Northumbria Research Link

Ultraviolet-Induced Fluorescence and Photo-degradation in Zinc Oxide Watercolour Paints

Vanessa Marie Johnson

A thesis submitted in partial fulfilment of the requirements of the University of Northumbria at Newcastle for the degree of Doctor of Philosophy

Research undertaken in the Faculty of Arts, Design & Social Sciences

July 2020

Abstract

Paper conservators tasked with the care and treatment of collections containing watercolours often encounter paper which has undergone severe discolouration and deterioration around Chinese white pigments, an effect caused by the photocatalytic reaction between surface electrons on the pigment particles and atmospheric moisture, leading to peroxide formation and oxidation of surrounding paper. This discolouration is difficult to treat and best avoided if possible. While conservators use ultraviolet-induced fluorescence to identify zinc oxide pigments by their intense visible fluorescence, they cannot presently relate zinc oxide's variety of fluorescent colours and intensities to its rate of photocatalysis. This thesis aims to link types of ultraviolet-induced fluorescence with zinc oxide's photocatalytic behaviour by examining the physical, chemical and optical properties of mock-up zinc oxide pigments in gum medium and historic watercolour painting case studies and determine whether this fluorescence could be quantified using commercially available DSLR cameras for predicting and diagnosing degradation in watercolours.

The investigation first collected and summarising art manuals and literature detailing zinc oxide's history and use as a watercolour pigment. This uncovered a near-consensus in the nineteenth century about the inert nature of zinc oxide, along with evidence that Winsor and Newton, the only supplier for nearly a century, annealed their pigments to improve their working properties and reduce their photoconductivity. No other suppliers could produce a good pigment and there were lone voices warning that zinc oxide may be damaging to surrounding materials.

Physical properties of pigments produced by the *direct* and *indirect* method as well as commercial and historic case study pigments were examined via x-ray diffraction

(XRD), x-ray fluorescence (XRF), energy-dispersive x-ray spectroscopy (EDX) and digital image analysis of micrographs and scanning electron microscopy (SEM) images. XRD and EDX verified the purity of all samples, while XRF revealed a much higher impurity content among *direct* method pigments than all others. Particle and crystallite sizes and morphologies derived from image analysis of micrographs and SEM images found that commercial and case study pigments were produced by the *indirect* method, that these had much smaller and shorter crystallites than *direct* method pigments and that these crystallites were more likely to be photoactive than the long crystallites of the *direct* method pigments.

The photocatalytic properties of mock-ups were studied via light exposure for 50 hours and subsequent measurements of peroxide formation via Russell-grams which imaged peroxides on *indirect* and commercial pigments. Colour changes were measured via a colorimeter and indicated that bleaching was the dominant effect, with most pigments causing browning on Whatman filter paper. Analysis of absorption spectra indicated that band gaps were narrowest for *direct* method pigments and wider for all others, a quality which lengthens the time that excited electrons are available for reactions. Visible deterioration was localised to materials in direct contact with pigments, evidenced by the embrittlement of binding media when paint sat on highly-sized paper and the browning of paper fibres when size was not present and paint was more embedded in the paper substrate.

Fluorescent characteristics were studied with fluorimetry and digital image processing with the goal of determining what qualities relate to photocatalysis. *Indirect* method pigments including commercial and case study pigments had a strong blue contribution, quantified via a green/blue ratio derived from the fluorescent peak areas and sRGB colour channel intensity values. This ratio was

consistently low for photocatalytic pigments as evidenced by peroxide formation and visual deterioration. Historic case studies which were photographed using different cameras and lighting scenarios still were grouped according to this ratio, which was low if visible deterioration was present.

Green/blue sRGB colour channel ratios increased after 50 hours of light exposure, indicating that the surface defects responsible for green fluorescence increased over time. These defects are also responsible for reducing photoactivity; however, given the age of case studies and the similarity in fluorescence between historic pigments and modern photoactive pigments, an endpoint for reactions could not be determined and may not exist. The green/blue ratio appears to be a reliable indicator of photoactivity even after periods of a century or more. More work is needed to standardise image processing procedures to make the method more quantitative, though comparisons within data sets in this study are a reliable indicator of peroxide formation on pigment particle surfaces.

Given the difficulty in treating watercolours damaged by zinc oxide and the evidence presented here of its lengthy photoactivity, paper conservators should avoid using the pigment for retouching and focus on stabilisation and prevention. Localised reduction of staining using alkalis below pH8 may be carried out with caution as strong alkalis dissolve zinc oxide pigments. Consolidation of cracked paint, when carried out after the removal of sulphate salts in a wash, both reintroduces the binder and provides a temporary barrier between surface electrons on pigment particles and surrounding paper, slowing the oxidation of paper cellulose by peroxides.

Table of Contents

List of Figures

author using scanning electron microscopy (SEM).

Chapter 4: Characterisation of Photocatalytic Degradation

and figure and distant mountains.

Chapter 5: Ultraviolet-Induced Visible Fluorescence of ZnO

Chapter 6 Discussion and Conclusions

Appendix 4: Miller Indexing and Miller-Bravais Indexing

Appendix 8: Particle and Crystallite Analysis: Procedure, Code, and Graphs

Appendix 9: Additional EDX Data and Sample Locations for Case Studies

Appendix 11: Analysis of Mock-Up Papers

Appendix 12: Light Exposure Rationale

Appendix 16: Fluorimetry Spectra

Appendix 17: Decomposition of Emission Spectra in MATLAB

Appendix 18: Wratten 2e Filter Diffusion Density

Appendix 19: Image Processing Procedure for UV-Induced Fluorescent Digital Images and Micrographs

List of Tables

Chapter 5: Ultraviolet-Induced Visible Fluorescence of ZnO

Chapter 6 Discussion and Conclusions

Appendix 1: Case Study and Mock-Up Sample Reference Tables

Appendix 2: Supplemental Information on Zinc Oxide Production

List of Auxiliary Content

Included in this thesis is supplementary data and analysis referenced in this work. They are arranged by the chapters in which they appear and contain the following folders:

- Chapter 3 physical properties
    - EDX data
    - Mapping
    - Particle analysis
    - XRD
    - XRF data
- Chapter 4 photocatalysis
    - Colorimetry
    - Fibre analysis
    - Photomicrographs
    - Reflectance spectra
    - Additional files: Russellgrams, Singh irradiance calculations and irradiance of light ageing lamp
- Chapter 5 fluorescence
    - Digital image analysis
    - Fluorimetry
- Chapter 6 discussion
    - Files include spreadsheets of various correlation calculations

Acknowledgements

I would like to thank first Jane Colbourne who first introduced me to the eccentricities of zinc oxide pigments and has supported and encouraged me in this work in more ways than I can enumerate here. I'd also like to thank Kate Nicolson for all her help with spectroscopic studies and instrument access as well as editing and general encouragement. Pietro Maiello provided hours of support with SEM and XRD studies as well as providing spectrophotometer access and advice on zinc oxide's band gap properties. Helen Creasy and Colin Liddie provided me with images and actual paintings for study and made themselves available for questions. More thanks goes out to Gordon Forrest for his XRF help and to Dave Thomas for helping me with ppm-atomic percentage conversions. Thanks to Lore Troalen for providing me with advice and a small historic sample for study. Thanks for Northumbria University for providing me with funding to attend the ICON 2016 conference and present my preliminary results to my peers. Thanks to my family and friends for their patience and support in my years of academic solitude. I couldn't have stayed sane without the humour and comradery of my Italian PhD cohorts. Extra thanks of course to my husband Anson Hancock for keeping this ship afloat with advice, tea, editing, funds, affection and patience.

Declaration

I declare that the work contained in this thesis has not been submitted for any other award and that it is all my own work. I also confirm that this work fully acknowledges opinions, ideas and contributions from the work of others.

Any ethical clearance for the research presented in this thesis has been approved. Approval has been sought and granted by the Faculty Ethics Committee on 6 October, 2016.

I declare that the Word Count of this Thesis is 39,474 words.

Vanessa Johnson

Signed 14 July 2020

1 Introduction

Winsor and Newton first developed a zinc oxide watercolour pigment called Chinese white in 1834. The new pigment led to a breakthrough in watercolour painting and the beginning of the international success of this newly-formed company. It mixed well with other colours and lent opacity to transparent watercolours, creating body-colours or gouache[1] which artists increasingly adopted in the late nineteenth century and applied thickly to approximate the more diffusely reflective surfaces of highly-pigmented oil paints (Avery, 2002). While the prevailing attitude of the time was that Chinese white, and by extension zinc oxide, was chemically stable, many watercolour paintings and pastels are today showing signs of severe degradation in both the paint film and surrounding areas of the paper (e.g. Kemp, Wise and Hamilton, 2004; Singer and Liddie, 2005). This degradation manifests in multiple ways: as efflorescence caused by the conversion of zinc oxide to soluble zinc sulphate salt crystals in the presence of moisture and sulphur dioxide and as darkening and embrittlement of paper as peroxides and free radicals formed on pigment particle surfaces oxidise cellulose in the paper fibres (Daniels, 1990; Liddie, 1998; Singer and Liddie, 2005).

The primary catalyst for degradation caused by zinc oxide is light, and zinc oxide is thus characterised as a photo-catalytic pigment. While photo-catalytic reactions are now considered typical of zinc oxide pigments on paper (e.g. Depew, 1941; Morley-

---

[1] The terms gouache and body-colour are interchangeably used to describe watercolour paints which are made opaque with the addition of white pigment; however, these two terms once referred to two different media. Gouache was a term introduced in the eighteenth century to describe a special paint prepared and sold for opaque painting on paper. It contained more binding medium than watercolours as well as a white pigment and additional white materials such as chalk to add opacity. Body-colour referred to 'any type of opaque water-soluble pigment' and has a history extending to the fifteenth century (Tate website, 'Art term: gouache').

Smith, 1958; Hey, 1987; Daniels, 1990), not all nineteenth century examples have been affected thus and some remain pristine over a century after their creation. Whilst the cause of this variation in reactivity is partially understood and linked to variations in exposure to light and moisture, it remains unclear why some zinc oxide pigments appear relatively stable. A possible factor is the method of pigment production. Two primary methods of production existed in the nineteenth century for zinc oxide: the *indirect* or French process and the *direct* or American process. These two production methods yielded zinc oxides with different physical qualities. Whilst the *indirect* method produced a whiter, finer and more visually pleasing pigment, it has been linked by Morley-Smith (1950; 1958) to higher levels of hydrogen peroxide production. However, *direct* method pigments, whilst more stable and less likely to produce these peroxides, are not widely used in pigment production today. It is unclear to what extent each method was used in the past for pigment production, prompting further research into the photocatalytic qualities of both types.

Today, professional expedience focuses on prevention of damage through control of display conditions and reducing light exposure. However, conservation professionals typically follow general guidelines dealing with all art objects and making no mention of zinc oxide's variable deterioration rates (e.g. Feller, 1964; Loe, Rowlands and Watson, 1982; Thomson, 1986; Smith, 2010; Druzik and Michalski, 2012). Perhaps more importantly, the impactful work published about zinc oxide's photocatalytic properties often lies behind a paywall in journals catering to the physics or chemistry communities and uses language which is impenetrable to many practicing conservators (e.g. Winter and Whittem, 1950; Rubin *et al.*, 1953; Dodd *et al.*, 2006; Sáez-Pérez, Rodríguez-Gordillo and Durán-Suárez, 2016; Blashkov,

Basov and Lisachenko, 2017). Given the variation in reactivity outlined in this literature, more research is called for to understand how and why different zinc oxide pigments react the way they do so recommendations can be provided.

The most common, non-destructive method used by conservators for indicating the presence of problematic pigments such as zinc oxide involves technical examination using photography in various light sources. Diffuse light sources generate ultraviolet reflectance (UVr) (<400 nm), UV fluorescence (UVf) ((~400-700 nm emitted from a surface which is illuminated by wavelengths <400 nm), visible reflectance (~400-700 nm), and infrared reflectance (>700 nm). UVf is particularly suited for indicating zinc oxide as it captures a characteristic intense visible fluorescence. However, several factors complicate this method of identification when applied to zinc oxide pigments. For example, binding media such as oxidised gum arabic and paper supports with certain sizes can also fluoresce in UV light and significantly alter the colour of the paint's visible fluorescence (Clementi *et al.*, 2012). It is understood that the colour of zinc oxide's fluorescence originates from a ratio of blue and green fluorescing nanoparticles that cause wide variations in the perceived colour of this fluorescence (e.g. Nagle, 1928; Hey, 1987). Variations in standards regarding digital image capture can also lead to miscommunication about a pigment's fluorescence.

Despite these drawbacks, studies have indicated that zinc oxide's visible fluorescence derives from its photocatalytic properties. In the 1950s investigations into the ratio of blue to green fluorescing particles indicated higher photo-activity for zinc oxides with a greater number of blue fluorescing particles. These studies also indicated that they converted to green fluorescence after peroxide-producing photocatalytic reactions occurred (Morley-Smith, 1950; 1958). Whilst some studies

of nano-fluorescence have been conducted by the conservation community (e.g. Romani *et al.*, 2010; Clementi *et al.*, 2012; Bertrand *et al.*, 2013; Artesani *et al.*, 2017), many more with applicable results (e.g. Shalish, Temkin and Narayanamurti, 2004; Janotti and Van de Walle, 2009; Chen *et al.*, 2011; Rodnyi and Khodyuk, 2011; Bandopadhyay and Mitra, 2015) have been published in physics and chemistry journals and suffer from accessibility issues discussed previously. Clarifying the findings of these studies will allow for conservators to access this knowledge, whilst further studies into their applicability to historic watercolour pigments will facilitate application to paper conservation.

This study aims to bridge the gap between physicists and chemists and working conservators, combining a thorough review of the work done by these scientists with experiments designed to track chemical and optical changes in pigments, media and paper after light exposure. By then determining how fluorescence correlates to light-induced degradation, the viability of fluorescence as a diagnostic tool for paper conservators can be assessed. If a strong link is found, a paper conservator utilising standardised procedures to examine the fluorescence of zinc oxide with a camera and a computer could in theory determine the potential for deterioration of an artwork due to the pigment's photocatalytic properties.

1.1 AIMS AND OBJECTIVES

The aim of this thesis is to determine whether ultraviolet fluorescence can be used to predict or diagnose deterioration in watercolours on paper caused by zinc oxide pigments. The following objectives will facilitate this aim.

1. Detail the attitudes surrounding zinc oxide pigments in the nineteenth century and find any evidence in the literature of problematic examples.

2. Characterise the physical properties of zinc oxide pigments such as crystal structure, composition and particle size and morphology and relate them to the pigments' production method and known electrical behaviour.

3. Study photo-induced deterioration processes and products in artworks and mock-ups and relate these to physical and optical properties.

4. Study zinc oxide pigments' fluorescence spectroscopically and using digital image analysis to understand how fluorescence changes over time and assess the viability of digital photography for the study of zinc oxide fluorescence by conservators.

5. Determine through comparison of all data if the detection of fluorescence can be used to prevent or detect degradation reactions in zinc oxide pigments and outline any new information discovered through the course of this study.

By achieving these objectives, a more informed and confident approach can be adopted in the display and preservation of paper-based objects containing zinc oxide pigments. Additionally, new understanding about the changing composition and behaviour of zinc oxide will undoubtedly serve in informing future approaches to the treatment of this problematic pigment in the wider conservation field.

Each chapter of the thesis will address an objective. Chapter 2 will address objective 1, chapter 3 will address objective 2, and so on. The thesis will be structured as follows:

Chapter 2: Historical background and changes in attitudes towards permanence in nineteenth century

Chapter 3: Characterisation of zinc oxide pigments using particle size analysis, crystal structure analysis and compositional analysis

Chapter 4: Characterisation of deterioration of watercolours containing zinc oxide via light exposure of mock-ups in the presence of moisture and examination of these samples using visual and analytical techniques with comparisons to case studies

Chapter 5: Analysis of UVf via fluorimetry and digital image analysis with further evaluation of digital imaging techniques, limitations and applicability to case studies.

Chapter 6: Discussion of results from chapters 2-5, linking across methods to highlight new discoveries and determine the most significant factors for degradation over time, followed by a discussion of current paper conservation practice and whether digital imaging methods could be used by paper conservators given the results of this study. Limitations to implementation will also be discussed as well as future work.

1.2 METHODOLOGY

This serves to introduce the techniques and resources used in the present study including those utilized in the creation of the mock-ups, the rationale behind the selection of case studies, and a brief description of the analytical/technical examination techniques employed. Each chapter of this thesis beginning with chapter 3 involves the analysis of mock-up and case study samples to better understand zinc oxide in historic works.

1.2.1 CREATION AND STUDY OF MOCK-UPS

To reduce variables and facilitate the separate examination of materials, most analysis was carried out on mock-ups created to approximate historic samples. This allowed for controlled light and moisture exposure and scrutiny of the physical and

chemical properties before and after exposure. The results from these mock-ups were then compared with a range of watercolours from the nineteenth and early twentieth centuries exhibiting similar anomalies.

Mock-ups of paint samples were prepared according to historic recipes and painted onto a variety of paper substrates. They consisted of pigments, a binding medium and paper substrates.

Pigments: Three *indirect* method pigments, three *direct* method pigments and three zinc white pigments from various pigment suppliers were selected and studied. All were in the Burt Hall pigment archives and were produced after 2005. The Cornelissen zinc white was ordered in 2015 and was likely produced at the latest date.

They consisted of the following: [2]

Indirect method zinc oxides:

- **Sample 1:** Zinc oxide red seal from Norkem chemical suppliers

- **Sample 3:** Zinc oxide high purity from Norkem chemical suppliers

- **Sample 4:** Zinc oxide white seal, code 28170000 from Brüggemann Chemical, Ludwig, Germany

Direct zinc oxides:

- **Sample 6**: Zinc oxide American Process from Norkem chemical suppliers

- **Sample 7**: Zinc oxide 2011 from Grillo-Werke AG

---

[2] Numbers are not in strict order as some samples originally studied were discounted. The original number designations were maintained to avoid confusion during data processing.

- **Sample 9:** Zinc oxide spezial, code 28170000 from Brüggemann Chemical, Ludwig, Germany

Zinc oxide pigments from pigment suppliers:

- **Sample 14:** Winsor and Newton Chinese White

- **Sample 15:** Kremer Pigments Zinc White 46300

- **Sample 16:** Cornelissen Zinc White[3]

The first two categories contain zinc oxide powders with similar properties to pigments, but which are not specifically marketed as artists' pigments by suppliers. However, industrial production methods for both non-pigments and pigments are similar, if not identical.

Binding Medium: Gum arabic in water provided the binding medium for all samples. This is based on the work by Ormsby *et al*. which concluded, after analysing historic watercolour paints, that 'by the early nineteenth century, gum arabic was used almost exclusively for commercially available watercolour paints' (Ormsby *et al.*, 2005, p. 45).[4]

To make the binding medium, grade 1 gum arabic supplied by Cornelissen art suppliers was added to boiling water in a ratio of 1g gum : 4 mL distilled water. A

---

[3] Pigment supplied to Cornelissen by Messrs. Charles Roberson and Co., a major pigment supplier in London since 1810.

[4] Originally, glycerine was added to half of the samples to add flexibility to the paint film, a choice informed by the Roberson archive. This coincided with a modern recipe for artisan watercolours recommended by Seymour (2007). Glycerine was chosen over other traditional humectants (honey, cane sugar etc.) as it did not discolour with age and had been used in ageing experiments which required a clear binding medium (Feller, 1992). Additionally, adding glycerine to the binding medium approximated Winsor & Newton's moist colours introduced in 1832, which were likely used widely by watercolour artists after that date as they were easier to wet up due to the addition of glycerine (Avery, 2002). Due to limitations in the study and data set sizes which could be reasonably analysed in the time allotted, this sample set was largely eliminated from the body of the thesis.

1:4 w/v ratio was chosen as it produced a thick yet workable solution. This ratio derives from a gum arabic recipe by Seymour (2007) recommending a 1:6 v/v ratio of gum to water. A 1.4 g/cm^3 density value was measured for the gum used in this study and given that 1 mL of water is equal to a cm^3 and weighs 1 gram, a 1:6 v/v ratio was equal to 1.4 grams solid gum arabic for 6 grams water, or 1 part gum by weight to approximately 4 parts water by volume[5]. After dissolving for two days as recommended by Seymour (2007), the gum solution was poured through a clean linen cloth to remove foreign material and woody plant matter.[6]

The gum water was added to zinc pigments in a ratio of 1.5 mL gum water to 0.2 g pigment. This ratio was chosen as it was the most pigment-rich paint produced which also resisted flaking when dry. The paint was applied to the papers using a size 1 sable brush, loaded once and tapped once on the side of the ceramic dish to remove excess paint. The painted area was approximately 2 cm^2 and all materials were rinsed thoroughly in deionised water between samples.

Papers: Sample sets were painted onto paper substrates of varying complexity and acidity to study reactions between zinc oxide pigments, cotton fibres, fillers, and acidic degradation products present in aged papers[7]. Control samples of only binding

---

[5] 1.4g to 6 ml is approx. 1.5 to 6, so dividing both sides by 1.5 yielded 1 g and 4 mL. This was done to facilitate measurement of components.

[6] For the binding medium with glycerine, a 5% w/w solution was prepared. 5% glycerine recommended by Gettens and Stout (2011) though they did not specify if this was weight or volume. Weight percentage was used due to glycerine's higher density than water (1.26 g/cm^3), resulting in a more conservative quantity of glycerine than if volume had been used.

[7] Papers from the nineteenth and mid-twentieth century were used for substrates in order to most closely approximate some of the papers used at the time. Additionally, initial paper quality used by artists varied widely and usually included acidic, lignin-heavy papers. By using both Whatman filter paper as a simple, neutral cotton fibre paper as well as historic papers of varying composition, photodegradation experiments could be carried out which included the acids present in these papers and more closely approximated natural ageing.

medium were painted out onto paper as well. The substrates and substances studied were the following:

- Whatman #1 filter paper: to study interactions between zinc oxide, gums and cotton paper fibres[8]

- Highly sized, naturally aged (~40 years) Fabriano NOT cotton rag watercolour paper: to study additional interactions between zinc oxide, gums, sizing agents, cotton and linen fibres and fillers

- Mid-nineteenth-century wove, mixed-fibred handmade paper from an extant folio from the Duke of Northumberland's archive at Alnwick Castle: to study interactions between zinc oxide, gums, sizing agents, mixed linen and wood pulp fibres, and coloured acidic degradation products.

Sample referencing: Each pigment was identified by a given number, each set (delineated by substrate) identified by a letter, and the binding media by C or Cg to allow for ease of data collection and reference.

The sample sets are as follows:

- **Sample set P**: Pigment alone, not in binding medium, usually on a slide or SEM peg

- **Sample set W**: Pigment and binding medium on untreated Whatman #1 filter paper

---

[8] Glass slides were initially made as a control but were abandoned as the watercolour paint would separate from the glass after light exposure, even when painted onto textured glass. Additionally, Whatman paper was determined to be a better control as it contained only cotton fibres and was more representative of the ageing conditions this study aims to replicate.

- **Sample set F**: Pigment and binding medium on ~40-year-old Fabriano NOT paper, highly textured

- **Sample set B**: Pigment and binding medium on aged mid-nineteenth century folio paper, mixed wood/linen fibres

Gum medium is delineated as follows:

- **C:** Cornelissen gum arabic

A sample of this system is as follows: B1C = Norkem zinc oxide red seal in gum arabic binding medium painted onto mid nineteenth-century folio paper.

1.2.2 CASE STUDIES[9]

Five watercolours were studied which contained zinc oxide pigments and dated from the mid-nineteenth century through the early twentieth century. The alphanumeric delineation of the pieces, their identifying information, and the rationale for their study are listed below:

Figure 1.1 Irene Kendal, *Bouquet of Flowers,* early twentieth century, watercolour and body-colour on paper, National Trust collection.

- IK: *Bouquet of Flowers* by Irene Kendal (dates unknown), early twentieth century (Figure 1.1), watercolour and body colour on wove paper, from the National Trust – to study a zinc oxide mixed

---

[9] To facilitate later reference to case studies, Appendix 1 on page 224 contains a reference table of case study titles, artists, dates and sample codes.

with other pigments from the early twentieth century on a highly discoloured, acidic sheet of paper. This case study has also undergone conservation treatment including repainting some white areas.

- SSB: *S.S. Buda* by George Thomson (dates unknown), 1889 (Figure 1.2), watercolour on wove paper, private collection – to study a zinc oxide with a significant percentage of zinc sulphate salts and a khaki-coloured fluorescence. This piece has also undergone conservation treatment but shows no signs of new whites added to zinc oxide areas.
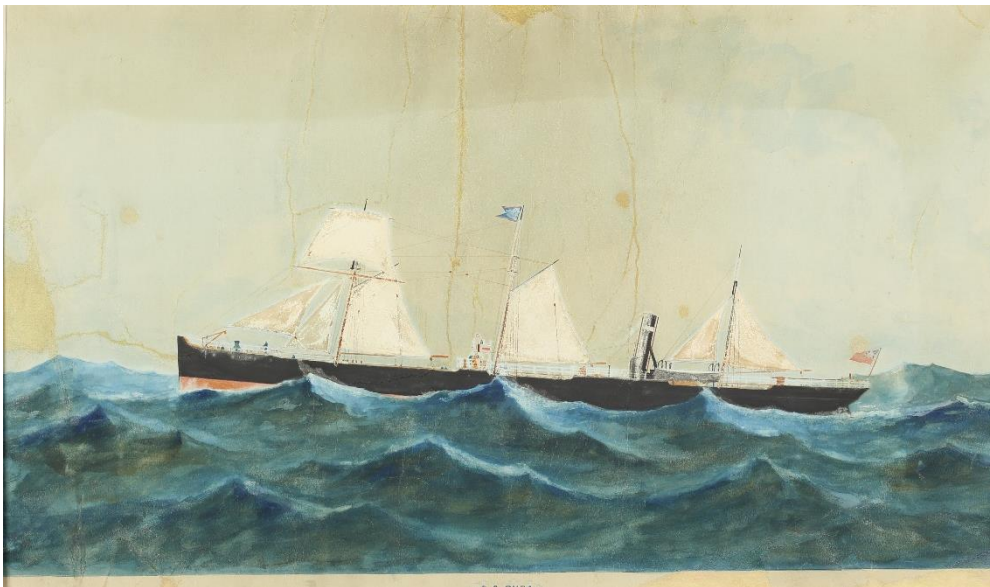
Figure 1.2 George Thomson, *S.S. Buda*, 1889, watercolour on paper, private collection. Image credit: Colin Liddie.

- TH: *View of the River Coquet* by Thomas Harper (1820-1889), watercolour and body colour on wove paper, mid-nineteenth century, on loan from the Laing Gallery, Newcastle upon Tyne (Figure 1.3) – to study a well-preserved zinc oxide from the golden age of its use. Harper exhibited between 1856 and 1875 in London and used zinc oxide pigments during this time and in this piece.

Figure 1.3 Thomas Harper, *View of the River Coquet,* mid-nineteenth century, watercolour on paper, The Laing Gallery collection.

- RD: ruins drawing, title and artist unknown, late nineteenth century, charcoal and white body colour on paper, in the study collection at Burt Hall, Northumbria University (Figure 1.4) – to study a well-preserved zinc oxide pigment from late in the nineteenth century.

Figure 1.4 Unknown artist, ruins drawing, late nineteenth century, charcoal with white body colour highlights on paper, Burt Hall study collection, Northumbria University.

- JC: 'General view of St. Mary's Cathedral, Iona' watercolour on paper, from Historic Environments Scotland, artist and data unknown[10] (Figure 1.5) – to study a zinc oxide which has clearly converted to zinc sulphate salts but which fluoresces differently to the zinc oxide in *S.S. Buda.*

Figure 1.5 Unknown artist, *General View of St. Mary's Cathedral, Iona,* date unknown, watercolour on paper, Historic Environment Scotland archive.

The decision to include case studies partially derives from a persuasive argument by J.S. Taylor, made in 1887 during the controversy over fading watercolours, that creating mock-ups and exposing them to light as a way of understanding watercolour behaviour is over-simplistic and far-removed from the actual life of an artwork. Whilst some of the physics involved in his argument is dated and inaccurate, his case for the direct observation of effects on naturally aged objects remains sound. He claimed, and probably accurately, that 'the scientific method [as

---

[10] Watercolour was acquired by HES in 1978 with 11 architectural drawings by JC and AC Buckler, though watercolour is stylistically dissimilar and not likely to have been painted by either architect. A date is given of 1850 in the accession records, but this probably refers to the architectural drawings which have watermarks in the paper saying Whatman 1850.

applied to the study of mock-ups]…is apt to lead to unnecessarily exaggerated conclusions' (Taylor, 1887, pp. 4-5). Whilst this study would likely yield valuable insights without the inclusion of case studies, the light exposure experiments in this study do not approximate actual ageing scenarios which are varied, complex and impossible to replicate. This can only be fully understood through the study of real-life case study scenarios.

Given the limitations of some forms of analysis, particularly destructive forms or those which required samples to fit into a chamber, not all analytical techniques were employed when examining each watercolour. Only those which were possible and least damaging to the works were carried out, such as photography and analysis of micro-samples either through microscopy or SEM/EDX analysis.

1.2.3 CHARACTERISATION OF MOCK-UPS AND CASE STUDIES

The following analytical techniques were used in each of these chapters.

Chapter 2 – Physical characterisation of pigments, analytical methods:

- **X-Ray diffraction (XRD) for crystal structure analysis:** XRD was utilised to determine the relative crystallinity of mock-up samples to one another.[11] This crystallinity relates to the level of defects in the zinc oxide crystals due to the absence or displacement of zinc or oxygen ions. These defects would theoretically alter the photocatalytic properties of

---

[11] As a correction due to line broadening was not applied, these measurements of crystallinity were qualitative, not quantitative, and useful when comparing one sample in this study to another. This correction would allow for a true interpretation of lattice properties but is beyond the scope of this study. Given that instrumental line broadening is constant if parameters in the instrument are not changed, it can be discounted when samples are compared to one another. They cannot, however, be compared with values reported in literature.

the pigment and change the rate of reactions with surrounding light and moisture.

- **X-Ray fluorescence (XRF) and EDX spectroscopy for compositional analysis:** Trace elements were measured using XRF spectroscopy as the resolution of the collected XRF spectra was better than that of the EDX spectra. Impurities could account for differences in deterioration rates as well as increasing or decreasing the intensity of certain fluorescent wavelengths. This analysis was carried out on mock-ups but not on case-studies as the required volume of pigment was significant. Case study pigments were verified as zinc oxide using EDX spectroscopy.

- **Particle size distribution using optical microscopy**: Measurements were collected of mock-up agglomerate particles suspended in Meltmount™ (refractive index 1.662) to determine clumping behaviour as this would affect total surface area and slow reactions.

- **Crystallite[12] size distribution and morphology analysis using scanning electron microscopy (SEM)**: Measurements were collected of the diameters and lengths of mock-up crystallites using SEM images and an image processing methodology to determine the size distribution of individual crystallites. These images provided additional data regarding pigment morphologies which further influence rates of photocatalytic reactions.

---

[12] A crystallite is an individual crystal of a pigment, as opposed to a particle which is often composed of many crystallites grown together or held together electrostatically.

Chapter 3 - Tracking deterioration, analytical methods:

- **Light-induced deterioration:** Two sets of mock-up samples were created, one set as a control whilst the other was exposed to light in a Q-SUN Xenon Test Chamber Xe-1 for 50 hours in total. These samples were attached to a foam core over a layer of wet Whatman #1 filter paper (3 sheets) and a layer of Gore-Tex®. This allowed moisture to be introduced slowly and steadily over time. Exposure was carried out in 5-hour increments to prevent the Whatman paper layer from drying completely during light exposure and to allow for rewetting.

- **Russell-grams:** hydrogen peroxide formation was measured by pressing a sheet of lithographic film onto the surface of light-exposed mock-up samples. Any peroxides reacted with the silver nitrate in the film, exposing those areas and rendering the film black. All areas of the film without contact with reaction products remained transparent after it was developed.

- **Visual examination of paint surfaces at magnification:** the surfaces of mock-up samples were photographed under magnification before and after light exposure using a Leica S6D microscope with microscope-mounted digital CCD camera (a Leica MC170 HD). This allowed cracking and discolouration to be documented and examined. Case studies were similarly photographed for comparison.

- **Colorimetry:** CIE 1976 $L*a*b*$ values were collected for zinc oxide pigments on paper, both in the pigmented areas and on the back of the Whatman mock-ups to track changes in pigment and paper tone with

light-induced degradation. This was carried out on mock-ups and some case studies for comparison. *L*a*b** values were used to calculate total colour change, $\Delta E *$, to further facilitate comparisons.

- **Spectrophotometry:** reflectance spectra from 300-1400 nm were collected using a Hitachi U-3010 Spectrophotometer to obtain information about band gap changes in zinc oxide pigments due to increased crystal defects after light exposure. This was done by converting reflectance to absorption, then extending the absorption edge to the x-axis to approximate the band gap energy. Control and exposed samples were compared in this way, as were pigments of different production types. Given instrumental limitations, only mock-ups were studied with this method.

- **Crystal structure analysis via elemental mapping and point scans with energy-dispersive X-ray (EDX) spectroscopy:** Distribution of zinc and oxygen ions were mapped using the mapping function provided by the program Aztec for EDX spectroscopic scans to determine if there was a concentration of defects in the lattice which would facilitate peroxide production on the crystal surfaces and if this defect gradient changed after light exposure or remained constant.

Chapter 4 - Ultraviolet-Induced Visible Fluorescence of ZnO, analytical methods:

- **Fluorimetry:** emission spectra were collected on a Horiba FluoroMax® 4 Spectrofluorometer using an excitation wavelength of 325 nm and a slit width of 2 nm over a range of 335-640 nm. 3 spectra were collected for

each mock-up sample as emission spectra varied according to thickness of paint and pigment-to-binder concentrations. These were normalised by area and plotted to compare controls to light-exposed samples. Case studies could not be studied with this method as the instrument required the sample to be loaded into a small (~1x2 cm) sample mount.

- **Digital image collection and processing:** UV-induced fluorescence images were taken of all control and light-exposed samples using a Canon EOS 6D digital camera with CMOS imaging chip and a Kodak Wratten 2e UV-cut-off filter to ensure only visible wavelengths of light were imaged. These were then processed using ImageJ to isolate the fluorescing area and allow easier visual comparison. Additional UV photos were taken at magnification using an Olympus BX51M microscope with mounted CCD camera (Olympus DP70). Both images were taken with UV lamps emitting at a dominant wavelength of ~360-365 nm. RGB values were analysed in all images and compared to determine if ratios between colour channels could be related to fluorimetry spectra and used for diagnostic purposes. UVf images of case studies were also collected and processed in this way and compared with mock-ups to determine if any relationship between the two could be established.

2 History of Zinc Oxide in Watercolour Painting

The greatest strength of English watercolours in the early nineteenth century was their transparent style, one that grew from an earlier tradition of monochromatic washes which were later stained with passages of colour reminiscent of tinted prints. One of the earliest exponents of the 'English style' was John Robert Cozens (b.1752, d.1797) who evolved his technique to incorporate applications of pure colour (Sloan, 2003). His watercolour techniques greatly influenced artists such as Joseph Mallord William Turner (b.1775, d.1851) and Thomas Girtin (b.1775, d.1802). Turner built on Cozens' technique by incorporating dabs of white or body-colour to add depth and texture to his compositions (Wilton and Lyles, 1993).

The growing popularity of watercolours was spurred on by exhibitions of these key artists' work and by the portability and speed of application of the painting medium compared with oil paints. Aimed at amateurs and artists alike manuals and compendia, devoted to the new technique, appeared with great proliferation, further promoting the style. Detailed instructions were provided on how to build up intense passages of colour using numerous washes of thin paint rather than a thick application of opaque pigment typical of body-colour techniques (Clark, 1807). The application of white was particularly discouraged, and instead the employment of the paper to provide the highlights was favoured. This was achieved by blotting, sponging and lifting colour with a cotton cloth (Fielding, 1830), by rubbing or scraping off pigment, or by leaving passages of the paper unpainted.

Specific details of the white pigments recommended for use during this period are largely absent from manuals. On the rare occasion they do appear the pigment is

generically referred to as 'white' as examples 'the trunk is beautifully streaked with white' (Francia, 1813)[13] and '[add] a small particle of White' to a sheep (Hassell, 1823, p. 29) illustrate. The sparse recommendations for using white could be due to the lack of any viable alternative to lead white. Chalk white and barium sulphate, sold as Constant or Permanent white, were available in the decades before the introduction of Chinese white, but these were difficult to paint with as they appeared transparent on working, having a similar refractive index to gum medium. This meant that the true colour of the mixed paint would only be revealed upon drying (Field, 1885). Muckley mentioned that attempts were made at using lead white as body-colour, which 'was immediately abandoned,' indicating that 'mixing white lead with their pigments…proved disastrous to the works in which it was employed' (Muckley, 1888, p. 50)[14].

Little evidence exists for the marketing or production of zinc oxide as a watercolour pigment before its introduction as Chinese White by Winsor and Newton in 1834. Louis-Bernard Guyton de Morveau (b.1737, d.1816), a French chemist in Dijon, had recommended zinc oxide as a possible white pigment in oils in 1780. Its lack of body however was to repress artists' hopes of this pigment providing a good substitute to the popular lead white. Shortly after this period two English patents were awarded to John Atkinson in 1794 and 1796 (Kühn, 1986; Harley, 2001) but whether they reached production is not clear. Rudolph Ackermann refers to 'white of zinc' and 'chemical white' in his treatise on Ackermann's superfine water colours, published in 1801, although neither pigment is listed for sale. His later manual of

---

[13] Pages in this artist's manual are not numbered.

[14] This is likely in reference to lead white's tendency to blacken when exposed to H_2SO_3, a common industrial pollutant, which converted lead carbonate to lead sulphide, a black substance (Daniels, 2007). Lead white pigments were prone to darken in watercolours as they were not varnished in the same way as oil paintings.

1844, written after the introduction of Chinese white by Winsor and Newton, similarly does not include a zinc oxide pigment (Fielding, 1844). Ackermann's watercolours were widely stocked in paint shops from the beginning of production in 1799 through their partnership with Roberson from 1820-1904. Ackermann himself was forward-thinking, read George Field's 1835 Chromatography and supplied pigments to Field for study (Simon, 2018). His stature as a colourman and his omission of zinc oxide from sale would suggest that there were serious obstacles at this period to the mass-production of a viable white pigment from this material.

Early documentary evidence of artists using zinc oxide are also rare. The French artist Théodore Géricault (b.1791, d.1824), worked in a style which combined transparent washes common to English watercolour method with the preferred opaque French technique. Géricault experimented with the new 'zinc white' pigment when he painted *English Horse Guard* around 1820-1821 (Figure 2.1). According to Cohn and Rosenfield (1977) he purposefully chose the pigment for its lack of opacity and blue tinge, perfect qualities for representing smoke and fur highlights. John Frederick Lewis also worked with various white pigments and used both lead white and zinc oxide in his sketchbooks whilst working in Spain from 1833-1834. These highlights were especially effective in bringing attention to objects drawn on tinted paper[15].

---

[15] Discussion of Lewis' sketch found on the Tate website at the following address: http://www.tate.org.uk/art/artworks/lewis-sheet-from-a-sketchbook-used-in-spain-t09624

Figure 2.1 Theodore Gericault, *English Horse Guard*, 1820-1821, watercolour and body-colour on wove paper, Harvard Art Museums/Fogg Museum collection. Image made available for non-commercial use by Harvard Art Museums.

J.M.W. Turner experimented with zinc oxide pigments in watercolours, with documented use as early as 1800-1804 (Townsend, 1993). This was atypical of his palette, however, and further examples are not established.

2.1 NOMENCLATURE: ZINC WHITE VS. CHINESE WHITE

Confusion exists in the use of the terms 'zinc white' and 'Chinese white'. Whilst the term Chinese white usually refers to the specific white paint sold by Winsor & Newton, there has been some disagreement about whether both zinc white and Chinese white are primarily composed of zinc oxide.

Zinc white often refers to the zinc-based pigment for oil, described by Standage in the artist's manual of pigments as composed of '65 atoms of zinc to 16 of oxygen, or

else it is the anhydrous oxide, the hydrated oxide, or hydrated basic carbonate of zinc' (Standage, 1887, p. 8). There was an assumption by Standage that the pigments in zinc white used for oils and Chinese white for watercolours were identical. This may have been influenced by an earlier manual released by the American Society of Painters in Water-Colors titled *Water-Color Painting: Some Facts and Authorities in Relation to its Durability* (Bellows *et al.*, 1868) which records the similarities of the pigments only differing in the medium used. Muckley also uses the terms interchangeably when arguing that when white is needed, only Chinese or zinc white should be used in watercolour painting (Muckley, 1882).

Despite these assertions that the two pigments are interchangeable, some nineteenth-century authors indicate fundamental differences. Field's *Chromatography* in later editions introduces Chinese white as a 'peculiar preparation of oxide of zinc' (Field, 1885, p. 102). Taylor describes it as 'oxide of zinc prepared by a peculiar process, the effect of which is to confer upon it great increase of body' (Taylor, 1887, p. 33). According to Winsor & Newton's current website, the original Chinese white pigment was heated to very high temperatures before paint production (*Spotlight on Chinese white*, 2011). This annealing process would drive out impurities from the zinc oxide and, depending on the levels of oxygen and airflow conditions in the furnace, create a pigment with consistent particle shape and size, conferring better working properties on the final product. It is the command of this process which is likely responsible for the success of Winsor & Newton's creation of Chinese white, a technique which elevated its working properties and compatibility in a range of painting and drawing media. This quality product was widely and effectively marketed as a viable and superior product in watercolour to that of the demonised lead white, so much so that other colourmen, unaware of the process, could not

compete. Within a short period of time, Winsor and Newton's Chinese white became synonymous with zinc oxide-based watercolour paints both in Great Britain and abroad.

2.2 INTRODUCTION OF CHINESE WHITE

Two years after the company of Winsor and Newton was founded, Messrs William Winsor and Henry Newton introduced Chinese white in 1834 to general acclaim. Positive reviews were many and included: 'It has a good body, retains its colour perfectly, and works easily' (Merrifield, 1851, pp. 15-16), is 'beautifully white' (Field, 1885, p.102), and 'brighter than the lightest parts of an oil picture' (Muckley, 1882, p. 109). At this period, and for many years thereafter, it was widely compared to other whites. It did not lose opacity like barium sulphate (Rowbotham and Rowbotham, 1850; Field, 1885) and had good body and increased density when compared to lead white[16] (Merrifield, 1851; Gullick and Timbs, 1859; Field, 1885; Taylor, 1887). Gullick & Timbs (1859) in their comprehensive treatise *Painting properly explained* also remarked on the pigment's capability in covering dark grounds, and later in 1885 Field found Chinese white to be exceptionally suited for mixing with other pigments.

Not all reviews were complimentary. Taylor observed 'a slight lack of opacity' (Taylor, 1887, p. 34) and in the introduction to chapter eight of Field's *Chromatography*, it was stated that Chinese white's opacity was 'rather wanting' (1885, p. 97). Muckley recommended only using it in thin washes as it was liable to 'scale off' in thick application (Muckley, 1888, p. 58). However, some of the early

---

[16] Muckley (1882, p. 109) referred to Chinese white as being 'more compact.'

criticism about zinc oxide pigments seems to derive from the perceived differences between zinc white and Chinese white. While zinc white was 'unpleasant' and thin, Chinese white was regarded as 'quite safe when properly employed' (Ellis, 1883, p. 48). Poor preparations of Chinese white could also produce an unsatisfactory pigment which 'possess[ed] pasty and clogging properties and a lack of body…altogether foreign to the genuine preparation' (Taylor, 1887, p. 34).

Professional rivalry seems to have been another source of criticism. Following its introduction, George Bachhoffner, a chemist and fellow colourman, wrote a scathing dismissal of zinc oxide, the basis of Chinese white. In his book *Chemistry as Applied to the Fine Arts* published in 1837 he described zinc oxide as 'much inferior both in body and colour to the whites with a base of lead, and but little, if any, superior to them in durability' (Bachhoffner, 1837, p. 116). Winsor and Newton refuted this claim with their own pamphlet which was widely distributed to artists, a strategy which restored the reputation of the new pigment (Harley, 2001).

Notably, other colourmen avoided releasing their own brand of zinc oxide pigment nor did they recommend Chinese white in their manuals. Ackermann was one such author whose *Manual of Colours used in the different branches of water-colour painting* (1844) goes as far as to discourage the use of white in the mixing of tints.[17]

Some of the earliest recommendations for Chinese white involved its use in highlights, a technique which was sometimes cautioned against in art manuals as it was thought to bring too much attention to local areas of the composition (Chapman, 1858; Ellis, 1883). Other manual authors, however, encouraged the artist to decide whether the technique was appropriate (Leitch, 1873). Barnard (1871) encouraged

---

[17] Ackermann does list Constant white for sale, possibly for use in highlights - a common technique during this period.

highlights for approximating flecks of snow while Merrifield (1851) added Chinese

white as reflective spots in shiny surfaces such as eyes, gold or as an easier way to

paint delicate lacework. These highlights could be 'glazed' over with a transparent

wash if too bright, incorporating them more easily into a composition (Rowbotham

and Rowbotham, 1850).

Glazing methods were especially useful for subjects such as the sun which required

greater impact and luminosity. The glazing technique found its most extensive use in

the work of William Henry Hunt (b.1790, d.1864). He would paint a Chinese white

ground over the entire surface of a sheet of paper and add stippled transparent layers

to build up a realistic colour (Johns, 2002) (Figure 2.2). John Ruskin admired this

technique and described it in detail in his *Elements of Drawing* as an appropriate

method for adding objects on top of backgrounds. By painting in the object using

white pigment, then glazing over with transparent washes, a more vibrant colour

could be obtained (Ruskin, 1858). His manuals on paintings were among the most
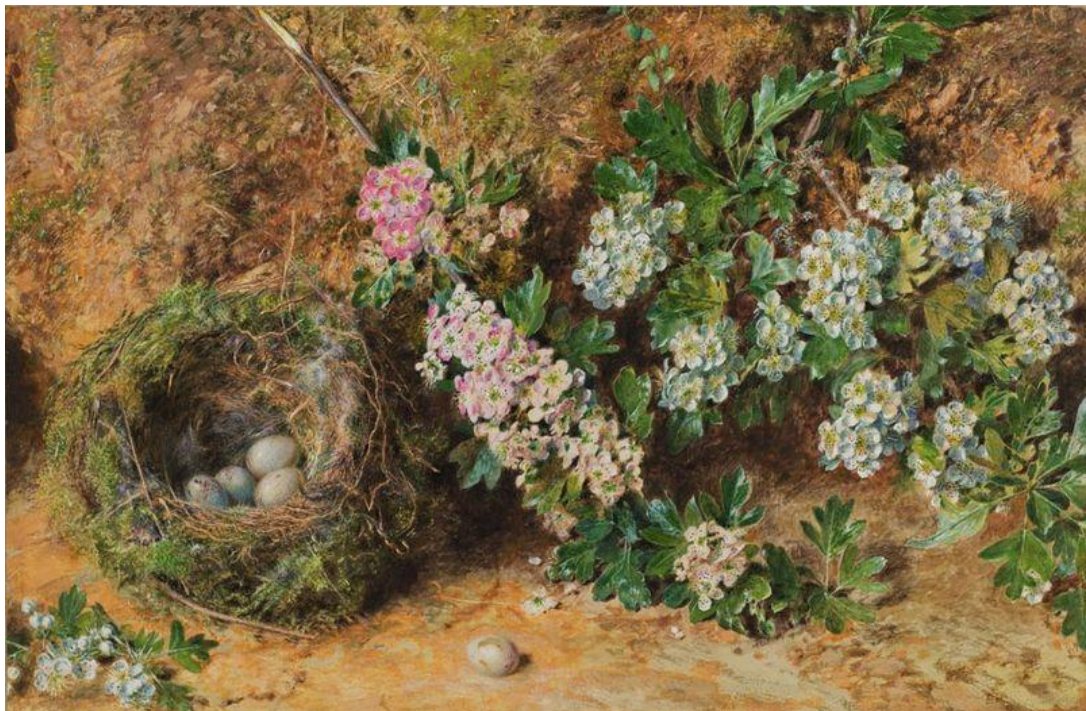
Figure 2.2 William Henry Hunt, *Chaffinch Nest and May Blossom*, 1845, watercolour on paper, the Courtauld Institute of Art collection. Image credit: The Samuel Courtauld Trust, image licensed for non-commercial use.

influential of the nineteenth century, nearly always in print and influencing artists in America as much as in Great Britain. His recommended techniques, particularly the glazing techniques, were readily adopted by artists and students (Avery, 2002).

One of the greatest benefits of Chinese white was that it facilitated painting on toned paper supports. Evidence of the popularity of this technique can be found in an advertisement for a special watercolour drawing box labelled for use when creating 'light and shade drawings on tinted paper' and which contained sepia, French blue and Chinese white (Merrifield, 1851, p. 6)[18]. This mode of painting on tinted paper was mentioned by Barnard as evidence of the merits of the pigment and its usefulness in watercolour painting when compared with the beautiful handling of washes without its addition (Barnard, 1871).

Experiments with Chinese white led artists to incorporating the white with other pigments to create opaque body colours, a technique that previously relied on mixing the less desirable lead white, chalk, or barium sulphate pigments into transparent colours. Chinese white, once predominantly used for highlights now began to define the medium of watercolours (Muckley, 1882).

Prominent advocates of body colour included John Ruskin and George Barnard who both recommended stippling in colour mixed with a little Chinese white to create smoother gradations and accelerate the painting process (Ruskin, 1858; Barnard, 1871). Barnard however cautioned overuse, claiming that a face painted with pigments mixed with Chinese white looked like a woman wearing too much makeup[19]. Chinese white allowed for a quicker and more accurate mixing of colours

---

[18] Advertisement is found in the back of the manual, after page numbers for main text end and begin again for advertisements.

[19] In contrast to this negative opinion, Merrifield listed Chinese white in her manual on portrait painting as an appropriate pigment for depicting flesh (Merrifield, 1851).

(Foster, 1884) and was especially useful in flower painting, creating a soft surface like the texture of petals.

Body colour in depictions of skies could also be quite useful although somewhat cautioned against. Barnard argued that white in skies created the appearance of fog which the viewer would rather be rid of, although in a later chapter he recommended its use in achieving this very same effect (Barnard, 1871). Carmichael claimed that small additions of Chinese white to blue prevented 'the colour from granulating and looking gritty,' thus creating a smoother effect (Carmichael, 1859, p. 50). The painting entitled *Olive Trees at Tivoli* by the American landscape painter George Inness (b.1825, d.1894) (Figure 2.3) is notable in its use of white in the sky creating a strong sense of atmosphere and humidity from the foreground into the distance (Avery, 2002). Being primarily a painter in oils, he treated the watercolour medium in a similar way, creating atmosphere with a thick application of paint rather than using the transparent washes typical of watercolour skies.

Figure 2.3 George Inness, *Olive Trees at Tivoli*, 1873, body-colour, watercolour and graphite on blue wove paper, the Metropolitan Museum of Art collection, image licensed for non-commercial use.

2.3 NINETEENTH-CENTURY ATTITUDES ABOUT PERMANENCE

Zinc oxide was overwhelmingly revered as a safe and stable pigment upon its introduction and for decades following, with manuals from the latter half of the nineteenth century describing its permanence as 'unquestionable' (Rowbotham and Rowbotham, 1850, p. 17) and 'unexceptionable' (Field, 1885, p. 97). It was 'not impermanent under any circumstances' (Standage, 1887, p. 8) and indeed zinc white, and by extension Chinese white, was 'the only perfectly permanent white' (Ellis, 1883, p. 48). Advertisements by Winsor & Newton described it as 'one of the most unchangeable substances in nature' (Merrifield, 1851, p. 12). Additional emphasis was placed not only on its permanence, but on its safe mixing with other colours, particularly valuable for those painting with body colour or opaquely (Gullick and Timbs, 1859; Taylor, 1887).

In this environment and amongst the fervour of praise there began to emerge small doubts about the long-term chemical instability of the pigment. Barnard insisted that the pure zinc oxide was permanent, but if exposed to iron, it would change colour due to 'sulferetted [sic] hydrogen' or 'foul air' from gas lighting or drains. To test his hypothesis, he suggested to the reader to perform their own tests and paint out their own sample and expose half to similar gases to see if a particular zinc oxide was immune to this type of chemical change (Barnard, 1871, p. 54). This suggestion indicates that watercolourists by this time may have been relying on zinc white pigments which were mixed with lead white in addition to the Chinese white sold by Winsor & Newton. It also suggests that there may have been some awareness of the conversion by sulphurous acid pollution[20] of zinc oxide to soluble zinc sulphate salts. These salts were white, however, suggesting the inclusion of iron would have

---

[20] Chemical formula H_2SO_3, a common industrial pollutant.

caused a red rusty colour to emerge. This comment suggests that observable changes in the pigment were beginning to occur around this time.

As the nineteenth-century neared its end, watercolours dating from the medium's 'golden era' (~1750-1850) began to show signs of change due to age (Wilton and Lyles, 1993). Ruskin described one of his Turner watercolours as 'much faded' but also claimed to 'find in their faintness more to discover through mystery than to surrender as lost' (Ruskin, 1878, p. 29). It was this fading of Turner's watercolours which first alarmed artists and the public to the problems of permanence in watercolours and prompted more study by scientists into the problem (Ellis, 1883).

2.3.1 THE CRISIS AT SOUTH KENSINGTON AND THE RUSSELL AND ABNEY REPORT

According to Taylor (1887), *The Times* in London reported in 1886 that damage by diffuse sunlight to watercolour paintings in the national collection in South Kensington had been so severe and irreversible that steps needed to be taken to prevent further damage. This included storing the works in portfolios or only displaying them at night. The ensuing controversy led to a panic among artists and dealers that watercolour artworks would lose value, or that the medium itself was too unstable for continued use. Ruskin wrote a letter at the time 'like the sound of a trumpet' (Taylor, 1887, p. 2) in defence of the medium and brought many sceptics back in favour of the technique.

In response to the controversy, Parliament commissioned two scientists, Dr. W. J. Russell and Captain W. de W. Abney, to investigate the chemical stability of watercolour paints. The resulting study, later known as The Russell and Abney

Report[21] of 1888 , was the most thorough scientific investigation of its time into the permanence of watercolour pigments under various conditions. The report received much attention and prompted intense debate. It isolated variables such as air, moisture and specific wavelengths of light to determine which was most responsible for the chemical changes in watercolour pigments. The authors measured chemical change via fading but for obvious reasons of colour did not study Chinese white alone, only in mixtures common to the body colour technique. Most pigments mixed with Chinese white faded as expected, though Prussian blue faded much more quickly than usual, and vermilion darkened more than expected. No conclusions were drawn at the time about Chinese white's impact on the accelerated fading and darkening.[22]

2.3.2 THE AFTERMATH: TENTATIVE WARNINGS ABOUT ZINC OXIDE

In a later watercolour manual titled *A Descriptive Handbook of Modern Water Colours*, John Scott Taylor expressed concern for zinc oxide specifically, saying that the pigment might not be inert due to its 'metallic oxide' composition, indicating that the contemporary knowledge of inorganic chemistry was aware of possible adverse reactions. He conceded however that in practice, zinc oxide seemed to be inert, though his decision to express doubt is notable (Taylor, 1887, p. 34). A year

---

[21] Full title 'Report to the Science and Art Department of the Committee of Council on Education on the Action of Light on Water Colours,' though commonly referred to as the Russell and Abney Report for brevity.

[22] The controversy prompted others, particularly artists' manuals, to question the permanence of various pigments. Standage, writing in 1887, noted that works by the old masters did not fade to the same degree that contemporary watercolours. He placed blame on both artists and manufacturers. He claimed that since old masters made their own paints and obtained pure pigments, they understood permanency. Standage blamed the rise of the colourman and the availability of premade paints. He commented on colourmen misrepresentation and using pigments which were not pure which lead to unreliable paints and a propensity towards fading (Standage, 1887). He admitted the causes of impermanence were not fully understood but strove to catalogue those pigments which were safe to use. His manual set out to provide artists with a definitive list of permanent pigments and to counter their rising ignorance of materials.

later, William J. Muckley recommended Chinese white, but cautioned against seemingly high-quality pigments 'prepared for *industrial* purposes by French makers' which were reported to be 'not only fleeting in themselves, but they damage all colours with which they come in contact' (Muckley, 1888, pp. 56-57). It is possible that the Winsor & Newton brand had not been observed to change over time, unlike French zinc oxide watercolour paints. As previously mentioned, Winsor & Newton claimed to have heated their pigments before preparing them into paints, likely creating a more stable pigment. Clearly, the physical properties of zinc oxide resulting from production and preparation methods greatly influenced their behaviour as pigments in watercolours.

3 Physical Characterisation of Zinc Oxide Powders

3.1 INDUSTRIAL METHODS OF PRODUCTION FOR ZINC OXIDE PIGMENTS

John Scott Taylor's warning about zinc oxide in 1887 suggests that some of its chemical and physical properties were known at the time (Taylor, 1887) and Muckley's warning about French-made pigments indicated that production was known to be a factor in permanence (Muckley, 1888). The two methods of producing zinc oxide for industrial purposes has changed little since the mid-nineteenth century (Kühn, 1986; Auer, Griebler and Jahn, 2005). These methods, the *indirect* or French method of production and the *direct* or American method, account for most zinc oxide produced both historically and currently[23] and produce pigments with different physical and chemical properties.

3.1.1 INDIRECT METHOD (FRENCH PROCESS) OF PRODUCTION

The first efficient production process for obtaining zinc oxide from the ore was the *indirect* method. This was discovered by chance by Stanislas Sorel who found that zinc oxide would collect on the edge of molten zinc baths during steel galvanisation, a process which he patented in 1837.[24] Sorel later partnered with the chemist E.C. Leclaire in 1840 to develop the *indirect* or French method (Remington and Francis, 1954; Downs Jr, 1976).

---

[23] For a discussion of the *wet* method, an additional production method sometimes used to produce zinc oxide powders but rarely pigments, refer to Appendix 2: Supplemental Information on Zinc Oxide Production.

[24] Although not produced commercially until the Industrial Revolution it is clear from historic records that zinc oxide was known as far back as 2000 B.C. when it was gathered from the sides of furnaces during brass production and then used as ointments (Moezzi, McDonagh and Cortie, 2012).

The *indirect* method was named for the indirect way in which the zinc oxide was obtained from the ore. The zinc metal is first melted out of the ore[25] then boiled in a large crucible. The resulting zinc vapour is then ignited and burnt in an oxygen-rich atmosphere. The zinc oxide particles are finally gathered in a series of collection hoppers which sort the product by quality and density (Fleury, 1912; Moezzi, McDonagh and Cortie, 2012). The resultant pigment consists of nodular crystals which are approximately round in shape and extremely small, ranging from 30–2000 nm (Figure 3.1) (Moezzi, McDonagh and Cortie, 2012).

SEM HV: 20.0 kV	WD: 15.09 mm		MIRA3 TESCAN
View field: 12.0 µm	SEM MAG: 33.2 kx	2 µm	
Det: SE	Date(m/d/y): 01/11/17	Northumbria University - Newcastle	
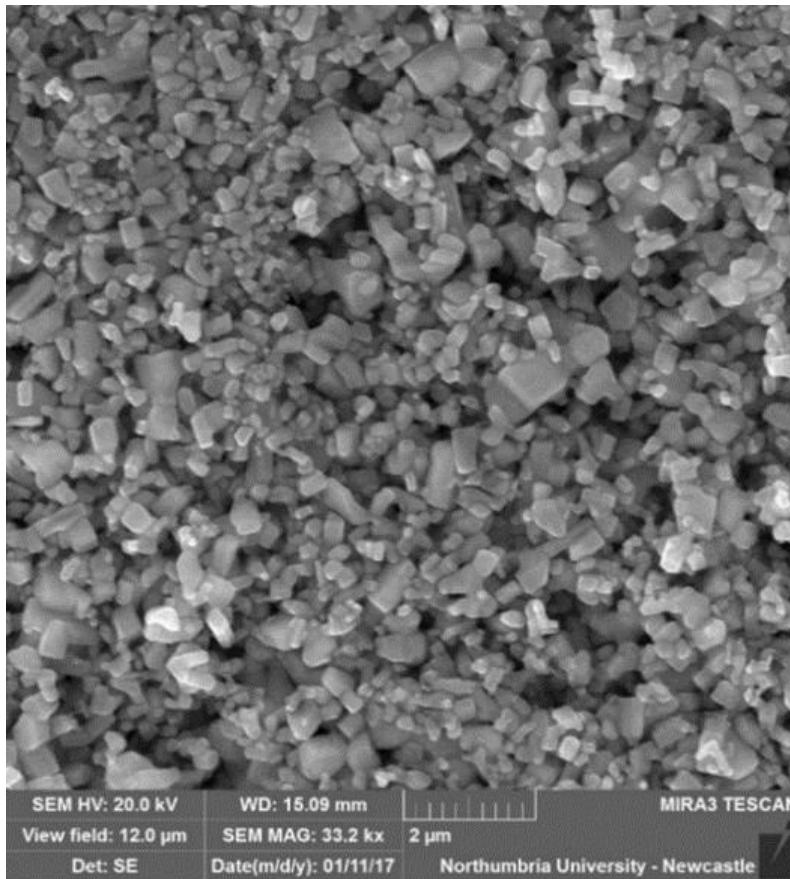
Figure 3.1 Nodular zinc oxide crystals produced by the *indirect* method. Image magnified 33,200 times and captured using a scanning electron microscope.

---

[25] Kühn (1986) reported that the *indirect* process in Europe preferred using boiled scrap metal instead of the ore as it was more readily available.

The *indirect* method is expensive but produces the purest zinc oxide of all available methods (Morgan, 1985). Impurities from the ore[26] such as cadmium, iron, lead and aluminium are removed from the zinc metal before combustion and oxidation take place. Auer, Griebler and Jahn (2005) list four purification methods: a) pouring off impurities after heating zinc metal in retorts; b) purifying the vapour using a fractional distillation process[27]; c) separating impurities in two connected chambers (the second being anoxic); and d) via a smelting process in a rotary kiln which allows for lead content, particle shape and size to be controlled by varying partial pressure and temperature of the surrounding gases.

The *indirect* method of production made zinc oxide widely available for paint manufacture and facilitated a shift in white pigment usage by a growing number of artists. Hiding power was of principle concern when producing zinc oxide crystals and the size of zinc oxide crystallites produced by the *indirect* method were maintained at an optimum value of 0.2-0.25 μm (Depew, 1941; Brown, 1957; Stephenson, 1973). Zinc oxide was still prohibitively expensive in the United States and would remain so until it could be manufactured locally. This occurred in the 1850s with the development of the *direct* method of zinc oxide production.

---

[26] The composition of the manufactured zinc oxide is a result of the composition of the ore or starting material such as scrap metal (Remington and Francis, 1954) and while the composition of modern zinc oxide can vary widely due to the variation in recycled material, historic zinc oxide was produced from ores mined geographically near a factory dedicated to its production. For a discussion of mines which supplied ores for zinc oxide production in the nineteenth century, refer to Appendix 2: Supplemental Information on Zinc Oxide Production.

[27] Refer to Kühn (1986) for description and illustration of fractional distillation process.

3.1.2 DIRECT METHOD (AMERICAN PROCESS) OF PRODUCTION

The *direct* method was named for the way the oxide was obtained directly from the ore rather than by melting out the zinc metal first[28]. The New Jersey Zinc Company developed the method in 1850 to render the expensive import of *indirect* process zinc oxide from France unnecessary. Until 1892, the *direct* method was the only process used in the USA for zinc oxide production, resulting in its name the 'American process' (Kühn, 1986).

The *direct* method was simple and efficient. Auer, Griebler and Jahn (2005) described an initial reduction at ~1000-1200 °C by burning coal and a zinc-containing material together which resulted in zinc vapour and carbon monoxide[29]. These were then oxidised to zinc oxide and carbon dioxide in an ignition chamber like those used in the *indirect* method and the resultant zinc oxide collected. The product resulting from the *direct* method was of lower quality and purity than the *indirect* method because of the poorer starter materials used (Moezzi, McDonagh and Cortie, 2012).

3.1.3 CONTROLLING PARTICLE SIZES

Particle size was controlled in both methods by varying the conditions in the oxidation and combustion chambers. Fine particle zinc oxide was obtained by creating air turbulence in a small oxidation chamber using jets, then rapidly cooling

---

[28] The *direct* process is and was more reliant on ores than the *indirect* process as outlined by Kühn (1986). For a discussion of the composition of the ores used, refer to Appendix 2: Supplemental Information on Zinc Oxide Production.

[29] In the past ores were primarily used and are still used to an extent today along with zinc concentrates, *indirect* process residues, galvanisation ash, skimmings from casting furnaces, and lower grade zinc oxides (Auer, Griebler and Jahn, 2005; Moezzi, McDonagh and Cortie, 2012). Galvanisation ash was pre-treated to remove lead and chloride by roasting at 1000 °C in rotary kilns, while sulphur-containing ores were pre-roasted to remove excess sulphur and create a purer zinc oxide (Holley, 1909).

the resulting product (Morgan, 1985). Larger particles were created by increasing the time spent at high temperatures and reducing the rate of cooling to allow more time for crystal growth. If acicular or needle-shaped particles were required, growth occurred in a very large combustion chamber containing an excess of air and little to no turbulence (Morgan, 1985). These acicular particles were typical of the *direct* method (Figure 3.2) but are not seen in the *indirect* method.
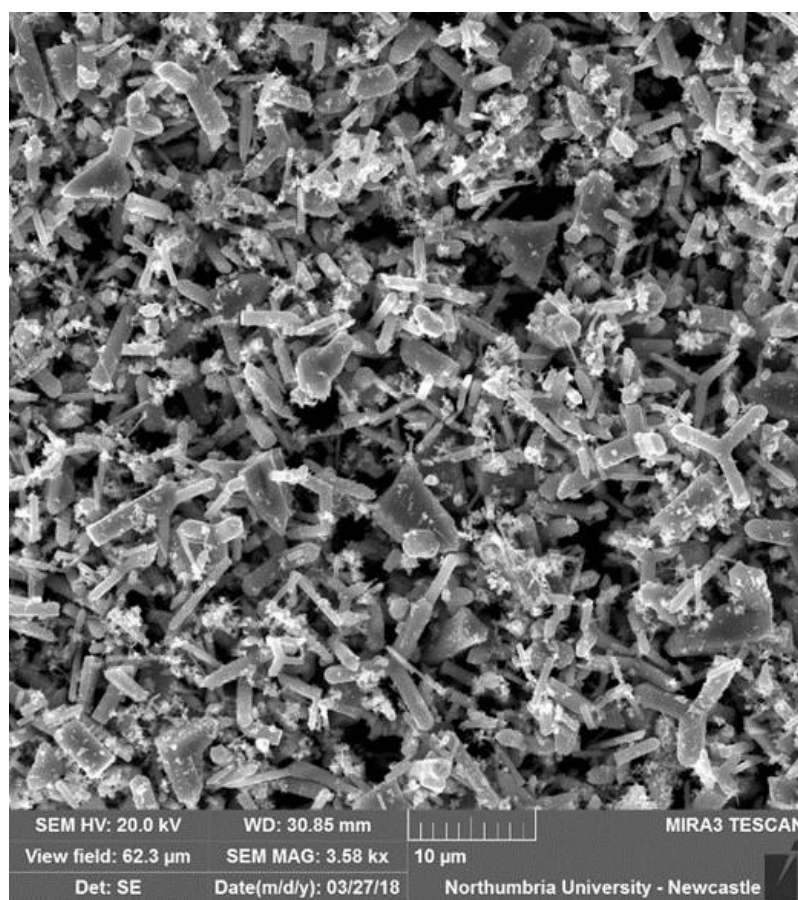
Figure 3.2 Acicular zinc oxide crystals typical of zinc oxide produced using the *direct* method. Image magnified 12,000 times and captured by thesis author using scanning electron microscopy (SEM).

3.1.4 AFTERTREATMENTS: ANNEALING

Many zinc oxides, particularly those created using the *direct* method, were roasted at high temperatures (~1000 °C) to improve their properties in paints and drive off some volatile impurities which affected the colour and chemical properties of the pigment (Auer, Griebler and Jahn, 2005). Church suggested the purest zinc oxide

was made by subjecting the whitest, densest pigment to 'powerful mechanical compression when red-hot' (Church, 1890, p. 135). Increasing pressure in this way would be an effective method of concurrently increasing temperature as atoms collide more frequently when they are compressed. Annealing reduces the number of crystal defects in the bulk of the pigment crystals but increases them significantly on the surface (Wang *et al.*, 2005; Srinivasan *et al.*, 2008). This alters the electrical and photocatalytic properties of the pigment.

The Chinese white introduced in 1834 by Winsor and Newton was heated 'to a very high temperature' which 'produced the first real alternative white with good opacity' (*Spotlight on Chinese white*, 2011). This was a significant admission by Winsor & Newton as no other colour-makers released a zinc oxide watercolour pigment in the nineteenth century. It is almost certain that the pigment sold by Winsor and Newton was created by the *indirect* or French method given its availability and better colour than the *direct* method. By annealing their product, Winsor and Newton created a more stable and uniform pigment which avoided the discolouration characteristic of untreated, impure pigments. Perhaps it was this annealing that differentiated their pigment from the French pigments Muckley warned about.

3.2 PHOTOCONDUCTIVITY AND REACTIONS OF ZINC OXIDE POWDERS

Recently, zinc oxide has been the subject of countless scientific studies as its photoconductivity makes it a promising and affordable material for solar cells (e.g. Klingshirn, 2007; Leake, 2010; Ellmer and Bikowski, 2016; Penfold *et al.*, 2018) and wastewater treatment (e.g. Pardeshi and Patil, 2008; Kumar and Rao, 2015; Singh, Saha and Pal, 2015). On the surface these studies do not seem to relate to

paper conservation; however, the electrical properties they discuss are primarily responsible for the deterioration caused by zinc oxide pigments on paper.

3.2.1 BAND STRUCTURE: ZINC OXIDE AS SEMICONDUCTOR[30]

A semiconductor is a material which is neither an insulator or a conductor[31]. Instead, electrons normally reside in a 'valence band' or energy level comprised of all valence orbitals. For a material's electrons to become free-flowing, they must be excited to a higher energy level called the 'conductance band.' Both valence and conductance bands can be explained by zinc oxide's electron configuration.

Equation 3.1 describes the electronic configuration of a neutral zinc atom:

$$Zn = [Ar]3d^{10}4s^2 \qquad (3.1)$$
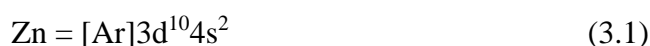
where Ar represents Argon, element 18, with an electron configuration of $1s^2 2s^2 2p^6 3s^2 3p^6$. Remove two electrons from zinc and the lowest unfilled molecular orbital, or LUMO, is the 4s orbital in Equation 3.1. This ionizes the zinc and gives it a 2+ charge. Oxygen, with a 2- charge, has an electron configuration of $1s^2 2s^2 2p^6$. The highest occupied molecular orbital, or HOMO, is the 2p orbital. The conductance band, or band in which electrons are excited and free-flowing, is formed by zinc's LUMO, while the valence
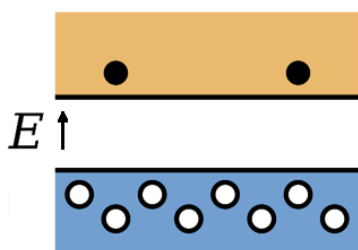
Figure 3.3 The filled valence band or HOMO (blue) and unfilled conductance band or LUMO (orange) in a material's resting state. The white area between bands represents the band gap while the *E* represents the energy required to cross the band gap. When electrons jump to the conductance band, unfilled holes are formed in the valence band.

---

[30] The following section assumes the reader possesses a basic understanding of the configuration of an atom as well as how to fill orbitals with electrons and the relationship of orbital filling to bonds.

[31] An insulator is defined as a material in which all valence electrons are tightly bound to their respective atoms while a conductor's electrons have free movement through a material.

band, or resting state of electrons, is formed by oxygen's HOMO (Klingshirn, 2007) (Figure 3.3).[32]

The energy required for a jump from the valence to conductance bands is called the band gap energy and is related to the orbital states of the ions in the crystal. Zinc oxide's band gap is reported from 3.3-3.4 electron volts (eV)[33], a rather large value for semiconductors resulting from the significant ionic portion of its bonding character.[34] Light can provide the energy required for band gap jumps. Given a band gap energy of 3.3 eV, the wavelength required for an electron to cross the band gap is 376 nm[35]. Any longer wavelengths will not be energetic enough and shorter wavelengths will exceed the energy required and cause the jump to occur.

3.2.2 REACTIONS WITH ADSORBED MATERIALS

When an electron jumps to the conductance band, it leaves behind a 'hole'[36] or positively-charged state. Holes can, along with excited electrons, react with adsorbed materials. Oxygen and water both readily adsorb onto the surface and initially react with these electrons and holes in two ways. Oxidative reactions occur when UV radiation causes adsorbed water molecules to hydrogen bond with each other, initiating dissociation of surrounding water via interaction with holes in the following oxidative reaction (Dodd *et al.*, 2006; Jacobs *et al.*, 2017):

---

[32] The information preceding this footnote is general knowledge but is well-summarised in the cited paper.

[33] Recent values have been given of 3.37 eV (Bindu and Thomas, 2014; Krithiga, Sankar and Subhashree, 2014), 3.3 eV (Penfold *et al.*, 2018), and 3.35 eV (Lyons *et al.*, 2017).

[34] The bonding character of zinc oxide lies almost midway between an ionic and covalent character (Klingshirn, 2007). The covalent character is responsible for zinc oxide's semiconductor behaviour, while the considerable ionic character means the band gap of zinc oxide is quite wide.

[35] Wavelengths of light have associated energy values in eV. For conversion equations, refer to Appendix 3: Relationship Between Energy and Wavelength of Light.

[36] While the term 'hole' may sound colloquial, it is the scientific term for positive energy wells remaining after the removal of an electron from a neutral atom or bond in a semiconductor.

$$\textbf{Oxidation Reaction: } H_2O + h^+ \rightarrow {\cdot}OH + H^+ \qquad (3.2)$$
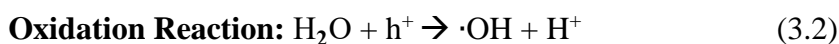
Reduction reactions occur when oxygen is chemisorbed onto the particle surface via an interaction with an electron in the conductance band, resulting in a superoxide (Dodd *et al.*, 2006; Jacobs *et al.*, 2017):

$$\textbf{Reduction reaction: } O_2 + e^- \rightarrow O_2^- \qquad (3.3)$$
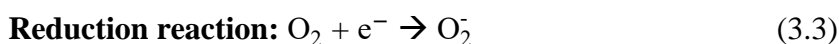
This reduction reaction leaves holes which facilitate reaction 3.2. The products of the two reactions, hydroxyl radicals (${\cdot}OH$) and superoxides (O_2^-), while highly reactive in themselves, can combine with another electron to form hydrogen peroxide (Singh, Saha and Pal, 2015):

$$O_2^- + 2H^+ + e^- \rightarrow H_2O_2 \qquad (3.4)$$

Hydrogen peroxide can then react with a proton and an electron to form a hydroxyl radical and a water in the following reaction (Singh, Saha and Pal, 2015):

$$H_2O_2 + H^+ + e^- \rightarrow {\cdot}OH + H_2O \qquad (3.5)$$
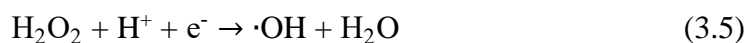
Most of the previous reactions required free electrons to convert water and oxygen into reactive products, while reaction 3.2 required a positive hole. There are three main factors influencing conductivity and electron concentration in the conductance band, namely crystal defects, elemental impurities, and particle size.

3.3 PHYSICAL CHARACTERISTICS INFLUENCING CONDUCTIVITY

3.3.1 CRYSTAL DEFECTS

Crystals are organised in repeated units called cells.[37] Figure 3.4 shows a typical unit cell for zinc oxide. In a perfect crystal, the unit cell is tessellated, no atoms would be missing, there would be no additional elements and the crystal would maintain a neutral charge.
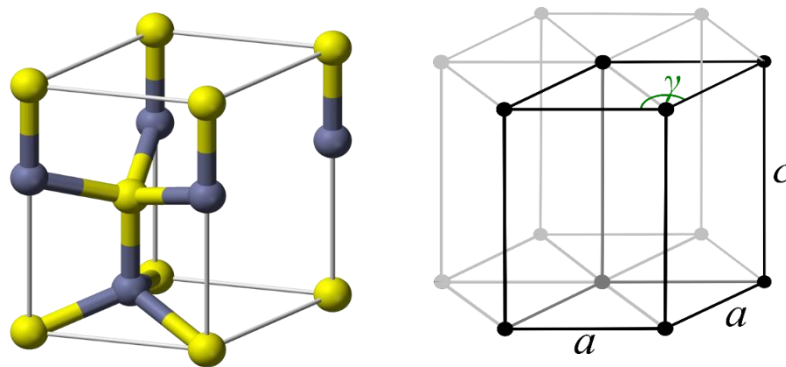
Figure 3.4 Left: Zinc oxide's hexagonal wurtzite structure. The yellow balls represent oxygen while the grey balls represent zinc. The unit is a rhombic prism. **Right:** Hexagonal structure defined as three unit cells clustered together. Cell parameters *a* and *c* are shown as well as the angle γ between the *a* parameters, equalling 120°.

No crystal structure is perfect, however, and all contain defects which interrupt neutrality and can introduce electrons and holes. When a defect or impurity is introduced which increases the electron concentration near the conductance band, it is known as a shallow donor. A defect or impurity which introduces a hole in the valence band which increases conductivity is called a shallow acceptor. A deep defect is one which lies in the band gap far from either conductance or valence bands.[38] These deep defects are often called 'trap states' and introduce new energy

---

[37] Unit cells are measured along the three parameters *a, b,* and *c*. Zinc oxide is classified as a hexagonal wurtzite-type crystal, meaning that cell parameters *a* and *b* are of equal length and therefore can both be represented by *a*, while the *c* parameter differs in length and is orthogonal to *a*.

[38] It can be assigned as a 'donor' or 'acceptor' even in a deep state depending on in which half of the band gap it resides.

levels into which electrons and holes can fall (Bonosewicz, Hirschwald and Neumann, 1986; Penfold *et al.*, 2018).

Zinc oxide is an *n-type* semiconductor. [39] However, the cause of this *n-type* conductivity remains controversial (e.g. González, 2012) as it cannot be directly tied to impurities or defects.

'Native point defects' are crystal defects due to changes in the elements already present in a perfect crystal. The three main native point defects in zinc oxide are:

- **Ion vacancies:** the absence of an ion in a space normally occupied by one

- **Ion interstitials:** ions in spaces not usually occupied in the lattice, called interstitial sites

- **Ion antisites:** an ion residing in a position normally occupied by another ion.

Three native point defects are thought to be the greatest contributors to zinc oxide's electronic properties: oxygen vacancies, zinc interstitials and zinc vacancies.

---

[39] As opposed to a *p-type* semiconductor, which is always positively charged.

(0001) (polar Zn plane)

c

a_3

a_2

a_1 (000$\bar{1}$) (polar O plane)
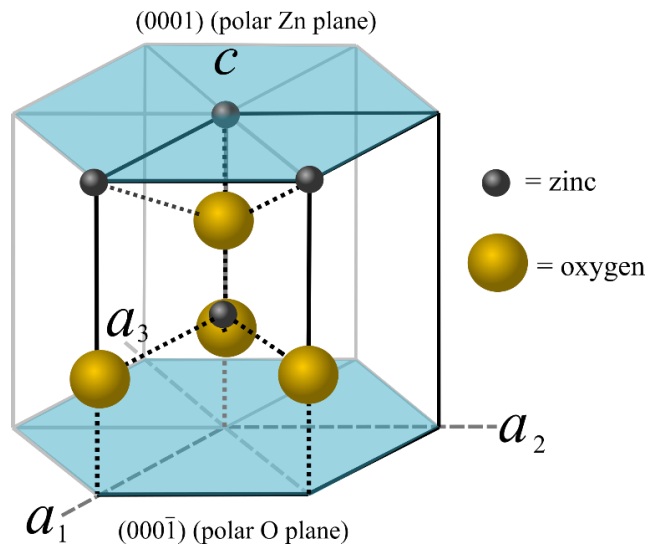
● = zinc

● = oxygen

Fig 3.5 Polar planes of ZnO crystals and relationship to crystal lattice and unit cell (shown as black outline)

Oxygen vacancies: In photocatalytic experiments, the (0001) polar face[40] of zinc oxide is found to be the most active in hydrogen peroxide production (Kumar and Rao, 2015) (Figure 3.5). Additionally, oxygen evaporates from the (0001)[41] polar zinc surface at elevated temperatures and in an oxygen-deficient atmosphere, creating oxygen vacancies and mirroring conditions present during *direct* method zinc oxide production (McVicker, Rapp and Hirth, 1975; Sengupta *et al.*, 1987). The formation energy for oxygen vacancies may be too high for the defect to account for zinc oxide's *n-type* conductivity (Janotti and Van De Walle, 2007; Ellmer and Bikowski, 2016) but may instead interact with another defect to produce this conductivity.

When analysing the photocatalytic properties of native point defects, Zhu *et al.* found that fewer native point defects, particularly oxygen vacancies, meant that excited electrons in the conductance band were freer to take part "in possible photocatalytic reactions rather than to recombine at the shallow energy levels of

---

[40] Notations such as (0001) and (000$\bar{1}$) are in Bravais-Miller notation and are ways of indicating where a plane crosses the crystal lattice in a hexagonal crystal habit. The first 3 numbers are referred to by the letters *h, k* and *i* and are the reciprocals of the a_1, a_2 and a_3 intercepts. The fourth number is referred to by the letter *l* and indicates the *c* intercept. Lines above numbers indicate that those numbers are negative. Miller notation is similar but excludes the third redundant term. For a more in-depth discussion of the indexing systems as applied to zinc oxide crystals, refer to Appendix 4: Miller Indexing and Miller-Bravais Indexing.

[41] The greater distance between the remaining three oxygens and the (000$\bar{1}$) face is known as the internal *u* parameter.

planar defects" (Zhu *et al.*, 2014, p. 1) referring to the longer length of time required for electrons to fall to the valence band than to fall to a trap state.

Zinc interstitials: Surface oxygen vacancies caused by removal of oxygen ions also cause interstitial zinc defects to form in the bulk material. With the removal of a negative oxygen ion near the (0001) plane, surrounding zinc ions are repelled from one another and move further into the crystal to rest in more energetically-neutral interstitial locations (Weidenkaff *et al.*, 1999), to the second nearest neighbour positions (Ellmer and Bikowski, 2016). These interstitial zinc ions carry lone electron pairs in the conductance band and when hybridized with oxygen vacancies, may contribute to zinc oxide's negative charge (Bandopadhyay and Mitra, 2015). The energy required for the formation of zinc interstitials is low, as is the migration energy, and zinc vacancies form in abundance as a result (Zhang, Wei and Zunger, 2001).

While some researchers feel that zinc interstitials are responsible for zinc oxide's *n-type* conductivity (Zhang, Wei and Zunger, 2001; Ellmer and Bikowski, 2016), others argue that the defects diffuse too quickly and have high formation energy under *n-type* conditions, eliminating them as the potential source (Janotti and Van De Walle, 2007). Controversy over this topic is ongoing and arises from the difficulty in experimentally linking defects and conductivity. [42]

Zinc vacancies: The vacancies left by zinc ions which have migrated to other positions or been removed from the crystal lattice are known to act as compensating

---

[42] Mathematical models can provide links between defects and possible shifts in conductivity using Density Field Theory and Local Density Approximations. However, these defect density approximations are prone to error. These calculations are beyond the scope of this thesis and involve mathematics not known to most members of the conservation field. They deal with electronic densities and can be found at this web address
http://www.tcm.phy.cam.ac.uk/castep/CASTEP_talks_06/montanari1.pdf

defects, meaning that they positively shift the overall charge of the naturally negative crystal. (Janotti and Van De Walle, 2007; Lyons *et al.*, 2017). Most meaningfully, they compensate for electron concentration, meaning they remove free electrons from the conductance band and prevent photocatalytic activity by providing recombination sites for excited electrons (Ellmer and Bikowski, 2016).

3.3.2 ELEMENTAL IMPURITIES AND CONDUCTIVITY

Elemental impurities are always present in zinc oxide and can act as donors or acceptors. Extremely small numbers of impurities and defects (0.01 ppm) can affect a semiconductor's conductivity (Janotti and Van de Walle, 2009). A strong case is made for hydrogen as a significant contributor to *n-type* conductivity. Hydrogen impurities act as a shallow donor, contributing electrons near the conductance band (Janotti and Van de Walle, 2009; Ellmer and Bikowski, 2016). The formation energy for these hydrogen defects is very low, meaning they are likely always present in zinc oxides and may be responsible for the overall negative charge of the crystal (Brown, 1957; Van De Walle, 2000; Janotti and Van de Walle, 2009). In oxygen-poor atmospheres, their incorporation interstitially and at the site left by oxygen vacancies would explain the *n-type* conductivity particularly since oxygen vacancies would not be abundant given their high formation energy requirements (Oba *et al.,* 2008).

Other impurities such as trivalent elements can substitute for zinc ions and increase electron concentration in the conductance band. Group 13 elements aluminium and gallium have been identified as particularly efficient donors at room temperature when replacing zinc ions (Klingshirn, 2007; Steiauf *et al.*, 2014) while indium, boron and thallium can also substitute for zinc (Moezzi, McDonagh and Cortie,

2012; Ellmer and Bikowski, 2016). Though anion substitution or 'doping'[43] is not as well-studied as cation doping, they can also act as donors with halogens substituting for oxygen and providing an extra electron. The energy required for fluorine substitution is low and theoretically substitutes readily for oxygen ions (Zhang, Wei and Zunger, 2001; Janotti and Van de Walle, 2009).

In the same way that trivalent elements can substitute for zinc to increase electron concentration in the conductance band, monovalent elements can substitute for zinc while elements from Group 15, particularly nitrogen can substitute for oxygen. Both create holes and increase conductivity while positively shifting the overall charge (Park, Zhang and Wei, 2002; Meyer *et al.*, 2005; Klingshirn, 2007). Group 1 elements, which are often proposed as acceptors in zinc locations, tend not to ionize at room temperature, largely maintaining neutrality (Klingshirn, 2007). However, conductivity was increased significantly with the introduction of lithium, which acts as a shallow acceptor, although the overall charge still remained negative (Klingshirn, 2007; Moezzi, McDonagh and Cortie, 2012). Interestingly, while monovalent lithium acts as an acceptor when replacing divalent zinc, it is a donor when present interstitially, as its valence electron increases electron concentration in the conductance band by virtue of being unbound (Klingshirn, 2007; Janotti and Van de Walle, 2009). A high lithium concentration also increases the rate of oxygen loss at both polar surfaces (McVicker, Rapp and Hirth, 1975). Figure 3.6 illustrates the energy levels of several discussed crystal defects and impurities.

---

[43] Doping refers to an intentional introduction of impurities or crystal defects to shift a crystal's conductivity.
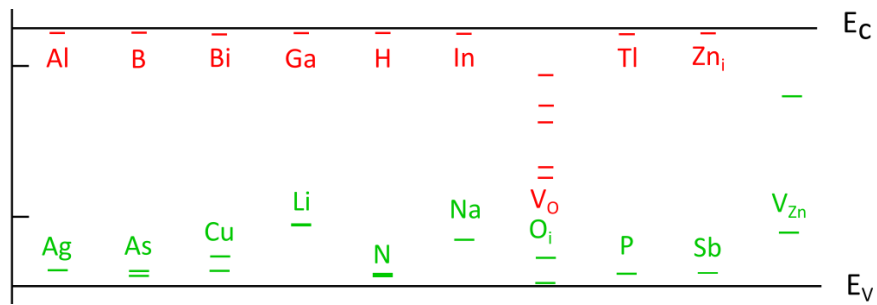
Figure 3.6 Energy levels of acceptors (green) and donors (red) compared with the conductance (E_c) and valence (E_V) band energies (eV). Image modified from Ellmer and Bikowski, 2016.

3.3.3 PARTICLE SIZE AND MORPHOLOGY

The percentage of surface area taken up by more electronically active crystal surfaces strongly influences the rate of reactions. Wahl *et al.* (2013) found that many zinc ions on the (0001) polar surface are ionized to 3+, while oxygen ions on the $(000\bar{1})$ surface ionize to -3. This means that electrons normally occupying the valence shells on the (0001) surface are pushed to the conductance band, while the valence band on the $(000\bar{1})$ surface is unfilled, creating holes. This causes both polar surfaces to contribute heavily to photocatalytic reactions described in Equations 3.2-3.5.

More reactive polar surfaces indicate that a shorter length-to-width ratio should translate to a more photocatalytic pigment. This is because with less length, a greater percentage of total surface area will be accounted for by the polar faces.
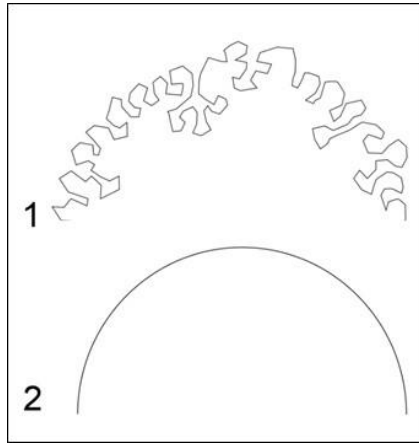
Figure 3.7 1) profile of a rough surface area vs. 2) profile of a smooth surface area. When projected into two dimensions, the disparity between the lengths of the profile lines illustrates the increase in surface area which results from a rougher surface.

Smaller particles also have a larger surface-area-to-volume (SAV) ratio; however, very small particles may pack closely together, reducing overall exposed surface area by creating large agglomerate particles. Most pigment particles are in fact comprised of multiple crystallites either grown together or packed together in an agglomerate or ball. A smooth ball will have a smaller surface area than a rough or porous one (Figure 3.7).

Both the crystallite morphology and the particle size influence the working and ageing properties of pigments by changing the texture and overall available surface area of the pigment.

3.4 ANALYTICAL METHODOLOGY

Crystal structure, composition and particle size and morphology were characterised for *indirect* and *direct* zinc oxide powders as well as for pigments sold by pigment manufacturers. They were as follows:

- *Indirect* **method powders:** P1, P3, P4

- *Direct* **method powders:** P6, P7, P9

- **Commercial pigments:** P14, P15, P16

Select case studies were also examined when possible to link findings with historic examples.

3.4.1 CRYSTAL STRUCTURE ANALYSIS VIA X-RAY DIFFRACTION (XRD)

Powder samples[44] were analysed using x-ray diffraction to determine lattice strain, a property resulting from lattice defects. The samples were studied using a Siemens Kristalloflex Diffraktometer D5000 at 40 kV and 40 mA from 20-80 degrees. The source beam was emitted through a 2 mm slit, while the detector was fitted with a 1 mm slit, followed by a 0.2 mm slit. X-rays were sourced by a CuKα source at 0.15406 nm and peaks from the source were filtered with a nickel filter then stripped in the program Eva. Diffractograms were collected at 0.02° steps with a collection time of 1 second per step. After data collection, diffractograms were saved as raw files then converted to UXD files for processing and graphing.

Characterising peaks: Prior to data processing, no instrumental line broadening correction was applied[45] as all data was analysed for comparison within the data set and is therefore qualitative, not quantitative. Broadening of peaks is due to both crystallite size and internal strain. Both were accounted for in the methodology.

Full-width at half-maximum (FWHM) values were obtained using the MATLAB workflow described in Appendix 5: Diffractogram Processing Methodology in MATLAB.

Calculating lattice parameters: Lattice parameters *a* and *c* were calculated using the following equations (Bindu & Thomas, 2014):

---

[44] X-ray diffraction required either a large powder sample of around 1 gram or a small painted area on paper mounted with adhesive. Samples could not be obtained from the watercolour paintings, so case study pigments were not analysed in this way.

[45] Both time and material restraints made instrumental line broadening correction impossible. To do so, a substance with a known crystallinity would have to be run, then corrections applied to the data sets. Given the excellent crystallinity of the powder samples as evidenced by the high, narrow peaks, correcting for instrumental line broadening was deemed unnecessary.

$$a = \frac{n_a \lambda}{\sqrt{3}\, sin\theta} \tag{3.6}$$

$$c = \frac{n_c \lambda}{sin\theta} \tag{3.7}$$

where λ is the incident wavelength (0.15406 nm for CuKα x-ray source) and θ the location of the peak in degrees. Both n_a and n_c values were calculated for all samples using Bragg's law (Equation 3.8). θ angle values and d lattice spacing values were provided by the (10$\bar{1}$0) peak for the a parameter and by the (0002) peak for the c parameter:

$$n = \frac{2d sin\theta}{\lambda} \tag{3.8}$$

Calculating crystallite sizes[46] from Scherrer plots: The Scherrer equation estimates crystallite values based on one diffraction peak and is stated as follows:

$$D = \frac{K\lambda}{\beta cos\theta} \tag{3.9}$$

where D = crystal size (nm), K is a constant (0.94 was used), λ is the incident wavelength (0.15406 nm for CuKα x-ray source), β is the FWHM of a peak in radians, and θ is the angle in radians of the incident beam. To obtain one crystallite size value from all peaks, the equation was rearranged and a size value obtained from the slope of a fitted line (Khorsand Zak, Abd. Majid, *et al.*, 2011):

$$cos\theta = \frac{K\lambda}{D}\left(\frac{1}{\beta}\right) \tag{3.10}$$

---

[46] Crystallite size values calculated from this equation are assumed to be the cube root of the volume of a crystal, assuming all crystallites have the same size and shape. This was assumed to represent a mean value (Speakman, n.d.).

Using this equation, $\frac{1}{\beta}$ values are plotted as x values and $cos\theta$ values as y values[47].

The slope of the line gives $\frac{K\lambda}{D}$, which can then allow for D to be solved. These

Scherrer plots were created for all XRD powder samples.

Calculating Zn-O bond lengths: The bond length L between adjacent Zn and O

ions was calculated for each sample by inputting parameters a and c into Equation

3.11:

$$L = \sqrt{\left(\frac{a^2}{3} + \left(\frac{1}{2} - u\right)^2 c^2\right)} \tag{3.11}$$

The internal parameter u^{48} was calculated with Equation 3.12 (Bindu & Thomas,

2014):

$$u = \frac{a^2}{3c^2} + 0.25 \tag{3.12}$$

Calculate Crystallite Size and Strain from Williamson-Hall Uniform

Deformation Model (UDM): Assuming that strain is uniform in all directions

(isotropic), the Williamson-Hall UDM equation can be used to derive crystallite size

and strain via a fitted plot. This equation can be expressed as (Bindu & Thomas,

2014):

$$\beta_{hkl}cos\theta_{hkl} = \varepsilon 4sin\theta_{hkl} + \frac{K\lambda}{D} \tag{3.13}$$

Where β_{hkl} is the FWHM of a peak associated with direction hkl whilst $cos\theta_{hkl}$ and

$sin\theta_{hkl}$ are the cosine and sine of the angle of the incident beam. Using the standard

$y = mx + b$ equation as a template, where m is the slope and b the y-intercept of a

---

[47] This is based on the standard formula for a plotted straight line, $y = mx + b$. The y-intercept b was not taken into account using this method.

[48] u is defined as an internal parameter for wurtzite structure crystals which measures 'the amount by which each atom is displaced with respect to the next along the 'c' axis' (Bindu & Thomas, 2014).

graph, $\beta_{hkl}cos\theta_{hkl}$ values are plotted as y values and $4sin\theta_{hkl}$ are plotted as x values for the first 6 peaks. A line is fitted to this. The slope value of the line gives the micro-strain ε and the y-intercept gives $\frac{K\lambda}{D}$ from which D can be calculated since K and λ are constants. While D was previously calculated using the Scherrer plots, the UDM plot can give a slightly different D value. It is understood that the Williamson-Hall method is not necessarily reliable for absolute values due to the number of assumptions it relies upon. It is however useful for comparing similar materials as it highlights relative differences between them in strain and size values (Barnes, Jaques and Vickers, 2006).

3.4.2 ELEMENTAL IMPURITIES ANALYSIS VIA X-RAY FLUORESCENCE (XRF) AND ENERGY-DISPERSIVE X-RAY (EDX) SPECTROSCOPY

All mock-up samples were characterised using a Spectro X-Lab 2000 X-Ray Fluorescence (XRF) spectrometer in geo-powder cuvette mode[49]. The XRF data was acquired using the program SPECTRO X-LAB and results were reported in parts-per-million, which were then converted to percentages. Correction factors were applied to raw data values to obtain more accurate ppm values[50]. XRF detected elements present in amounts undetectable by EDX and so was useful in determining the presence of trace elements in the powders.

All five case studies were characterised using EDX spectroscopy rather than XRF as the latter required a large sample size (~1-2 g of material). Most samples for EDX were coated in 5 nm of platinum prior to analysis to increase conductivity and

---

[49] Refer to Appendix 6: Sample Masses for XRF Analysis for a table of the powder masses measured in cuvettes using XRF spectroscopy.

[50] Refer to Appendix 7: XRF Correction Factors for a list of correction factors applied to XRF data.

produce clearer SEM images. This platinum peak did not obscure elements expected in pigments[51]. The instrument used was the Oxford Instruments X-Max 150 EDX detector mounted on a TESCAN MIRA3 SEM using 10 kV. SEM secondary electron detector was used to acquire image and select locations of EDX scans.

3.4.3 PARTICLE SIZE ANALYSIS VIA DIGITAL IMAGE PROCESSING

Particle sizes as a function of clumping behaviour was measured using an image processing method in ImageJ[52] and size was defined as the cube root of a particle's volume. A digital image analysis method was chosen as it is a well-established method and did not require specialist equipment (Mora, Kwan and Chan, 1998; Kwan, Mora and Chan, 1999; Li, Wilkinson and Patchigolla, 2005). This method tends to give the largest estimation of size when compared to other methods (Li *et al.,* 2005); however, values obtained were not be treated as absolute size values but used for comparison with other samples processed in the same way and with other variables such as UV fluorescence and ageing characteristics.

Pigments were mounted on glass slides in Meltmount™ (refractive index 1.662) on which a cover slip was placed. They were imaged at 200x magnification using a microscope-mounted Olympus DP70 camera with CCD chip in dark field mode to provide greatest contrast between particles and background and avoid distortions introduced at higher magnifications. Image size was set to 4080x3072 pixels to

---

[51] Other elements sharing its peak energy were gold and zirconium. Sodium shared a peak energy with zinc and was not accounted for as it was often overlapped by the zinc peak. Pigments containing sodium were identified by other elements present (such as ultramarine, which contains sodium but also aluminium, silicon and sulphur.

[52] Also called Fiji. This is a free program written in Java for image analysis and developed by a team led by Wayne Rasband at the National Institute of Health in the United States. It is particularly useful for particle size analysis and fluorescence analysis.

minimise spatial coverage per pixel. Using such a high-resolution image should also reduce the error percentage of analysed particles[53].

A reference image was taken with a scale bar in the lower right corner. This was measured in Gimp to obtain a pixel/µm conversion factor. All images of pigment particles were saved as tiffs and did not contain scale bars as this would have affected processing.

Images were imported into ImageJ and the following steps carried out to obtain image size data:[54]

- Set scale – pixels were assigned values based on measurement of scale bar (pixels per µm.)

- RGB to Luminance and Duplicate – the image was converted to luminance (intensity values only), then duplicated.

- Manual Background Subtraction: Gaussian Blur and Image Subtraction – With the duplicate image selected, a Gaussian blur was applied with a Sigma value of 2,000,000 to produce a uniform grey image in which all pixel intensity values were greater than the background but less than the particles. The blurred image was subtracted from the original luminance image leaving only particles with non-zero intensity values.

- Auto Brightness/Contrast and Threshold – In the Image → Auto brightness/contrast was applied, then auto threshold.

---

[53] For example, particles consisting of 20 pixels when imaged and analysed have a 5% error associated with each pixel, while a particle consisting of two pixels has a 50% error associated with each pixel.

[54] For a more in-depth discussion of each step and the theory behind them, refer to Appendix 8: Particle and Crystallite Analysis: Procedure, Code and Graphs.

- Watershed –A Watershed algorithm was sometimes utilised to break up slightly overlapping adjacent particles. Images were chosen where overlap between particles was minimal and images with watershed applied were compared with the original to ensure accuracy.

- Analyse Particles – The Analyse Particles function obtained projected area values of particles in the final processed image. A lower limit of 0.1 μm^2 was applied as this was the calculated area of a particle containing 10 pixels. Restricting the range in this way reduced the error of the estimation to less than 10% per pixel (Mora et al., 1998). An outline map of particles was selected as the output format along with a spreadsheet of particle areas associated to each particle in the map. Both images and the spreadsheet were saved and the entire process repeated for each image (Figure 3.8).
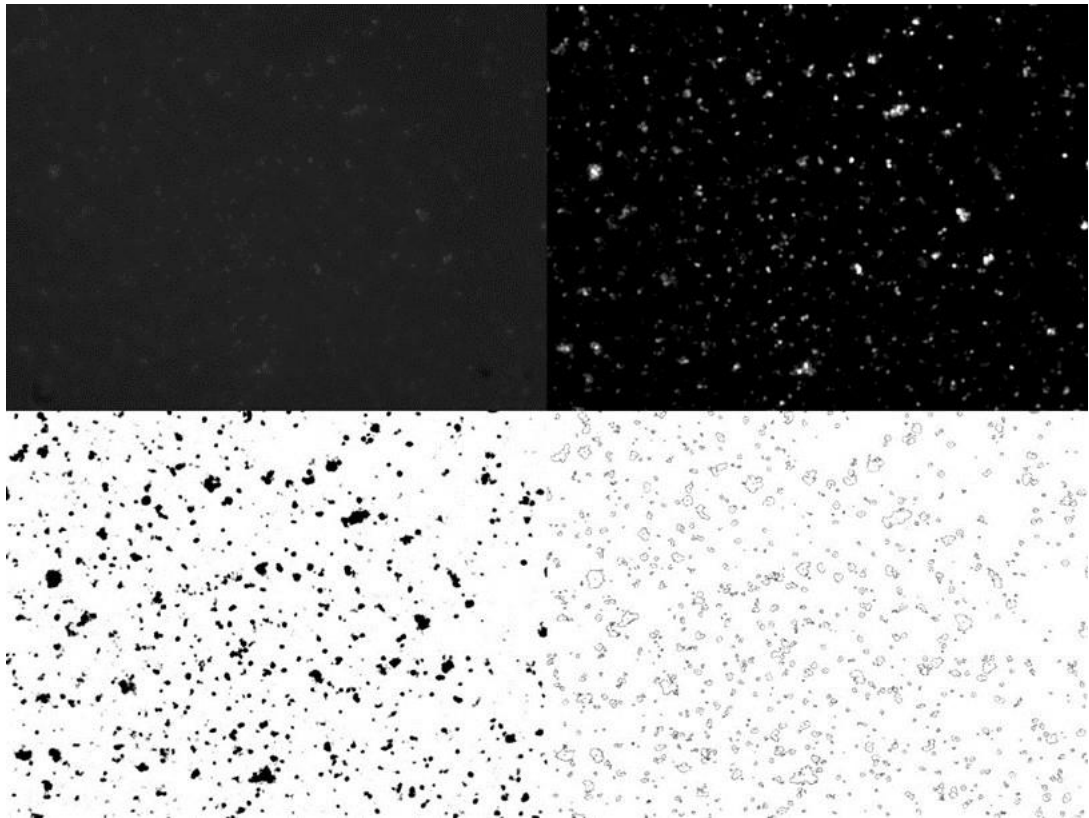
Figure 3.8 Particle analysis image processing procedure. Images magnified 200x. **Upper left:** luminance image of pigment particles. **Upper right:** image of particles after background subtraction and auto brightness/contrast. **Lower left:** threshold image. **Lower right:** outlines of particles over 10 pixels in area.

5,000 particles were analysed for each pigment. Area values were reported as the projected area of a sphere given the approximately spherical nature of pigment clumps. Values for diameter and size were derived assuming a spherical geometry.

Processing Data in MATLAB: Particle sizes (size vs count) excluding the smallest and largest 10% of values[55] were binned in MATLAB[56] then graphed in Microsoft Excel to create a histogram of counts per size range. Additionally, Excel was used to

---

[55] Excluding the lowest 10% of values and highest 10% of values eliminates most outliers and gives a better distribution of particle sizes (Horiba, 2014, p. 11).

[56] Binning is the process of setting parameters for bars in a histogram. In this case, it gives the minimum and maximum values for sizes represented. For MATLAB code, refer to Appendix 8: Particle and Crystallite Analysis: Procedure, Code and Graphs.

obtain values for average size, SAV ratio, median size, mean diameter and median diameter from the 80% of projected particle area values.

3.4.4 MORPHOLOGICAL AND CRYSTALLITE SIZE ANALYSIS VIA SCANNING ELECTRON MICROSCOPY (SEM)

Morphologies and sizes of individual crystallites for all mock-ups and select case studies[57] were examined and measured using a TESCAN MIRA3 scanning electron microscope[58] which allowed for very high magnification up to 50,000x and gave clear images of the crystallites. These were exported as tiff files to avoid compression of image data. Four morphological characteristics were catalogued: pyramids, overall rod-like shape, nodular or round crystallites and acicular or long needle-like crystallites. Crystallites were then measured using the following procedure.

The images were opened in ImageJ and assigned a scale value using the same methodology as used with the agglomerate images. 100 crystallites were measured by hand as they were largely overlapping and could not be differentiated by tone. Lines representing length and diameter were drawn over crystallites using the line tool (Figure 3.9) then measured[59]. The method parallels the techniques used by Li and Haneda (2003) who measured 200 crystallites in this way. These values were imported into MATLAB for binning then graphed in Excel.[60] Unlike spherical

---

[57] Some case study samples did not image well in SEM. This was due to the pigments being mixed or, more often, to the binding medium obscuring the shape of the particles. The case studies examined for morphological characteristics were sample RD1, TH3, and SSB-J.

[58] Microscope ran using the program MiraTC x64.

[59] The draw function was applied with the shortcut keys Ctrl+d, while measurements were taken using Ctrl + m. The measurement function used the pixel-to-μm conversion set by the user in the Set Scale function to measure the drawn line.

[60] For the code and MATLAB data processing procedure, refer to Appendix 8, section A8.2 Crystallite Size Analysis.

agglomerates, crystallites were analysed as cylinders due to the wurtzite crystal habit approximating a hexagonal prism.
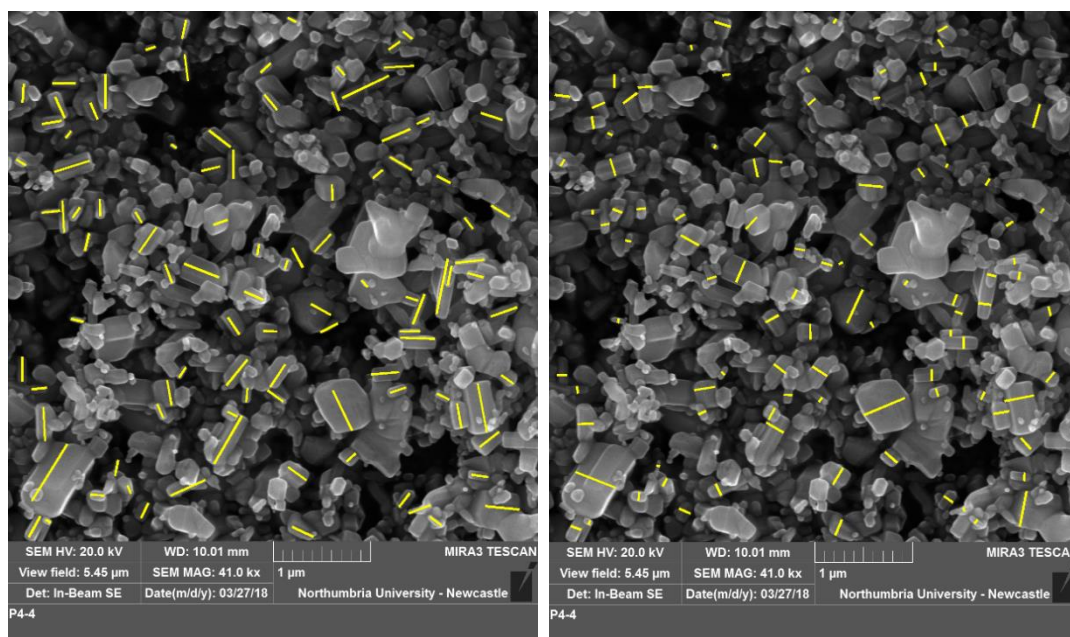
Figure 3.9 Left: length measurements. **Right:** diameter measurements of sample 4 crystallites using SEM.

3.5 RESULTS

3.5.1 XRD RESULTS

All powder samples except those supplied by Brüggemann (samples 4 and 9) yielded diffractograms with comparable data and peak intensities. It is likely the slits in the instrument were changed before samples 4 and 9 could be analysed. XRD data from these two samples were therefore not included.

Peak shapes and intensities: Diffractogram peaks were narrow overall, indicating that the pigment crystals are highly organised and lacking in excessive defects (Figure 3.10). Sample 14, the contemporary Winsor and Newton pigment, had the lowest intensity peaks of all samples for every peak despite the same instrument parameters.
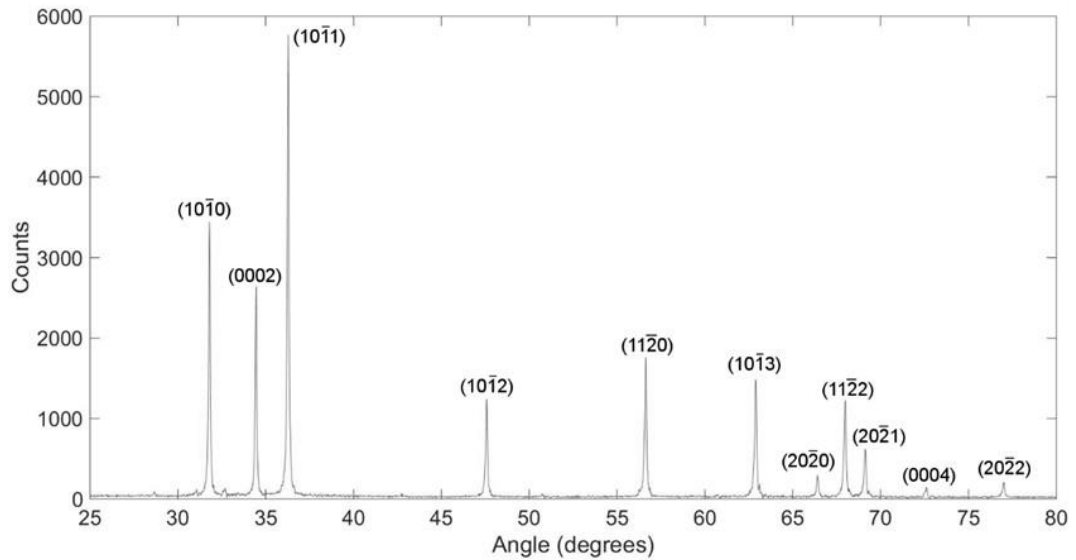
Figure 3.10 Typical diffractogram for zinc oxide powder samples. Peaks are labelled with associated planes using Miller-Bravais indices

The most intense peak for all samples measured was the $(10\bar{1}1)$ peak. The plane indicated by this peak passes through the crystal diagonally from the front plane through the *c* axis and through two cell units (Figure 3.11, top). The *direct* method samples 6 and 7 returned the strongest $(10\bar{1}1)$ peak while the *indirect* and commercial pigment samples 3, 15, 16, 1 followed in decreasing intensity. This same pattern repeats in the $(10\bar{1}0)$ peaks (Figure 3.11, middle). A greater intensity in these peaks could indicate a longer crystal in the *c* direction which would be consistent with the acicular crystal shape of *direct* method zinc oxide powders.

The peak intensities were more consistent along the (0002) plane with 7, 3, 6, and 15 giving the greatest return (in decreasing order) followed by 16 and 1 (Figure 3.11, bottom). The similarities among samples could indicate that there is not much variation in the width of crystals perpendicular to the *c* axis.
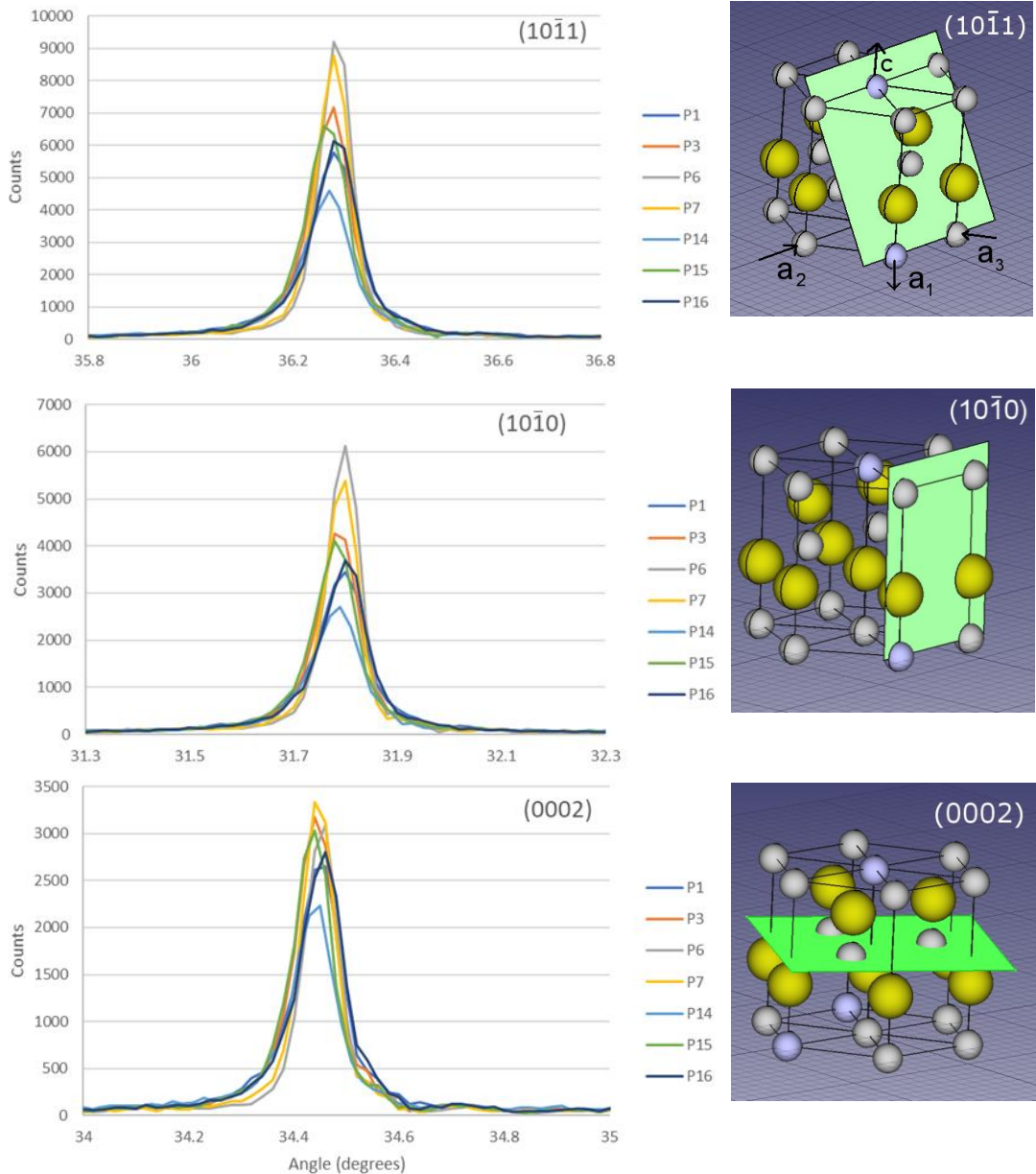
Figure 3.11 diffractogram peaks and 3D models of **top:** (10$\bar{1}$1) plane **middle:** (10$\bar{1}$0) plane **bottom:** (0002) plane

Lattice Parameters: Lattice parameters were calculated using Equations 3.10, 3.11 and 3.12 and agreed with values reported in the literature (Clementi *et al*., 2012; Landolt & Börnstein, 1999). The differences between them is negligible, however, and only discernible when comparing thousandths of an angstrom (Table 3.1). These values and other values derived from diffractogram peaks are qualitative and only meant for comparison within the data set.

Table 3.1 Lattice parameters (Å) for powder samples calculated from diffractogram data

Sample	*a*	*c*	*c/a*	*u*
1	3.2487	5.2025	1.6014	0.3800
3	3.2477	5.2040	1.6024	0.3798
6	3.2477	5.2011	1.6015	0.3800
7	3.2467	5.2025	1.6024	0.3798
14	3.2477	5.2025	1.6019	0.3799
15	3.2487	5.2040	1.6019	0.3799
16	3.2467	5.2011	1.6020	0.3799

Crystallite Size from Scherrer Equation and Williamson-Hall Plots: Crystal sizes returned from the Scherrer plots were very low, from ~40-60 nm, while sizes returned from the Williamson-Hall plots were slightly larger at ~60-80 nm (Table 3.2).

Table 3.2 Crystallite size values derived from Scherrer and Williamson-Hall plots

Sample	Scherrer size (nm)	WH UDM size (nm)
P1	39	60
P3	41	69
P6	44	82
P7	39	77
P14	58	60
P15	39	66
P16	47	66

Scherrer plots for *direct* method pigments were shifted to higher x values as the diffractogram peaks were narrower (Figure 3.12). Given that line broadening as measured using Scherrer methods only account for size differences, this indicates that *direct* method pigments are larger than the *indirect* pigments. *Indirect* method powders P1 and P3 and commercial pigments P14, P15 and P16 had similar distributions of FWHM values, indicating the crystal sizes are similar.
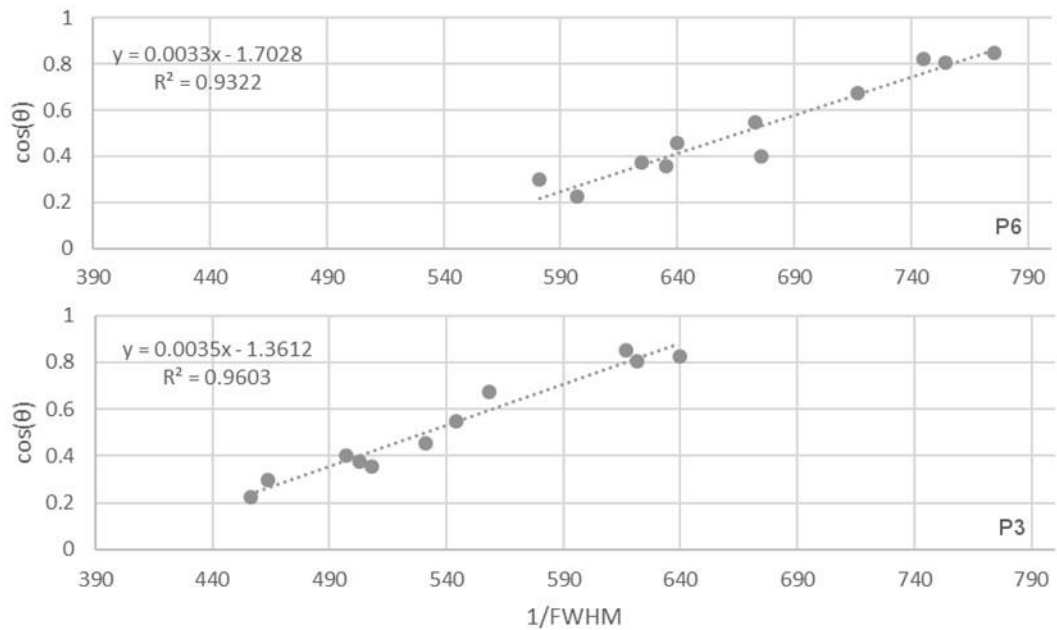
Figure 3.12 Scherrer plots of **above:** *direct* method sample P6 and **below:** *indirect* method sample P3.

Strain estimates from Williamson-Hall plots were identical, indicating that they may not be different enough to measure using the instrument and processing methods employed in this work. Lower intercept values for *direct* method pigments indicated that these were larger than the *indirect* method or commercial pigment samples due to the FWHM values acting as a scaling factor for the y-axis (Figure 3.13).
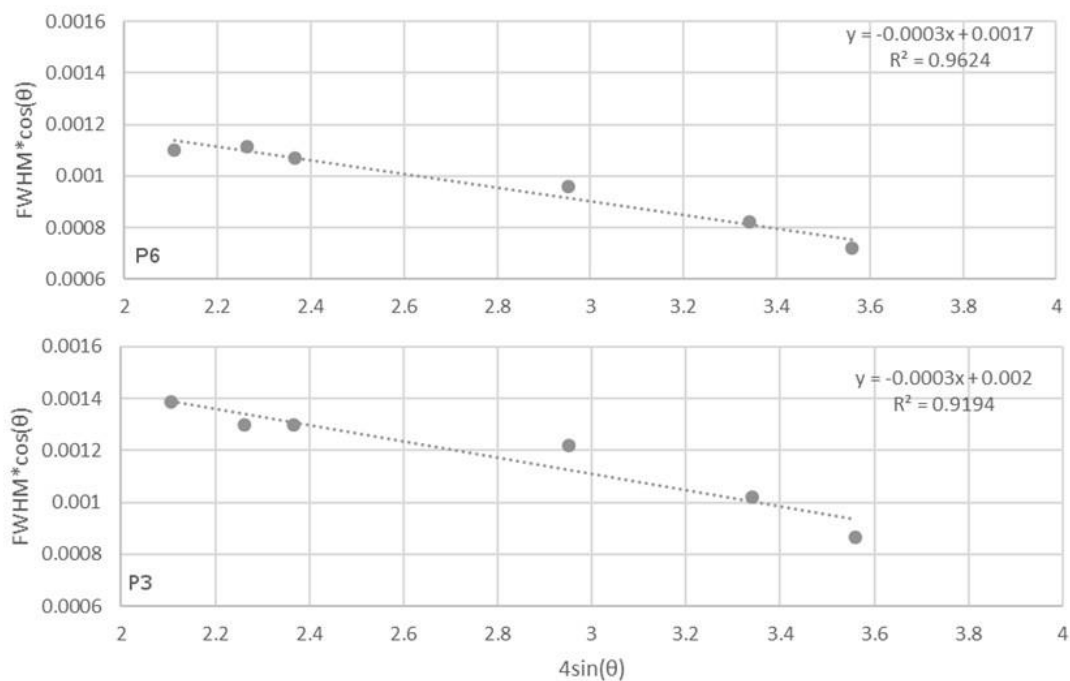
Figure 3.13 Williamson-Hall plots of **above:** *direct* method sample P6 and **below:** *indirect* sample P3.

Zn-O bond lengths: The calculated bond lengths between Zn and O atoms in the lattice were about 1.98 Å for all samples and in agreement with reported bond lengths (González, 2012) (Table 3.3).

Table 3.3 Calculated Zn-O bond lengths

Sample	ZnO bond length (Å)
P1	1.9768
P3	1.9766
P6	1.9763
P7	1.9760
P14	1.9764
P15	1.9770
P16	1.9758

3.5.2 XRF AND CASE STUDY EDX RESULTS

XRF results for powder samples: All samples contained impurities such as iron, cobalt, nickel, and copper, as well as slightly less chlorine, potassium and calcium (Figure 3.14).
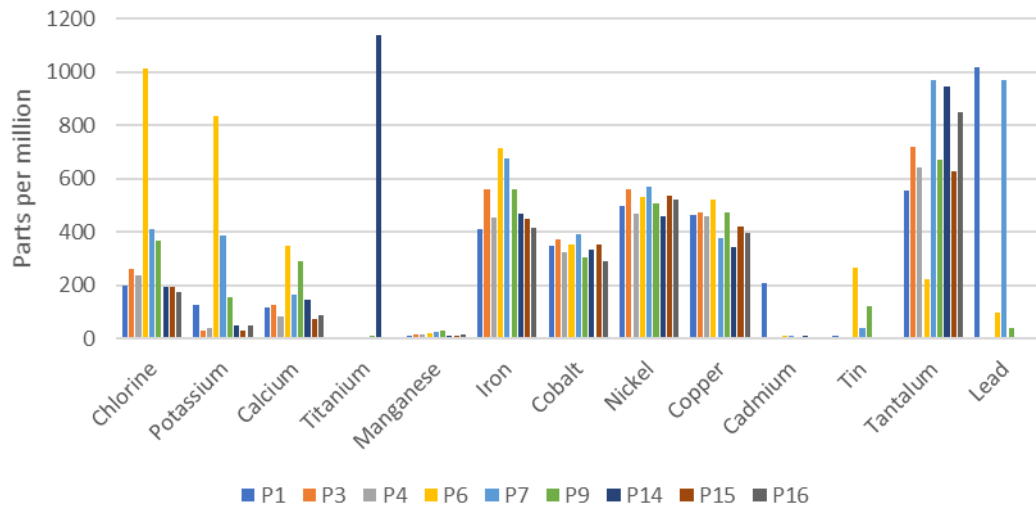
Figure 3.14 Trace elements found in powder samples

Samples P3, P4, P15 and P16 were compositionally similar (Figure 3.15), as was sample P14 except that it contained 1137 ppm of titanium, the only sample to contain titanium in any significant quantity. Sample P9 was somewhat like this group but contained more chlorine, potassium, and calcium as well as containing tin and lead unlike the other samples mentioned.
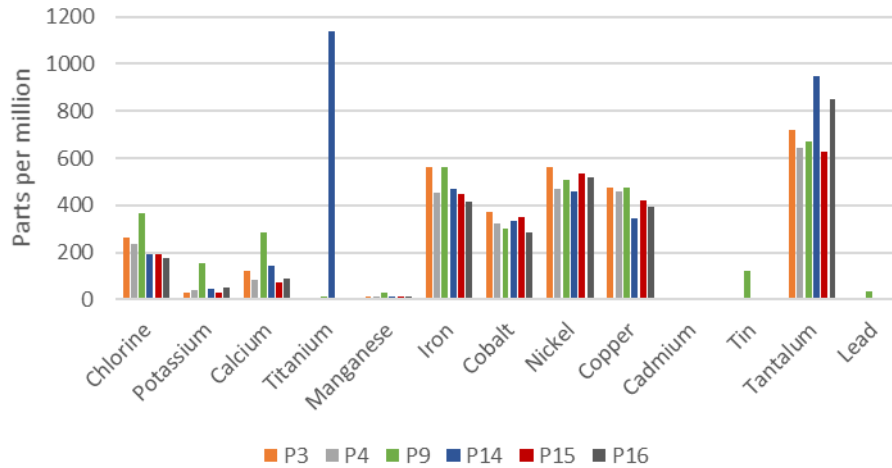
Figure 3.15 Compositionally similar pigments. All pigments except P9 are *indirect* method or commercial pigments, while P9 is a *direct* method pigment.

Samples P1 and P7 contain by far the most lead with 1016 and 971 ppm respectively. Sample P1 is also the only sample with significant amounts of cadmium (206 ppm while all other samples contain less than 11 ppm). Sample P6 contains the most chlorine, potassium, calcium and tin of all samples (Figure 3.16).
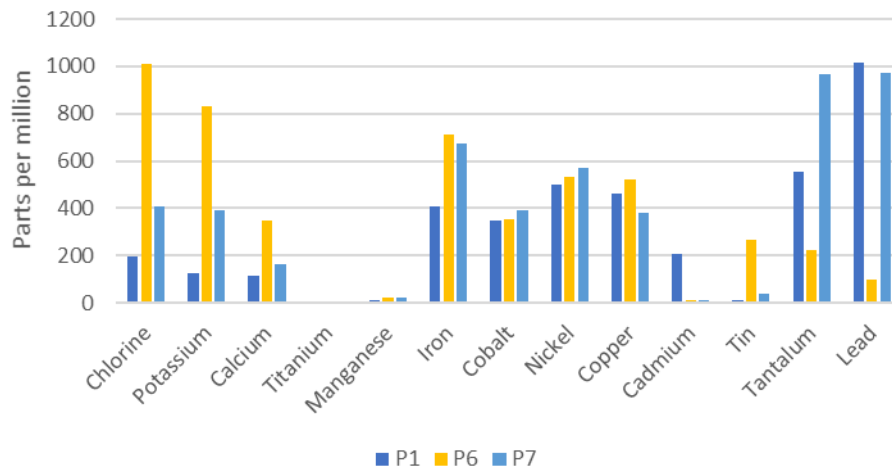
Figure 3.16 Compositionally unusual pigments

Total impurities were greatest for sample P7, then P6, P14, and P1 (Figure 3.17). Samples P3, P4, P15 and P16 contained the fewest impurities. These last four samples are largely the *indirect* method powders or assumed to be *indirect* in the case of the commercial pigments.
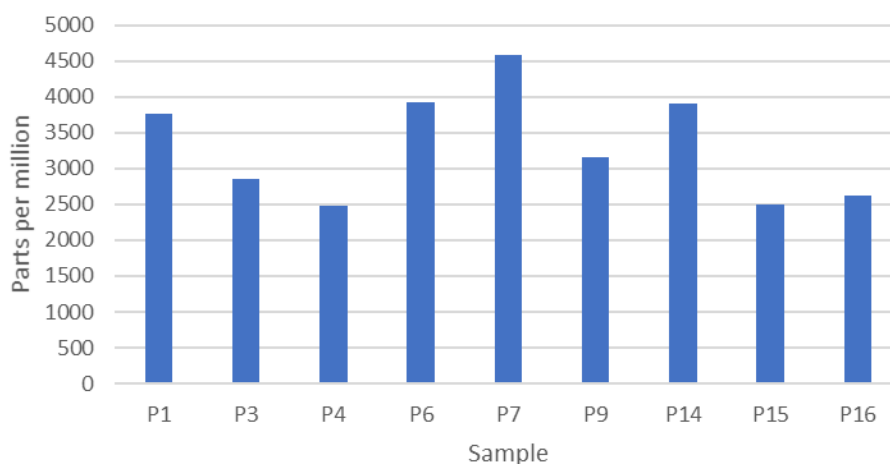
Figure 3.17 Sum of all impurities for each sample

Case study EDX results[61]: Attempts to compare spectroscopic EDX results for case studies with XRF results for pigment samples were unsuccessful given the differences in sensitivity of the methods. When converted to atomic %, the XRF results appear extremely small compared with the EDX results (Figure 3.18). All case studies were found to contain zinc in representative white pigment areas. Table 3.4 lists the atomic percentage of elements in each sample.[62] The percentages of zinc and oxygen ranged widely due to the presence of other impurities and elements in the pigment mixture and binding medium. Zinc oxide was identified by determining the percentage of zinc compared to other cations and then comparing the sulphur-to-zinc ratio. A low ratio indicated the sample was mostly zinc oxide, while a high ratio indicated a sizable zinc sulphate salt contribution. These are represented in the last two columns of Table 3.4.

---

[61] EDX scans for case studies were unable to detect trace elements and were largely used to verify that case study pigments were zinc oxide and not overly mixed with other pigments. Scans did not focus on single crystallites but rather were meant to characterise an area containing many pigment crystals and a fair amount of binding medium. For locations of EDX scans refer to Appendix 9: Additional EDX Data and Sample Locations for Case Studies.

[62] Oxygen and carbon were excluded as they were present in the binding medium and carbon pad under the mounted sample and therefore could not be attributed to the pigments alone. Sodium was omitted because the zinc peak usually overwhelms it.
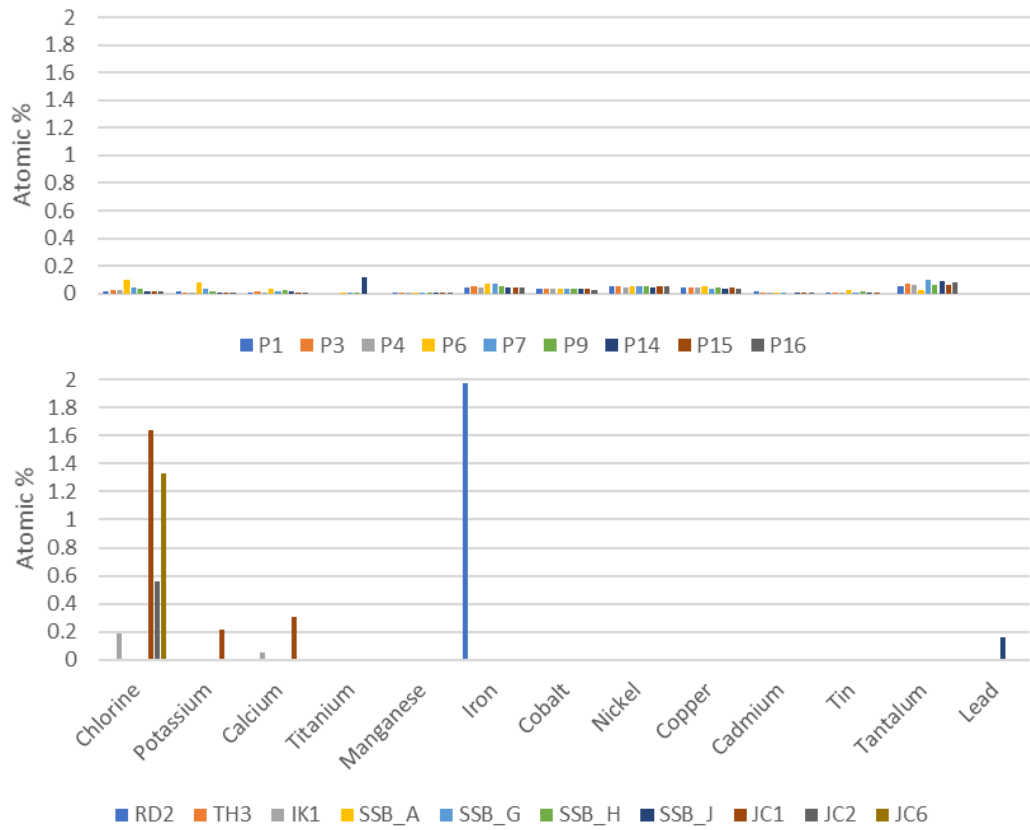
Figure 3.18 Comparison of results from **above:** XRF spectroscopy of powder samples with **below:** EDX spectroscopy of case studies showing that they are not comparable due to differences in instrument sensitivity.

Table 3.4 Atomic percentages of elements obtained from EDX analysis of case study paint samples

Sample	Zn	S	Al	Si	Ba	Fe	Ca	Cl	Ti	K	Pb	Mg	Co	N	P	As	Sn	% Zn/cations	S/Zn
RD2	8.48	0.79	0.16	0.19	------	1.97	------	------	------	------	------	------	------	------	------	------	------	80	0.09
TH1	26.68	1.09	3.85	5.84	------	------	------	------	------	------	------	------	------	------	------	------	------	87	0.04
TH2	15.30	1.13	8.26	7.91	------	------	------	------	------	7.36	------	------	------	------	------	------	------	65	0.07
TH3	16.92	2.31	0.63	2.27	------	------	------	------	------	------	------	------	------	------	------	------	------	96	0.14
IK1	9.68	0.14	------	0.12	------	------	0.05	0.19	------	------	------	------	------	------	------	------	------	99	0.01
IK2	6.09	0.42	0.45	0.25	------	------	0.12	0.10	6.05	0.05	------	------	------	------	------	------	------	48	0.07
IK3	------	5.13	0.04	------	4.70	1.86	------	------	------	0.06	3.57	------	------	6.41	0.09	------	------	0	------
IK4	4.17	0.10	0.09	0.23	------	------	0.05	0.08	0.36	------	------	------	------	------	------	------	------	89	0.02
IK5	6.71	0.29	0.14	0.37	------	------	0.09	0.18	------	------	------	0.10	------	6.40	------	0.15	------	93	0.04
SSB-A	18.38	2.46	0.48	0.72	------	------	------	------	------	------	------	0.37	------	4.21	------	------	------	96	0.13
SSB-D	2.38	1.72	1.44	2.15	0.70	0.27	0.34	------	------	------	------	0.90	0.19	------	------	------	0.47	36	0.72
SSB-E	4.42	2.06	0.31	------	------	------	------	------	------	------	------	------	------	------	------	------	------	93	0.47
SSB-F	0.52	0.16	2.11	1.65	------	------	0.26	------	------	------	------	------	------	------	------	------	------	82	0.31
SSB-G	22.85	3.88	------	0.21	------	------	------	------	------	------	------	------	------	3.91	------	------	------	100	0.17
SSB-H	18.49	0.78	------	1.55	------	------	------	------	------	------	------	------	------	------	------	------	------	100	0.04
SSB-I	0.35	0.31	------	2.70	------	------	7.68	------	------	------	------	0.12	------	------	------	------	------	4	0.88
SSB-J	18.98	1.27	0.27	0.35	------	------	------	------	------	------	0.16	------	------	1.73	------	------	------	98	0.07
SSB-K	0.27	0..48	1.26	0.93	------	0.11	0.25	------	------	------	0.06	0.14	------	------	------	------	------	13	1.77
SSB-L	0.66	0.38	1.36	2.82	------	------	0.15	------	------	------	------	------	------	------	------	------	------	30	0.58

Key: Sample names: RD – ruin drawing, TH – Thomas Harper watercolour, IK – Irene Kendall watercolour, SSB – *SS Buda* watercolour. **Bold sample names** indicate those which meet following criteria: 1) sample contains ~10% or more of Zn 2) zinc constitutes over 90% of cations present, and 3) ratio of sulphur to zinc is under 0.2.

Table 3.4 continued Atomic percentages of elements obtained from EDX analysis of case study paint samples

Sample	Zn	S	Al	Si	Ba	Fe	Ca	Cl	Ti	K	Pb	Mg	Co	N	P	As	Sn	% Zn//cations	S/Zn
JC1	18.60	4.63	0.49	0.83	------	------	0.31	1.64	------	0.22	------	0.32	------	------	------	------	------	94	0.25
JC2	16.00	3.47	0.23	0.35	------	------	------	0.56	------	------	------	0.25	------	3.24	------	------	------	97	0.22
JC3	12.30	10.15	------	------	------	------	------	------	------	------	------	------	------	------	------	------	------	100	0.83
JC4	12.49	2.22	5.46	0.30	------	------	------	0.87	------	------	------	------	2.18	------	------	------	------	59	0.18
JC5	10.50	8.24	3.16	0.32	------	------	------	------	------	------	------	0.33	1.78	2.71	------	------	------	67	0.78
JC6	19.93	6.76	0.26	0.38	------	------	------	1.33	------	------	------	------	------	------	------	------	------	99	0.34
JC7	20.91	5.51	3.98	0.35	------	------	0.42	1.98	------	------	------	------	1.17	------	------	------	------	79	0.26

Key: Sample names: JC – *View of St. Mary's Cathedral* watercolour. **Blue bold sample names** indicate those which meet following criteria: 1) contain ~10% or more of Zn 2) zinc constitutes over 90% of cations present, and 3) ratio of sulphur to zinc is under 0.4. **Red bold sample name** indicates sample with very high sulphur to zinc ratio and without any impurities.

3.5.3 PARTICLE SIZE ANALYSIS RESULTS

All *indirect* method pigments (P1, P3, P4) and commercial pigments P15 and P16 contained particles with sizes from 0.37 - 2.37 µm (Figure 3.19). Sample P14 formed large clumps and had a maximum particle size of 10 µm (Figure 3.20).
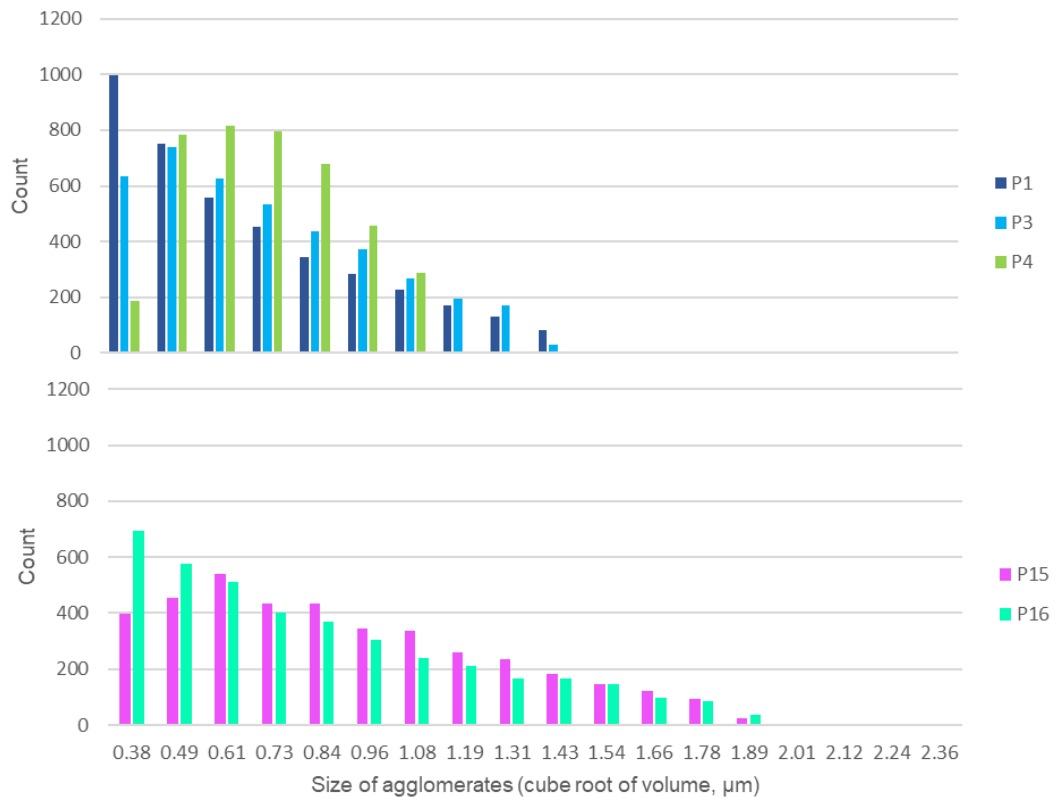
Figure 3.19 Above: Size distribution of *indirect* method samples. **Below:** Select commercial pigments.
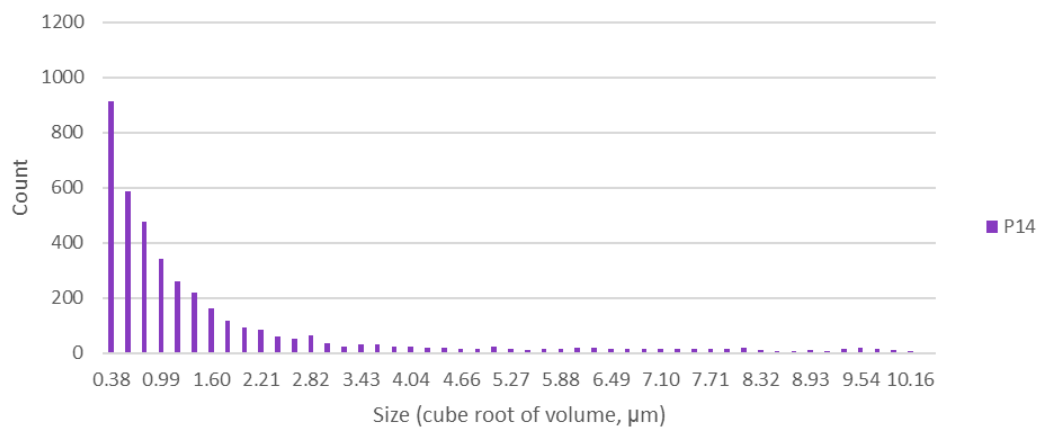
Figure 3.20 Size distribution of commercial pigment sample P14 showing wide range of particle sizes.

The next largest particles were measured in *direct* method pigments and were 3.8 µm. Of the *direct* method pigments, P7 had a range of values most in agreement with the *indirect* and commercial pigments, about 0.4 – 2.7 µm (Figure 3.21). Sample P4 had the most restrained domain, about 0.5 – 1.8 µm, but also the greatest increase between the smallest and second-smallest bin, from about 200 to 800 particles, or an increase of about 600 particles.
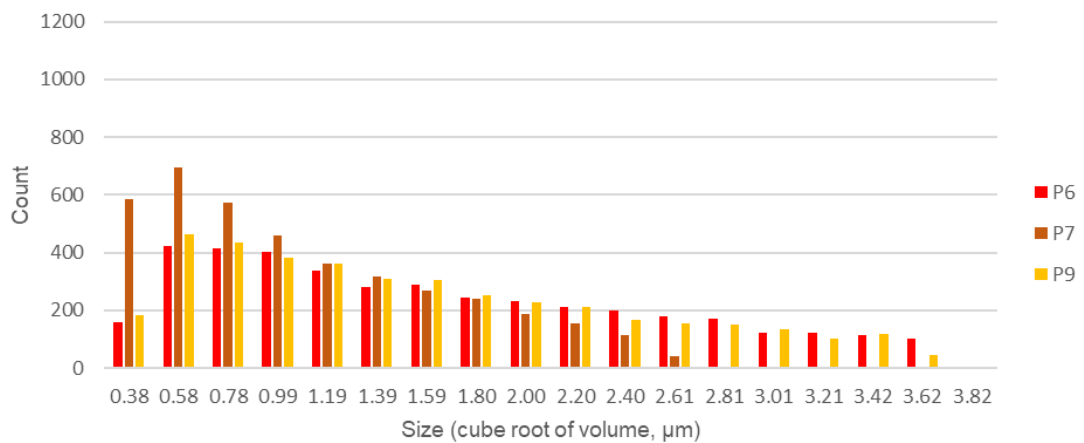
Figure 3.21 Size distributions of *direct* method samples

Size values and SAV[63] ratios are given in Table 3.5. The median and mean values agree closely for all samples except P14, which is skewed towards smaller particles with a few very large particles skewing the mean. High SAV ratios correspond to small particles and vice versa, reflecting the greater total surface area available for reactions on smaller pigment particles.

---

[63] Surface-area-to-volume

Table 3.5 Particle size ranges and values for all powder samples (µm)

Sample	SMean	S50 (median)	S10	S90	SAV ratio
1	1.00	0.867	0.378	2.36	3.25
3	1.08	0.992	0.412	2.26	3.28
4	1.07	1.04	0.518	1.79	3.84
6	1.75	1.58	0.509	3.83	1.88
7	1.19	1.04	0.433	2.67	2.78
9	1.68	1.50	0.510	3.72	1.95
14	1.80	1.00	0.390	10.4	0.745
15	0.957	0.892	0.402	1.91	3.87
16	0.887	0.791	0.378	1.95	3.91

Key: S = size, SAV = surface-area-to-volume ratio

A general comparison of particle size trends for *indirect*, commercial and *direct* method pigments highlights the similarities between the former two types and the wider particle size range for *direct* method pigments (Figure 3.22).
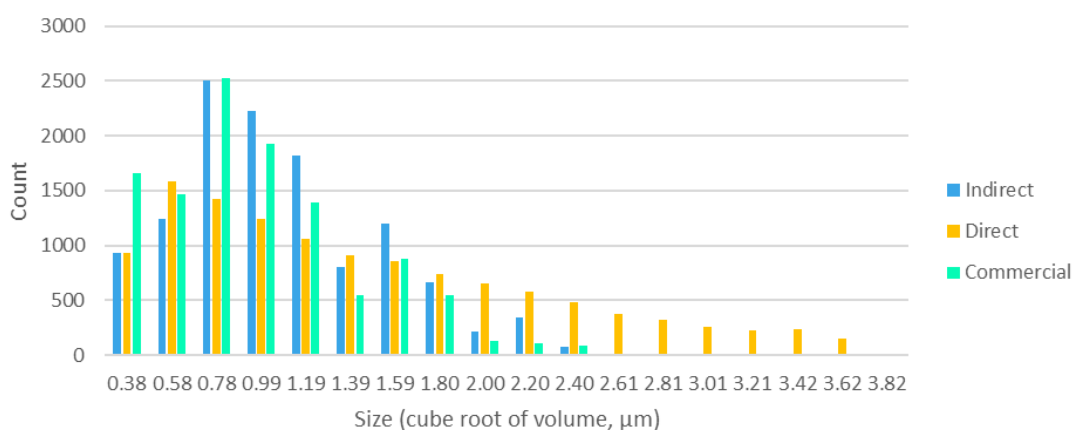
Figure 3.22 Particle size distributions of summed *indirect* method, *direct* method and commercial zinc oxide samples.

3.5.4 CRYSTALLITE SIZE RESULTS

Indirect method samples and commercial pigments were generally composed of smaller crystallites than *direct* method samples (Figures 3.23 and 3.24, Table 3.6). Whereas sample P14 covered a very large size range when measured as a particle, the crystallite measurements were more confined and agreed more closely with other commercial pigment samples.
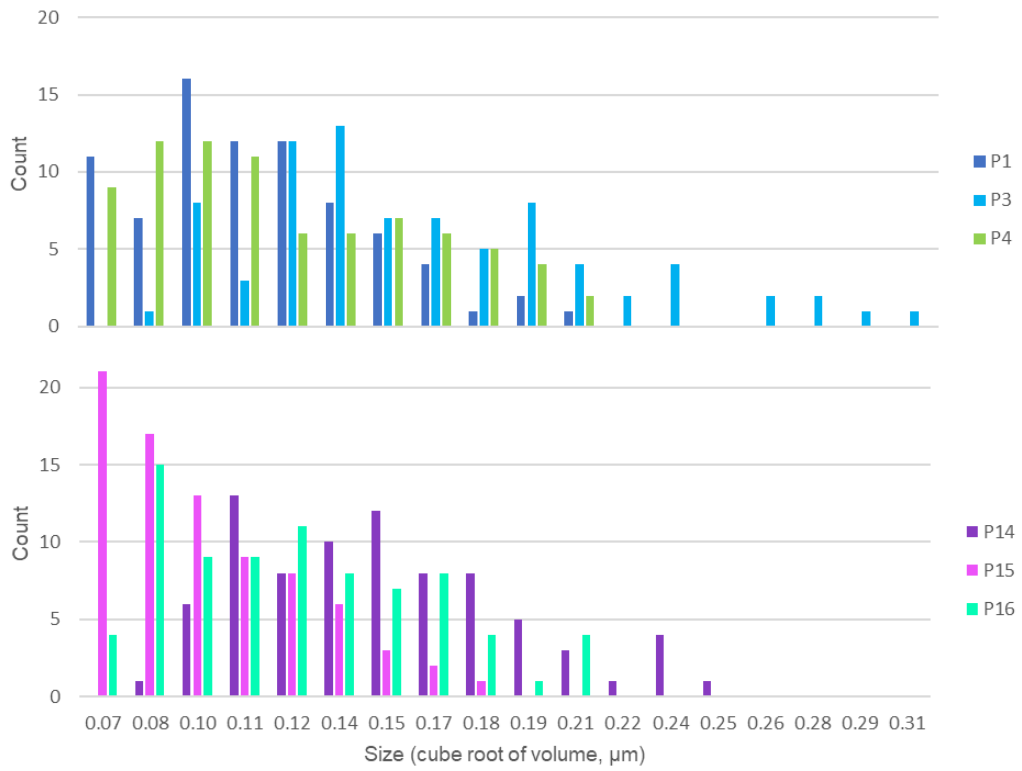
Figure 3.23 Crystallite size distributions of **above:** *indirect* method samples and **below:** commercial pigments
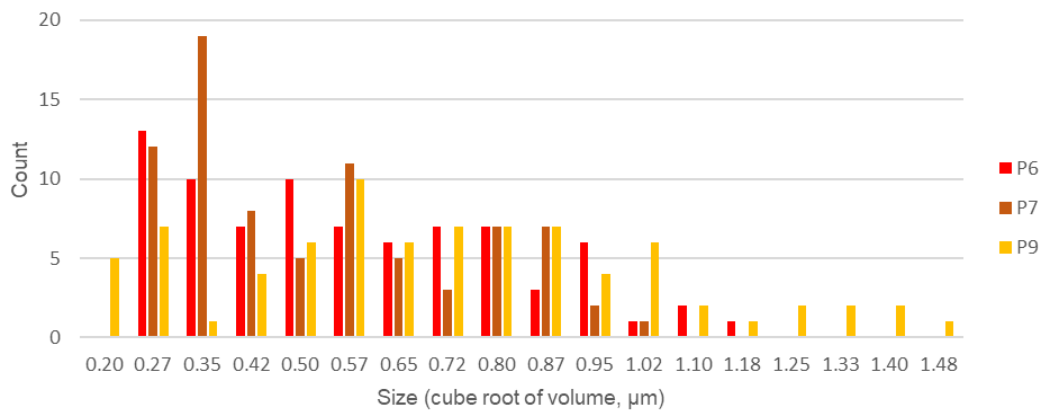
Figure 3.24 Crystallite size distribution of *direct* method powder samples.

Table 3.6 Crystallite size ranges and values for all powder samples (µm)

Sample	SMean	S50 (median)	S10	S90	SAV ratio
1	0.121	0.120	0.0707	0.214	41.8
3	0.170	0.157	0.0945	0.307	28.9
4	0.128	0.117	0.0681	0.215	38.4
6	0.618	0.575	0.286	1.20	8.21
7	0.566	0.540	0.322	1.13	8.78
9	0.749	0.737	0.196	1.48	6.73
14	0.158	0.155	0.0946	0.259	32.3
15	0.105	0.0973	0.0679	0.182	48.5
16	0.131	0.129	0.0716	0.218	38.1

Direct method samples had a greater length-to-width ratio (Table 3.7) meaning a greater percentage of surface area was accounted for by the lateral crystal faces than by the polar faces. *Indirect* and commercial pigments all had smaller, similar length-to-width ratios and around a quarter of their surface area accounted for by polar faces.

Table 3.7 Dimensional analysis of pigment samples[64]

Sample	Length-to-width ratio	% polar surface area
1	1.63	23
3	1.54	26
4	1.76	22
6	3.56	12
7	2.81	17
9	3.89	11
14	1.57	25
15	1.83	21
16	1.75	22

---

[64] Length-to-width ratio calculated by dividing the sum of all measured lengths by the sum of all measured widths. Likewise, % polar surface area was calculated by dividing the sum of all polar surface areas by the sum of all total surface areas, then multiplying the result by 100.

Case studies: Three of the five case studies were imaged and analysed for crystallite size distribution. The Irene Kendall pigments were not analysed as the pigment was too embedded in binding medium to image well while the *St. Mary's Cathedral* watercolour samples were too mixed to ensure accurate results. The Thomas Harper (TH3) pigment had the smallest crystallites with the narrowest range of sizes, followed by *SS Buda* (SSB_J) which had mostly small crystallites but included many larger crystallites. The ruin drawing (RD1) sample had the widest range and largest crystals, though there was some overlap with the other two case study samples (Figure 3.25).
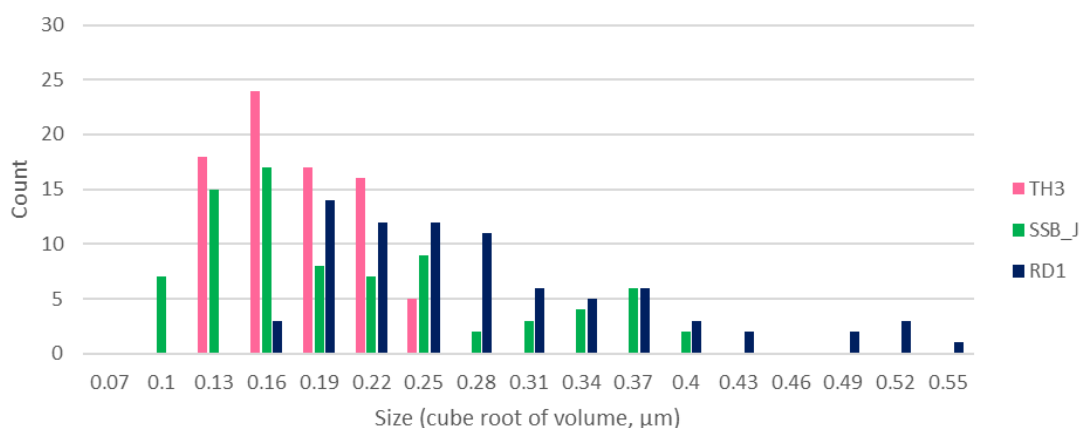
Figure 3.25 Crystallite size distribution of case study pigments from Thomas Harper watercolour (TH3), *SS Buda* watercolour (SSB_J) and ruin drawing (RD1).

Length-to-width ratios were all small for case studies, with the shortest being the SSB pigment (Table 3.8). This translated to a high percentage of surface area accounted for by polar surfaces, nearly a quarter in all cases.

Table 3.8 Length-to-width ratios and % polar surface area for three case study pigment samples

Sample	Length-to-width ratio	% polar surface area
RD1	1.70	24
SSB-J	1.57	25
TH3	1.73	22

SAV ratios for case studies were wide-ranging and reflected the variation in crystallite sizes measured in historic pigments (Table 3.9).

Table 3.9 Crystallite size ranges and SAV ratios for three case study pigment samples (µm)

Sample	SMean	S50 (median)	S10	S90	SAV ratio
RD1	0.271	0.242	0.155	0.538	17.3
SSB-J	0.193	0.162	0.0940	0.392	21.7
TH3	0.159	0.155	0.106	0.227	33.2

Overall, crystallites followed a similar size distribution as particles, with *indirect* and commercial pigments occupying very similar ranges and *direct* method pigments typically made up of larger particles. Case study pigments were more like the *indirect* and commercial pigments with a slightly higher instance of larger particles, though never as large as the *direct* method samples (Figure 3.26).
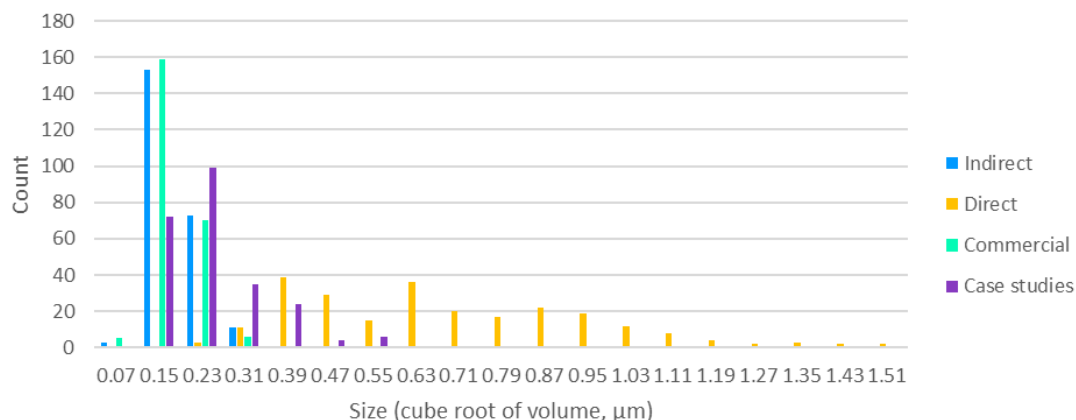
Figure 3.26 Crystallite size distribution for all *indirect, direct,* commercial and case study pigments.

3.5.5 CRYSTALLITE MORPHOLOGY RESULTS

Mock-up samples typically were divided morphologically by production method, with *indirect* and commercial pigments generally containing both rod-like and nodular particles (except for P14 which was purely nodular) and *direct* method pigments containing rod-like, acicular particles with pyramidal ends. Case-study

samples were all nodular, with RD1 containing some obvious rod-like particles. Other samples were obscured by the binding medium but could be determined as nodular rather than acicular (Table 3.10).

Table 3.10 Morphological characteristics of mock-up and case-study samples

Sample	Pyramids	Rod-like	Nodular	Acicular
1		●	●	
3		●	●	
4		●	●	
6	●	●		●
7	●	●		●
9	●	●		●
14			●	
15		●	●	
16		●	●	
RD1		●	●	
TH3			●	
SSB-J			●	

3.6 DISCUSSION

3.6.1 STRAIN VALUES FROM WILLIAMSON-HALL PLOTS

Strain values derived from Williamson-Hall plots were identical and all negative. Most literature describes a positive strain value for zinc oxide (Scardi, Leoni and Delhez, 2004; Khorsand Zak, Abd. Majid, *et al.*, 2011; Bindu and Thomas, 2014), but negative strain is not necessarily meaningful especially if the instrumental line broadening is not corrected, a procedure which was beyond the scope of this study. Strain values in this case were disregarded.

3.6.2 INFLUENCE OF XRF ON XRD RESULTS

Both data and the literature suggest that elemental impurity content does not correlate in any way to lattice changes as measured by x-ray diffraction. In studies

of the influence of individual impurities to lattice parameters, Krithiga, Sankar and Subhashree (2014) could find no relationship between lithium content and the diffractogram, only finding a slight decrease in the *c* lattice at high concentrations due to the replacement of zinc with lithium. Yun and Lim (2011) could similarly find no correlation between increasing the amount of aluminium and changes to either the diffractogram or the lattice parameters.

3.6.3 XRF RESULTS AND ELECTRONIC EFFECTS

All *direct* method pigments had a detectable level of lead. This impurity carries a charge of +2 and is a neutral impurity when replacing a zinc ion (Bonosewicz, Hirschwald and Neumann, 1986). If it were present interstitially, it would make the crystal slightly more positively charged. It has not been extensively studied as a defect, however, due to its tendency to replace zinc rather than sit interstitially; meaning this defect likely has no effect on conductivity. Cadmium similarly contains a +2 charge and is present only in sample P1, an *indirect* method pigment. It also does not affect conductivity as it replaces zinc ions in the lattice. However, it indicates that sample P1 likely came from a sphalerite source, an ore consisting mainly of zinc sulphide. It also suggests that any distillation process used to purify the zinc oxide after production was not rigorous.

Chlorine, potassium and calcium were also dominant in sample P6. None have been studied sufficiently as dopants and potassium as a positive defect was only briefly studied mathematically. Authors found that its positive contribution to charge would easily be compensated by oxygen vacancies (Park, Zhang and Wei, 2002).

Of the elements which could contribute significantly to conductivity, most were undetectable by the XRF instrument due to its energy limit. The instrument did not

collect data below sodium as the x-ray wavelength used was not appropriate for detecting such light elements. As a result, these defects cannot be examined.

The most unusual and stand-alone result is the high titanium content in sample P14. This same sample showed extreme clumping behaviour, with a very wide range of particle sizes, although the crystallite sizes were comparable to other *indirect* method pigments. In addition, the P14 XRD results were poor, indicating predominantly zinc oxide with small additional peaks. These peaks could not be positively related to those caused by titanium dioxide. The pigment did not disperse well in gum arabic and behaved very poorly as a watercolour due to the extreme clumping and resistance to colloidal dispersion. This sample will be excluded from further study as it was not representative of pigments that would typically be used either today or during the nineteenth century.[65]

3.6.4 XRF RESULTS AND HISTORIC PIGMENTS IN LITERATURE

Comparing XRF spectroscopy results from this study with results from papers which studied historic zinc oxide pigments highlights the similarities between the powder samples chosen for this study and historic pigments. Artesani *et al.* (2016) analysed early 20th century Lefranc-Bourgeois pastels using XRF and EDX spectroscopy and found most were mixed with zinc white, which may have had a zinc sulphide component. Additionally, calcium and barium would have been more prevalent as both were used as fillers in pastels. Nevertheless, samples from this study compare well with results obtained from the historic pastels, particularly Artesani *et al.*'s first

---

[65] The presence of titanium is also evidence of pigment mixing. Titanium dioxide was produced commercially only in the 20th century and therefore was unlikely to have been mixed with zinc oxide in the 19th century unless as the natural mineral, thus providing further justification for exclusion from this study.

four samples which were white and consisted only of zinc white and possibly zinc sulphide (Table 3.11).

Table 3.11 Results from Artesani *et al.* (2016) pastels (SO1-SO4) compared to test pigments

	Fe	Co	Ni	Ca	Pb	Ba	Al	Si	Cu
SO1	●	●	●	●			●	●	●
SO2	●	●	●		●		●	●	●
SO3				●			●		●
SO4	●	●	●	●		●	●	●	●
P1	●	●	●	●	●				●
P3	●	●	●	●					●
P4	●	●	●	●					●
P6	●	●	●	●	●				●
P7	●	●	●	●	●				●
P9	●	●	●	●	●				●
P14	●	●	●	●					●
P15	●	●	●	●					●
P16	●	●	●	●					●

Capogrosso *et al.* (2015) also analysed early 20th century Lefranc-Bourgeois samples and identified zinc oxide as the main pigment in a pastel (LF1) and a powder watercolour pigment (LF2). They also studied a Winsor and Newton Chinese White paint tube (WN1) (Table 3.12).

Table 3.12 Results from Capogrosso *et al.* (2015) (top three) compared to test pigments

	Fe	Mn	Cl	Ti	Cd	Ca	Pb	Ba	Sn	Cr	K	S	Si
WN1	●		●			●		●	●	●	●	●	●
LF1	●	●	●	●	●	●	●	●		●	●	●	●
LF2	●		●		●	●	●			●		●	●
P1	●	○	●		●	●	●		○		●		
P3	●	○	●			●					○		
P4	●	○	●			●					○		
P6	●	○	●		○	●	●			●	●		
P7	●	○	●			●	●			○	●		
P9	●	○	●			●	●			●	●		
P14	●	○	●	●		●					○		
P15	●	○	●			●					○		
P16	●	○	●			●					○		

Key: ● = includes over 50 ppm of the element, ○ = includes 10-50 ppm of the element
WN1 = Nineteenth-century Winsor and Newton Chinese White from the Courtauld Institute, LF1= A piece of a Lefranc-Bourgeois Raffaelli pastel identified as zinc oxide in a lipidic compound, LF2 = A Lefranc watercolour pigment powder from a bottle labelled Blanc de Neige, Vieille-Montagne Mars, Le Mans 1893, identified as zinc oxide with some zinc carbonate

There is slightly less agreement between samples analysed by Capogrosso *et al.* (2015) and when compared with the powder samples from this study. Samples mostly share impurities such as iron, chlorine, calcium and potassium. Cadmium is a common impurity in *direct* method zinc oxide, leading the authors to tentatively exclude the *indirect* method of production as the source of the zinc oxide. A decent percentage of cadmium was found in *indirect* sample P1, a zinc oxide red seal of lower purity than other *indirect* test samples. Perhaps sample P1 would not have been used as a pigment, being sourced from Sigma Aldrich for study, not painting. Regardless, the authors provide some evidence that a *direct* method pigment was used at least in a pastel form in the early twentieth century[66].

Casadio and Rose (2013) found when analysing Picasso's Ripolin paints using nanoprobe XRF spectroscopy that some of the more common impurities like iron

---

[66] This time period is assumed by the presence of titanium dioxide, a pigment not used until after 1916 when mass production was improved.

and lead were more often localised and found outside of the zinc oxide pigment particles, rather than inside them.

3.6.5 CRYSTALLITE SIZE TRENDS AND COMPARISON TO LITERATURE

The range of crystallite sizes determined through SEM image analysis agreed with ranges given in the literature (Figure 3.27).
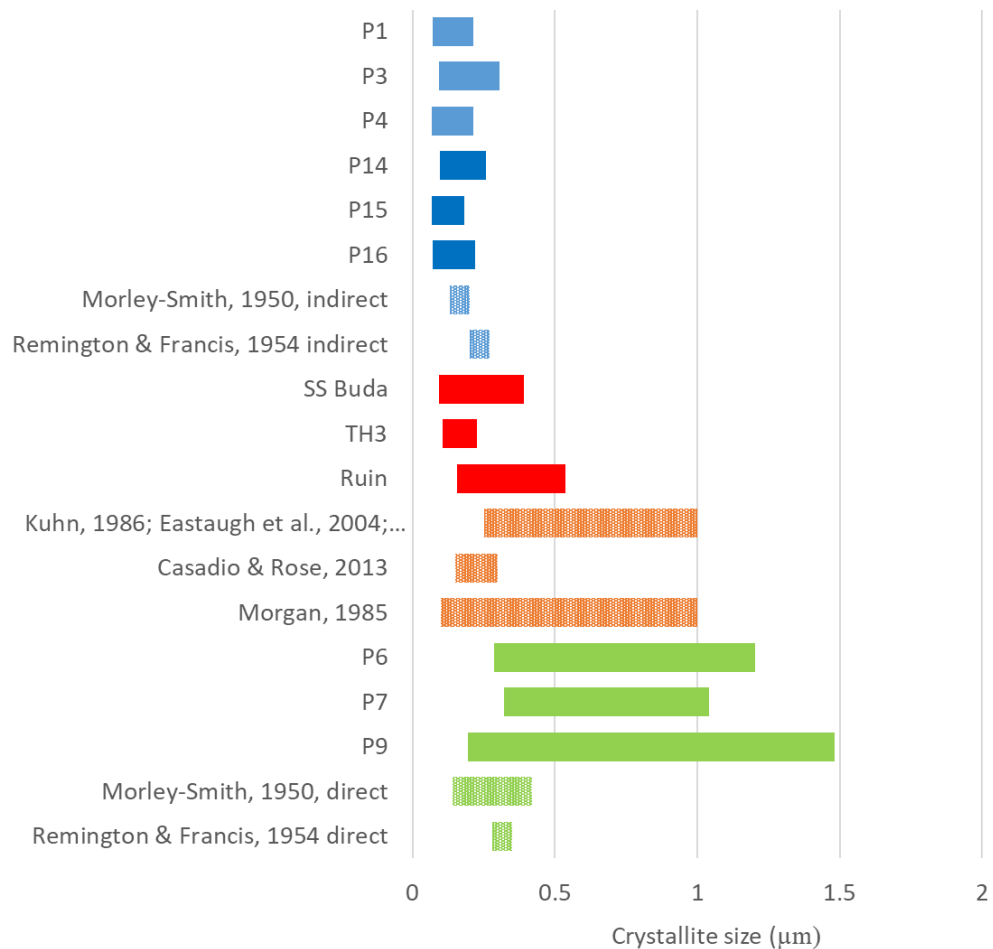
Figure 3.27 Range of crystallite sizes measured using SEM for study powders and case studies as well as reported sizes from select papers. **Key:** light blue = *indirect* pigments, dark blue = commercial pigments, red = case studies, orange = unspecified production method, green = *direct* pigments. Solid bars = measurements in this study, textured bars = measurements from literature

They also revealed similarities in size between *indirect* method pigments and commercial pigments. Historic pigments from case studies SSB, TH and RD all fell within these ranges. TH most closely matched the size ranges measured in *indirect* pigments, while the other two case studies had a slightly broader range, although not

nearly as broad as the *direct* method pigments and broader still than sizes reported in the literature. This suggests the case studies may contain *indirect* method zinc oxide pigments.

3.6.6 THEORETICAL RELATIONSHIP OF SIZE AND MORPHOLOGY TO REACTIVITY

Size and surface area have both been linked with rates of photocatalysis and deterioration of surrounding materials. Dodd et al. (2006) found an optimum crystallite size of 33 nm (approximately 0.033 µm) for producing hydroxyl radicals when irradiated by UV light at a 300 nm wavelength. Crystallites both smaller and larger than 33 nm had lower rates of hydroxyl creation, either due to less overall surface area for large particles or increased recombination rates for small particles.

Another investigation of catalysis and its relationship with physical properties (Li & Haneda, 2003) found that the highest photocatalytic rates were measured for single crystallite zinc oxides and the lowest for rod-like particles. The single crystallites are more nodular than the rod-like particles, indicating a clear connection between length-to-width ratio and photocatalytic activity.

When compared with Dodd et al. (2006) values derived from SEM crystallite size analysis were closest to the optimum size of 0.033 µm in *indirect* method and commercial pigments, with minimum values measured from ~0.07 to 0.09 µm. *Direct* method pigments were measured with minimum values starting from ~0.20 to 0.30 µm. While the method of measuring crystallites was very limited, the actual, rather than the measured, range of sizes for *indirect* and commercial pigments will likely contain a significant number of crystallites at the optimum size of 0.03 µm given the high concentration of smaller pigment crystallites measured when

compared to the *direct* method pigments as well as the limitations of measuring crystallites by hand, causing very small crystallites to be largely excluded.

Further work in photocatalytic reactions for sample pigments can confirm whether those with smaller length-to-width ratios are more reactive than those with longer values, as predicted by Li and Haneda. Results so far indicate that this should include both *indirect* and commercial pigments.

3.7 CONCLUSIONS

Based on analysis of physical properties, the following conclusions were reached:

- Procedures for collecting and analysing XRD data allowed for confirmation of relative purity and high crystallinity among all zinc oxide samples but did not yield results about defect concentrations.

- Commercial pigments (P14, P15, P16) are most like *indirect* method pigments in size, morphology and composition. The polar surface area of both types accounted for 20-25% of total surface area, much higher than *direct* method pigments' 11-17% of total area. As oxygen evolves from these surfaces most readily (Kumar and Rao, 2015) and ionization leads to excess electrons (0001) and holes (000$\bar{1}$) on the polar surfaces (Wahl *et al.*, 2013), this could translate to higher rates of photocatalytic behaviour for *indirect* and commercial pigments.

- When compared with results from Li and Haneda (2003) who identify nodular-like crystallites as the most photocatalytic and rod-like as the least, *direct* method pigments should be the least photocatalytic as they are

composed entirely of rod-like crystallites, while *indirect* and commercial contain a mix, indicating they may be more reactive.

- *Direct* method pigments (P6, P7, P9) have the highest percentage of elemental impurities, although *indirect* sample P1 contained a comparably high percentage of impurities. This may influence their rate of reactions, but not knowing whether the impurities are added or interstitial limits conclusions that can be drawn from this result. They compared favourably with historic pigments analysed by Artesani *et al.* (2016) and Capogrosso *et al.* (2015) with slight differences in composition largely accounted for by the presence of fillers in their samples.

- All case studies were confirmed to have zinc present. A high zinc-to-sulphur ratio confirmed that the pigments were oxides and not sulphates.

- Case study crystallites were most like *indirect* and commercial pigments, having similar length-to-width and SAV ratios as well as containing mostly nodular crystallites. This indicates they may have similar photocatalytic rates as these pigments and were likely produced using the *indirect* method of production.

4 Characterisation of Photocatalytic Degradation

4.1 TWENTIETH-CENTURY ATTITUDES

Despite the warnings generated from the Russell and Abney report [67] and research by Standage (1887) and Muckley (1888), zinc oxide's reputation for permanence remained largely unaffected until the early twentieth century. This reputation was reinforced by lead pigment scientist and Professor of Chemistry at the Royal Academy, Sir Arthur Church in his influential publication of 1890 *The Chemistry of Paint and Paintings*. He held the strong view that the pigment was 'practically perfect, being unchangeable in hue or opacity under the most adverse influences' (Church, 1890, p. 119). The author maintained his opinions even in the revised third edition published eleven years later (Church, 1901, p. 135). Others supporters who affirmed the pigment's stability included Zerr and Rübencamp who described it as 'very fast to air and light…unaffected by corrosive and sulphureous [sic] gases, and…specially suitable for mixing with other colours, since it does not alter their tone' (Zerr and Rübencamp, 1908, p. 88). Clifford Holley even suggested mixing zinc oxide with Prussian blue and comparing the colour to the blue mixed with lead white as a proof of zinc oxide's superior colour and working properties (Holley, 1909). No mention was made to the highly-publicised experiments [68] by Russell and

---

[67] Described in section 2.4.1.

[68] The report itself was sold in art shops and discussed in the Royal Academy so Arthur Church, Professor of Chemistry, would have surely consulted the report when teaching the science of pigments to his students.

Abney which clearly showed Prussian blue to fade more quickly in zinc oxide's presence[69].

The light experiment involving Prussian blue was revisited two years later by a German painter and paint chemist named Alexander Eibner who finally acknowledged evidence of zinc oxide's detrimental effects on surrounding materials (Eibner, 1911). He concluded that 'zinc white indeed accelerates light-fading of artists' paints and this manifested itself when '"coats of the corresponding mixtures with gum arabic, i.e., in aquarelle colors, [were] exposed to light, this being most pronounced when under glass"' (Kühn, 1986, p. 174)[70].

Further research into zinc oxide's role in the degradation of art works took decades to emerge. Scientists in physics, chemistry, and paintings conservation all made important discoveries about zinc oxide's properties as a photo-catalytic material beginning in the late 1930s[71], but it was not until the 1980s that links to works of art on paper were made (Figure 4.1).

---

[69] A more recent study into the chemical mechanisms of fading in Prussian blue indicate that free electrons are involved in a one-step reduction reaction (Kirby and Saunders, 2004):

$$Fe^{III}[Fe^{II}(CN)_6]^- + e^- \rightleftharpoons Fe^{II}[Fe^{II}(CN)_6]^{2-}$$
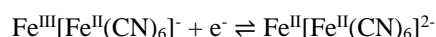
These are readily generated on the surface of zinc oxide particles in the presence of UV or blue wavelengths of light, explaining the results obtained in both Eibner's and Russell and Abney's study.

[70] Article by Eibner written in German, quote is taken from 'Zinc white' by Kühn who offers the translated summary on page 174.

[71] Publications with rigorous methodologies detailing zinc oxide's optical and chemical properties begin to increase in number in the 1950s, though earlier publications acknowledge some of the unique properties of the pigment such as its varying fluorescence (Nagle, 1928) and electronic band structure (Leverenz and Seitz, 1939). See Chapter 4: Fluorimetry and Spectrophotometry for a deeper discussion of these topics.

1910

1911 Eibner, *Uber die lichtwirkungen auf malerei-farbstoffe*

- Zinc oxide accelerates degradation of surrounding pigments in water-based paints

1911 Fleury, *The preparation and uses of zinc white paint*

- The more metallic zinc oxide is, the more stable. A unique opinion.

1920

1920 Holmes, *Notes on the science of picture making*

- Praise for body colour's appearance
- No comment on chemical stability
- Body colours usually include zinc white

1940

1941 Depew, *Zinc oxide - a product of complex physical and chemical properties*

- A full understanding of ZnO as a reactive pigment
- Describes ZnO use in vulcanisation of rubber
- ZnO was coated when used in enamel paints
- Describes conversion to sulphate salts and carbonation

1941 Jacobsen and Gardner, *Zinc soaps in paints: zinc oleates*

- reaction of zinc oxide with certain binding media in oil paintings

1950 Morley-Smith, *The development of anti-chalking French process zinc oxides*

- Contribution of particle size and ratio of blue/green fluorescing particles to chalking in oil paints

1950 Winter and Whittem, *Fluorescent and photo-chemical activity of zinc oxides*

- Concern about chalking in oil paints
- Connects fluorescence to photocatalytic activity
- Details effects of heat treatments

1953 Rubin et al, *Photochemical synthesis of hydrogen peroxide at zinc oxide surfaces*

- Degradation due to surface reactions with humidity

1950 Rischbieth, *Weathering tests on zinc oxide paints*

- Weathering tests to study chalking in oils

1953 Markham and Laidler, *Kinetic study on the surface of zinc oxide in aqueous suspensions*

- Study of hydrogen peroxide formation on zinc oxide particle surfaces in water

1957 Brown, *Zinc oxide rediscovered*

1960

- Description of hydrogen peroxide formation on particle surfaces along with summary of scientific knowledge to date

1958 Morley-Smith, *Zinc oxide: a reactive pigment*

- Photochemical properties of ZnO and relationship to soap formation

1966 Feller, *Problems in retouching: chalking of intermediate layers*

- Describes problems with retouching paintings exhibiting chalking due to zinc white pigments

1970

1987 Daniels, *Discolouration of paper induced by pigments containing zinc*

- Describes oxidation and discolouration of paper by hydrogen peroxide formed on ZnO particles, outlines reaction sequence
- Case studies of paper artworks discoloured by ZnO

1981 Kelly and Williams, *Inhibition of light sensitivity of paper treated with diethyl zinc*

- Paper degrades more quickly in presence of high humidity and ZnO

1987 Michalski, *Damage to museum objects by visible radiation (light) and ultraviolet radiation (UV)*

- Description of light damage to various object types types
- Chalking of ZnO in oil gives false appearance of fading

1987 Hey, *Chinese white - a potential source of trouble on paper?*

- Summary of studies of hydrogen peroxide forming on ZnO surfaces due to UV light exposure
- Studies browning of paper using W&N ZnO pigments painted onto sized paper, H_2O_2 effect neutralised with application of alkali

1990

Figure 4.1 Timeline of selected zinc oxide degradation literature: 1910 – 1990. **Key:** red text: studies of zinc oxide degradation problems on paper; orange text: studies of zinc oxide degradation in oil paints; green text: general study of zinc oxide as a photo-catalytic pigment; blue text: scientific papers studying zinc oxide as a photo-reactive material, not specific to pigments.

The bulk of the research shown in Figure 4.1 dealt with zinc oxide's electrical properties or effects on oil paintings such as soap formation and chalking.[72] In the period between 1911 and the 1980s, there was little comment on zinc oxide's potential danger to other pigments in watercolours. C.J Holmes, the Director of the National Portrait Gallery and a Slade Professor at the University of Oxford as well as writer of the seminal text *Notes on the Science of Picture-Making*, commented in 1920 only on zinc oxide's beauty in the context of body colour and not on its tendency to fade some pigments (Holmes, 1920). For such a prominent figure to omit the fact of zinc oxide's danger to surrounding pigments is significant. It was only after the 1970s that conservators and scientists began to discuss and publish accounts of visible changes to paper substrates caused by zinc oxide pigments.

4.2 DEGRADATION IN ARTWORKS ON PAPER CONTAINING ZINC OXIDE PIGMENTS

Most case studies dealing with visible degradation of paper related to interactions with zinc oxide pigments describe three types of changes: discolouration of paper around or behind pigments in the form of browning, shielding of paper from UV-induced browning, and conversion of zinc oxide into zinc sulphate salts resulting in pigment loss.

4.2.1 LOCALISED DISCOLOURATION OF PAPER

Vincent Daniels, Chief Conservation Scientist at the British Museum, and Margaret Hey, Chemist at the National Gallery in London, were among the first to notice and document discolouration of paper behind and adjacent to areas of Chinese white

---

[72] Refer to Appendix 10: Zinc Oxide's Use in Oil Paintings for more information on conservation issues stemming from zinc oxide in oil paints.

application. Hey documented unpublished discussions with colleagues in the 1970s about these phenomena (Hey, 1987) while Daniels, using XRD analysis, identified zinc oxide pigments as the cause of severe brown discolouration on the verso of two prints with watercolour additions (Daniels, 1990).

More recently, Kemp, Wise and Hamilton (2004) reported a pastel drawing by the Australian artist Grace Cossington Smith titled *Portrait of Diddy* which had suffered similar severe localised discolouration as well as planar distortions (Figure 4.2). Cross-sectional analysis and EDX spectroscopy revealed a white under-layer in severely degraded areas containing zinc, barium and sulphur, a typical composition for a zinc white pastel extended with barites and chalks. This under-layer directly corresponded to the severe degradation in the paper substrate.

Figure 4.2 Left: *Portrait of Diddy* by Grace Cossington Smith (b.1892, d.1984, work from 1920), soft pastel on paper, visible light photo of recto before treatment. **Right:** Brown, severely degraded areas on the verso corresponding to the application of the white pigment. In the collection of the National Gallery of Australia. Images credit: Kemp, Wise and Hamilton (2004).
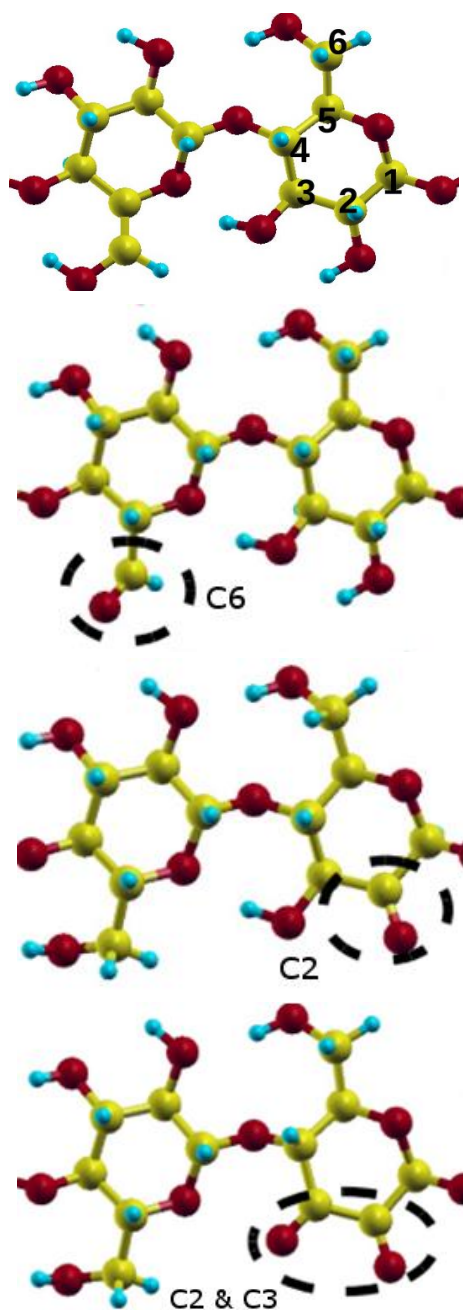
Figure 4.3 Positions of carbon atoms in the glucose monomers which make up cellulose (top), oxidised C6 side group (second from top), oxidised C2 side group (third from top) and oxidised C2 and C3 groups (bottom). Images of molecule structures from Conte *et al*., 2012.

Daniels identified the cause of discolouration adjacent to zinc oxide pigments as peroxide formation on the pigment particle surfaces (Daniels, 1990). Paper discolouration can result from the photo-oxidation of cellulose side groups (Daruwalla and Narsian, 1966; Conte *et al.*, 2012) during which hydroxides at the C2 and C6 positions oxidise to carbonyls[73], along with occasional conjugated oxidation at the C2 and C3 positions (Figure 4.3)[74] (Feller, Lee and Curran, 1985; Potthast, Rosenau and Kosma, 2006; Conte *et al.*, 2012). In low-relative humidity (RH) conditions, the C6 hydroxide oxidises to a carbonyl, forming an aldehyde (Daruwalla and Narsian, 1966; Conte *et al.*, 2012). At RH greater than 50%, oxidisation to carbonyls occurs mainly at the C2 position (Daruwalla and Narsian, 1966).

---

[73] Carboxyls, though a product of cellulose deterioration, occur mostly during pulp bleaching processes and are less involved in natural ageing or discolouration (Potthast, Rosenau and Kosma, 2006; Conte *et al.*, 2012).

[74] Cellulose consists of D-glucose monomers with 6 carbon atoms numbered according to position. They are linked with a β 1,4 glycosidic bond, meaning that the glucose molecules are oriented opposite one another and bonded between the 1 and 4 carbons.
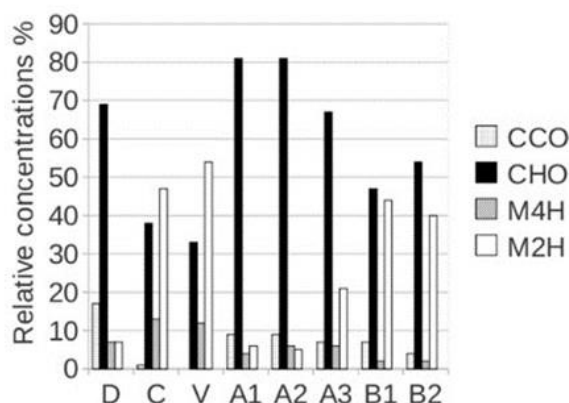
Figure 4.4 Concentrations of oxidized side groups in aged paper samples. C and V were thermally aged in normal air, while D was aged in dehydrated air. Samples A1-A3 and B1-B2 are from the 15th century. For A1-A3, all conservation treatments performed on them were dry. Samples B1 and B2 had wet treatments. CCO is complete oxidation of C6, CHO oxidation of C6 to aldehyde, M4H is coordinated oxidation of C2 and C3 to ketones and M2H is oxidation of C2 to a single ketone. Graph was modified from Conte *et al.*, 2012.

Conte *et al.* (2012) [75] identified the most common oxidation reactions associated with paper discolouration in thermally and naturally aged papers. C6 oxidises[76] more often in naturally aged papers without hydrous conservation treatments, while C2 oxidises at a much higher rate after aqueous treatment[77] (Conte *et al.*, 2012)[78] (Figure 4.4). Hemicellulose undergoes similar oxidation patterns but oxidises more readily than cellulose, meaning that papers with a higher hemicellulose content discolour more readily (Carter, 1996). Lignin, a component of paper made from wood pulps, can shield cellulose and hemicellulose from degradation by absorbing UV light but unfortunately creates acids and chromophores upon oxidation (Carter, 1996). Reaction mechanisms again involve oxidation of hydroxyls to carbonyls, in this case creating conjugated double bonds (Daniels, 2007) (Figure 4.5).

---

[75] Oxidised side groups were quantified using light absorption data and Density Functional Theory calculations.

[76] CHO in Figure 4.4

[77] M2H in Figure 4.4

[78] All papers also contained lesser amounts of C2 and C3 coordinated oxidation of hydroxyls to carbonyls (M4H in Figure 4.4) as well as completely oxidised C6 moieties (CCO in Figure 4.4).
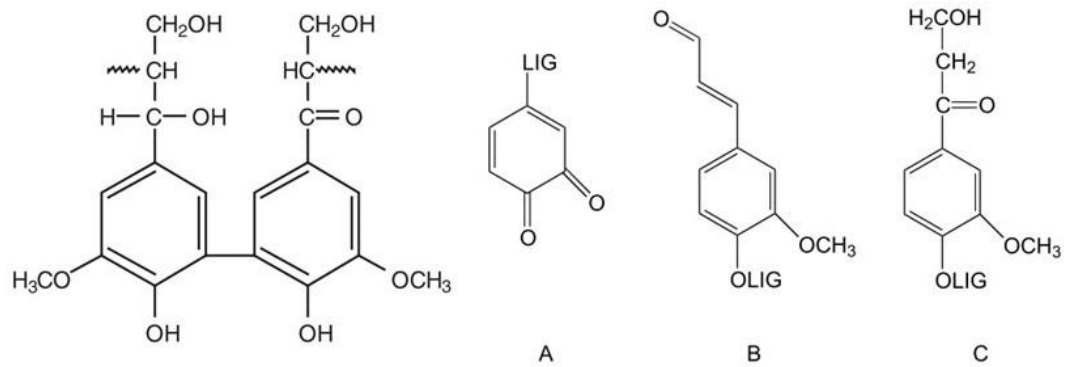
Figure 4.5 Lignin molecule (left) and main coloured by-products of lignin degradation A) orthoquinone, B) coniferaldehyde, C) aromatic ketone. LIG refers to rest of the lignin molecule. Image credit: lignin molecule from Daniels, 2007, coloured by-products from Carter, 1996.

Oxidation reactions with these paper components are catalysed by zinc oxide pigments as they react with adsorbed water in reactions 3.2-3.5 outlined in Chapter 3 and detailed again below:

$$\textbf{Oxidation Reaction: } H_2O + h^+ \rightarrow \cdot OH + H^+ \tag{3.2}$$

$$\textbf{Reduction reaction: } O_2 + e^- \rightarrow O_2^- \tag{3.3}$$

$$O_2^- + 2H^+ + e^- \rightarrow H_2O_2 \tag{3.4}$$

$$H_2O_2 + H^+ + e^- \rightarrow \cdot OH + H_2O \tag{3.5}$$
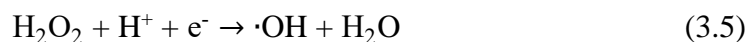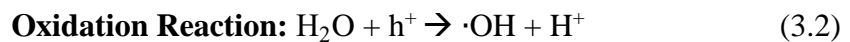
The oxidation of cellulose begins with the first half of reaction 3.5. First, hydrogen peroxide removes hydrogen from a cellulose molecule with the help of electrons in zinc oxide's conductance band. This creates a hydroxyl radical which can then remove another hydrogen from cellulose to form water, oxidising the hydroxyls in cellulose to carbonyls. The location of these reactions depends on the humidity levels present in the environment.

4.2.2 UV ABSORPTION AND SCREENING OF SUPPORT

In contrast to zinc oxide's tendency to catalyse cellulose oxidation, the pigment also screens underlying paper from UV-induced photolysis by strongly absorbing wavelengths of light below ~390 nm (Stutz, 1925; Bacci *et al.*, 2007). This manifests as distinct changes in paper tone from dark exposed paper to lighter paper where the pigment has been applied. At this interface between the applied pigment areas and surrounding paper, the sheet can become brittle and strained due to dissimilar expansion and contraction rates in the presence of moisture.

Singer and Liddie described these extreme distortions in the watercolour *S.S. Buda* by George Thomson. In the top image of Figure 4.6, the exposed paper has undergone severe hydrolysis exacerbated by its display over a stove in a Shetland cottage, an environment which would have clearly yielded extreme fluctuations in both temperature and humidity (Singer and Liddie, 2005). A very distinct ridge was also observed around the sails (lower left image in Figure 4.6). The authors attributed this to a deflated hydrogen peroxide bubble within the paper substrate (Singer and Liddie, 2005). This ridge could also be caused by uneven expansion of the support. The lower right image in Figure 4.6, taken in raking light, highlights the shift from flatter dark areas to more wrinkled paper behind the zinc oxide pigments.
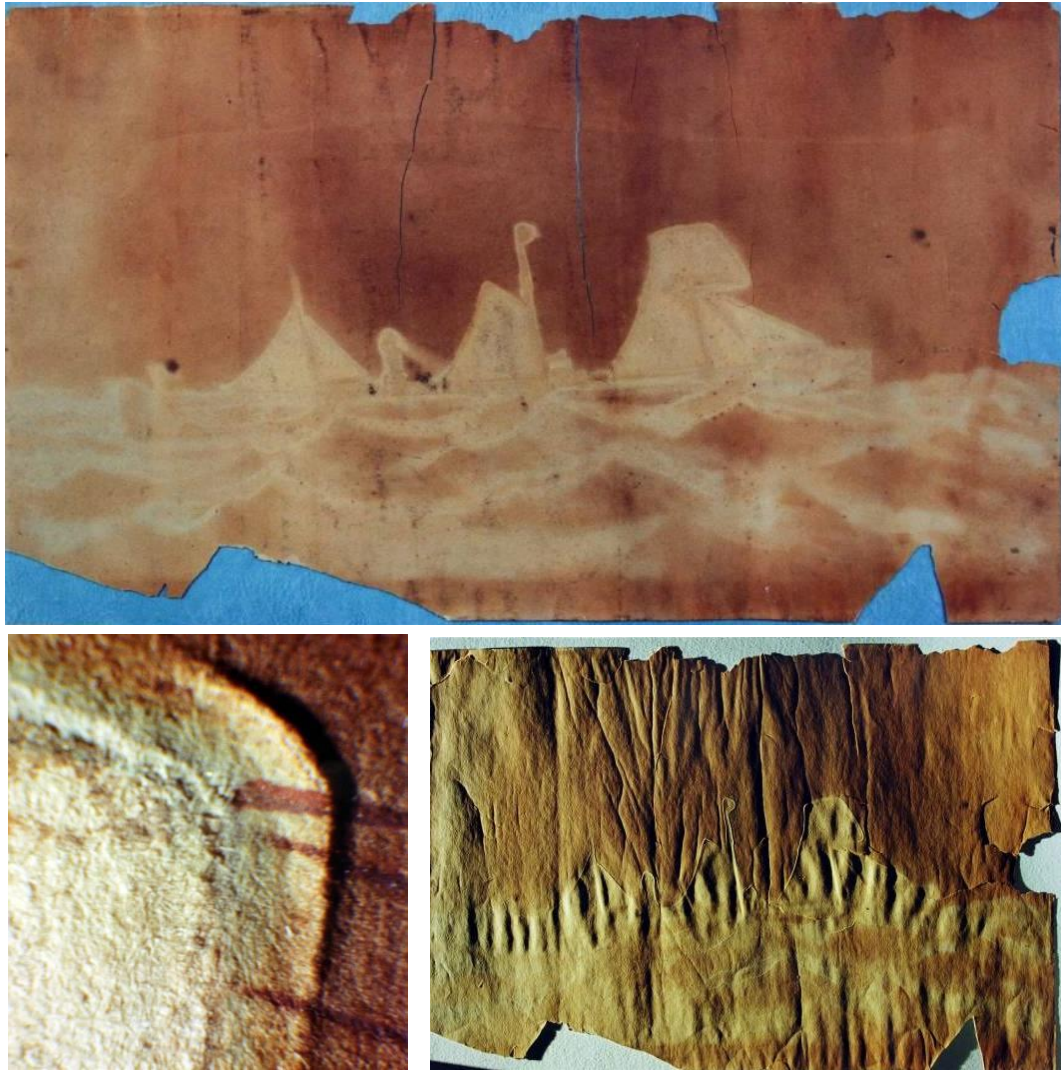
Figure 4.6 Top: Reflected light photograph in reflected light of the verso of *S.S. Buda* by George Thomson, 1889. **Lower left:** Photomicrograph of ridge present between dark and light paper areas. **Lower right:** Raking light shows distinct differences in expansion rates of paper at pigment/paper interface. Image credit: Colin Liddie.

While the absorption of UV light is beneficial for paper by preventing photolysis, it can increase the conductivity of the surface of zinc oxide particles. When illuminated by UV light, conductivity on the surface of the pigments increases and persists after the light source is removed. It has been suggested that this effect derives from UV-induced desorption of oxygen from the surface (Mollow, 1956; Bao *et al.*, 2011). This would leave a singly ionised oxygen vacancy, acting as a shallow donor and contributing electrons to the conductance band, immediately increasing conductivity and continuing to do so until the vacancy degrades to the

neutral state. Importantly, this desorption can occur even in the presence of 'white' or visible light without a UV component (Gurwitz, Cohen and Shalish, 2014). The effect of this desorption is a positive charge forming on the surface of particles, pulling electrons out of the bulk of the pigment crystallites onto the surface and allowing for better catalysis of degradation reactions (Kumar and Rao, 2015).

4.2.3 EFFLORESCENCE: ZINC SULPHATE SALT FORMATION

In the presence of atmospheric sulphur dioxide pollution, zinc oxide can convert to zinc sulphide which readily oxidises in the presence of hydrogen peroxide to form soluble zinc sulphate salts ($ZnSO_4$) (Singer and Liddie, 2005; Ebert, Singer and Grimaldi, 2012). This can lead to efflorescence,[79] a phenomenon which occurs when salts migrate from the bulk of a material to the surface, forming a deposit. These salts deposit onto the surface of the artwork or dissolve in the presence of moisture and spread outward into the surrounding substrate. This sometimes leads to the formation of white halos around pigmented areas (Colbourne, 2006).

A clear example of efflorescence is illustrated once more by Singer and Liddie (2005). Very light halos are observed around the sails which were originally painted with a white pigment, extending all the way to the ridges previously described (Figure 4.7).

---

[79] The term derives from the French root meaning 'to flower out.'

Figure 4.7 *S.S. Buda* by George Thomson reflected light photograph of 'halos' where paper is lightest around white pigment area. Image credit: Singer & Liddie, 2005.

Samples from the ridges were analysed with Energy-dispersive X-ray (EDX) spectroscopy and found to contain zinc and sulphur, whereas surrounding unpigmented paper only contained very small amounts of sulphur and no zinc, indicating they were likely caused by solubilised zinc sulphate salts. No pigment remains in these areas and they appear to derive their tone solely from the paper, though the presence of zinc sulphate salts and the effects of UV screening indicate that they were originally painted with a zinc oxide pigment (Singer and Liddie, 2005).

4.2.4 OTHER FACTORS INFLUENCING CHEMICAL REACTIONS

In addition to previously mentioned physical and optical properties, pH can affect the rate of reactions taking place on zinc oxide surfaces. Pardeshi and Patil (2008) studied the efficiency of phenol degradation in aqueous solution by zinc oxide photo-catalysed radicals and peroxides and found that the reactions were most

efficient when illuminated by natural sunlight and when the solutions were slightly acidic or neutral. These pH conditions are typical of aged paper objects and optimal for photocatalytic reactions on zinc oxide particles.

It is also possible that the binding medium and paper play an active role in the perpetuation of hydrogen peroxide formation. Markham and Laidler (1953) investigated hydrogen peroxide production from zinc oxide in the absence and presence of various organic compounds. They concluded that organic materials were required to remove hydroxyl groups which, when present in high concentrations as they prevented the further production of hydrogen peroxide. The amount of peroxides produced was much higher in the presence of the organic compounds[80] than if only water was used. In the latter, peroxide formation would slow to a halt in the presence of vapour, only resuming with the re-introduction of liquid water.

The photo-excitation of electrons to the conductance band in the presence of a carbon-containing molecule can remove oxygen ions from the crystal lattice at room temperature (Bonosewicz, Hirschwald and Neumann, 1986; Bao *et al.*, 2011; Gurwitz, Cohen and Shalish, 2014). Gaseous, atmospheric carbon dioxide and monoxide can remove oxygen ions from zinc oxide's polar surfaces when illuminated by wavelengths of light as long as 500-650 nm (Gurwitz, Cohen and Shalish, 2014). This means that illumination by UV-filtered visible light could potentially initiate reactions on zinc oxide surfaces as the pigment particles are typically exposed to the air, unlike oils which can be varnished. Visible wavelengths of light can also induce electron exchange between organic dyes or coloured metal

---

[80] Organic compounds included resorcinol, phloroglucinol, phenol, catechol, toluene, benzene, chlorobenzene, acetanilide, aniline, quinone, and hydroquinone.

ions and zinc oxide, facilitating superoxide formation and exacerbating degradation of paper (Thomas, 2012).

4.3 METHODOLOGY

There are three degradative processes that occur in paper:

- **Hydrolytic degradation:** According to standard reaction-kinetic principles, the rate of the hydrolytic process is determined by the temperature, the acidity (pH value), and the amount of moisture present in the paper. The moisture content is again dependent on the (relative) humidity in the storage/display environment (Porck, 2000). This process at low pH levels can lead to chain scission via β-elimination of the glucosidic bond connecting glucose units in cellulose (Daruwalla and Narsian, 1966; Feller, 1986).

- **Oxidative:** characterised by the conversion of hydroxyls on cellulose to ketones and carbonyls via reactions with surrounding materials

- **Thermal degradation:** additional oxidative and hydrolytic degradation, particularly discolouration of hemicelluloses, can be induced thermally (Lee & Feller, 1986).

This study is only concerned with oxidative and hydrolytic processes, not thermal as the reactions taking place due to zinc oxide involve moisture, UV light, peroxides and radicals which oxidise the cellulose. Thermal ageing would therefore be inappropriate. The principle reaction concerned in this study is therefore oxidative: however, given the participation of moisture in the ageing regime outlined below, hydrolytic reactions must be accounted for.

To understand the photo-oxidation of paper in the presence of zinc oxide, the following three papers were used as substrates:[81]

- Whatman #1 filter paper: regarded as a 'standard' in paper studies because of its pure cotton content and lack of size, though it does not resemble papers used historically for watercolours (Daniels, 2001).

- Fabriano cotton rag watercolour paper: contains fillers and is highly sized. This paper more closely resembles nineteenth-century high-quality watercolour papers.

- Folio paper: mixed-fibred lower-quality handmade paper with high lignin content. This paper will allow for study of zinc oxide reactions on cheaper papers, as were sometimes used by artists such as Turner and Ruskin. It will also provide some indication of how oxidative reactions occur alongside hydrolytic reactions and to what extent they influence one another.

4.3.1 LIGHT-INDUCED DETERIORATION OF MOCK-UPS

Zinc oxide watercolour paint on paper was humidified and exposed to bright light to induce photocatalytic reactions and the formation of peroxides and radical species. Samples were then compared to a control to study the detrimental effects on the degradation of the paper substrate and binding medium.[82]

---

[81] For results of paper analysis and data indicating fibre types and presence of fillers, refer to Appendix 11: Analysis of Mock-Up Papers.

[82] In this way, hydrogen peroxide is the 'critical product' formed during photo-oxidative reactions on zinc oxide surfaces (Fromageot & Lemaire, 1991). Singh, Saha and Pal (2015) found hydrogen peroxide conforms to Feller's (1992) criteria for a critical product: the material must 1) change measurably at an early stage of the degradation process, 2) change in a dramatic way near the 'time of failure' or during a critical point in degradation, and 3) must change predictably throughout the entire ageing regime.

Mock-ups for this experiment were created following the methodology outlined in

section 1.2.1 Creation and Study of Mock-Ups[83]. Samples were exposed to light in a

Q-SUN Xenon Test Chamber Xe-1 light ageing machine with a xenon arc lamp

tungsten bulb (1800W). The temperature inside the machine was moderated at 25°

C. Two UV filters were used, a Daylight Q and Window Q filter, which approximate

indoor conditions and restrict the UV light present. The machine was calibrated to

1.1 W/m^2 at 420 nm (Figure 4.8).
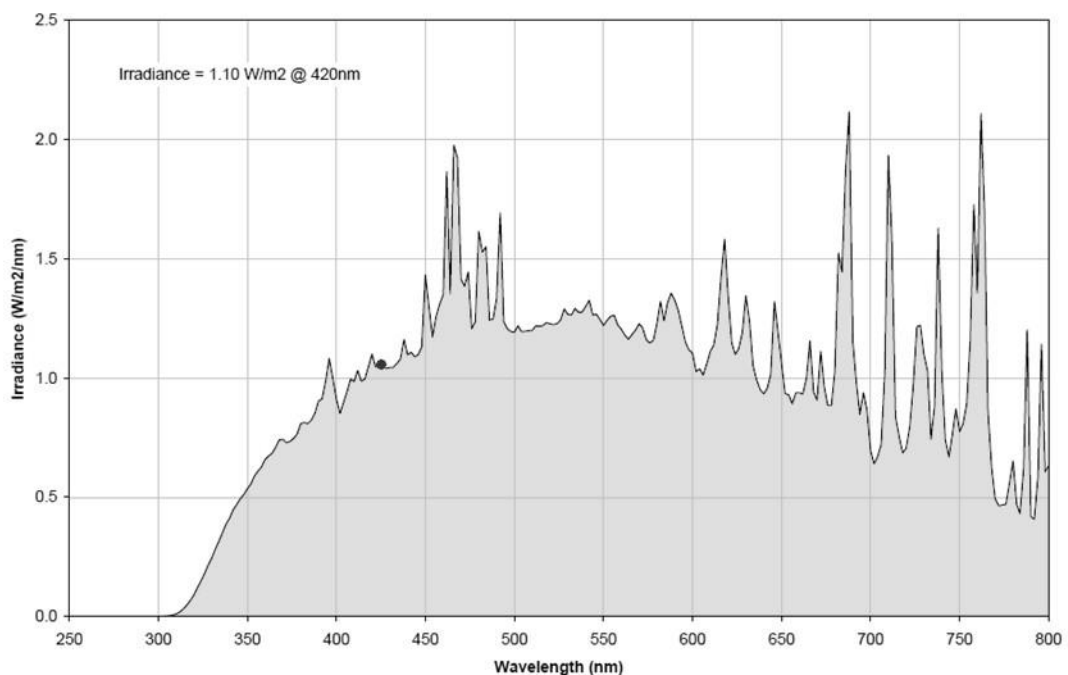
Figure 4.8 SPD (Spectral Power Distribution) for the lamp in the Q-Sun light ageing machine
after application of Daylight and Window-Q filters and after calibration of instrument to 1.10
W/m^2 at 420 nm (black dot). Grey area under curve represents total irradiance. Image
modified from Q-Sun Technical Bulletin LX-5056.

Mock-ups were exposed to moisture over a layer of Gore-Tex® which allowed

gradual humidification from a triple layer of dampened Whatman #1 filter paper. All

test samples were exposed to a total of 50 hours of light[84] in 5-hour increments, with

---

[83] Page 7.

[84] Based on experiments by (Singh, Saha and Pal (2015). By replicating the author's exposure levels
in the presence of moisture, peroxide formation was assured in the time allotted. For calculations and
rationale behind ageing timescale, refer to Appendix 12: Light Exposure Rationale.

re-wetting of Whatman paper occurring between each exposure. Samples were dried overnight between increments. This was partly out of necessity as the light ageing machine could not be run overnight but would also induce deterioration to the paint layer by expanding and contracting the paint layer and paper substrate.

Light exposure was measured by the total irradiance imparted to the test site. Irradiance is defined as the watts per metre squared imparted to a surface. A watt is a joule per second and describes the energy imparted to an object over time. As it is a standard scientific unit[85], it is a more widely-accepted and specific measurement of light energy than lux, a unit commonly used by conservators for recommending display conditions[86].

Previous studies indicate that cellulose in paper begins to deteriorate immediately upon exposure to light (Lee, Bogaard and Feller, 1989). Additionally, reaction of organic materials from zinc oxide's photocatalytic by-products is logarithmic, as demonstrated by Singh, Saha and Pal (2015), who found that 40% of a methyl red dye had reacted with peroxides formed after 10 minutes exposure at 365 nm, with the percentage dropping every 10-minute increment thereafter. By exposing samples to similar irradiance levels of irradiance as those used in this experiment, reactions between zinc oxide, water and the paper substrate was guaranteed.

---

[85] Known collectively as the International System of Units.

[86] Additionally, spectral irradiance, or the irradiance per nanometre of light, can describe the total energy in Joules over time imparted to a material from a specific wavelength range. For this study, 17,863 joules of energy were imparted over all wavelengths, while the energy imparted by UV light was 1757.16 Joules. By multiplying irradiance, which is Watts/metres2, or joules/seconds x metres2, by pigment area (metres2) and seconds, those units cancel out and what remains is joules. For a discussion of lux vs. irradiance and a justification for the use of irradiance rather than lux in this study, refer to Appendix 13: Lux vs. Irradiance.

4.3.2 RUSSELL-GRAMS

Russell-grams were created using a similar methodology to Liddie (1998), a method originally outlined by William J. Russell who also contributed to the Russell and Abney report in 1888. It involved exposing sensitised film to reaction by-products, particularly peroxides which in turn reduced the silver nitrate in the film resulting in an image corresponding to areas of degradation (Russell, 1908; Daniels, 1986).

Method: In the photographic dark room in absence of light, Kodak lithographic film was sensitised in a 1.5% ammonium hydroxide solution after which it was air-died in a light-sealed box for 2-3 hours, then blow-dried. Continuing in the dark and using the Kodak box as a guide for placement, the lithographic film was positioned emulsion-side-down over the zinc oxide light-exposed samples. A lead sheet ensured good physical contact between the film and the samples and the box was sealed (Figure 4.9).
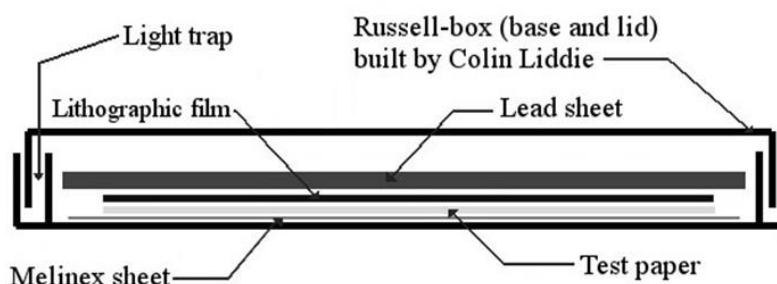
Figure 4.9 Russell-gram set-up.

After 36 hours, a 1:1 mixture of Kodak Xtol developer with water was prepared alongside a 1:4 solution of Structurix fixative with water. The film was carefully removed from the Russell-box in the dark then transferred to the developer which was then agitated for 6 minutes, followed by 2 minutes in the fixative solution. Finally, the film was rinsed in water for 15 minutes, with the light turned on after the

first minute. The resulting image on the film was starkly contrasting and mapped the hydrogen peroxide formation clearly.

4.3.3 VISUAL COMPARISONS AT MAGNIFICATION

Both control samples and mock-ups were imaged at 6.3x and 12.5x magnifications with a Leica S6D microscope with microscope-mounted Leica MC170 HD digital CCD camera to track visible changes such as paper discolouration and paint cracking after light exposure.

4.3.4 COLORIMETRY

A Konica Minolta CM-2600d portable spectrophotometer was used to collect $L*a*b*$ values[87] for the pigmented areas and verso for all control and test samples. Both SCI and SCE[88] values were collected, but only SCI values were analysed as they include both diffuse and specular wavelengths, meaning values are independent of surface texture effects on $L*a*b*$ values. Three readings were taken at different points within the pigmented area then averaged. Similar readings were taken of aged paper with only gum arabic applied to gauge the influence of discolouration on colour change in the pigment layer. Data were collected using standard illuminant D65 at a viewer angle of 10°, the illuminant representing average midday light in Western Europe[89] and the angle appropriate for wide-field viewing.

Colour change ($\Delta E*$) values were calculated from CIE 1976 $L*a*b*$ values using Equation 4.1 provided by Buxbaum and Pfaff (2005):

---

[87] These values are part of the CIELAB or CIE 1976 $L*a*b*$ colour space and describe lightness, $*L$, position between red and green, $a*$, and position between blue and yellow, $b*$.

[88] SCI stands for Spectral Component Included, while SCE stands for Spectral Component Excluded.

[89] This is a very common standard illuminant used in colour analysis, despite the odd specificity of the light source being approximated.

$$\Delta E^* = \sqrt{(\Delta L *)^2 \; + \; (\Delta a *)^2 \; + \; (\Delta b *)^2} \qquad\qquad (4.1)$$

4.3.5 SPECTROPHOTOMETRY

Semiconductor absorption spectra always contain an absorption edge, defined by the part of its spectrum where a sudden shift occurs from high to low absorption percentage, plotting a nearly vertical line. This shift typically begins at around 3.20 eV or 387 nm for pure zinc oxide substances (e.g. Viezbicke *et al.*, 2015). The location and slope of this edge shifts with degradation or with annealing and can indicate whether either has occurred (Khorsand Zak, Ebrahimizadeh Abrishami *et al.*, 2011; Viezbicke *et al.*, 2015). Additionally, optical band gap widths can be obtained from the absorption edge when converted to Tauc plots (Tauc, 1968). A Tauc plot fits a linear regression to the absorption edge, extending this fit line to the x-axis to determine the energy of the material's band gap via the x-intercept.

Tauc plots determine band gap energies by plotting the absorption coefficient multiplied by energy then squared for direct band gaps[90] ($(\alpha h v)^2$) on the y-axis against wavelength energy (eV). The absorption coefficient is calculated from the Kubelka Munk theory and utilises variables including the thickness of the paint film and the reflectance of the substrate and a white and black substrate (Tauc, 1968; Krithiga, Sankar and Subhashree, 2014; Wells, 2015). However, the paint used in this study is on paper, and it does not have a readily measurable thickness as it both sits on top of and sinks in between the paper fibres. To approximate a band gap value for comparison between samples and avoid complications presented by calculating an absorption coefficient, measured absorption percentages were used

---

[90] A direct band gap occurs when an electron can directly emit a photon upon relaxation. Electrons in materials with indirect band gaps must transfer momentum to the crystal lattice and cannot directly emit photons. Calculating the power for the Tauc plot y-axis changes depending on the band-gap of the material.

for y-values assuming a consistent influence of the substrate as the paint was applied consistently using the same recipes and number of brushstrokes for each sample. Differences between samples would be minimal in the part of the spectrum being studied given zinc oxide's strong absorption in the UV and given the purity of the pigments. Data derived from this method are comparable within the data set and appropriate as an approximation of band gap changes due to degradation processes.

Reflectance spectra were measured using a Hitachi U-3010 spectrophotometer with integrating sphere. Spectra were all in excellent agreement when taken from multiple locations, so rather than averaging spectra, the spectrum with the strongest return per sample was chosen for analysis. The following settings were used when operating the spectrophotometer:

- Wavelength range: 300-1400

- Scan speed: fast (sufficiently smooth signal produced)

- Scan mode: single

- Detector: External2detector

- Slit width: 5 nm

- White reference: barium sulphate powder

To find the best approximation of the band edge slope, the steepest point of the absorption edge was determined using the first derivative of the spectrum which produced a peak at the steepest point (Khorsand Zak, Razali, *et al.*, 2011). The following MATLAB code was used to convert reflectance spectra to absorption, then find the steepest point:

```
%convert y to absorption
y = 100-y;

%find derivative of line
dy = diff(y)./diff(x);

%plot y derivative over x, with x adjusted for derivative (+- 0.5
%error value given derivative method)
plot(x(1:end-1),dy)
```

Then four points to either side of this y-value were used to fit a line extending to the x-axis in Excel. Solving the equation for this line when y = 0 gave the x-intercept.

The intercept values along with their error ranges[91] were then plotted together to determine if changes in band gap had occurred after light exposure or if certain samples may have undergone annealing during the production process.

4.3.6 ELEMENTAL MAPPING AND POINT SCANS WITH ENERGY-DISPERSIVE X-RAY (EDX) SPECTROSCOPY

The distribution of zinc and oxygen ions in case studies and powder samples before and after light exposure were measured using an Oxford Instruments X-Max 150 EDX detector mounted on a TESCAN MIRA3 scanning electron microscope (SEM). The area of interest was focused upon using the SEM and secondary electron (SE) imaging at a beam intensity of 10kV. Magnification varied from sample to sample as particle sizes required a range of magnifications.

Mapping: Images were acquired using the computer program Aztec then the area of interest was mapped. Maps were collected for each sample as the image dictated.

---

[91] To determine the error for this line, the standard error for a sample population was calculated in Excel then multiplied by 1.96 to obtain a confidence level of 95%.[91] Equation 4.2 was used to calculate standard error:

$$SE = \sqrt{\frac{p(1-p)}{n}} \tag{4.2}$$

This calculation was necessary in that the value derived is an extrapolation. It is a value derived from a fitted line and will have associated error as a result.

They were acquired as verification and visualisations of EDX point scans. Settings were adjusted as needed. [92]

Point scans (EDX): 6-7 points were scanned in a line down the centre of a mapped crystallite. This was to obtain a ratio of oxygen to zinc ions along the length of the crystal, indicating any changes towards the poles. Additional scans were taken if other faces were seen which evolve oxygen at similar rates to the polar faces (Newberg *et al*., 2018; Jacobs *et al.,* 2017; Niskanen *et al*., 2013). All point scans were in count mode with a count set at one million.

Point scan data was allocated position values from 0-1 and assigned values in relation to the 0 and 1 points. The point with the highest oxygen percentage was assigned 0. If the 1 point was 500 pixels from the 0 point, then a point 300 pixels from the 0 point would be assigned a value of 300/500 or 0.6.

4.4 RESULTS

4.4.1 RUSSELL-GRAMS

Only Russell-grams of samples on new Whatman paper were clear enough to differentiate between pigmented areas and paper. The naturally aged Fabriano and Folio papers imaged black, meaning the paper itself likely generated a lot of peroxides and free radicals after light exposure.

Of the samples on paper, only samples 1, 3, 6, 7, 15 and 16 yielded clear results[93], and all but *direct* method samples 6 and 7 showed signs of peroxide formation on

---

[92] For information on exact image acquisition settings in Aztec, refer to Appendix 14: Elemental Mapping Supplemental Information.

[93] Samples 4 and 9 were not included in the Russell-gram samples and subsequent Russell-grams failed due to faulty film. As the film can no longer be purchased, samples 4 and 9 were not studied using this technique and should not be ruled out as potentially reactive.

the surface. Both *indirect* and commercial pigments showed signs of significant

peroxide formation after light exposure (Figure 4.10).
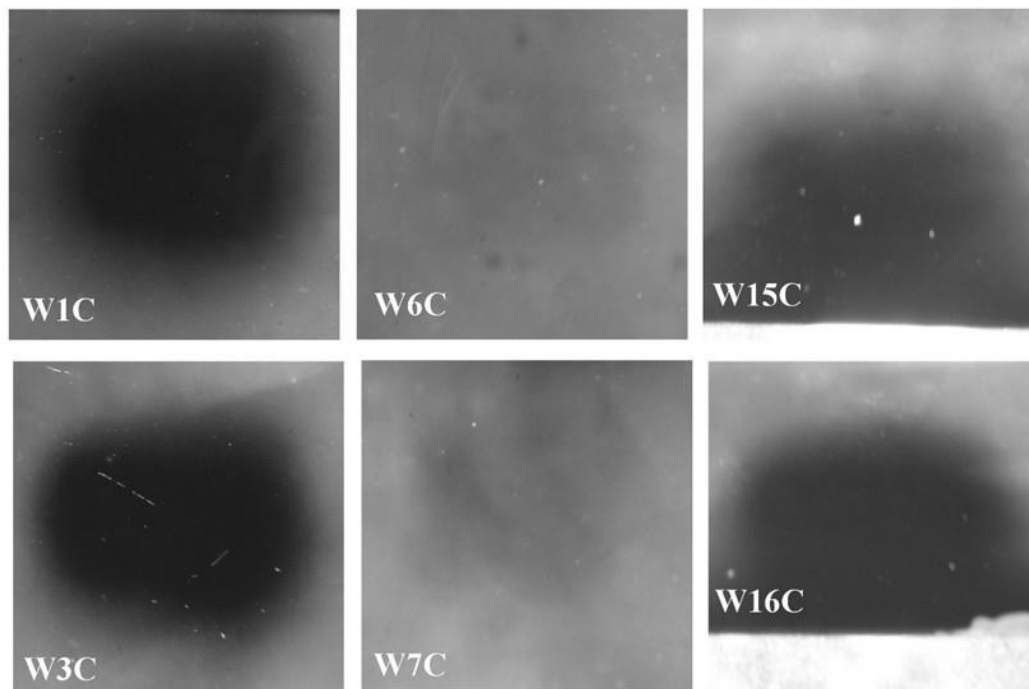
Figure 4.10 Russell-gram results, with dark areas representing exposed film. **Left column:** *indirect* method samples 1 and 3, **central column:** *direct* method samples 6 and 7, and **right column:** commercial pigments 15 and 16, all on Whatman paper in gum arabic binding medium.

4.4.2 VISUAL COMPARISONS

Mock-ups: Browning of the paper adjacent to the applied pigments after prolonged

light exposure was observed in all samples painted onto Whatman paper (W) except

for *indirect* sample 1. None showed cracking in the paint layer (Figure 4.11).

Browning on the verso of papers was most severe for *indirect* sample 4 on Whatman

paper. (Figure 4.12).
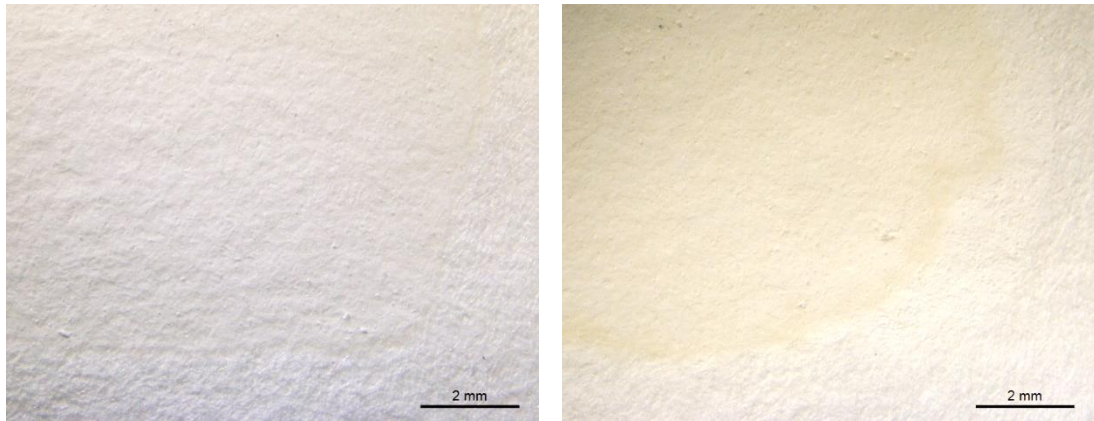
Figure 4.11 *Recto* of *indirect* sample W3C **left:** before light exposure and **right:** after light exposure. Magnified 6.3x and photographed in same light at same distance from light source.
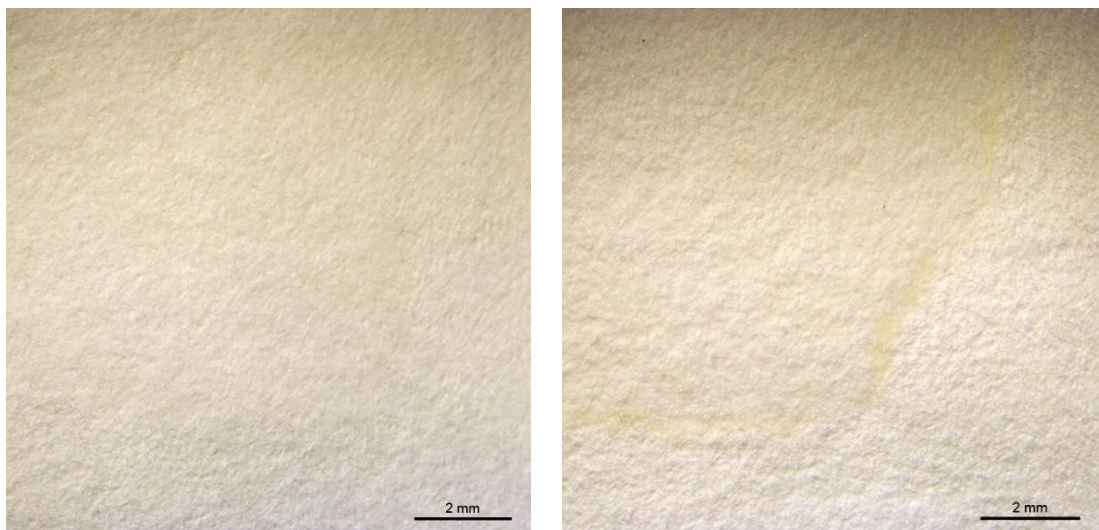
Figure 4.12 Verso of *indirect* sample W4C before light exposure (left) and after light exposure (right). Magnified 6.3x and photographed in same light at same distance from light source.

The paint films of all samples painted onto Fabriano paper (F) except for commercial sample 15 cracked after light exposure, indicating some shrinkage and loss of flexibility (Figure 4.13).
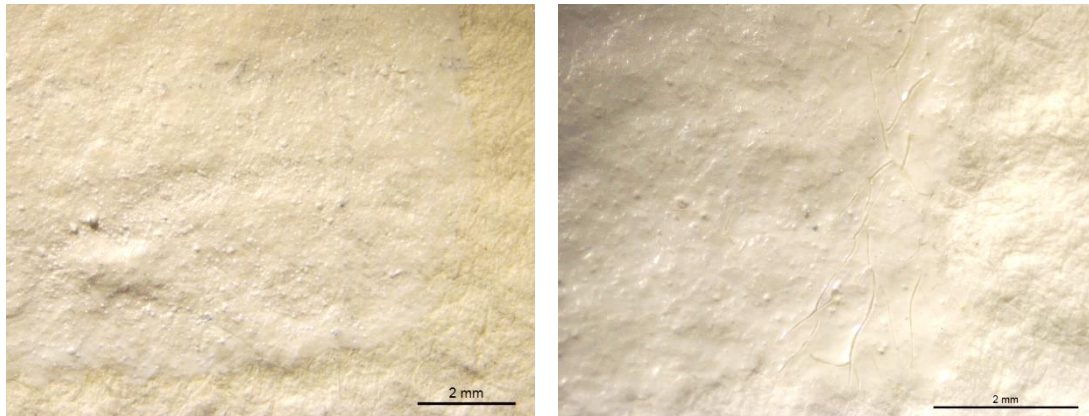
Figure 4.13 *Recto* of *indirect* sample F3C **left:** before light exposure and magnified 6.3x and **right:** after light exposure, magnified 12.5x. Photographed in same light at same distance from light source.

All samples painted onto Folio paper (B) cracked after light exposure. *Direct* method sample 7 showed browning underneath the entire painted surface (Figure 4.14). *Indirect* method samples 1 and 3 contain brown tidelines which were probably formed from over-wetting of the surface during light exposure, transferring discoloured degradation products to the wet/dry boundary. While discolouration in commercial sample 16 appears to be like the discolouration in Whatman samples, it may also be a result of tidelines from over-wetting.
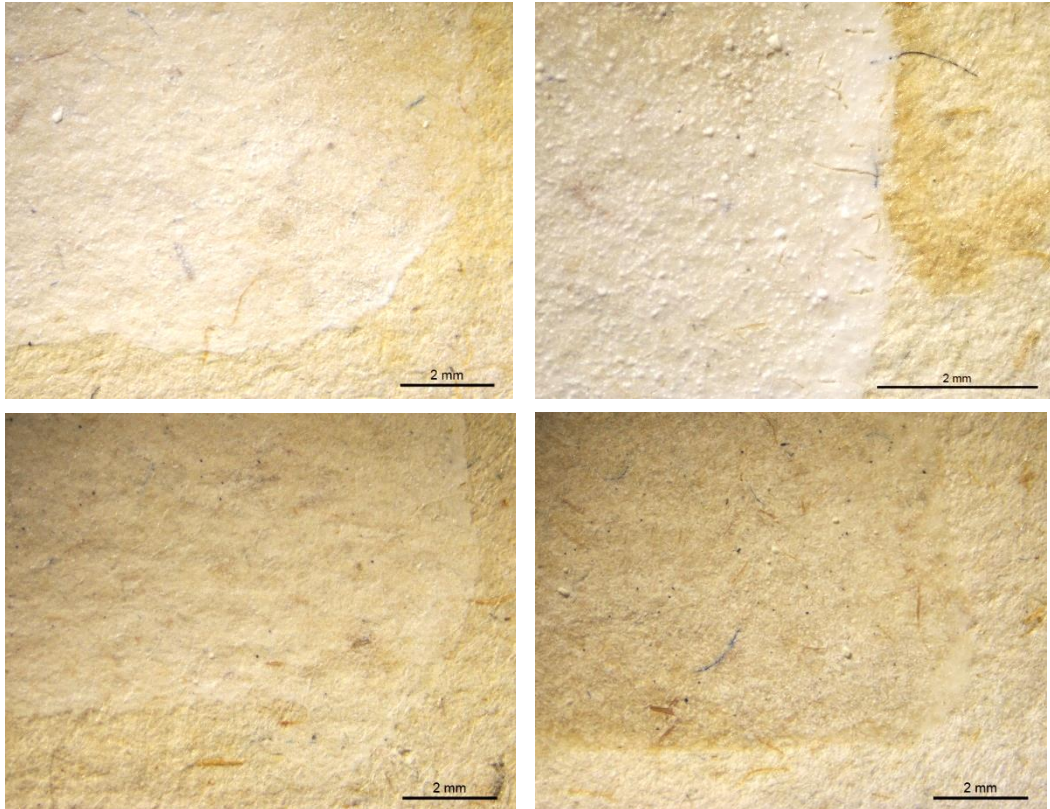
Figure 4.14 Upper left: *Indirect* sample B3C before light exposure and **upper right:** after light exposure. **Lower left:** *Direct s*ample B7C before light exposure and **lower right:** after light exposure. Photographs on left and bottom right taken at 6.3x magnification, on top right at 12.5x magnification, all photographed in same light at same distance from light source.

Gums painted onto all paper types did not appear to change considerably after ageing. Fabriano and Folio papers still bleached and Whatman papers did not appear to change.

Case studies: Of the naturally-aged case studies visually examined for signs of deterioration, two contained no noticeable changes due to zinc oxide pigments: Thomas Harper's *View of the River Coquet* and the late-nineteenth century ruin drawing. Two others, *S.S. Buda* by George Thomson (Figure 4.15) and *General view of St. Mary's Cathedral, Iona* (Figure 4.16) had undergone extensive zinc sulphate salt conversions which resulted in very little original pigment remaining in the pieces.
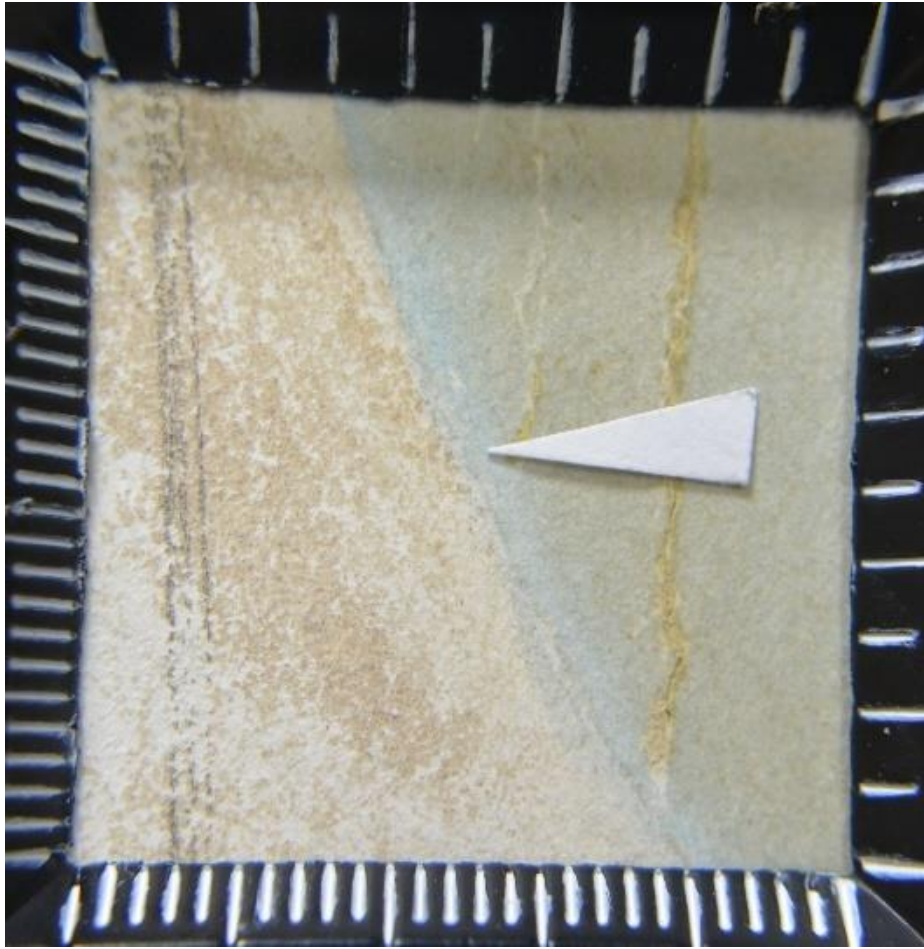
Figure 4.15 Detail from *S.S. Buda* showing sail area where all pigment is lost. Solubilised zinc sulphate salts have also caused light halo to remain around the lost pigment area, indicating it may have provided some protection from deterioration.

Figure 4.16 Zinc sulphate salt crystals can be seen sitting on top of the painted area on the left side of this detail of *General view of St. Mary's Cathedral, Iona*. The right side of the paper has been protected by a frame or window mount and maintains some of the original zinc oxide pigment.

Irene Kendall's *Bouquet of Flowers* primarily experienced loss of paint through cracking and tenting[94] (Figure 4.17). There is no apparent localised darkening of paper associated with the pigments, though this cannot be ruled out as the artwork has undergone conservation cleaning.

---

[94] Tenting occurs when a paint layer separates from the support, often raising up and cracking at the same time. This can sometimes resemble a tent, hence the term.
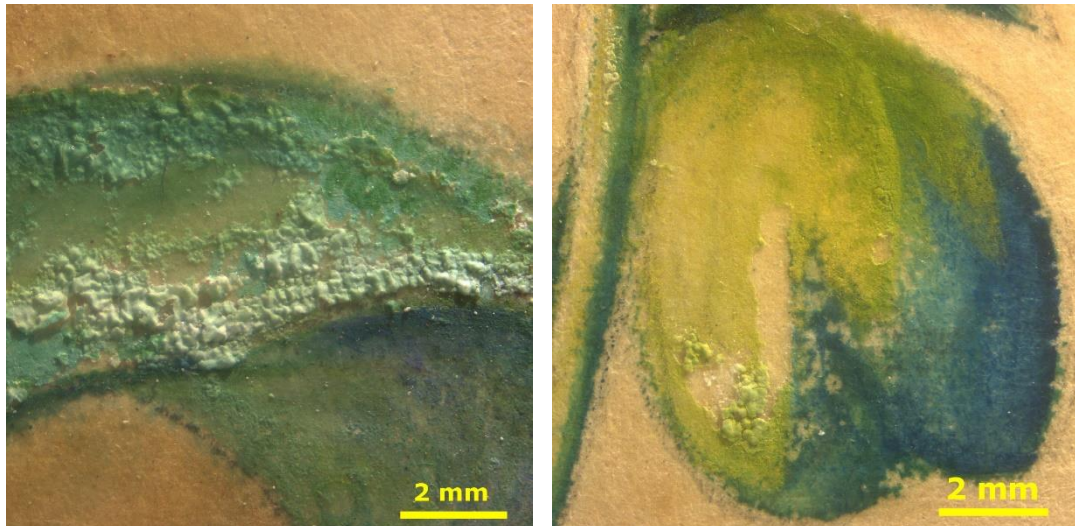
Figure 4.17 Left: tenting of white pigment areas contrasting sharply with green pigments which lay flat on the highly sized hot press paper. **Right:** losses shown near areas of tenting associated with zinc oxide application.

When the *verso* of *General view of St. Mary's Cathedral, Iona* was compared with the recto, darkened paper areas could be associated with potential areas of zinc oxide application, though little original pigment remains, rather these areas contain extensive zinc sulphate salt deposits (Figure 4.18).

Figure 4.18 Left: *Recto* view of upper right section of *General view of St. Mary's Cathedral, Iona.* **Right:** *Verso* of same area shows browning of paper in locations of white pigment application such as lake near the shore and figure and distant mountains.

4.4.3 COLORIMETRY

Most samples were bleached in the pigment areas after light exposure, as indicated by an increase in L^* value. *Direct* sample 7, however, darkened considerably after light exposure on Whatman (WC) and Folio (BC) papers. *Indirect* samples 1 and 4, and *direct* sample 9 darkened on Fabriano (FC) paper while *indirect* sample 3 darkened on Whatman (Figure 4.19). When averaged, zinc oxide areas on Folio papers increased L^* values by 1.88, Fabriano increased by 0.52, and Whatman papers by 0.067.
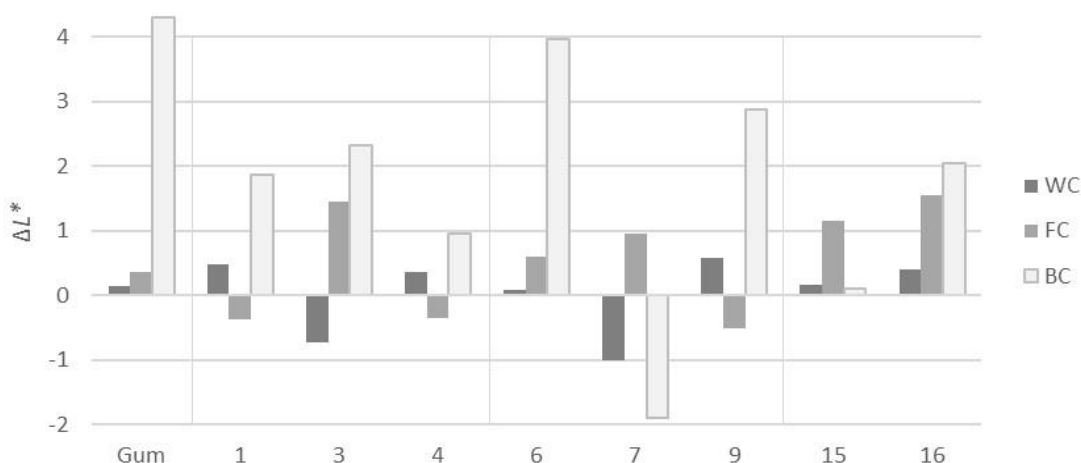
Figure 4.19 Change in lightness measured by ΔL^* for all pigment samples on all three paper substrates after light exposure. W = Whatman paper, F = Fabriano, and B = Folio paper. C indicates a gum arabic binding medium. Samples 1, 3 and 4 are *indirect* method zinc oxide pigments, samples 6, 7 and 9 are *direct* method pigments and samples 15 and 16 are commercially supplied pigments.

Significant and consistent decreases in a^* were observed and indicated a shift away from red after light exposure. Whatman gum samples , *indirect* sample 1, *direct* sample 9 and commercial samples 15 and 16 showed slightly increased a^* values (Figure 4.20).
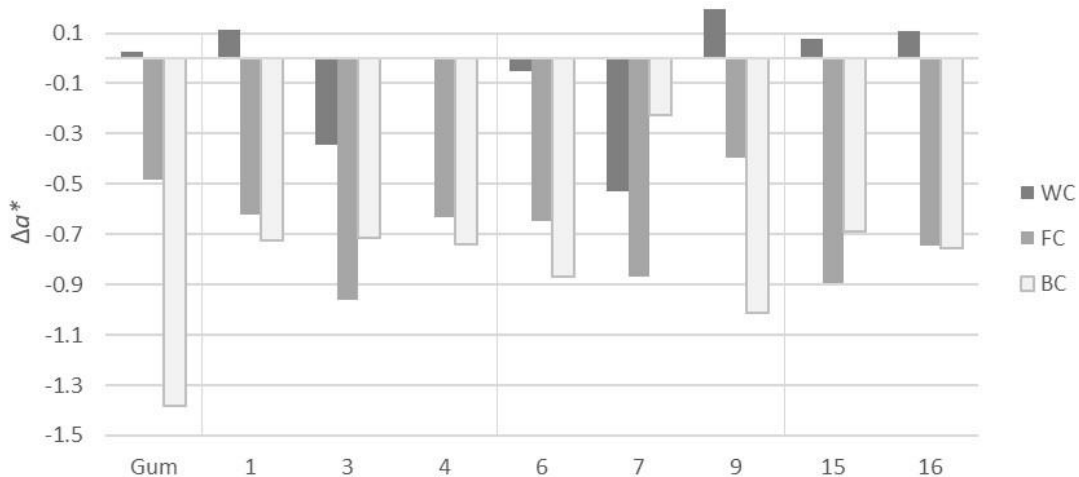
Figure 4.20 Changes in *a** for all samples on paper after light exposure. W = Whatman paper, F = Fabriano, and B = Folio paper. C indicates a gum arabic binding medium. Samples 1, 3 and 4 are *indirect* method zinc oxide pigments, samples 6, 7 and 9 are *direct* method pigments and samples 15 and 16 are commercially supplied pigments.

Whilst most samples decreased in *b** values after light exposure, *indirect* sample 3 on Whatman paper, *direct* sample 7 on Whatman and Folio paper and commercial sample 16 on Folio paper increased *b** values, which is associated with yellowing (Figure 4.21).
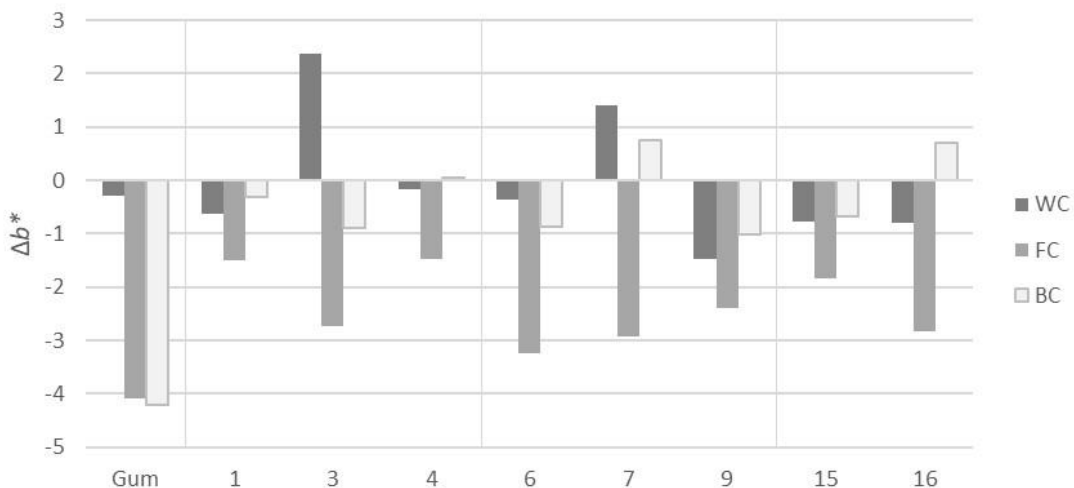
Figure 4.21 Changes in *b** for all samples on paper after light exposure. W = Whatman paper, F = Fabriano, and B = Folio paper. C indicates a gum arabic binding medium. Samples 1, 3 and 4 are *indirect* method zinc oxide pigments, samples 6, 7 and 9 are *direct* method pigments and samples 15 and 16 are commercially supplied pigments.

Pigments on Fabriano paper had the highest overall colour change as measured by ΔE ($\Delta E = 2.81$), while pigments on Folio papers changed only slightly less ($\Delta E = 2.74$), and pigments on Whatman paper changed the least ($\Delta E = 1.05$). When averaged across paper samples, ΔE values were lowest for *indirect* samples 1 and 4 and commercial sample 15 (Figure 4.22).
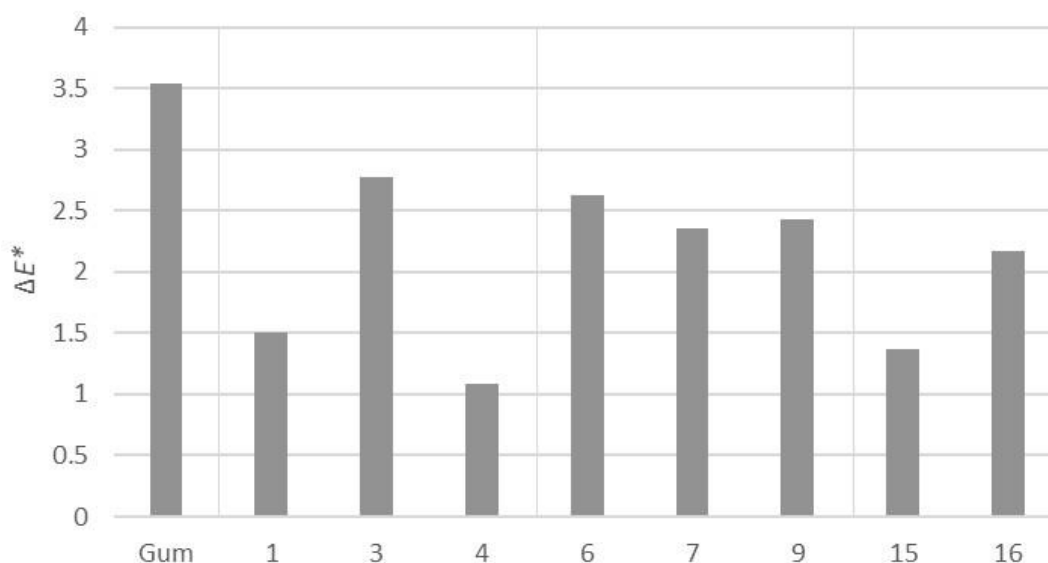
Figure 4.22 Averaged ΔE^* values from Whatman, Fabriano and Folio papers for all samples. Samples 1, 3 and 4 are *indirect* method zinc oxide pigments, samples 6, 7 and 9 are *direct* method pigments and samples 15 and 16 are commercially supplied pigments.

Case studies: colorimetry data was collected for case studies, but the results were inconclusive and not comparable to mock-ups. This was due to mixing of pigments and to differences in the paper tone influencing results.

4.4.4 SPECTROPHOTOMETRY

Band gaps extrapolated from all *indirect* and commercial pigments' absorption edges were between 3.02 and 3.12 eV while band gaps for *direct* method pigments were much less, between 2.72 and 3.02 eV for *direct* samples 6 and 7 and between 2.42 and 2.82 eV for *direct* sample 9.

Changes in the absorption edge were very different from one paper type to another, indicating likely contributions by paper and gum confounding results. The clearest trends were rather between production types (Table 4.1, Figure 4.23).

Table 4.1 Calculated band gap values and standard errors x1.96 for all reflectance spectra

Samples	W	SE	W50	SE	B	SE	B50	SE	F	SE	F50	SE
1	3.033	0.006	3.073	0.006	3.043	0.010	3.036	0.005	3.069	0.009	3.057	0.006
3	3.063	0.005	3.054	0.006	3.046	0.008	3.055	0.007	3.080	0.007	3.074	0.008
4	3.056	0.010	3.084	0.006	3.056	0.006	3.061	0.006	3.086	0.005	3.070	0.006
6	2.969	0.009	2.977	0.005	2.858	0.017	2.907	0.010	2.985	0.009	2.991	0.010
7	2.971	0.010	2.951	0.013	2.900	0.012	2.816	0.023	2.990	0.010	3.003	0.011
9	2.695	0.003	2.695	0.007	2.434	0.003	2.541	0.006	2.743	0.005	2.761	0.005
15	3.063	0.006	3.096	0.007	3.070	0.007	3.040	0.007	3.082	0.007	3.102	0.006
16	3.077	0.005	3.097	0.006	3.053	0.006	3.059	0.010	3.096	0.005	3.096	0.007

Key: W = Whatman paper, W50 = Whatman exposed 50 hours, B = Folio paper, B50 = Folio paper exposed 50 hours, F = Fabriano paper, F50 = Fabriano paper exposed 50 hours, SE = standard error x 1.96, samples 1, 3 and 4 are *indirect* method, samples 6, 7 and 9 are *direct* method, and samples 15 and 16 are commercial pigments.
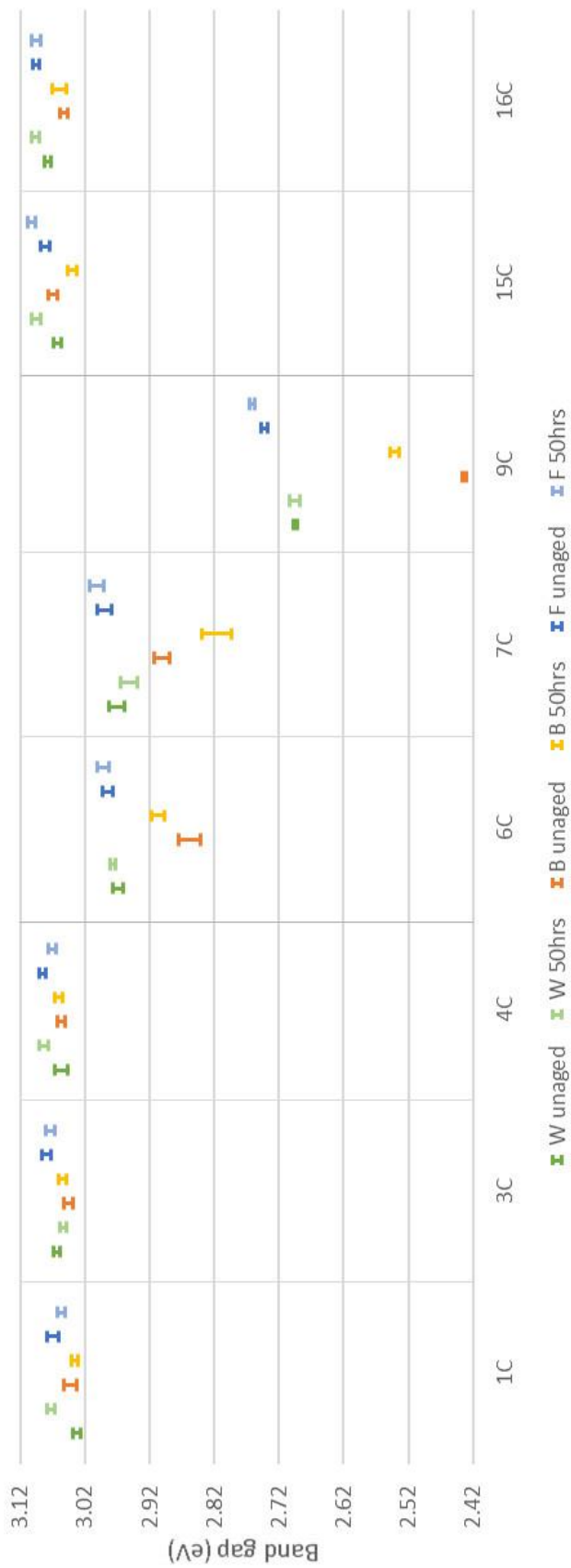
Figure 4.23 Band gap changes for all samples after 50 hours light exposure with error bars (+/- SE x 1.96). Samples 1, 3 and 4 are *indirect* method zinc oxide pigments, samples 6, 7 and 9 are *direct* method pigments and samples 15 and 16 are commercially supplied pigments.

The slopes of these absorption edges were most steep for *indirect* and commercial pigments and significantly shallower for *direct* method pigments. Unexposed pigments on Whatman paper appeared to group together according to slope steepness (Figure 4.24). Sample 16 has the steepest edge at the shortest wavelength, while samples 3, 4 and 15 are almost as steep and located at a slightly longer wavelength. Sample 1 is more gradual, then samples 6 and 7. Sample 9 is far less steep than any other sample and would intercept at a very long wavelength.
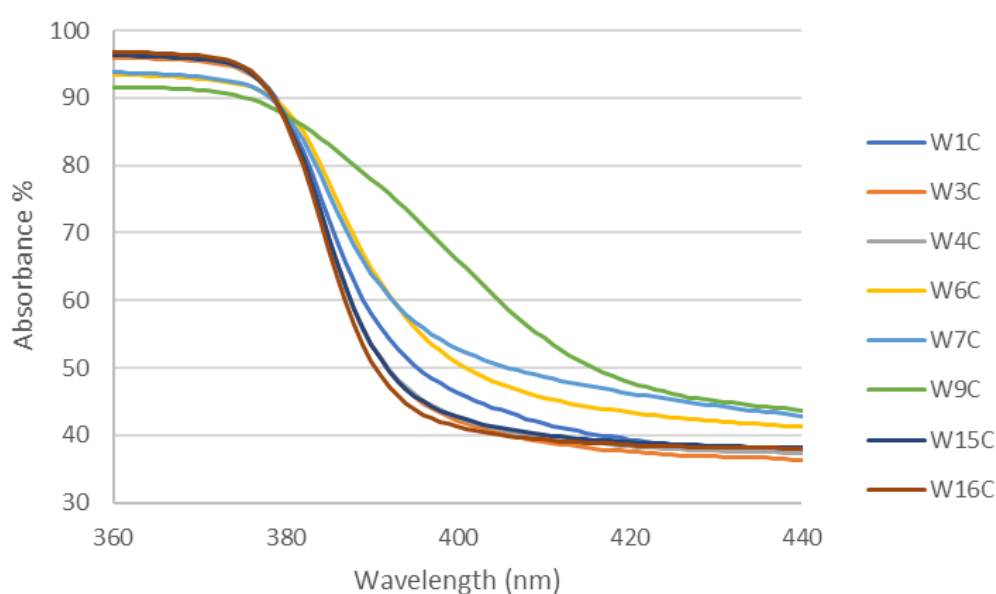
Figure 4.24 Absorption over wavelength values for all pigment samples on Whatman paper. Samples 1, 3 and 4 = *indirect* method pigments; 6, 7, and 9 = *direct* method pigments; 15 and 16 = commercial pigments.

Sample 9 had a very shallow slope across all paper samples, followed by samples 6 and 7. When comparing across paper samples, changes in steepness for each pigment sample were slightly different, though the relationship of slopes across pigments was the same (Figure 4.25).
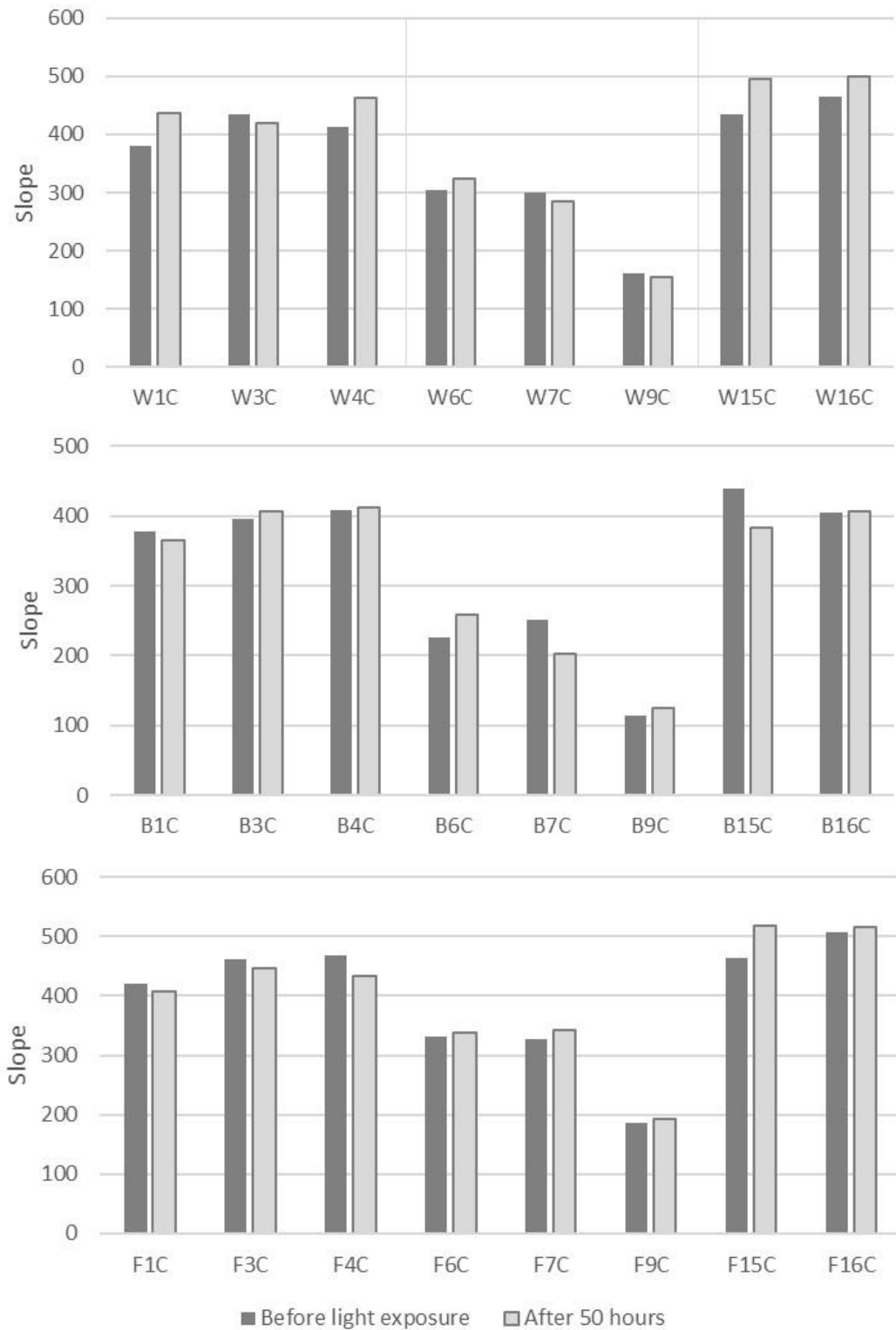
Figure 4.25 Slopes of absorption edges for all samples on Whatman paper (top), Folio paper (centre) and Fabriano paper (bottom). Samples 1, 3 and 4 = *indirect* method pigments; 6, 7, and 9 = *direct* method pigments; 15 and 16 = commercial pigments.

4.4.5 ELEMENTAL MAPPING AND EDX POINT SCANS

Overall results from EDX point scans during mapping detected no sulphur ions, meaning conversion to sulphate salts was not observed in this study. Such conversion could have been induced by the inclusion of an off-gassing sulphurous solution; however, this was not possible given the instrumentation available.

When oxygen content was plotted against position, 5 out of 8 pigment samples appeared to have an overall decrease in oxygen content after light exposure. In contrast, *indirect* sample 1, *direct* sample 9 and two of the maps from commercial sample 15 indicated an increase in oxygen content.

Measurements from *direct* method sample 7 were taken from crystallites with the same morphology. A decrease in slope occurs near position 0 and an increase near position 1 when oxygen percentage is graphed against position. Oxygen percentage decreased overall after light exposure (Figure 4.26).
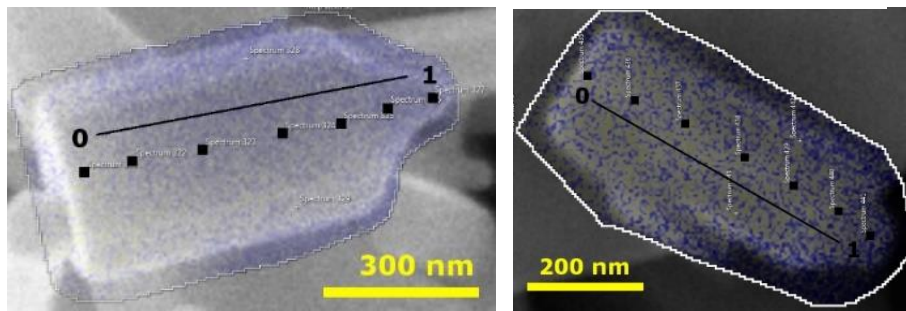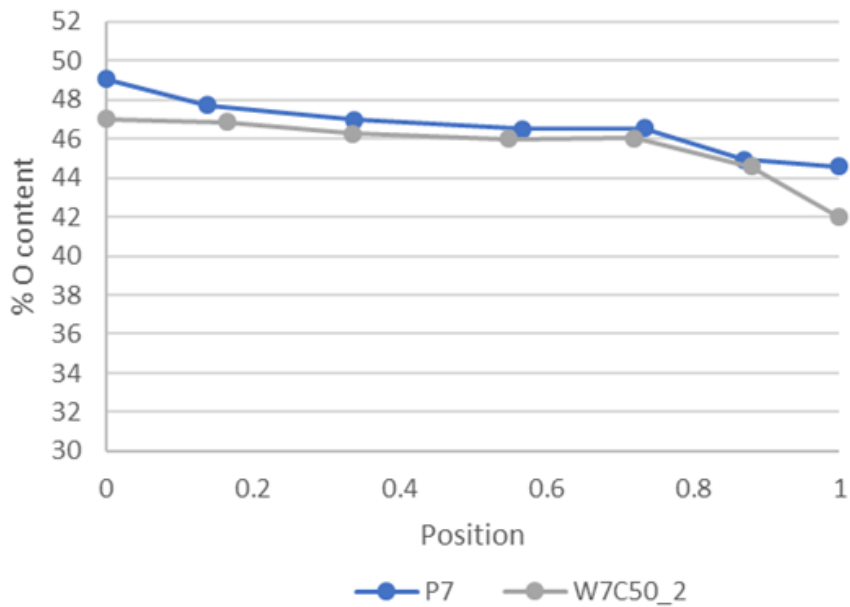
Figure 4.26 Top: Graph of oxygen content over position derived from elemental maps of *direct* method pigment 7. **Bottom left:** unexposed crystallite and **bottom right:** 50 hours exposed crystallite from Whatman paper sample W7C50_2. Oxygen in maps is indicated by yellow pixels, zinc by blue.

Unexposed and exposed crystallites from *indirect* method sample 4 also had a somewhat similar morphology and a slight decrease in oxygen content after 50 hours of exposure (Figure 4.27). The exposed crystallite had a very unusual morphology, with lots of surface variation unlike the smooth, unexposed crystallite.
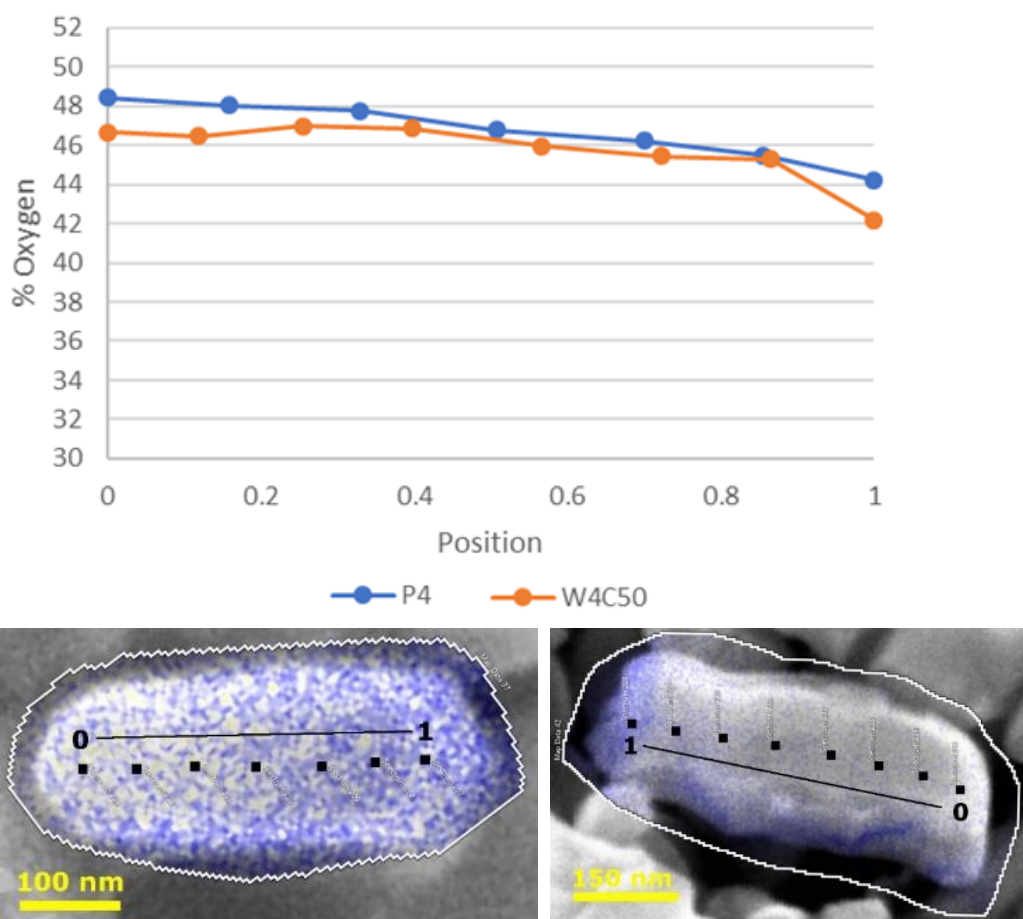
Figure 4.27 Top: Graph of oxygen content over position derived from elemental maps of *indirect* method pigment 4. **Top right:** unexposed crystallite and **bottom right:** 50 hours exposed crystallite from Whatman paper sample W4C50. Oxygen content in maps indicated by yellow pixels, zinc by blue.

Measurements from commercial sample 15 consisted of particles roughly similar in size and morphology. A pattern was seen in light exposed samples in which all had fitted lines with a shallower slope than the unexposed sample (Figure 4.28). The slope of the line for P15 was -6.22, while the slopes for exposed samples ranged from -0.91 to -4.04[95].

---

[95] W15C50 slope = -1.09, W15C50_2 slope = -0.91, W15C50_3 slope = -4.04
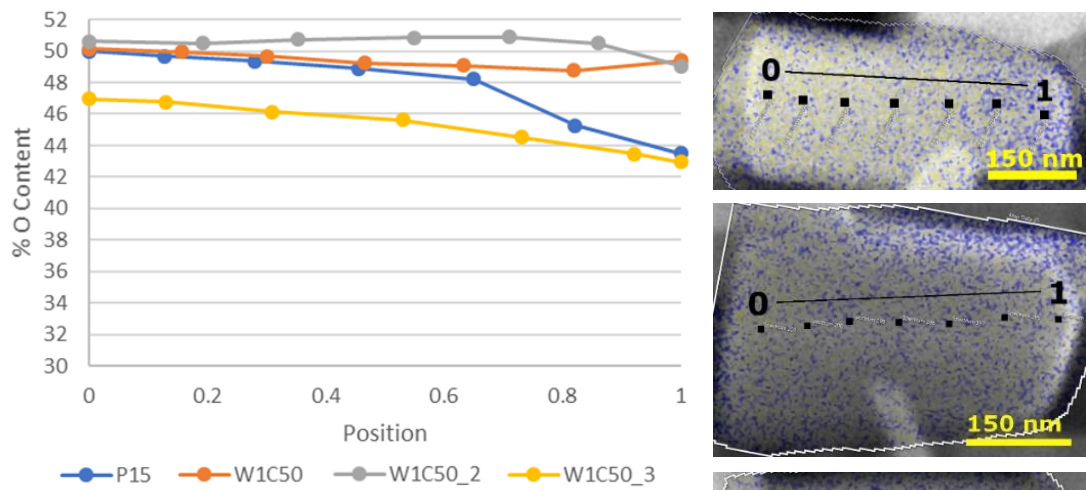
Figure 4.28 Left: Graph of oxygen content over position derived from elemental maps of commercial pigment 15. **Top right:** unexposed crystallite. Next three images are 50 hours exposed crystallites from Whatman paper samples **second from top, right:** W15C50, **third from top, right:** W15C50_2, and **bottom right:** W15C50_3. Oxygen in maps indicated by yellow pixels, zinc by blue.

Indirect sample 1 followed an opposite trend than commercial sample 15 when fitted line slopes were compared. The unexposed slope of P1 was -1.6, while the exposed slopes were -2.57 for sample W1C50 and -2.53 for sample W1C50_2 (Figure 4.29).
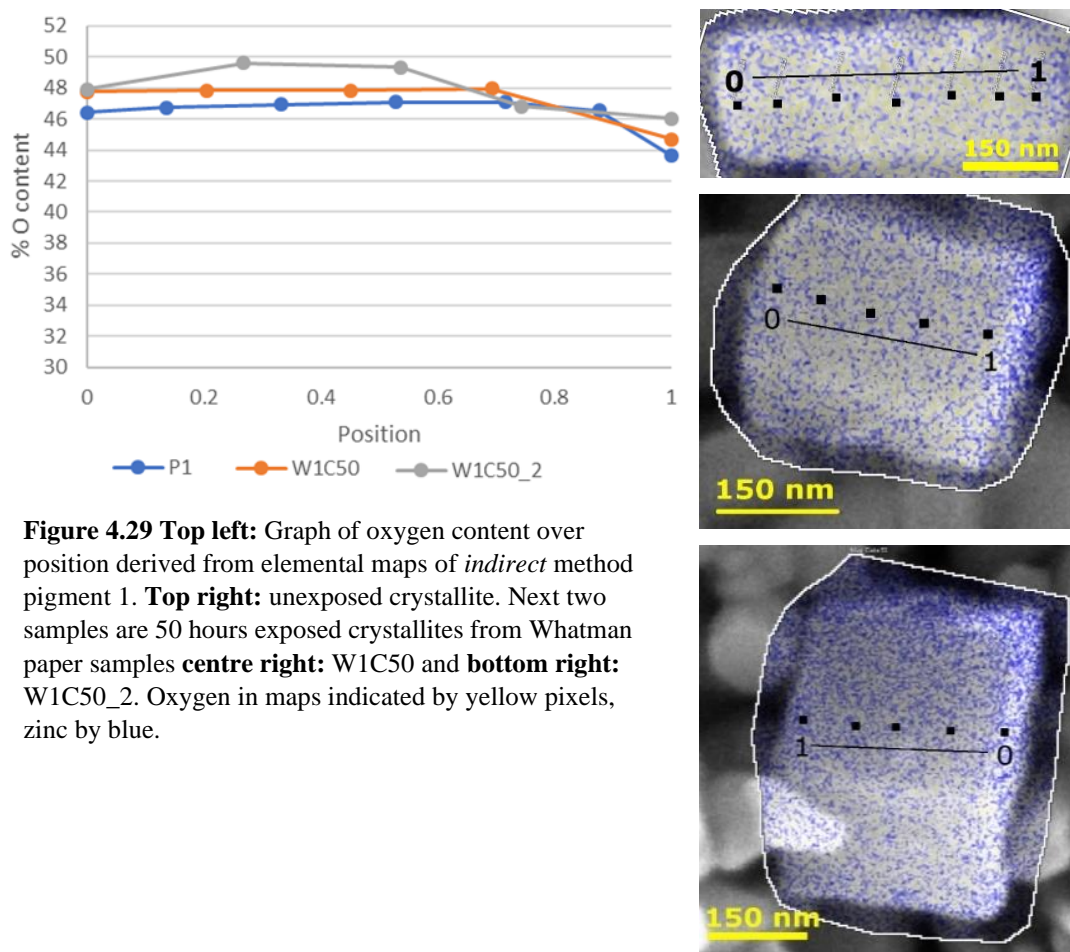
Figure 4.29 Top left: Graph of oxygen content over position derived from elemental maps of *indirect* method pigment 1. **Top right:** unexposed crystallite. Next two samples are 50 hours exposed crystallites from Whatman paper samples **centre right:** W1C50 and **bottom right:** W1C50_2. Oxygen in maps indicated by yellow pixels, zinc by blue.

Measurements from *indirect* method sample 3 followed both trends, with the fitted line for the unexposed sample P3 having a slope of -2.45, in comparison with exposed sample W3C50's slope of -0.68 and exposed sample W3C50_2's slope of -2.95 (Figure 4.30).
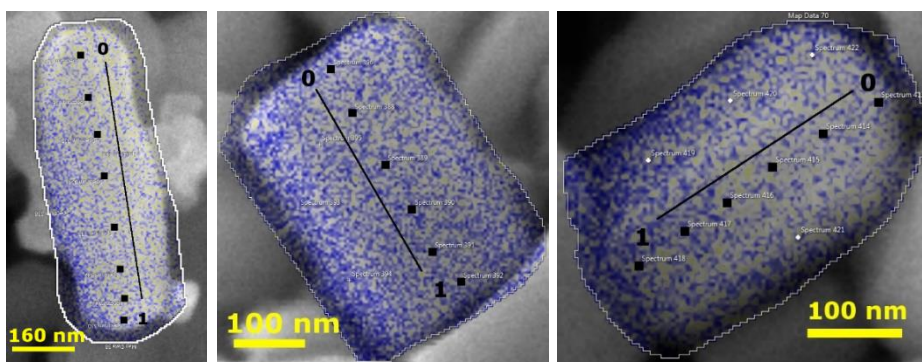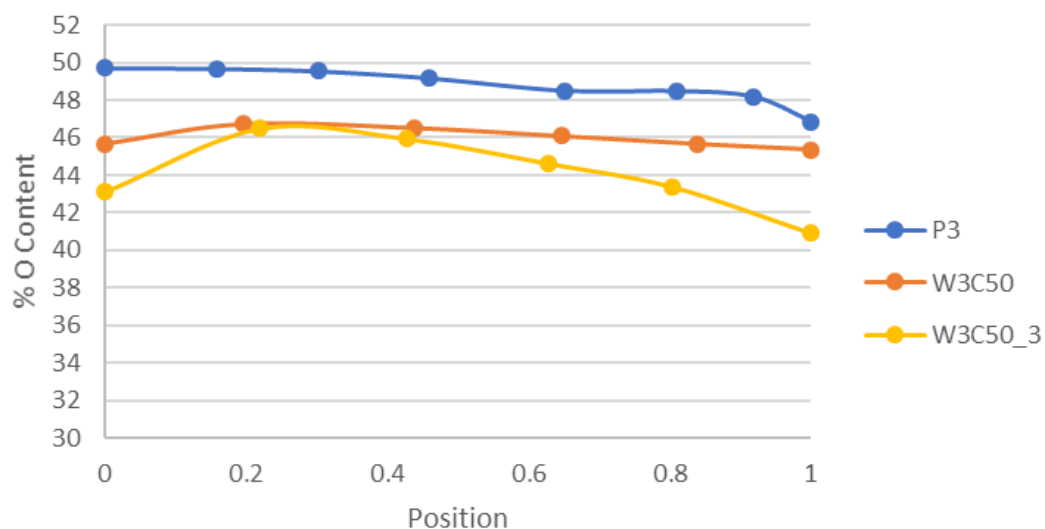
Figure 4.30 Top: Graph of oxygen content over position derived from elemental maps of *indirect* method pigment 3. **Bottom left:** unexposed crystallite. Next two samples are 50 hours exposed crystallites from Whatman paper samples **bottom centre:** W3C50 and **bottom right:** W3C50_3. Oxygen in maps indicated by yellow pixels, zinc by blue.

The fitted line for commercial pigment 16 increased steepness after exposure and appeared to have a much lower oxygen content in the exposed versus the unexposed crystallite (Figure 4.31).
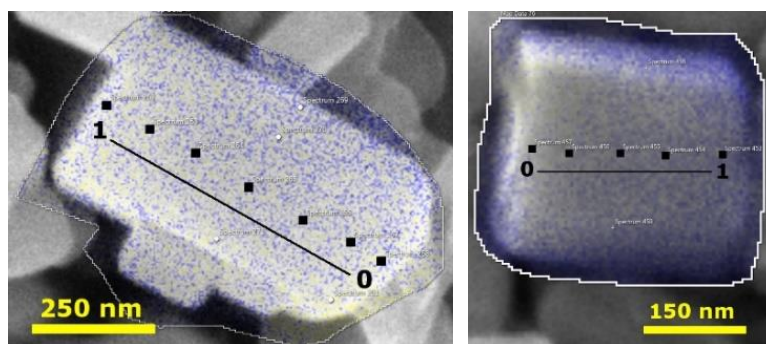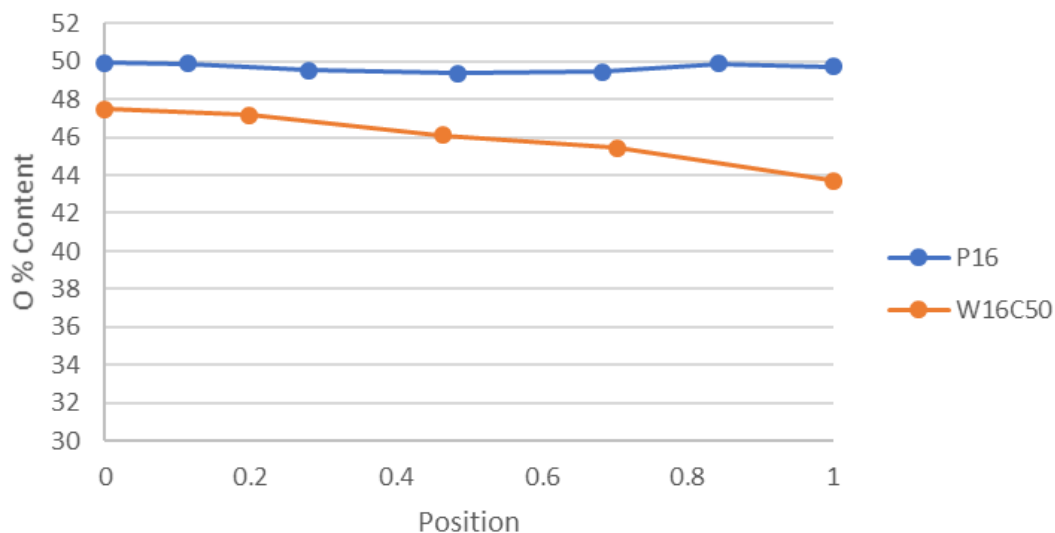
Figure 4.31 Top: Graph of oxygen content over position derived from elemental maps of commercial pigment 16. **Bottom left:** unexposed crystallite and **bottom right:** 50 hours exposed crystallite from Whatman paper sample W16C50. Oxygen in maps indicated by yellow pixels, zinc by blue.

Oxygen content of *direct* method sample 6 after exposure was much less than before exposure. The measurements taken along both crystals were also in different areas of the elemental map, with measurements from the unexposed crystal taken in a predominantly yellow area indicating high oxygen content, and the exposed measurements taken from a predominantly blue area, indicating mostly zinc (Figure 4.32).
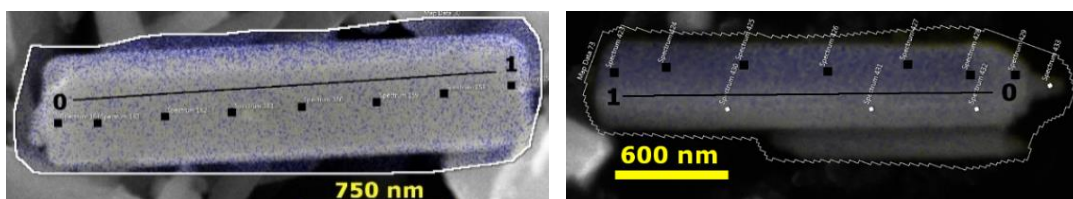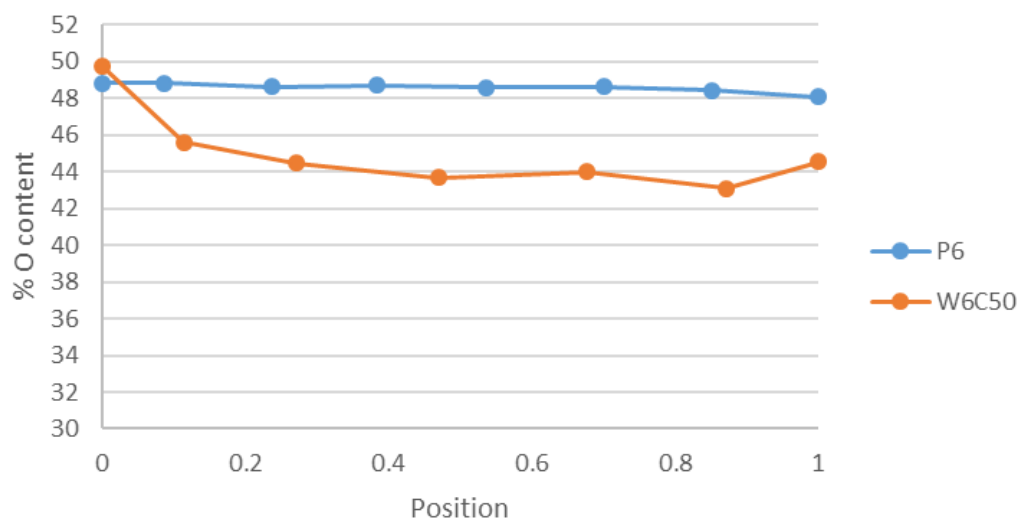
Figure 4.32 Top: Graph of oxygen content over position derived from elemental maps of *direct* method pigment 6. **Bottom left:** unexposed crystallite and **bottom right:** 50 hours exposed crystallite from Whatman paper sample W6C50. Oxygen in maps indicated by yellow pixels, zinc by blue.

In contrast with *direct* method sample 6, *direct* method sample 9 contained a much higher percentage of oxygen in the exposed sample than in the unexposed sample (Figure 4.33).
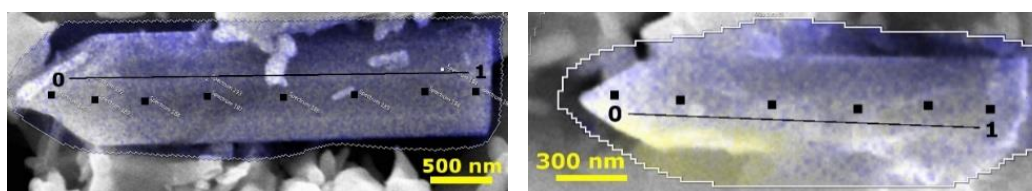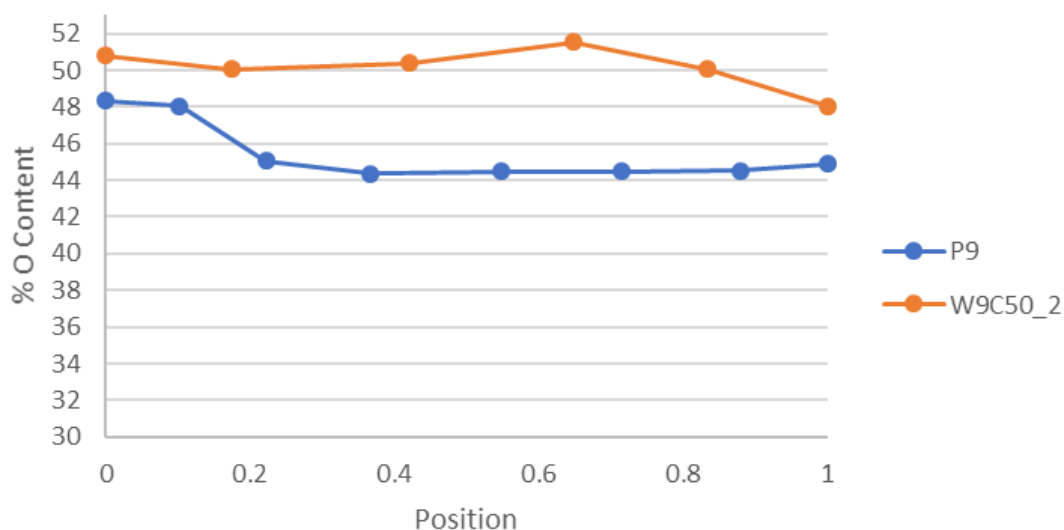
Figure 4.33 Top: Graph of oxygen content over position derived from elemental maps of *direct* method pigment 9. **Bottom left:** unexposed crystallite and **bottom right:** 50 hours exposed crystallite from Whatman paper sample W9C50_2. Oxygen in maps indicated by yellow pixels, zinc by blue.

4.5 DISCUSSION

The following observations are made after comparing results across methods and between mock-ups and case studies. Ineffective or inconclusive methods are also discussed alongside ways in which to progress future research.

4.5.1 CHANGES TO BINDING MEDIUM IN MOCK-UPS AND *BOUQUET OF FLOWERS*

Prevalent cracking in highly-sized papers indicates that some change occurred in the binding medium. Zinc oxide paints in both Fabriano and Folio paper as well as zinc oxide from Irene Kendal's *Bouquet of Flowers* primarily degraded via binding medium disintegration. All three papers are highly sized and do not allow much penetration of the pigments into the paper fibres. Reaction products would therefore be confined to the pigment and binding medium rather than coming into direct

contact with paper fibres. This could explain why browning did not occur in these three cases.

Cracking of the binding media was likely caused by a combination of two factors: 1) a loss of film elasticity from the wet/dry cycles involved in light ageing and natural ageing; 2) hydrolysis of glycosidic bonds in gum arabic's constituent polysaccharide molecules, changing their intermolecular interactions. Gum arabic consists of large, branched polysaccharides with weak intermolecular interactions. The exact structure of these molecules is still not fully resolved, though they are mostly composed of galactose and arabinose monosaccharides (70-85%) with branching structures of rhamnose and glucuronic acids (Dror, Cohen and Yerushalmi-Rozen, 2006; Williams and Phillips, 2009). A combination of acids in the aged papers, ambient UV light, repeated exposure to moisture and drying and oxidative products formed on zinc oxide surfaces probably reduced elasticity in the paint layer by breaking down the glycosidic bonds in these polysaccharides. Gum sugar monomers themselves have been found to be very stable when analysed with gas chromatography-mass spectrometry (GC-MS) and their composition over time is independent of zinc oxide pigments with which they are mixed (Bonaduce *et al.*, 2007; Riedo, Scalarone and Chiantore, 2013). Bonaduce *et. al.* could not, however, determine whether chain scission within the polysaccharides had occurred.

Additional work will involve the wetting and drying of similar mock-ups without light exposure to compare the extent and type of cracking of the paint layer to those samples exposed to light. This could help determine whether the cracking was due primarily to light-induced peroxide formation or to the repeated expansion and contraction of the paint layer due to the wet/dry cycle.

4.5.2 FTIR AND ADSORBED WATER

ATR spectra of paper substrates before and after light exposure were collected to identify changes in hydroxyl bands around 3300 cm^{-1} and carbonyl peaks in the 1500-1900 cm^{-1} range to establish whether degradation processes discussed in Section 4.2.1 had occurred. Unfortunately, both bands are largely dominated by vibrations due to adsorbed water in the paper, particularly the carbonyl peaks (Łojewska *et al.*, 2005). Spectra could be taken at elevated temperatures to desorb water molecules and measure only carbonyl groups; however, appropriate instrumentation was not available at the time of study. Therefore, FTIR and ATR techniques were abandoned as an option although they may prove useful in future work.

4.5.3 RUSSELL-GRAMS AND VISUAL COMPARISONS

Changes in overall paper tone tended to be dominated by the bleaching effect of visible light rather than the darkening of paper via UV-induced degradation processes visible around the pigments. Colour change is an example of 'net change' after exposure to light, called a 'single point determination' (Feller, 1992, p. 22) and may not occur alongside chemical change, particularly if molecules are bleached by the light (Feller, 1992). Colour change is often cited as a result of the oxidation of paper due to zinc oxide pigments (Daniels, 1990; Kemp, Wise and Hamilton, 2004; Singer and Liddie, 2005) and the observed browning of paper surrounding zinc oxide pigments on Whatman paper, coupled with results from cellulose oxidation research (Daruwalla and Narsian, 1966; Conte *et al.*, 2012) indicates that cellulose oxidation occurred as a result of peroxide formation on pigment surfaces. Additionally, the successful dark imaging of the Russell-grams for samples with

visible discolouration after exposure confirms that discolouration was induced by peroxides.

Russell-grams could not be made for six months after light exposure due to difficulties with obtaining materials and aligning schedules with the appropriate technician. Even so, peroxides were strongly detected with 36 hours of contact with the lithographic film. This indicates that even after the light source has been removed, peroxide formation is ongoing and likely would continue to be detected until peroxides had been completely reduced by surrounding materials. It may also indicate that some peroxide formation occurred on *direct* method samples but perhaps had reduced to water by the time Russell-grams could be made. They did not, however, produce the levels of peroxides for as long as *indirect* or commercial pigments (Figure 4.34).
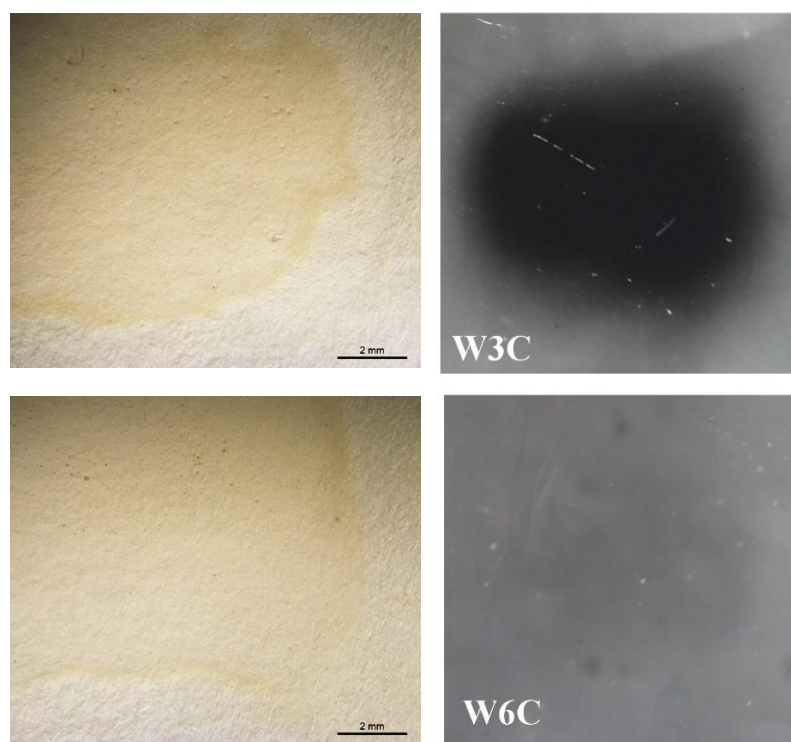
Figure 4.34 Upper left: Discoloured *indirect* sample 3 and **Upper right:** Russell-gram of the same sample indicating high levels of peroxides on pigment surfaces. **Lower left:** discoloured *direct* sample 6 and **lower right:** Russell-gram of the same sample indicating very little hydrogen peroxide on the pigment at the time of imaging.

4.5.4 $\Delta E *$ AND THE UV ABSORPTION EDGE

The band edge was most apparent in the samples on Whatman paper due to its high reflectance in the visible spectrum. The paper did not bleach as dramatically as the Folio or Fabriano papers and did not alter the blue regions too dramatically, keeping the absorption edges more consistent. The overall lack of colour change for *indirect* samples 1 and 4 and commercial samples 15 and 16 on Whatman paper as measured by low $\Delta E *$ values correlates well to their steep UV absorption edges (Figure 4.35). Conversely, *direct* method samples 7 and 9 have the shallowest slopes and the highest colour change. This indicates that the *indirect* method and commercial pigments are most effective at absorbing harmful UV wavelengths which could induce colour change in paper. Their high reflectance in the visible range could also prevent bleaching by visible wavelengths of light.
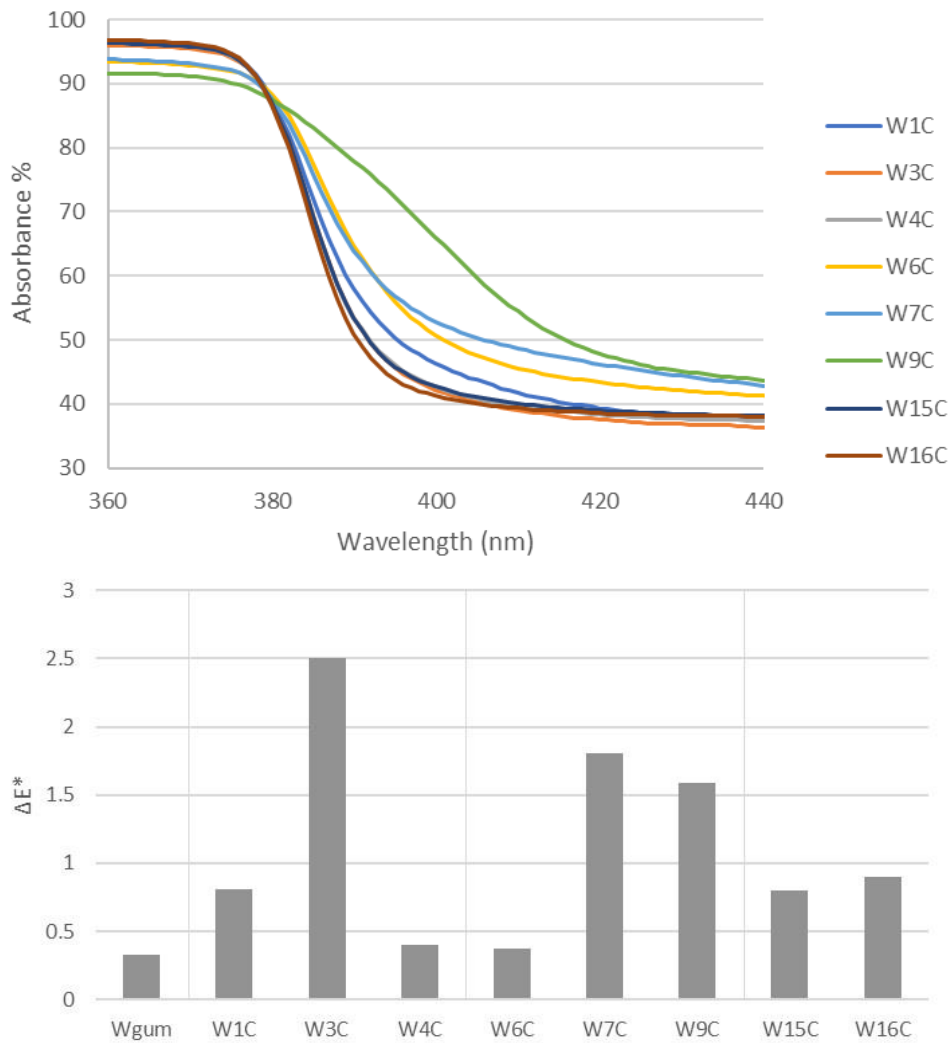
Figure 4.35 Above: Absorption edges of all pigment samples on Whatman paper. **Below:** Whatman $\Delta E*$ values. Samples 1, 3 and 4 = *indirect* method pigments; 6, 7, and 9 = *direct* method pigments; 15 and 16 = commercial pigments.

Indirect sample 3 does not fit the trend described here because the severe browning caused by degradation after light exposure raised its $\Delta E*$ value higher than other similar samples with similarly steep slopes. Additionally, *direct* sample 6 does not have a high $\Delta E*$ value like the other *direct* method pigments, containing a value more like *indirect* sample 4. As the colour change was measured through the pigment itself, this may be due to a pigment property unrelated to paper changes

such as hiding power.[96] *Direct* samples 6 and 7 imaged extremely faintly using the Russell-gram technique, indicating that peroxide formation on their particle surfaces is minimal and the two pigments have a similar photo-response.

4.5.5 THE ABSORPTION EDGE AND OXYGEN GRADIENT

A redshift of the absorption edge has been associated with increased annealing temperatures (Khorsand Zak, Ebrahimizadeh Abrishami, *et al.*, 2011), a quality previously described as a more gradual slope (Brown, 1957). By this criteria, *direct* method samples, particularly 9, would have been annealed at the highest temperatures, while sample 1 may also have been annealed but at a lower temperature given its shallow slope when compared with other *indirect* pigments.

Annealing drives out impurities and defects from the bulk but also increases the occurrence of crystal defects on the surface by facilitating the movement of ions within and out of the crystal (Wang *et al.*, 2005; Erhart and Albe, 2006; Srinivasan *et al.*, 2008). Elemental maps indicated that at least some crystals had a notable concentration of defects at one pole in the form of oxygen vacancies. All samples other than P6 and P16 had a defect gradient along the c axis.

These defects have a pronounced effect on fluorescence and their presence could be inferred by the type and colour of fluorescence of pigment particles before and after light exposure. While mapping did not allow for the direct detection of these defects, fluorescence studies show promise in allowing for their study.

---

[96] Hiding power specifically refers to the amount of surface a litre of paint can cover. It relates to a particle's size and refractive index compared to a binding medium such as linseed oil or gum arabic. A pigment with higher hiding power can cover more area than an equal amount of pigment with less hiding power.

4.5.6 MORPHOLOGICAL DEPENDENCY OF OXYGEN GRADIENT

When graphed according to morphological characteristics, oxygen gradients were the same for samples of similar morphology, regardless of whether those crystallites were exposed to light or not. This indicates that the greatest determinant of the slope and shape of the oxygen gradient for crystallites is not light exposure, but morphology[97].

4.5.7 DEPENDENCE OF OXYGEN CONTENT ON LOCATION PERPENDICULAR TO *c* AXIS

Elemental mapping revealed an uneven distribution of oxygen ions perpendicular to the *c* axis. EDX point scans were collected from the lateral faces of *indirect* method sample P3 and *direct* method sample P7 and showed an increase or decrease in the oxygen values when compared with corresponding central points (Figure 4.36).

---

[97] For graphs and results of this exercise, refer to Appendix 15: Morphological Trends in Mapping Data.
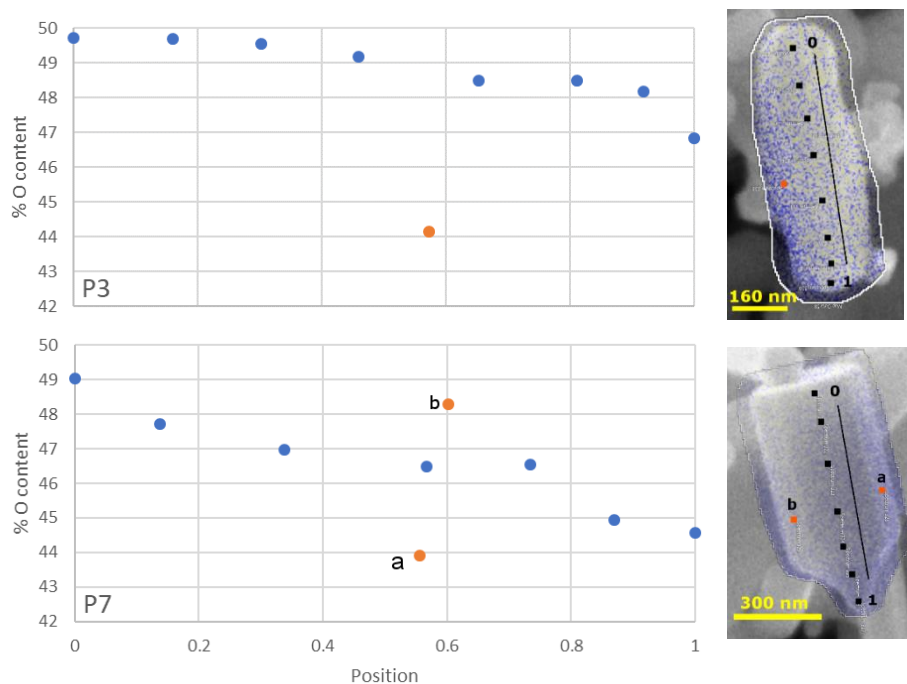
Figure 4.36 Graphs and maps of oxygen content along *c* axis (blue points) and lateral to that axis (orange points). The point from *indirect* sample 3 indicates an area of oxygen deficiency along the side of the crystallite, while points from *direct* sample 7 indicate a gradient may exist perpendicular to the *c* axis.

To determine if another oxygen gradient was present, EDX point scans were taken in a line perpendicular to the *c* axis on a crystallite from commercial pigment sample P16. A gradient in that perpendicular direction was verified (Figure 4.37).
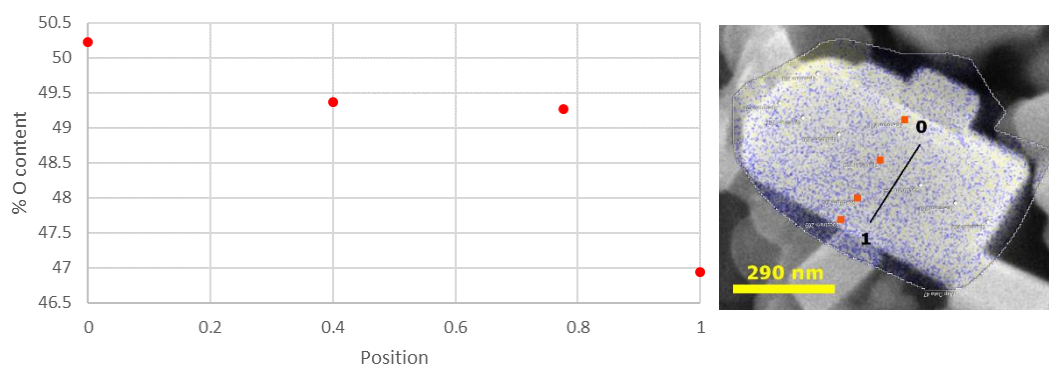
Figure 4.37 Graphs and maps showing gradient of oxygen content perpendicular to *c* axis in crystallite from commercial pigment sample P16.

The facet with the highest oxygen deficiency measured in these three samples is likely the (10$\bar{1}$0) face. This face is prone to oxygen vacancies and adsorbs -OH groups readily at RH above 10^{-4} % (Newberg *et al.*, 2018). A (10$\bar{1}$0) hydroxylated

surface with oxygen vacancies is 69% more likely to adsorb atmospheric oxygen and water than a hydroxylated surface without vacancies (Meyer, Rabaa and Marx, 2006; Jacobs *et al.*, 2017). This $(10\bar{1}0)$ surface is largest in comparison to the total surface area in *direct* method pigments[98]. However, Russell-grams showed inactivity in *direct* method pigments, indicating this face may not be very reactive even if it attracts hydroxyls.

4.5.8 HYDROGEN AS SUBSTITUTE FOR OXYGEN VACANCY

While oxygen vacancies are clearly important for the adsorption of moisture onto zinc oxide surfaces, and potentially for increasing the likelihood of further reactions, theoretical studies shed doubt upon their role as a contributor of negative conductivity. They have been categorised as deep donors, meaning they do not contribute electrons to the valence band (Janotti & Van De Walle, 2007). They also require a lot of energy to form and maintain. Instead of oxygen vacancies accounting for the mapped oxygen gradients in this study, it is possible that hydrogen has substituted for oxygen in the crystal lattice. This substitutional hydrogen has a low formation energy, acts as shallow donors and bonds strongly with -OH groups, explaining the hydrogenation of the $(10\bar{1}0)$ surface (Janotti and Van De Walle, 2007; Oba *et al.*, 2008; Ellmer and Bikowski, 2016). The absence of oxygen ions detected by EDX mapping in this study could be explained by this substitution of hydrogen, an atom not detected by EDX spectroscopy.

---

[98] This is due to the *direct* method pigments being longer on average than *indirect* method pigments, as evidenced by a greater length-to-width ratio.

4.5.9 ELEMENTAL MAPS: CASE STUDY COMPARISONS TO MOCK-UPS

The sample RD2, taken from the ruin drawing, had a very similar oxygen gradient as contemporary pigment sample P15 (Figure 4.38) implying they were produced by a similar method. Although no other case study provided conclusive data for comparison, the available case studies for sampling were limited and confounded by the pigments being embedded in gum medium.
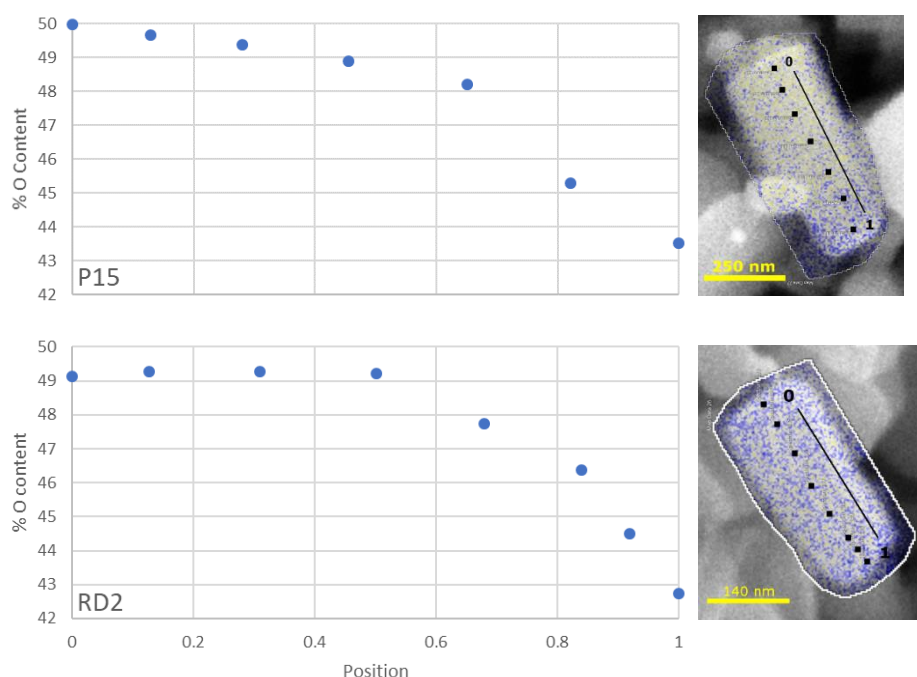
Figure 4.38 Graphs and maps of oxygen content highlight similarities between contemporary pigment P15 and historic pigment RD2.

4.5.10 LIMITATIONS OF ELEMENTAL MAP DATA

Given the length of time required for a single elemental mapping (typically 1-3 hours), only one crystallite per powder sample was processed. This meant that results were based on one type of particle which may or may not be representative of the entire powder sample. Measurements were also influenced by position along the *a* axes and morphology of the crystallites.

Samples 1, 3, and 16 all had unexposed particles measured with a much higher length-to-width ratio than the exposed particles. This may have influenced the results as shorter particles may have less of an oxygen gradient, particularly if they were originally part of longer particles which were previously broken.

Sample 6 results were confounded by the location of the measurements along the *a* axis. Measurements for W6C50 seem to be largely from the $(10\bar{1}0)$ face, which is oriented towards the detector in the SEM image. Other samples may also have been influenced by their position along this perpendicular gradient, a confounding variable which was not accounted for during data collection. Mapping data using this method is therefore unreliable in detecting defect changes after light exposure.

4.6 CONCLUSIONS

- The predominant visual effect of light exposure on paper was bleaching due to visible light, which accounted for 90.2% of irradiance imparted to the samples, while only 9.8% of irradiance was from UV light.

- *Indirect* and commercial pigments produced the most hydrogen peroxide after light exposure as evidenced by Russell-grams while *direct* method pigments did not show signs of peroxide production using this method.

- Visible degradation in unsized Whatman paper was confined to browning, while in sized mock-ups and the Irene Kendal piece, cracking and cupping of the paint layer were prominent. Without size, pigments are absorbed within the paper fibres and react more readily with cellulose, while highly-sized papers confine pigments to surfaces where they may degrade the binding medium.

- Morphology rather than light exposure is the greatest determinant of oxygen gradients in crystallites.

- *Direct* method crystallites have the highest length-to-width ratios and therefore the largest $(101\bar{0})$ face, an area associated with the adsorption of hydroxyl groups. Despite this tendency, *direct* method pigments did not produce detectable peroxides in the course of ageing as in the case of the shorter *indirect* and commercial pigments. This research therefore demonstrates that this face may not be important for peroxide formation despite its abundance of hydroxyls.

- A relationship was found between production type and steepness of the absorption edge, with *indirect* method pigments having the steepest edge and *direct* method pigments having the least steep edge. This may relate to post-production annealing, a process possibly employed in *direct* method production in order to eliminate residual impurities from the ore. The process would have the added effect of creating crystal defects on the surface through ion diffusion, decreasing the energy released as electrons fall into trap states produced by crystal defects and producing a shallower absorption edge.

- Steep absorption edges such as those found in *indirect* and commercial pigments provide better protection from UV light but may also indicate higher photocatalytic activity as evidenced by Russell-gram results.

- The untitled ruin drawing (RD) has a similar oxygen gradient to sample P15, indicating they may have been produced in similar conditions and by similar methods.

5 Ultraviolet-Induced Visible Fluorescence of ZnO

When photons which are more energetic than a semiconducting material's band gap hit its surface, electrons are excited into its conductance band. These electrons lose excess energy gradually until they drop out of the conductance band. Fluorescence results from these excited electrons falling back to the ground state and emitting a longer wavelength of light than the one which was absorbed. The emitted wavelength of light is proportional to the energy gap crossed upon relaxation, while the difference between the photon energy absorbed by an electron and the energy emitted through fluorescence is known as the Stokes shift and is unique to the material. Impurities and defects in a material's crystal structure can create additional energy levels within the band gap called traps which electrons can fall into, fluorescing in longer wavelengths related to the shorter energetic distance. The time electrons spend in the conductance band will also be less in the presence of these traps.

Not all 'recombinations,' as these returns to resting states are called, result in fluorescence. van Dijken et al. (2000) characterizes recombinations which result in visible emission as those which occur 'following the tunneling [sic] of the surface-trapped hole back into the particle' (p. 1721) while those which are nonradiative 'can be the result of either of two different processes, trapping of a hole at the surface followed by trapping of an electron at the surface or trapping of an electron at the surface followed by trapping of a hole at the surface' (p. 1721). This chapter deals only with radiative processes.

Defects in zinc oxide, particularly oxygen vacancies and zinc interstitials, have been linked with both faster recombination rates (Zhu *et al.*, 2014; Penfold *et al.*, 2018) and green fluorescence (i.e. Kröger and Vink, 1954; Janotti and Van de Walle, 2009; Fabbri *et al.*, 2014) while fewer defects can extend excitation times and allow for more photocatalytic reactions to occur (Zhu *et al.*, 2014; Penfold *et al.*, 2018). Additionally, transitions from zinc to oxygen ions are associated with the near-band edge (NBE) emission, visible as blue fluorescence, and would be more prevalent in a crystal with fewer defects (Fabbri *et al.*, 2014). Linking the fluorescence of mock-ups before and after light exposure with their degradation behaviour will aid in correlating the two phenomena and setting the groundwork for a predictive model of fluorescence in zinc oxide watercolours.

5.1 QUALITIES OF ZINC OXIDE FLUORESCENCE

Zinc oxide crystallites have two distinct fluorescent colours which dominate when viewed under a microscope. The NBE emission corresponds to UV light emitted due to absorption and re-emission across the band-gap and appears blue in colour (Fabbri *et al*., 2014). Green fluorescence derives from electron transitions not across the band gap, or from oxygen to zinc ions and back, but from transitions made by excited electrons in the conductance band down to 'trap states' or energy levels within the band gap resulting from elemental impurities or lattice defects and distortions (van Dijken *et al.*, 2000). Morley-Smith (1950) first identified these two types of fluorescing particles when searching for a cause of chalking in house paints and found his results heavily augmented by the ratio of these blue-to-green fluorescing particles, with higher rates of blue fluorescing particles correlating with higher rates of chalking. He further linked the blue fluorescing particles to *indirect*

method zinc oxides and noted their absence when looking at *direct* method pigments under magnification.

The colour of fluorescence for those viewing the phenomenon with the naked eye is a result of the ratio of microscopic green and blue fluorescence and ranges from a bright green to a dull khaki brown through magenta. Nagle (1928) described a full range of colours in his early work on the differentiation of zinc oxide powders via UV fluorescence for use in the rubber industry. The 'pure' zinc oxide fluoresced a 'rich deep violet,' while others ranged from 'orange-buff' to 'a fine bright apple green colour' (Nagle, 1928, p. 307).

5.1.1 BLUE/NBE FLUORESCENCE

The NBE emission peak location varies, with values reported at 390 nm (Artesani *et al.*, 2018), 370 nm (Chen *et al.*, 2011), 377 nm (Bandopadhyay and Mitra, 2015) and 381 nm (Fabbri *et al.*, 2014)[99]. A red-shift, or shift towards longer wavelengths (and narrowing of the band gap) was linked to an increase in a wide range of impurities such as nitrogen with aluminium, gallium, indium, tin and lead (Djurišić and Leung, 2006; Rodnyi and Khodyuk, 2011). Conversely, Yun and Lim (2011) associated increased aluminium concentrations with a blue-shift of the NBE peak.

By growing nanorods[100] of zinc oxide, Fabbri *et al.* (2014) located the NBE fluorescence at the base of the long zinc oxide crystallites and found it diminished as zinc defects increased along the $(10\bar{1}0)$ long axis. The intensity of the green

---

[99] The NBE emission is temperature-dependent and red-shifts at higher temperatures (Chen *et al.*, 2011) which could account for the variation in reported values. Chen *et al.* provide a graph of the position of the NBE emission across a wide range of temperatures in their 2011 publication. The effect is due to the conversion of some absorbed energy from exciting wavelengths into thermal energy, resulting in both a longer emitted wavelength when an electron settles back into a lower energy state and a less intense fluorescence overall at higher temperatures.

[100] The term is used by Fabbri *et al.* to describe acicular, rod-like zinc oxide crystallites grown on a gallium nitride substrate.

fluorescence was dependent on the surface-area-to-volume ratio and the morphology of the nanorods, suggesting that shorter rods with less growth time would be dominated by NBE wavelengths, both traits characteristic of *indirect* method zinc oxides.

Additional blue peaks at 410 and 425 nm in small, localised particles were identified by Artesani *et al.,* (2016) which do not correspond to the NBE peak. Earlier work by Bertrand *et al.* (2013) using cathodoluminescence to map fluorescent wavelengths at a nanoscale identified localised 425 nm emissions in sparsely-distributed nanoparticles. The dual peaks observed by Artesani *et al.* (2016) were previously identified by Viswanatha *et al.* (2006) as arising from copper impurities. They doped[101] or introduced copper ions into the zinc oxide lattice in concentrations from 0-4% and observed a dual emission peak at 410 and 430 nm. Of interest is the observation by Artesani *et al.* (2016) that these dual peaks were present in historic samples which all had evenly-distributed copper impurities but not control samples which contained far fewer impurities overall and no copper.

5.1.2 GREEN FLUORESCENCE

The cause of the broad green emission band has long been debated and never fully settled. The theories of its origin fall into two camps: green fluorescence arising from impurities or from crystal defects. While it is probable that there are multiple causes, there may be one dominant contributor.

Impurities: Impurity studies have focused largely on copper as a source of the green fluorescent band (Dingle, 1969; Mishra *et al.*, 1990; Alivov, Chukichev and

---

[101] Doping involves adding defects or impurities to a semiconductor to influence its electrical properties. This is done by either introducing materials which increase the electron concentration or the hole concentration and usually also introduce additional energy levels within the band structure.

Nikitenko, 2004). While the green emission band for copper impurities in ZnO is similar to the characteristic green emission band, Rodnyi and Khodyuk (2011) have shown that the strength and type of green fluorescence is unrelated to the concentration of copper in zinc oxide crystals. Additionally, Janotti and Van de Walle (2009) point out that while copper may contribute to the green fluorescent band, not all green fluorescing zinc oxides contain copper.

Defects: A stronger case has been made for lattice defects causing green fluorescence. Nagle observed in 1928 that all zinc oxides which he heated to a 'white heat' for ten minutes obtained a green fluorescence (Nagle, 1928, p. 311), a strong indicator that the origin of green fluorescence is related to crystal structure defects. Leverenz and Seitz (1939) linked zinc oxides created in a reducing atmosphere to fluorescence bands from 430-600 nm with a broad peak at 495 nm. This led to a theory that the green fluorescence derives from either neutral (De Angelis and Armelao, 2011) or singly ionized oxygen vacancies (Kröger and Vink, 1954; Vanheusden *et al.*, 1996; Bandopadhyay and Mitra, 2015).

The green band has been ascribed to contributions by oxygen vacancies, interstitial oxygen, and zinc vacancies (Kröger and Vink, 1954; Mikhailov, Neshchimenko and Li, 2011). Of the three defects, zinc vacancies have the lowest formation energy and are more favourable in oxygen-rich conditions (Janotti and Van de Walle, 2009). Zinc vacancies act as deep acceptors and can recombine with shallow donors such as hydrogen ions on the zinc vacancy site to cause a green emission band (Cox *et al.*, 2001; Shi *et al.*, 2004; Lyons *et al.*, 2017). Oxygen vacancies have been argued against as causes of green fluorescence (Fabbri *et al.*, 2014) though others feel it may play a part, either through the elimination of the NBE emission in some zinc oxides, concurrently strengthening the green band (Gurwitz, Cohen and Shalish,

2014) or when interacting with interstitial zinc ions (Krithiga, Sankar and Subhashree, 2014). Artesani *et al.* (2018) described a green fluorescence in both pure zinc oxide pigments and in those in oil paints. They associated a strengthening of this band with the creation of more zinc vacancy sites after zinc ions were removed by carboxylates in the formation of zinc soaps. Assigning the exact cause of the green band is extremely difficult and the research into this topic is ongoing, though defects are broadly thought to be the most likely cause.[102]

5.1.3 OTHER FACTORS INFLUENCING FLUORESCENCE IN PAINTS

Temperature influences fluorescence by reducing the intensity and energy of emitted light at higher temperatures. The effect is most dramatic moving from very low temperatures (near absolute 0, or 0 K) to those near the freezing point of water, but changes are negligible when observing fluorescence closer to comfortable room temperature (van Dijken *et al.*, 2000). Therefore, the effects of temperature on fluorescence are minimal in a museum or gallery context.

Binding media are known to influence fluorescence by enhancing or diminishing peaks or shifting their maxima. Gum arabic, the binding medium used in mock-ups, contains a large emission peak at 315 nm and a wide band from 420 to 470 nm (Dhenadhayalan, Mythily and Kumaran, 2014). When mixed with zinc oxide, the NBE emission is enhanced but the composition of the gum arabic does not change detectably with ageing (Bonaduce *et al.*, 2007; Chiantore, Riedo and Scalarone, 2009; Artesani *et al.*, 2018). As gum arabic contains an abundance of hydroxyl

---

[102] For an overview of current and past research, see González, G. B. (2012) 'Investigating the defect structures in transparent conducting oxides using x-ray and neutron scattering techniques', Materials, 5(12), pp. 818–850.

groups, Artesani *et al.* (2017) theorise that complexation of these hydroxyl groups promote zinc oxide defects which would enhance the NBE emission.[103]

Paper substrates may also influence fluorescence if paints are thinly applied. As watercolour paints are never entirely opaque, the absorption and emission characteristics of underlying paper could affect the appearance of fluorescing pigments by strengthening or dampening fluorescent bands.

Methodologies have been developed which aim to eliminate contributions by the binding medium and isolate pigment fluorescence from multispectral digital images (Verri *et al.*, 2008; Clementi *et al.*, 2009; Dyer, Verri and Cupitt, 2013). These studies have largely focused on opaque oil or tempera paints and not more transparent paints on paper. Irrespective of this, their methodology succeeds in obtaining more typical emission spectra for pigments, allowing for identification and characterisation of in-situ pigments in fluorescing or absorbing binding media.

5.2 RELATIONSHIP BETWEEN FLUORESCENCE AND RATE OF CATALYSIS

Morley-Smith observed a more active production of hydrogen peroxide on zinc oxide pigments with a higher proportion of blue-fluorescing particles, specifically *indirect* method zinc oxides. Additionally, these particles could be 'wholly converted into the green under controlled conditions' (Morley-Smith, 1950, p. 495). The shift from blue to green fluorescence in *indirect* method pigments could be explained by the defect gradient described by Fabbri *et al.* (2014) along the polar

---

[103] Some theories involve the adsorption of hydroxyl radicals on the polar faces of zinc oxide (Kumar and Rao, 2015), either on the positive zinc ion site or on oxygen ions. Subsequently, oxygen would become available for electron transfers across the band gap, producing a NBE emission and strengthening that fluorescent peak.

axis. In *indirect* pigments, the short nodular particles fluoresce a blue colour if the ratio of ions in the crystal lattice is nearly 1-to-1. Over time, as previously discussed in Section 3.3.1, oxygen evaporates from the polar surfaces, particularly from the (0001) surface, increasing defects and trap states[104] thus promoting additional migration of zinc ions to interstitial positions (McVicker, Rapp and Hirth, 1975; Sengupta *et al.*, 1987; Kumar and Rao, 2015).

Oxygen removal from the lattice requires a lot of energy; however, carbon-containing molecules such as gaseous carbon dioxide and monoxide may facilitate their removal at room temperatures via illumination by wavelengths of light up to 650 nm in length (Bonosewicz, Hirschwald and Neumann, 1986; Bao *et al.*, 2011; Gurwitz, Cohen and Shalish, 2014). This could indicate that UV cut-off filters for windows and light may not be enough to prevent certain photo-catalytic reactions.

5.3 ANALYSIS OF ARTWORKS USING UV FLUORESCENCE

Conservators already utilise UV-induced fluorescence to various degrees for pigment identification and its origins extend back to the earlier twentieth century (Eibner, 1933; Lyon, 1934; Rene de la Rie, 1982). Various publications in the conservation literature detail the types of fluorescence expected for different pigments, although they often disagree on the colour. Zinc white's fluorescence has been described as yellow (Cosentino, 2014; Carden, 1991) blue (Isacco & Darrah, 1993) and anywhere from 'orange-buff' to violet to 'bright apple green' (Nagle, 1928, p. 307). Some of this confusion derives from the varying fluorescence of zinc

---

[104] A trap state is a defect or impurity which recombines with an electron from the conductance band, essentially 'trapping' it and making it immobile. Traps tend to be located within the band gap, meaning that fluorescence from recombination with traps is less energetic and at a longer wavelength than fluorescence from band-to-band recombinations.

oxide, though it must be noted that there is uncertainty inherent in describing the subtleties of colour.

Additionally, human colour perception is surprisingly varied and normal colour vision in particular ranges so widely that attempts at describing the same colour often result in different language used (Barbur et al., 2008; Jordan & Mollon, 1995). To further complicate the matter, the time of year can influence an individual's perception of colour (Jordan & Mollon, 1993) as can the colour of one's iris (Jordan & Mollon, 1995). Famously, colours can appear radically different depending on the context in which they are viewed, as in optical illusions which place equivalent swatches of colour against differing backgrounds, seemingly creating new colours (Figure 5.1). In short, any method of analysis requires precision of language and a quantitative technique for measuring surface colour.
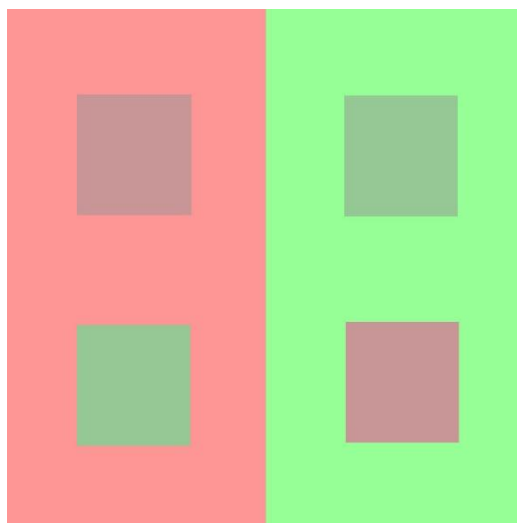
Figure 5.1 Four swatches in two colour fields demonstrate how context can alter perceived colour. The four swatches represent two colours but appear instead as four colours due to the changes in surrounding colour.

One solution is to use a fluorimeter to obtain exact emission spectra. This could be particularly useful for zinc oxide as it would allow for quantitative study of the two main emission peaks. Realistically, however, many conservators outside of museums do not have the means to purchase such a specialised piece of equipment or the background to interpret the spectral data. Portable fluorimeters can be assembled using components such as fibreoptic cables, UV light sources and portable detectors (Romani *et al.*, 2010; Doherty *et al.*,

2013). These can be especially useful for analysis of important pieces as they can be loaned out by institutions and easily repaired and transported.

Digital image processing presents the most viable solution to the problem of describing colour accurately. However, variations in sensor response, built-in filters, dark current, photographing distances and variations in lighting can all influence the information captured by digital cameras. Digital imaging for most conservators is typically qualitative and multispectral in order to obtain the most information about a pigment's possible identity. Most commonly, reflected visible, ultraviolet fluorescence, infrared, ultraviolet reflectance and false-colour infrared (IRFC)[105] (a composite image created in post-processing) images are employed (e.g. Baldia and Jakes, 2007; Cosentino, 2014). This useful method suffers from limitations previously discussed resulting from the range of human colour vision and the difficulties of language to describe colour, particularly when subtle differentiation of colour is required.

A more accurate method for describing digitally-imaged colour is needed, particularly in the case of fluorescent pigments which can be complicated by surrounding fluorescing paper and materials and by variations in image capture setup and equipment. Additionally, simple methodologies are preferable as conservators often do not possess the time or background for intense image processing procedures employed by conservation scientists. A review of the information derived from images with minimal processing may be useful to determine if patterns can be derived. Then further processing methods can be

---

[105] This type of image is a composite created using a visible light image and an IR image in which colour channels are switched so that IR occupies the red channel, the red is shifted to the green channel and the green to the blue channel.

discussed and employed which improve accuracy and comparability between cameras and conservators.

5.4 METHODOLOGY

5.4.1 ULTRAVIOLET FLUORIMETRY

Emission spectra were collected to establish a quantitative foundation for fluorescence analysis from digital image analysis. Fluorescent spectra of mock-ups on Whatman and Folio paper[106] were acquired using a Horiba FluoroMax 4 spectrofluorometer with an excitation wavelength of 325 nm, a slit opening of 2 nm, an output range of 335-640 nm and a sample angle of 60° from the detector. Dark count was less than 1000 counts per second and spectra were corrected by dividing the measured counts per second by microamps as measured by the reference detector.

Five spectra were collected for each unexposed and exposed mock-up sample. Initially processing was carried out in a|e - UV-Vis-IR Spectral Software 1.2 by FluorTools[107]. Minimum values were subtracted for background correction and the x-axis limited to 370-640 nm for *indirect* and commercial pigments and to 380-640 nm for *direct* method pigments. The three spectra with the highest return were kept as they represented areas with the thickest paint application and greatest opacity. Additionally, outliers were eliminated such as those spectra which were far too weak or strong or those with unusual or additional peaks. One data set was exported as an

---

[106] Data for Fabriano paper was not collected using this technique.

[107] Program and documentation can be found at www.fluortools.com.

ASCII file after this processing methodology while another set was exported after normalisation by area which set the total area to 1 to facilitate peak comparisons.

The three spectra were averaged and graphed against each other in MATLAB, with minimum and maximum values across the three spectra also graphed to provide a visual representation of the range of data (Figure 5.2). These averages represented trends in data and simplify data processing as the data ranges were neither too broad nor too overlapping[108].
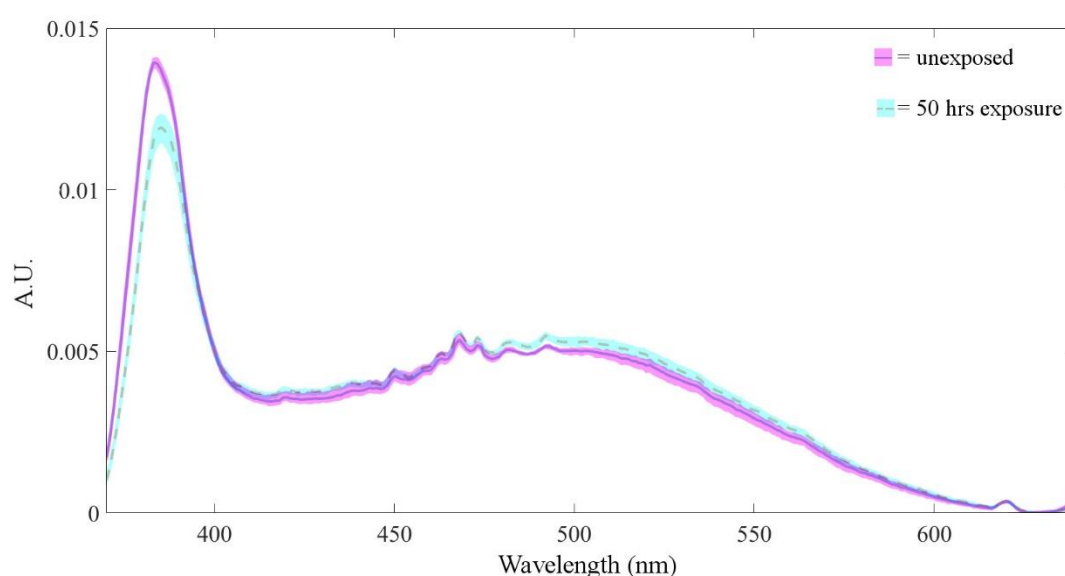
Figure 5.2 Normalised fluorimetry spectra of *indirect* sample 3 on Whatman paper. Pink and blue bands give the range of data while solid and dashed lines give the average intensities for unexposed and exposed samples.

The normalised averaged emission peaks were analysed using an Interactive Peak Fitter, an interface developed for MATLAB by Professor Tom O'Haver at The University of Maryland[109]. This program fits a user-specified numbers of peaks and shapes (Gaussian, Lorentzian, exponential, etc.) to spectra and returns peak

---

[108] For all processed fluorimetry spectra, refer to Appendix 16: Fluorimetry Spectra.

[109] The peak fitter can be found on O'Haver's website and instructions for its use found at this web address: http://terpconnect.umd.edu/~toh/spectrum/ifpinstructions.html.

locations, intensities (displayed as heights), areas, R^2 values and error % values

(Figure 5.3). These were then analysed and compared to determine what trends

could be found[110].
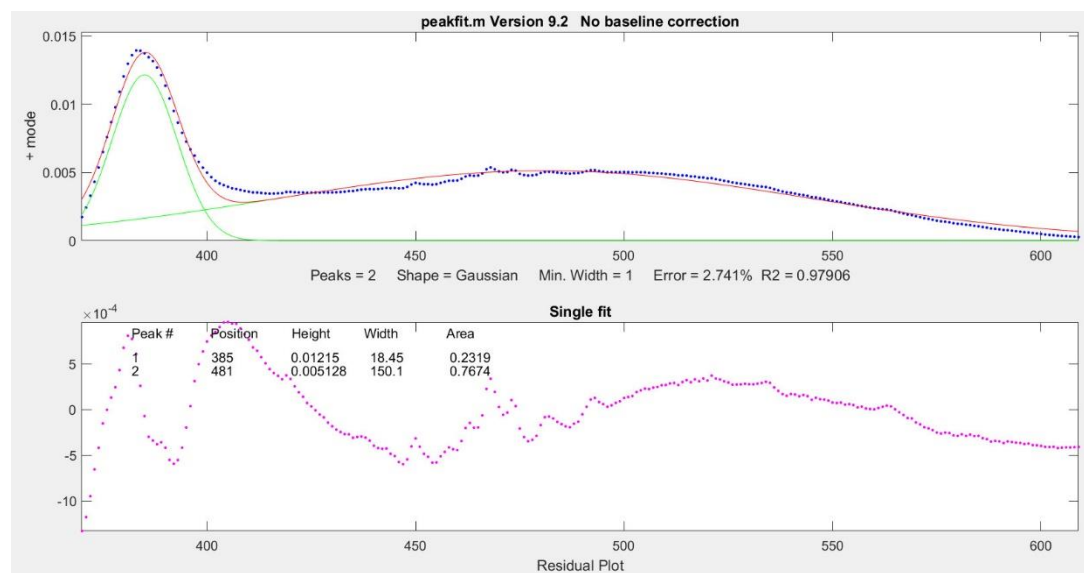
Figure 5.3 Peak fitting Whatman *indirect* sample 3 with the Interactive Peak Fitter using 2 Gaussian peaks. Green peaks in top graph represent fitted Gaussians, red line represents composite of two fitted peaks and blue dots represent data normalised by area. Lower graph is representation of residuals from fitting, with any divergence from 0 representing a divergence of the red line from the blue input data.

Fluorescent spectra were not collected from any of the case study watercolour

paintings as the instrument required an in-situ sample to be inserted into a small

chamber for data collection.

5.4.2 DIGITAL IMAGING AND ANALYSIS WITH COMMERCIAL DSLR

All samples were digitally imaged using a Canon EOS 6D commercial camera with

CMOS imaging chip with built-in IR filter and Kodak Wratten 2e UV-cut-off filter

attached to the lens to cut out wavelengths under 400 nm[111]. The room was blacked-

---

[110] For all peak fitting images and data, refer to Appendix 17: Decomposition of Emission Spectra in MATLAB.

[111] For a graph of the cut-off point of the filter as provided by Kodak, refer to Appendix 18: Wratten 2e Filter Diffusion Density.

out and two Narva LT 36W/073 blacklight blue UV lamps emitting at 365 nm were set up at 45° to the sample (Figure 5.4). Images were taken in CR2 format, the RAW format for Canon cameras, and mock-ups were imaged at 23cm distance.[112] This was to maximise the amount of emitted light captured and reduce total area of image, mitigating adverse effects from inconsistent illumination. Each mock-up sample was imaged at an exposure time of 0.5 seconds. The f/stop for each paper type had to be adjusted to avoid overexposure and were set to the following: Whatman paper - 5.0, Fabriano paper - 6.3, Folio paper - 4.5. The white balance for all was set to 8000K.
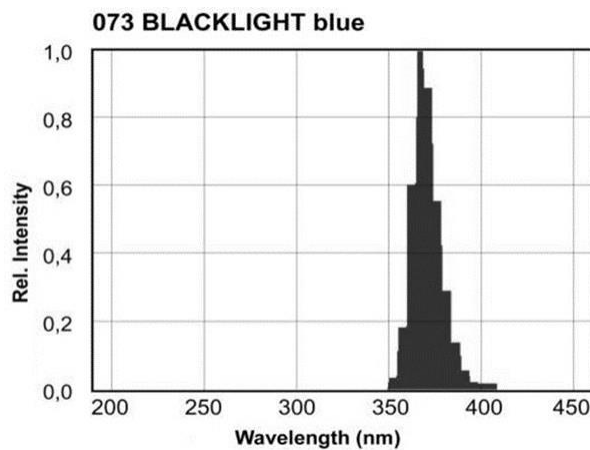
Figure 5.4 Distribution of wavelength intensities for N Narva LT 36W/073 blacklight blue lamp. Light is predominantly in the UV, with a small contribution by wavelengths between 400-410 nm. Image modified from Narva data sheet found at https://docs-emea.rs-online.com/webdocs/12ae/0900766b812ae575.pdf.

ISO values were maintained at 200 throughout. While this reduced the camera's sensitivity to light, it also reduced the noise in the final image. By imaging for 0.5

---

[112] Height of tripod legs was set at 93 cm, and the front leg touched the base of the easel on which the samples sat.

seconds and at appropriate f/stop values[113], which adjusts the aperture width, the low sensitivity could be somewhat mitigated.

In UFRaw[114], CR2 images were white balanced at 8000K if not already set to that value. Raw images were converted to Gimp PPM files and opened in Gimp, then cropped to 869x674 pixels and saved as tiffs. The tiffs were then opened in ImageJ, also known as Fiji, an open-source image processing program specifically developed for processing biological fluorescence images (Bankhead, 2014)[115]. Areas of the image not taken up by fluorescing pigment were subtracted using a background subtraction methodology.[116]

To extract RGB values for comparison, background-subtracted images were loaded into MATLAB and analysed there for mean and median pixel values, excluding black pixels. After verifying a normal distribution of values by comparing mean and median values, mean values were compared in Excel to determine what, if any, changes could be detected in the colour bands after light exposure and how they compared across paper types.

5.4.3 OPTICAL UV FLUORESCENCE MICROSCOPY

Magnified images were taken of mock-up samples to examine fluorescence at a micro-scale. Digital images were captured with a microscope-mounted Olympus

---

[113] Appropriate values were found by imaging samples of a similar paper type, then opening the images in UFRaw and analyzing histograms of the distribution of pixel values. Ideally, intensity curves would fill the histogram with values 0-255 and without peaks at either extremity or concentrated to one side. Once a histogram was found which was well-distributed and did not cut off the tails of the intensity curves, the f/stop value used would be selected for all images of that paper type. Paper type had the greatest impact on the position of the pixel distribution curves, hence why it delineated the sets of images.

[114] An open-source raw processing programmed developed by the makers of Gimp.

[115] This program was used in Chapter 3 for particle analysis.

[116] See Appendix 19: Image Processing Procedure for UV-Induced Fluorescent Digital Images and Micrographs.

DP70 digital camera with CCD chip mounted to an Olympus BX51M microscope. The UV lamp used was a USH-103D short-arc mercury lamp housed in an Olympus U-RFL-T unit. Images at 50x magnification were collected with ISO settings at 200 to reduce noise. Exposure times needed to be adjusted for magnification and types of pigment as *indirect* pigments were less bright than *direct* pigments. The exposure times used are listed in Table 5.1.

Table 5.1 Exposure times for UV fluorescent micrographs of mock-up paint samples

Samples	Exposure time at 50x mag (seconds)
All *indirect* and commercial (1, 3, 4, 15, 16)	1/15
Direct samples 6 and 7	1/20
Direct sample 9	1/40
Gum arabic	1/45

Images were saved as tiffs and processed in MATLAB[117]. These were then analysed similarly to digital images and imported into Excel where blue and green channels were compared.

Images of the edges of pigments were collected as changes in fluorescence are most visible to the naked eye in these regions. These were visually compared to observe qualitative changes to fluorescence.

5.4.4 CASE STUDIES: RGB ANALYSIS

Case studies were photographed in UV light, though often distances varied, meaning this data is more qualitative and not directly comparable in some cases. Areas of fluorescence were cropped to a size where most pixels were accounted for by

---

[117] See Appendix 19: Image Processing Procedure for UV-Induced Fluorescent Digital Images and Micrographs.

fluorescing pigments,[118] then these cropped images were analysed similarly to the mock-up photographs. The following conditions and image sizes were used for each sample:

- **Thomas Harper:** photographed in same photo studio as mock-ups, same lighting and Canon EOS 6D camera, ½ second exposure, ISO 200, f/stop 5, distance from image approximately one metre.

    o Cropped image size: 731x434 pixels (Figure 5.5)
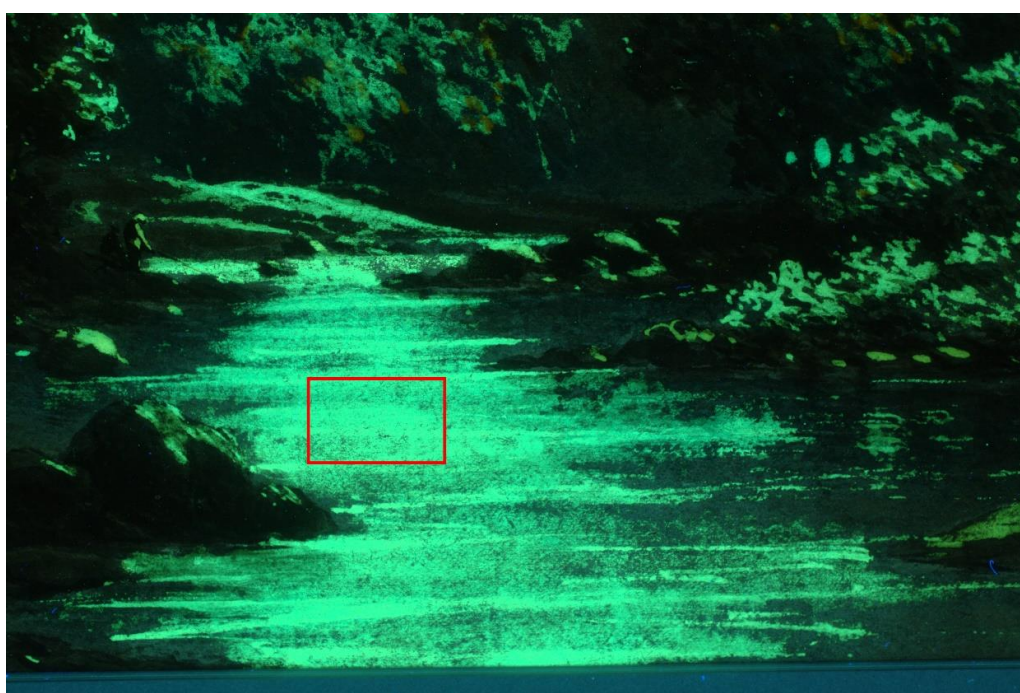
Figure 5.5 Detail of watercolour by Thomas Harper with cropped area outlined which was processed to extract RGB data for analysis.

- **St. Mary's Cathedral, Iona:** Photographed with Huawei cell phone camera with Darkbeam hand-held 365 nm UV torch in room with light coming from windows and fluorescent bulbs, photographed at distance of approximately 10 cm, torch at about 4 cm.

---

[118] The background subtraction procedure used for digital images of mock-up samples could not be applied to case studies as the contrast between fluorescing pigment and paper was not high enough to allow for the same methodology. Therefore, cropping presented the best option for RGB analysis.

- Cropped image sizes:

  - sample JC4 – 435 x 477 pixels (Figure 5.6, left)

  - sample JC7 – 238 x 230 pixels (Figure 5.6, right)
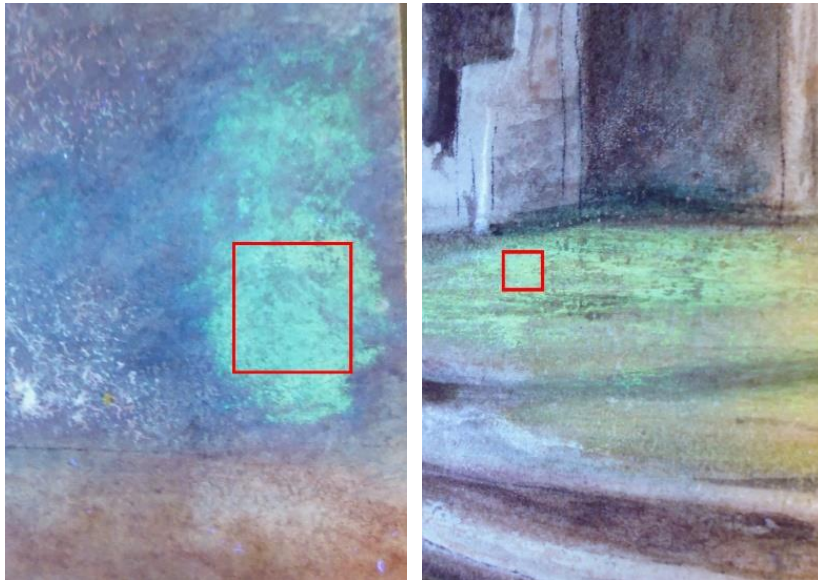
Figure 5.6 Details of watercolour titled *General View of St. Mary's Cathedral, Iona* with cropped areas outlined which were processed to extract RGB data for analysis. **Left:** sample JC4, **right:** sample JC7.

- **Irene Kendal:** photographed in same photo studio as mock-ups, same lighting and Canon EOS 6D camera, 1 second exposure, ISO 200, f/stop 8 at distance of approximately 2 metres.

  - Cropped image size: 67 x 104 pixels (Figure 5.7)

Figure 5.7 Detail of *Bouquet of Flowers* by Irene Kendall with cropped area outlined which was processed to extract RGB data for analysis.

- **Ruin drawing:** photographed in same photo studio as mock-ups, same lighting and Canon EOS 6D camera, 8 second exposure, ISO 200, f/stop 8 at distance of approximately 2 metres.

  - Cropped image size: 57 x 72 pixels (Figure 5.8)
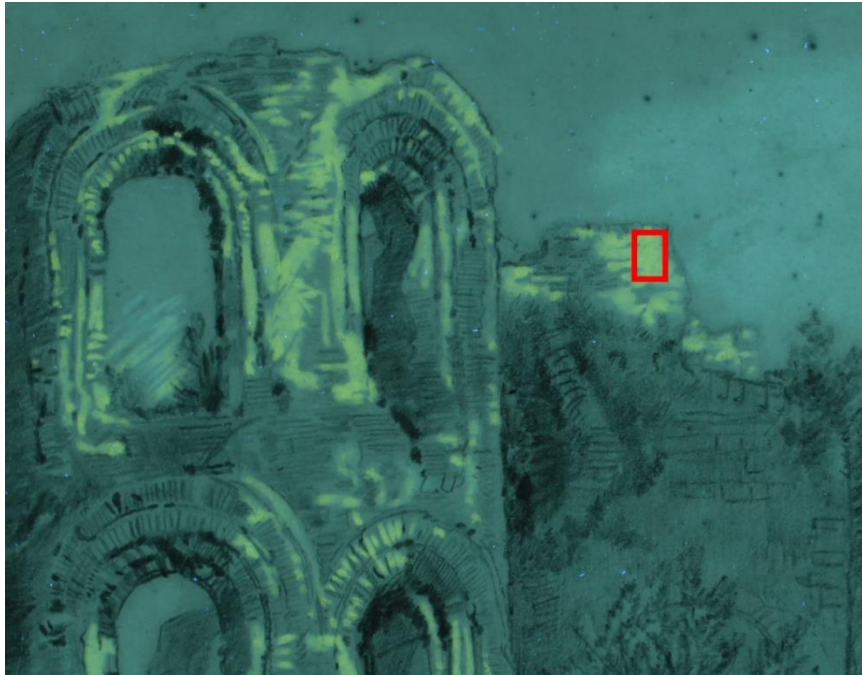
Figure 5.8 Detail of the ruin drawing with cropped area outlined which was processed to extract RGB data for analysis.

- **SS Buda:** photographed in same photo studio as mock-ups, same lighting and Canon EOS 6D camera, 15 second exposure, ISO 200, f/stop 8 at distance of approximately 2 metres.

  - Cropped image size: 17 x 18 pixels (Figure 5.9)
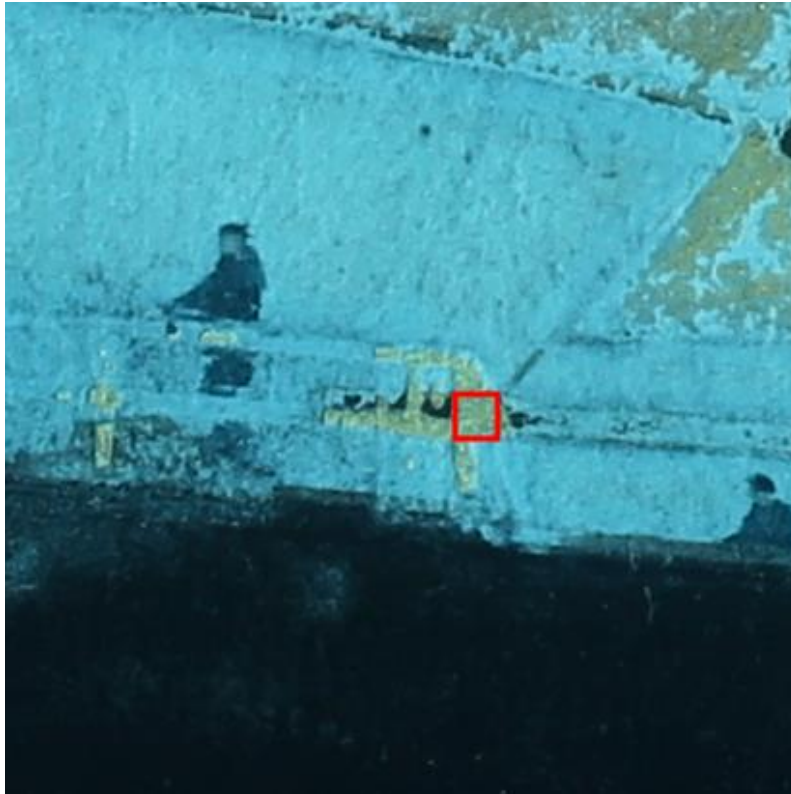
Figure 5.9 Detail of the watercolour *SS Buda* with cropped area outlined which was processed to extract RGB data for analysis.

5.5 RESULTS

5.5.1 FLUORIMETRY

Gum on paper samples: A relative decrease in emission intensity from 475-550 nm and increase at higher wavelengths was recorded in normalised spectra of gum arabic on Whatman paper. A similar decrease occurred in spectra from gum arabic on Folio paper, with an additional increase in intensity recorded from ~375-460 nm (Figure 5.10).
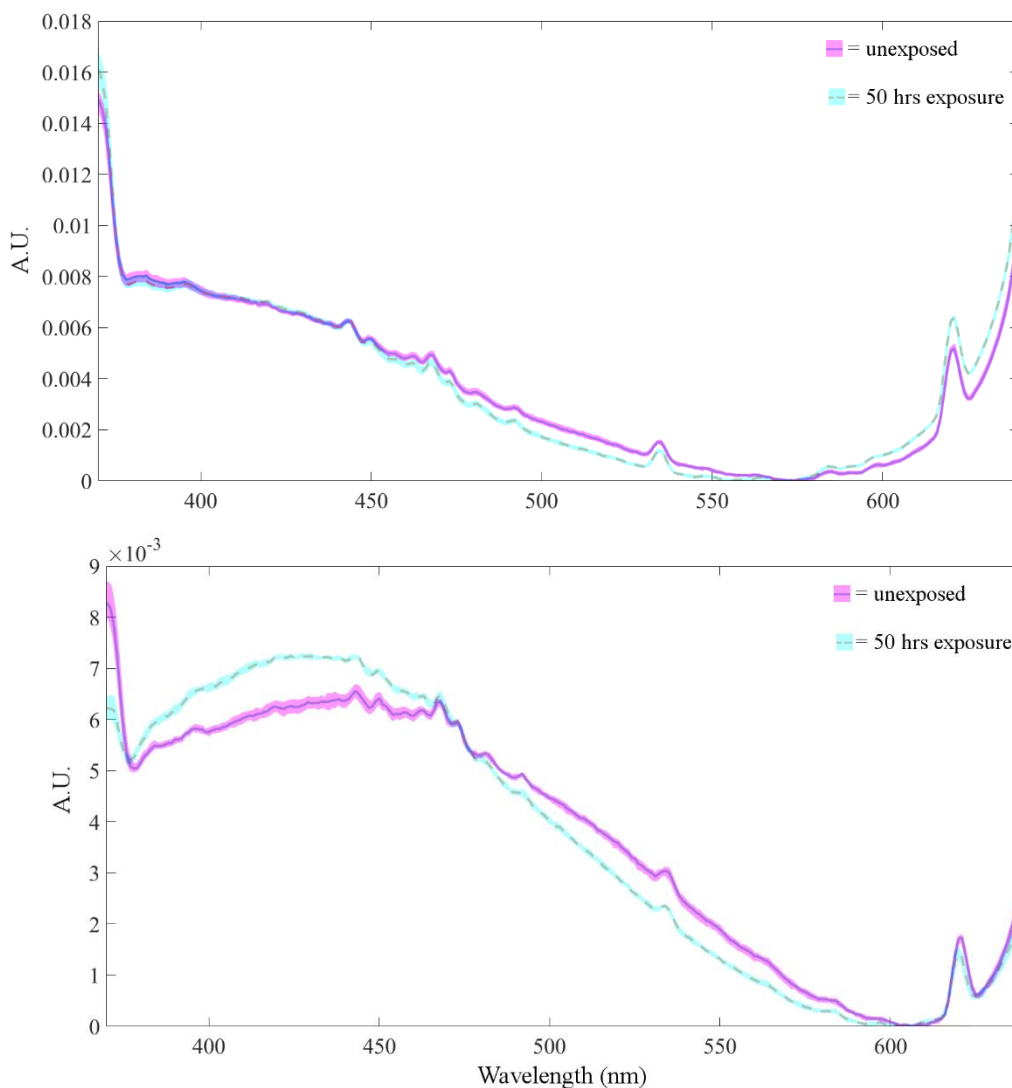
Figure 5.10 Emission spectra normalised by area (area = 1) for gum arabic on **above:** Whatman paper and **below:** Folio paper.

Comparison of green-to-NBE emission peak areas in pigment samples:[119] when dividing NBE emission peak areas from green areas, pigment samples fit into two types. Type 1 had green-to-NBE area ratios near or below 5. This group included *indirect* samples 3 and 4 and commercial samples 15 and 16 on both Whatman and Folio papers. Type 2 had ratios above 6, typically greater than 10. This group includes *indirect* sample 1 and *direct* samples 6, 7 and 9. (Figure 5.11).

---

[119] For all fluorescent peak area data, refer to Appendix 20: Fluorescent Spectra Peak Area and Intensity Values.
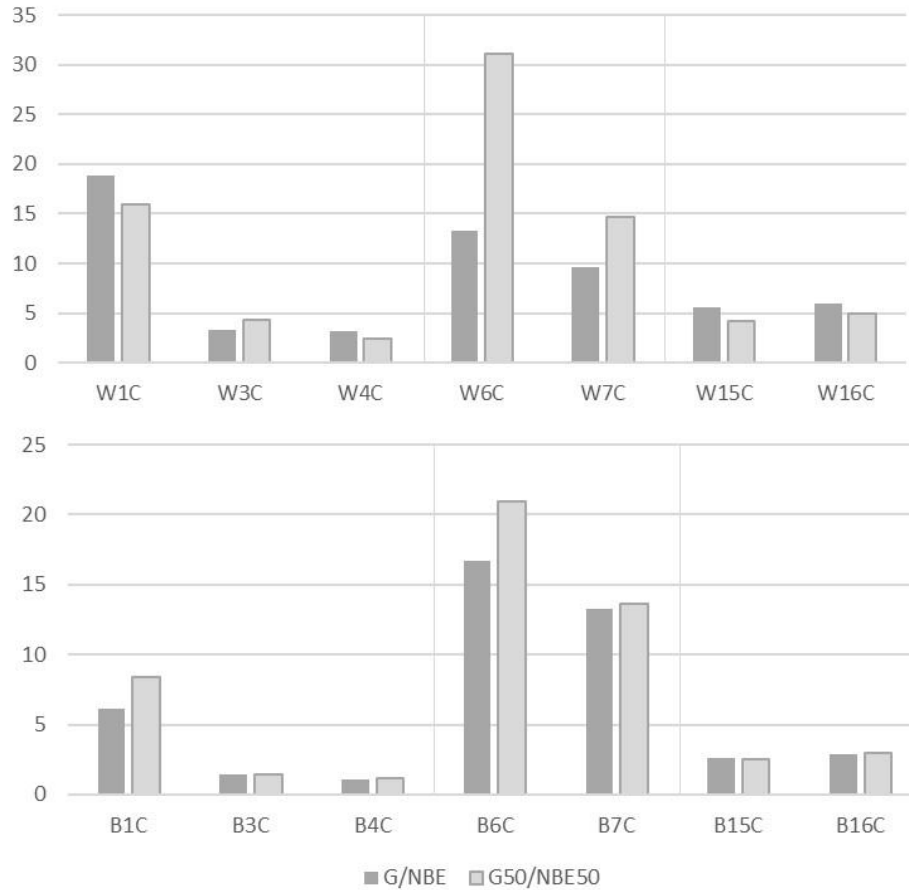
Figure 5.11 Ratios of green-to-NBE emission peak areas for samples on **above:** Whatman (W) and **below:** Folio (B) papers before (dark grey bars) and after (light grey bars) 50 hours of light exposure. *Direct* sample 9 is not included due to high ratio values.

Green-to-NBE ratios typically decreased in Type 1 samples apart from *indirect* sample 3 on Whatman paper and increased for Type 2 samples apart from *indirect* sample 1 on Whatman paper.

Sample 9 had ratios in the hundreds due to the near-absence of the NBE emission (Figure 5.12).
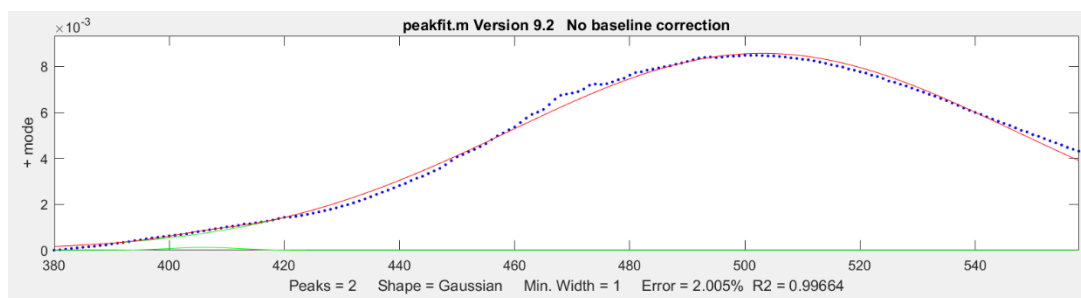
Figure 5.12 Peak fitting to *direct* method sample 9 on Whatman paper. Red line is composite peak made from two gaussians, one centred at 503 nm, the other, small peak at 406 nm. The extreme difference in area is evident.

Comparison of green-to-NBE emission peak intensities:[120] Peak intensities

followed the same trends as peak areas and grouped the samples into the same two

types. Type 1 contained ratios under one and Type 2 ratios were over one (Figure

5.13). Changes in intensity ratios also remained consistent with changes to peak area

ratios.

---

[120] For all fluorescent peak intensity data, refer to Appendix 20: Fluorescent Spectra Peak Area and Intensity Values.
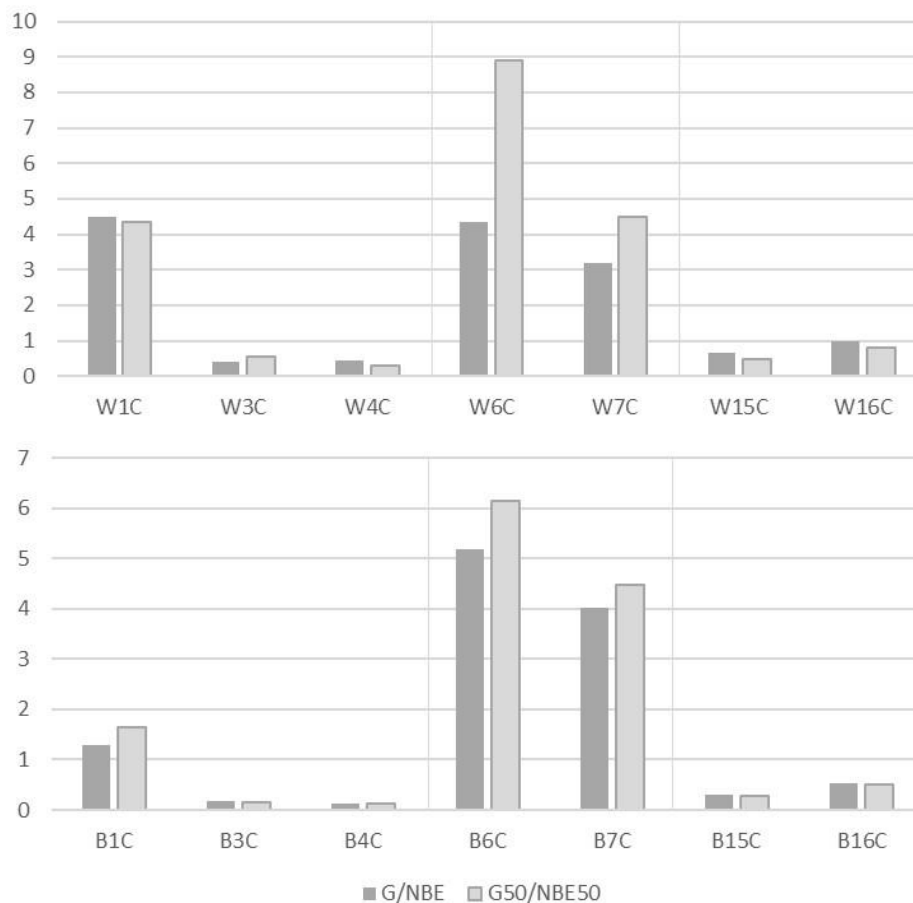
Figure 5.13 Ratios of green-to-NBE emission peak intensities for samples on **above:** Whatman (W) and **below:** folio (B) papers before (dark grey bars) and after (light grey bars) 50 hours of light exposure. *Direct* sample 9 is not included due to high ratio values.

Overall, Whatman *direct* samples 6, 7 and 9 on Whatman paper had the greatest increase of green/NBE peak intensity ratios, followed by *indirect* samples 1 on Folio paper and sample 3 on Whatman paper. *Indirect* sample 4 and *direct* method samples 6 and 7 on Folio paper increased their ratios by 10-20% while these ratios dropped for all other pigments on Folio paper. The green/NBE peak intensity ratio for *indirect* sample 1 on Whatman paper decreased slightly with light exposure while *indirect* sample 4 and commercial samples 15 and 16 decreased by approximately 20-30% (Figure 5.14)
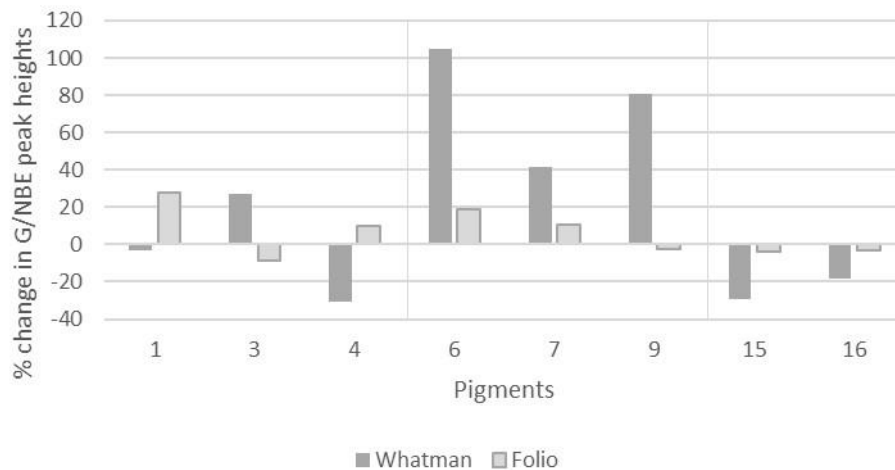
Figure 5.14 % changes to the green/NBE emission peak intensity ratios from fluorimetry spectra of samples on Whatman and Folio papers.

Peak shapes: Two distinct fluorescence shapes were seen corresponding to the green-to-NBE area ratios. Type 1 was characterised by a distinct NBE peak and a broad green band and type 2 was characterised by a small NBE peak and a broad, strong green band (Figure 5.15). Of the two types, the second type contains all *direct* method samples in addition to *indirect* Whatman sample W1C while the first contains only *indirect* and commercial pigments.
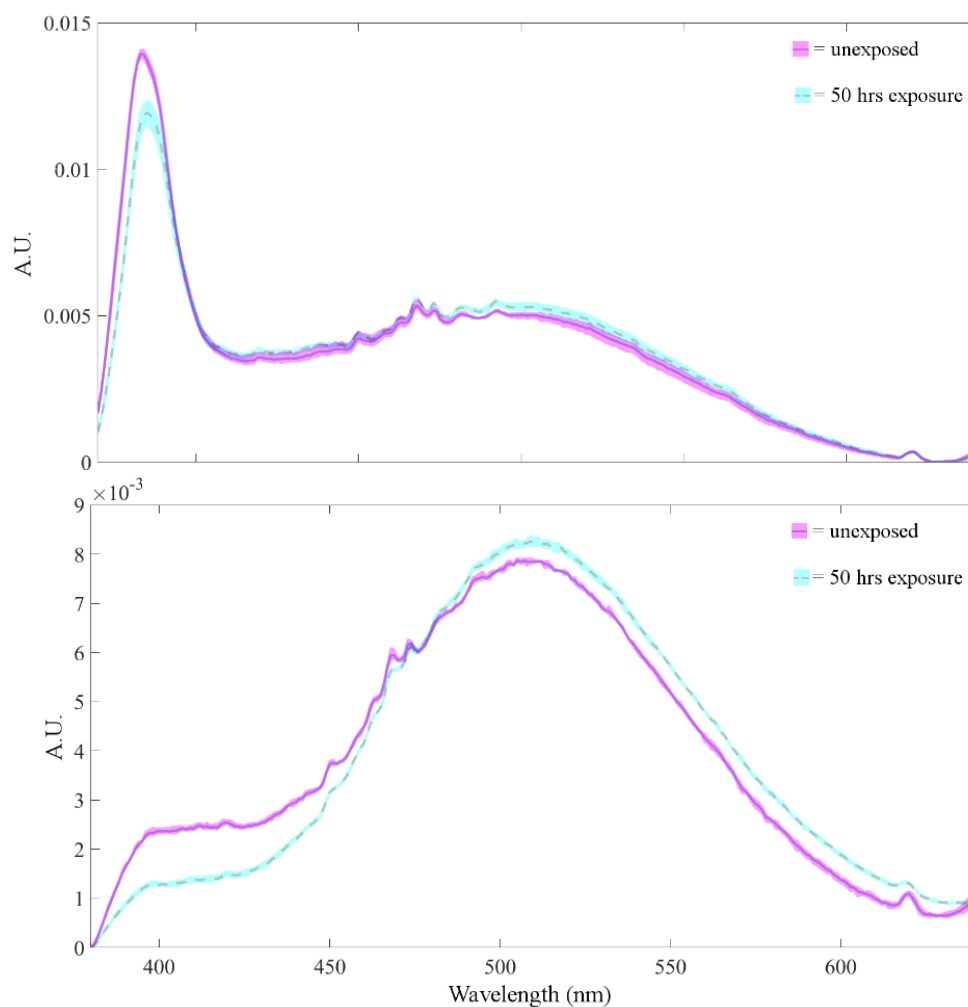
Figure 5.15 Two types of fluorimetry spectra: **above:** type 1 containing clear, strong NBE peak and **below:** type 2 with weaker, less well-defined peak. Top spectra from *indirect* sample 3 on Whatman paper and bottom from *direct* sample 6 on Whatman paper.

5.5.2 DIGITAL IMAGE PROCESSING

Mock-ups on Whatman paper: The greatest change in fluorescence after light exposure was observed in *indirect* samples 3 and 4 and commercial samples 15 and 16. Most change was seen around the edges which shifted to a darker green colour while the *indirect* pigments appeared to change more overall. Changes in commercial pigments were more confined to the edges. By contrast, *indirect* pigment 1 and *direct* pigments 6, 7 and 9 did not appear to change after light exposure (Figure 5.16).
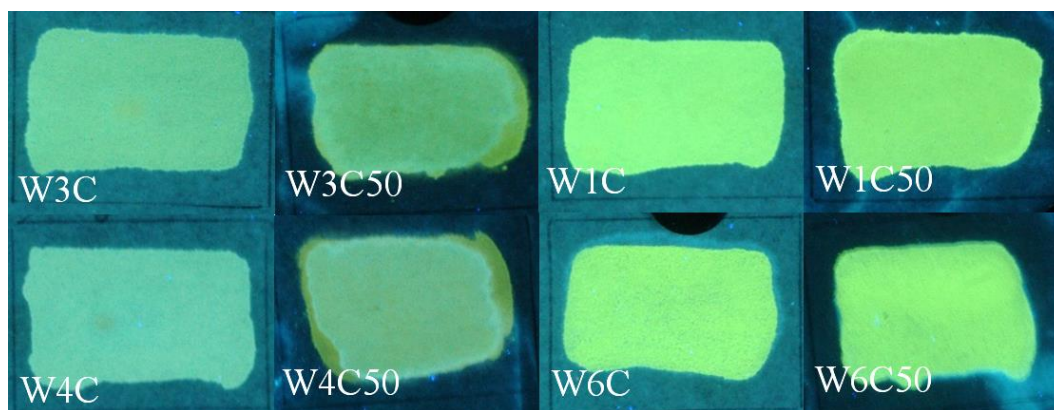
Figure 5.16 Left two columns: *Indirect* samples 3 and 4 on Whatman paper before and after light exposure demonstrating visible changes in colour and type of fluorescence. **Right two columns:** *indirect* pigment 1 and *direct* pigment 6 did not change visibly after light exposure.

After background subtraction and averaging of RGB values,[121] the ratio of the intensities of the green and blue channels were calculated before and after light exposure. Ratios below 1.7 were calculated for *indirect* samples 3 and 4, *direct* sample 9 and commercial samples 15 and 16. *Indirect* sample 1 and *direct* samples 6 and 7 had ratios over 1.7, while the control samples of gum on paper had very low ratios under 1. Ratios for all samples increased after light exposure except for the control gum sample (Figure 5.17).
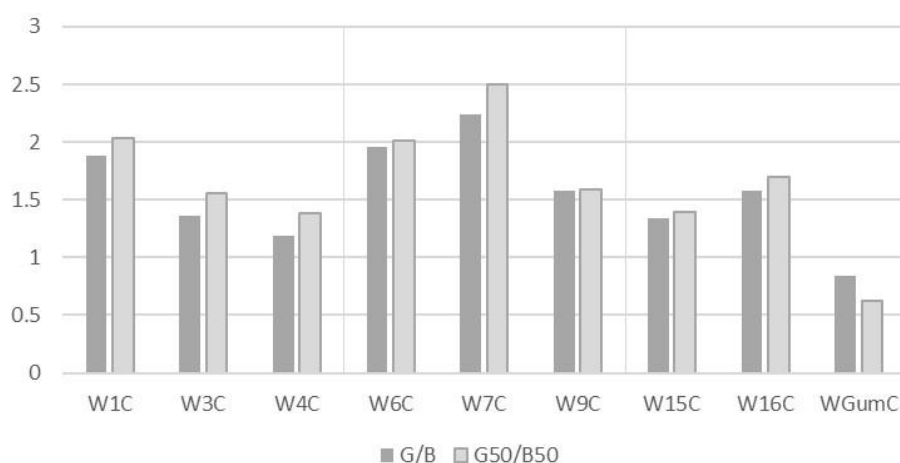
Figure 5.17 Green/blue channel ratios from digital UV fluorescent images of samples on Whatman paper before (dark grey bars) and after (light grey bars) 50 hours of light exposure.

---

[121] For all photography RGB data and green/blue channel ratios, refer to Appendix 21: RGB Values and G/B Ratios.

Mock-ups on Fabriano paper: Visual changes in fluorescence for samples on Fabriano paper were not as obvious as the changes seen on Whatman paper, particularly for the *indirect* method pigments 3 and 4 which changed dramatically on Whatman but remained visually unchanged on the Fabriano (Figure 5.18).
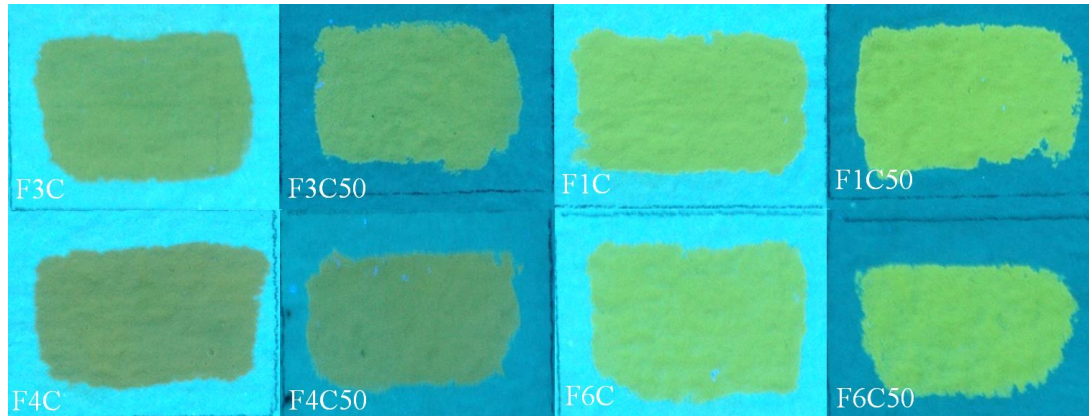
Figure 5.18 Left two columns: *Indirect* samples 3 and 4 on Fabriano paper before and after light exposure. Exposed samples do not appear visibly different. **Right two columns:** *indirect* pigment 1 and *direct* pigment 6 also did not change visibly after light exposure.

Pigments grouped by green-to-blue band ratios followed the same trend as in Whatman paper, though the difference between the two groups was less obvious. *Indirect* samples 3 and 4, *direct* method sample 9 and commercial samples 15 and 16 maintained ratios under 1.6 while all others except gum control samples maintained higher ratios. Ratio increases were observed in all samples except *indirect* sample 4 and commercial sample 15. Averaged RGB swatches appeared slightly darker after light exposure as did the gum sample which darkened significantly (Figure 5.19).
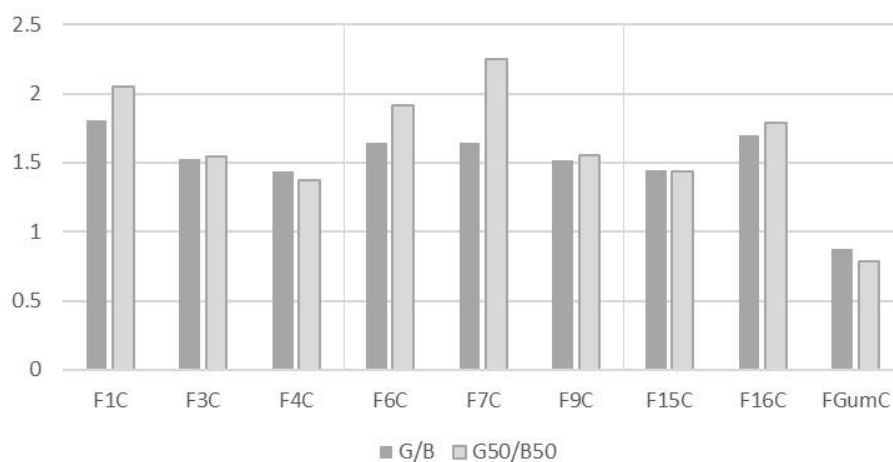
Figure 5.19 Green/blue channel ratios from digital UV fluorescent images of samples on Fabriano paper before (dark grey bars) and after (light grey bars) 50 hours of light exposure.

Mock-ups on Folio paper: changes to the fluorescence of pigment samples on Folio paper were very difficult to detect with photography or the naked eye, though the paper itself visibly decreased in fluorescence intensity (Figure 5.20).
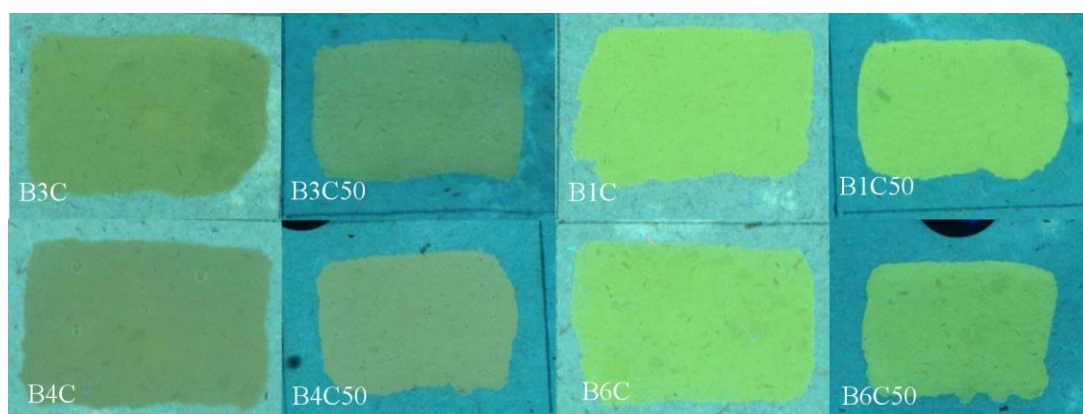
Figure 5.20 Left two columns: *Indirect* samples 3 and 4 on Folio paper before and after light exposure. Exposed samples do not appear visibly different. **Right two columns:** *indirect* pigment 1 and *direct* pigment 6 also did not change visibly after light exposure.

Ratios of green-to-blue bands fell at or below 1.6 in *indirect* samples 3 and 4, *direct* sample 9 and commercial pigment 15 while all other samples were higher. The control sample was around 1. Ratios of all samples reduced after light exposure except *indirect* sample 1 with increased (Figure 5.21).
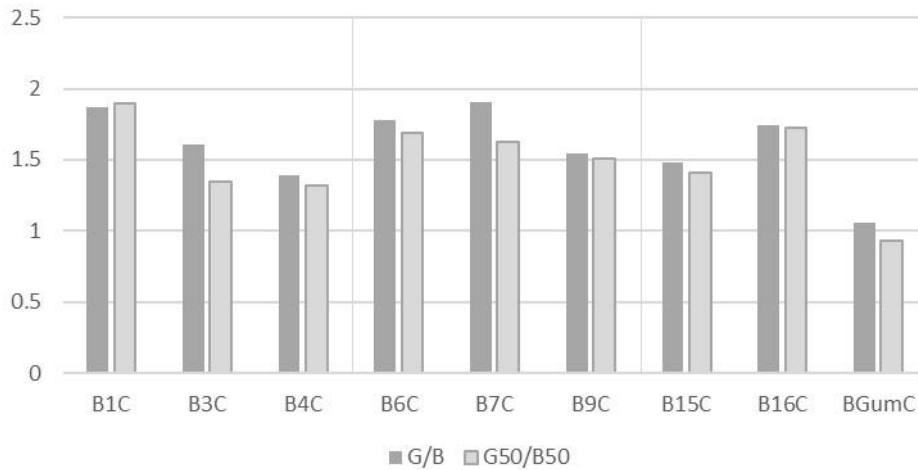
Figure 5.21 Green/blue channel ratios from digital UV fluorescent images of samples on Folio paper before (dark grey bars) and after (light grey bars) 50 hours of light exposure.

Comparison of colour channel ratio changes across paper types in digital photographs: when the percent change to the green/blue ratio was calculated[122] and compared, samples on Whatman paper had the most consist increase in green/blue ratio, followed by those on Fabriano. Samples on Folio paper consistently decreased in green/blue ratio values. All control samples consisting of gum on paper decreased significantly in green/blue ratios. On Whatman paper, the greatest change was seen in *indirect* samples 3 and 4. On Fabriano paper, *indirect* sample 1 and *direct* method samples 6 and 7 had the greatest change after light exposure. *Indirect* sample 3 and *direct* sample 7 changed the most of all samples on Folio paper. Samples 1, 3 and 7 experienced a large change in green/blue ratio most consistently across paper samples (Figure 5.22).

---

[122] The ratio before light exposure was subtracted from the ratio after light exposure, then this value was divided by the ratio before light exposure and multiplied by 100 to obtain the percent change values.
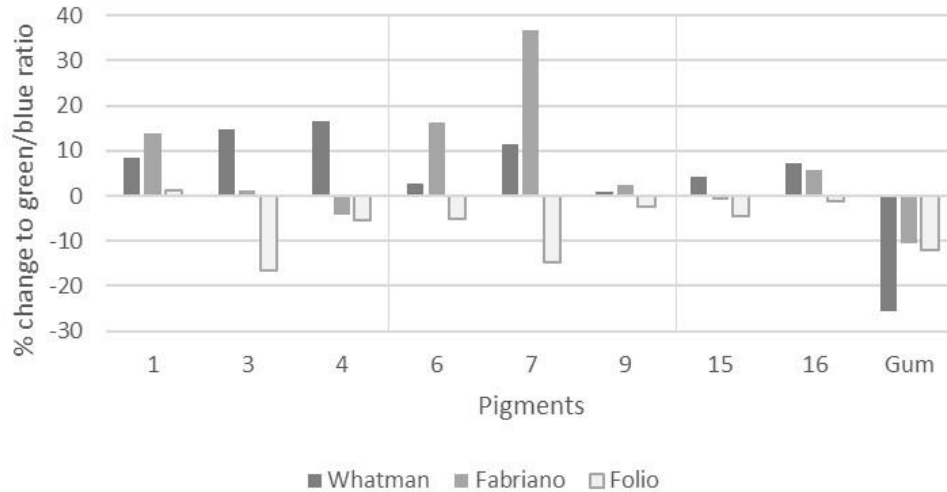
Figure 5.22 % changes to green/blue colour channel ratios from digital UV fluorescent images of samples on Whatman, Fabriano and Folio papers.

Case studies: Average RGB values appear very different from one another when representative swatches were made (Figure 5.23). These were much easier to compare than unprocessed images given the range of image sizes.
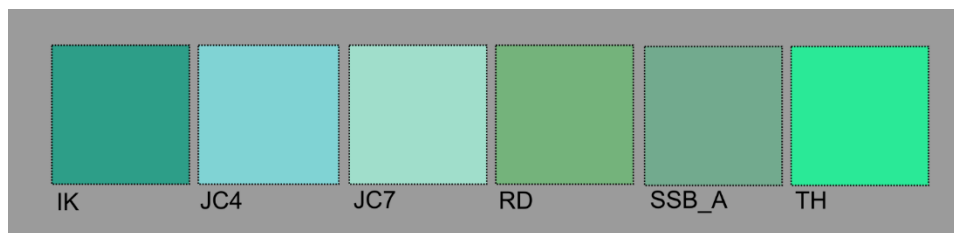
Figure 5.23 Colour swatches of average RGB values from fluorescent images of case study samples.

Case studies had green-to-blue ratios generally less than 1.6. The lowest ratio was found in sample JC4 from the *General View of St. Mary's Cathedral, Iona* followed by sample JC7 from the same piece, then IK from Irene Kendal, RD from the ruin drawing and TH from the Thomas Harper watercolour (Figure 5.24).
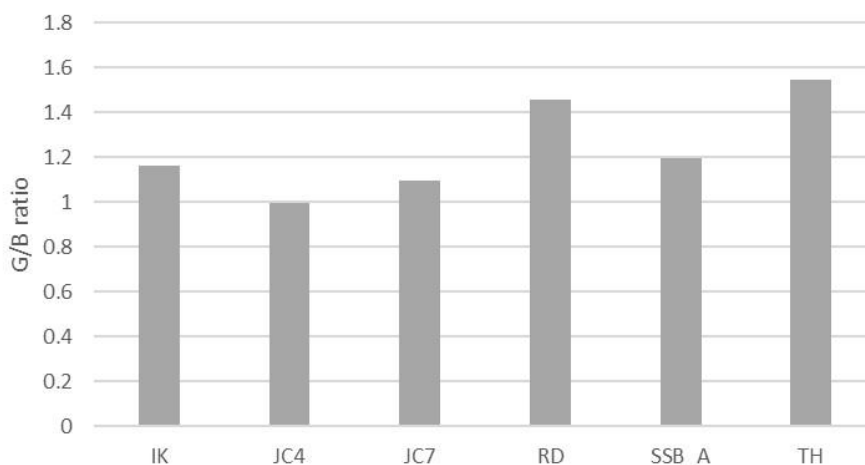
Figure 5.24 Green/blue colour channel ratios for select case study samples.

5.5.3 UV FLUORESCENT OPTICAL MICROGRAPHY

Whatman paper micrographs: When viewed at 50x magnification, there is a clear increase in green fluorescence after light exposure in *indirect* sample 3 and 4 and commercial pigments 15 and 16. These effects are most obvious when viewing sample edges under magnification. *Direct* pigment samples 6, 7 and 9 as well as *indirect* sample 1 do not appear to change after light exposure. (Figure 5.25).
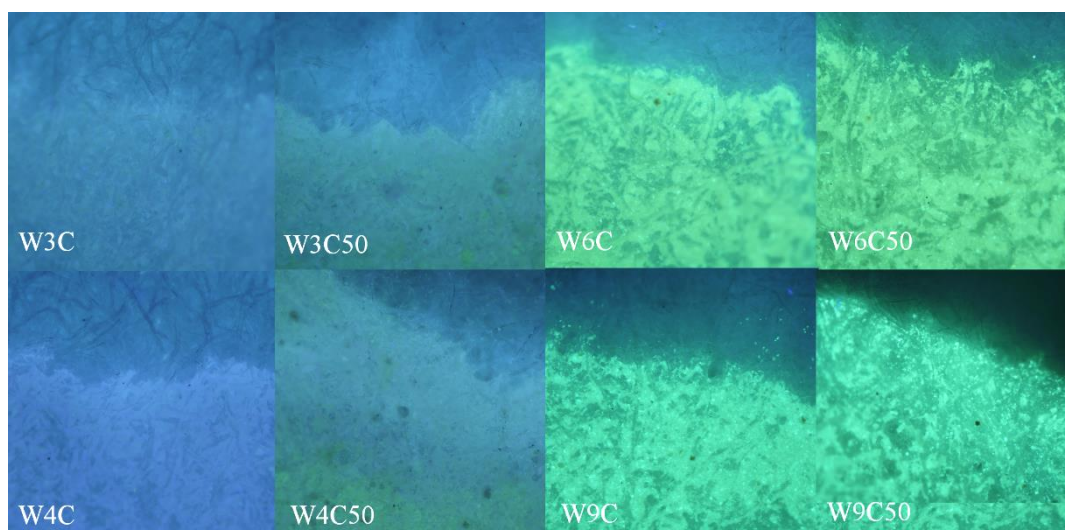
Figure 5.25 Micrographs of samples on Whatman paper at 50x magnification. **Left two columns:** *Indirect* samples 3 and 4 before and after light exposure. Exposed samples appear greener after exposure. **Right two columns:** *direct* pigments 6 and 9 did not change visibly after light exposure.

Ratios of green/blue channels were below 1 in unexposed *indirect* samples 3 and 4

and sample 15. These two *indirect* samples had the greatest increase in green-to-blue

ratio. After light exposure, sample 15 maintained the lowest ratio (Figure 5.26).
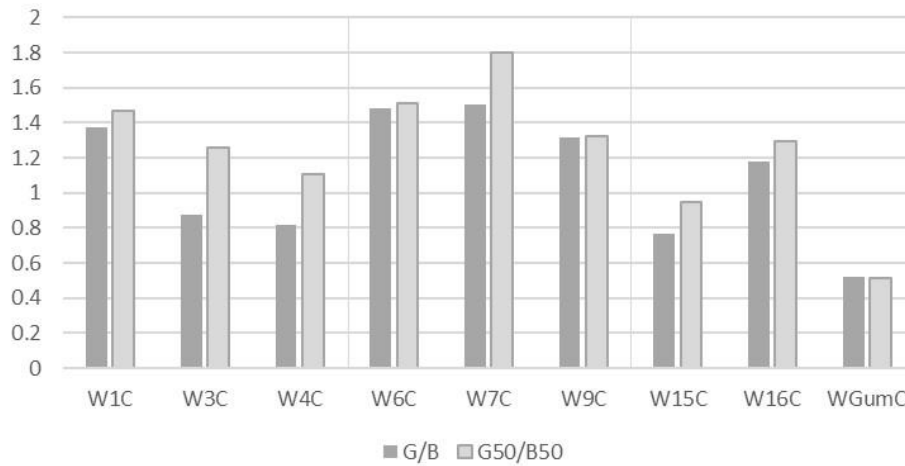
Figure 5.26 Ratios of green-to-blue channels from UV fluorescent micrographs of samples on
Whatman paper before (dark grey bars) and after (light grey bars) 50 hours of light exposure.

Fabriano: Fluorescence in samples on Fabriano paper did not appear to change

much after light exposure. Fluorescent intensity in the paper reduced significantly

but this did not alter the appearance of the pigments (Figure 5.27).
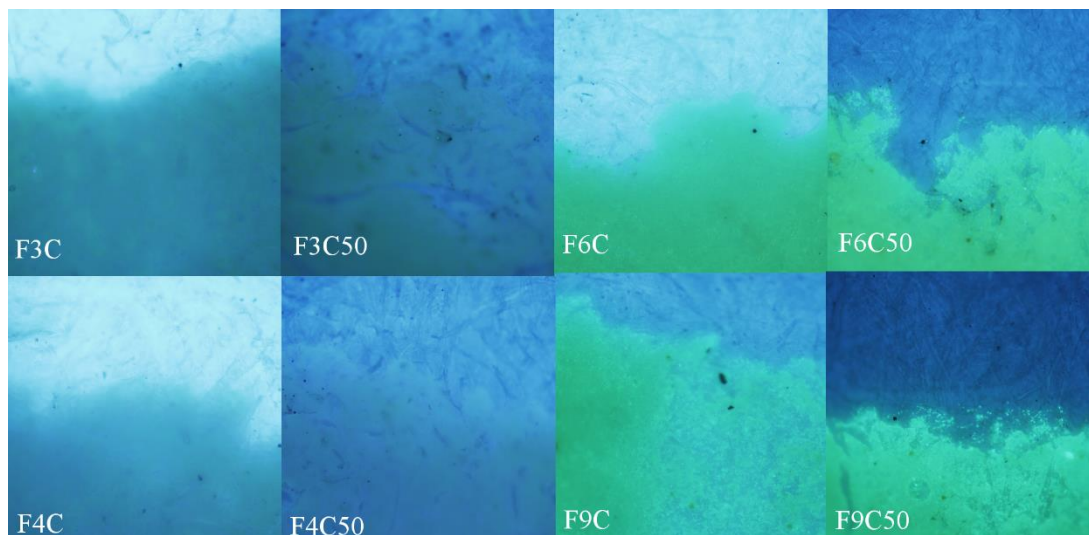
Figure 5.27 Micrographs of samples on Fabriano paper under 50x magnification. **Left two
columns:** *Indirect* samples 3 and 4 before and after light exposure. **Right two columns:** *direct*
pigments 6 and 9 after light exposure. Neither set of pigments appears to have changed in
fluorescent intensity or colour.

Indirect samples 3 and 4 and commercial pigment 15 all maintained green-to-blue ratios of below 1. This ratio decreased after light exposure for all *indirect* samples, *direct* method sample 7 and commercial sample 16, while it increased slightly for *direct* method pigments 6 and 9 as well as commercial sample 15. The ratio of the control sample decreased and remained below 1 (Figure 5.28).
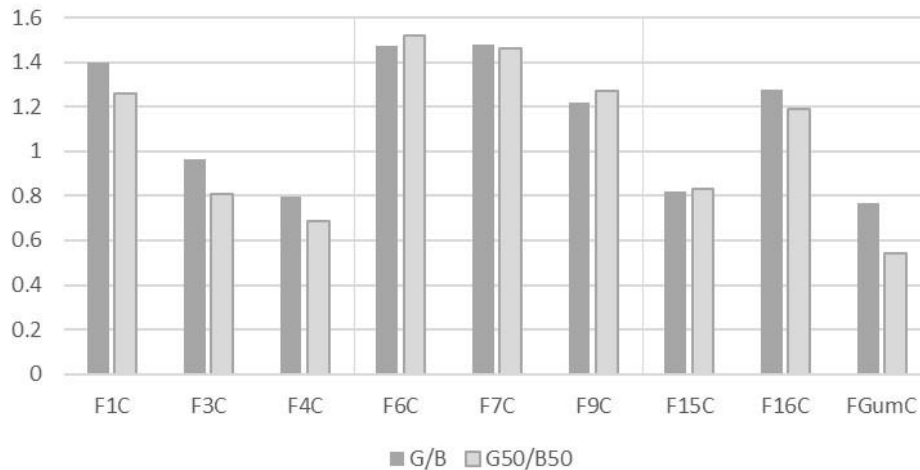
Figure 5.28 Green/blue colour channel ratios from UV fluorescent micrographs of samples on Fabriano paper before (dark grey bars) and after (light grey bars) 50 hours of light exposure.

Folio: *Indirect* samples 3 and 4 and commercial sample 16 appeared to change colour and increased in intensity somewhat after light exposure while all other samples appeared similar under magnification. *Direct* method samples 6 and 9 appeared slightly brighter after light exposure (Figure 5.29).
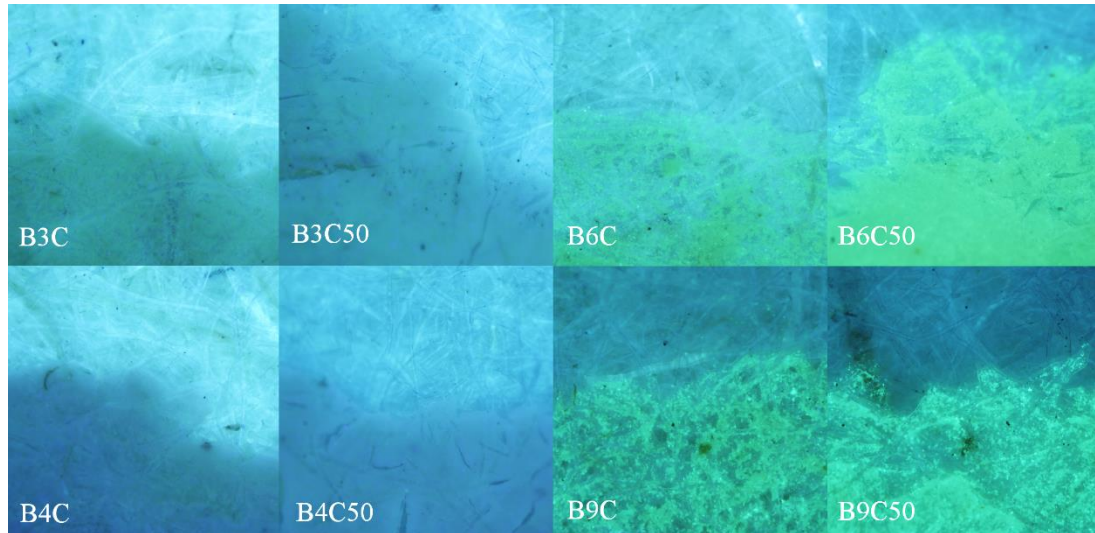
Figure 5.29 Micrographs of samples on Folio paper under 50x magnification. **Left two columns:** *Indirect* samples 3 and 4 before and after light exposure. **Right two columns:** *direct* pigments 6 and 9 after light exposure. *Indirect* pigments shown appear to change very slightly, while *direct* method pigments do not appear to change in colour but appear slightly brighter.

Direct method sample 7 changed appearance dramatically after light exposure, appearing to have a broken surface and fluorescing very blue between groupings of green pigment (Figure 5.30).
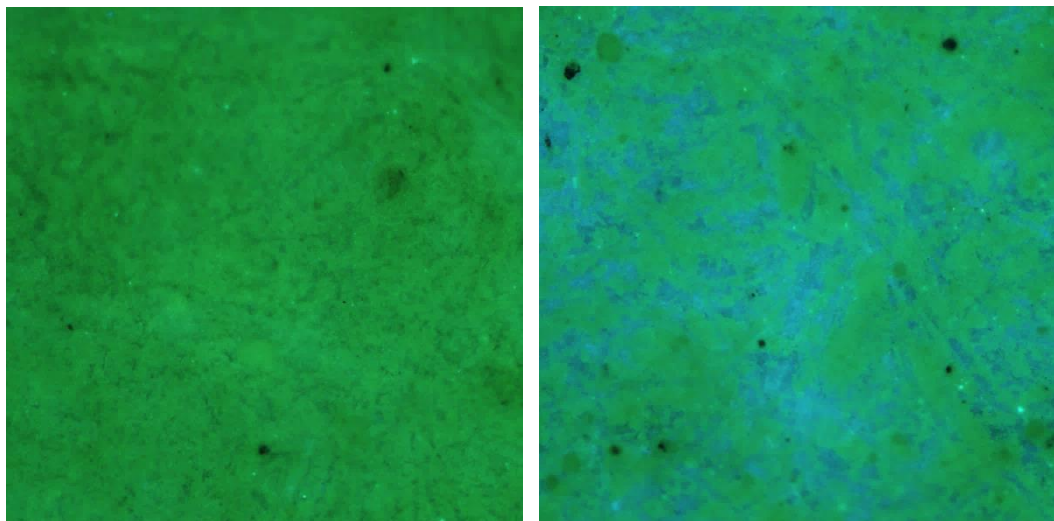
Figure 5.30 Micrographs of *direct* method sample 7 on Folio paper under 50x magnification **left:** before light exposure and **right:** after light exposure. A significant new blue contribution can be seen in the micrograph on the right.

When comparing green-to-blue RGB bands, *indirect* samples 3 and 4 and commercial sample 15 remained under 1 while all others contained ratios over 1.

The unusual new fluorescence in *direct* method sample 7 is evident as a sharp decrease in the green-to-blue ratio after light exposure. *Direct* method pigments 6 and 9 as well as commercial pigment 16 also had decreased ratios with light exposure while all *indirect* samples and commercial sample 15 increased ratios after exposure. The control sample decreased ratios slightly with light exposure and maintained a ratio under 1 (Figure 5.31).
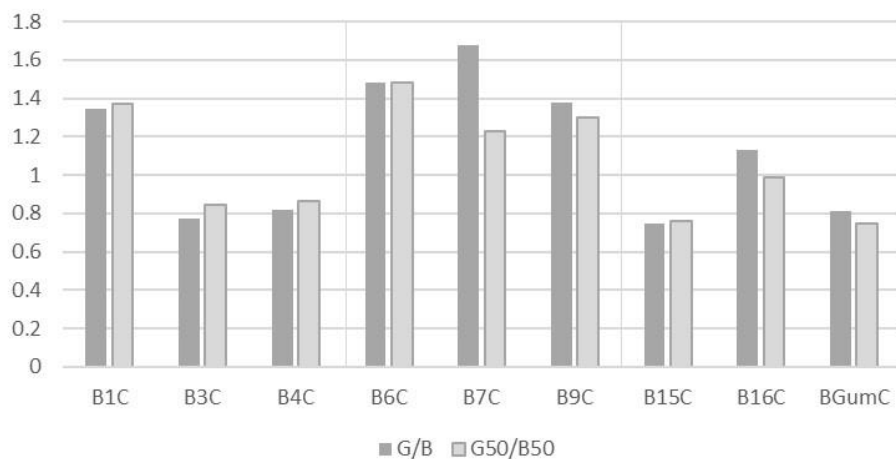
Figure 5.31 Green/blue colour channel ratios from UV fluorescent micrographs of samples on Fabriano paper before (dark grey bars) and after (light grey bars) 50 hours of light exposure.

Comparison of colour channel ratio changes across paper types in micrographs: the highest percent change in green/blue ratios derived from micrographs occurred in pigments on Whatman paper. Ratios in *indirect* method samples 3 and 4 increased by over 30% while commercial sample 15 increased by 24%, *direct* sample 7 by 20% and commercial pigment 16 by 10%. All other pigments increased by less than 10%. Green/blue ratios from samples on Fabriano paper generally decreased except for *direct* method samples 6 and 9 and commercial sample 15 which all increased slightly. Ratios from samples on Folio paper increased in all *indirect* samples and commercial sample 15 and decreased in *direct* sample 7 and commercial sample 16. *Direct* method sample 6 did not change appreciably. *Indirect* method samples 3 and 4 changed the most over all three paper

types, followed by *indirect* sample 1 and commercial sample 16. All control samples had decreased ratios after light exposure, with Fabriano paper decreasing the most and Whatman the least (Figure 5.32).
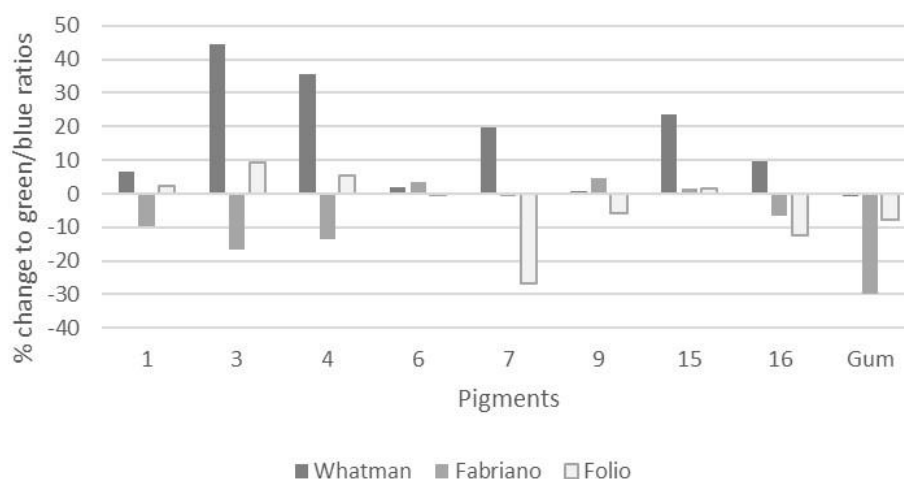
Figure 5.32 % change to green/blue colour channel ratios from digital UV fluorescent micrographs of samples on Whatman, Fabriano and Folio papers.

5.6 DISCUSSION

5.6.1 ORIGINS OF TWO FLUORESCENT TYPES

Fluorescence as measured by fluorimetry and photography fell into two types: those with a dominant NBE emission or blue channel and those with a dominant green emission or green channel. Additionally, the location of the green peak differed between types. The green band in the first type, comprising *indirect* samples 3 and 4 and commercial sample 15, was located between ~460-485 nm while its location for the second type, comprised of *indirect* sample 1, *direct* samples 6, 7, and 9 and commercial sample 16, was located between 500 and 515 nm (Figure 5.33).
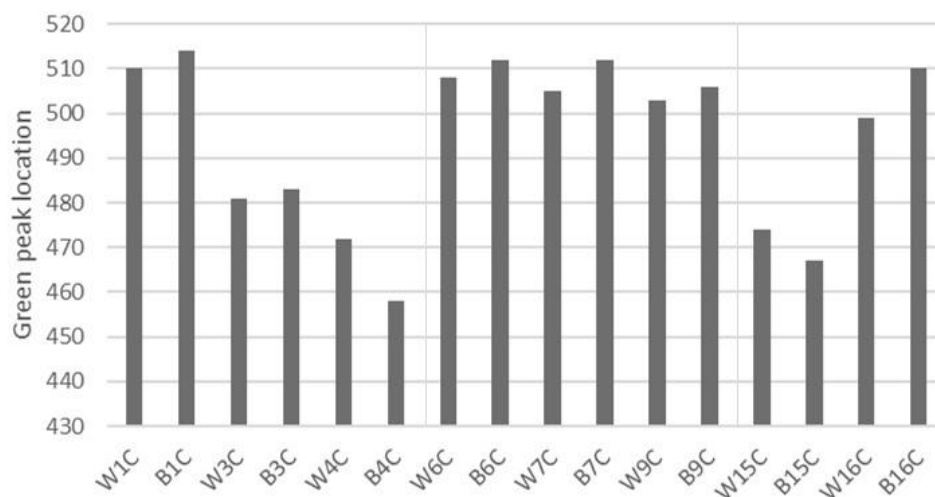
Figure 5.33 Position of the green band in fluorimetry spectra from unexposed pigment samples on Whatman (W) and Folio (B) papers

The prominence of the NBE peak in the first type of sample indicates a crystal structure with fewer defects. This band is well-established as the emission from band-gap relaxations, meaning that its intensity indicates a near-ideal ratio of zinc to oxygen ions. The presence of a green band suggests that defects are present, though the type is unclear. A green band with a reduced or absent NBE peak would indicate a strong deviation from the ideal ion ratio via either an excess of zinc or oxygen vacancies. Zhu *et al.* (2014) annealed zinc oxide samples at 400 ℃ in an oxygen atmosphere to convert stacking faults to defects and produced a fluorescent spectrum with a nearly-absent NBE peak and a stronger peak at 485 nm. They were unable to identify the cause of this peak, however. The data from this study indicates that the pigments in type 1 were likely produced in an oxygen-rich atmosphere and contain few vacancy defects.

The peak located at ~510 nm has been associated with zinc oxides annealed in anoxic environments (Shan *et al.*, 2005). Lyons *et al.* (2017) suggest that the transition energy between zinc ions and dangling bonds produces an emission at 515 nm. Such bonds are extremely common in zinc oxide and other semiconductors and

could be the cause of this emission band. These dangling bonds would increase with the removal of oxygen from polar surfaces by surrounding moisture or with excitation by light and catalysis by carbon atoms (Kumar and Rao, 2015). A strong 510 nm peak could indicate a less conductive pigment with fewer oxygen ions.

Oxygen removal from polar surfaces may be facilitated by reactions with adsorbed carbon-containing molecules such as carbon dioxides and monoxides in the atmosphere. This reaction is catalysed by light with wavelengths up to 650 nm. Carbon reactants oxygenate first to carbon monoxide, then again to carbon dioxide, potentially removing two oxygens from zinc oxide polar surfaces (Bao *et al.*, 2011; Gurwitz, Cohen and Shalish, 2014; Kumar and Rao, 2015). Watercolour pigments are not totally encased in binding media or varnished like oils, meaning they are more exposed to gaseous carbon molecules. This would facilitate oxygen removal and related conversion of fluorescence from blue to green along with a gradual reduction in peroxide formation and electrical activity. A blue-fluorescing *indirect* zinc oxide pigment could acquire a dominant green fluorescence over time via this mechanism.

5.6.2 COMPARISONS TO HISTORIC ZINC OXIDE PIGMENTS

Clementi *et al.* (2012) pointed to a difference in the shapes of fluorescent spectra from analytical sources of zinc oxide and historic zinc white samples. The analytical sources had spectra which fit with the type 1 shape, characterised by a strong NBE peak and a weak, broad green band while historic pigments were more like type 2 spectra with a stronger green band, though still containing a strong peak.

The historic samples analysed by Clementi *et al.* are most like *indirect* sample 1 in shape and peak intensity ratios while the analytical zinc oxide pigment is closer to

commercial sample 15 or *indirect* analytical sample 3. The binding medium used is different, as Clementi *et al.* used oil and alkyd binders, but the spectra are still comparable. The similarities discussed indicate a similarity in composition and crystal structure of sample 1, a red seal *indirect* zinc oxide, to historic zinc whites and implies that some pigments sold today as zinc white are closer to the analytical material than the pigments sold in the nineteenth century, though commercial sample 16 has a much stronger green peak and indicates some similarity to the historic sample (Figure 5.34).
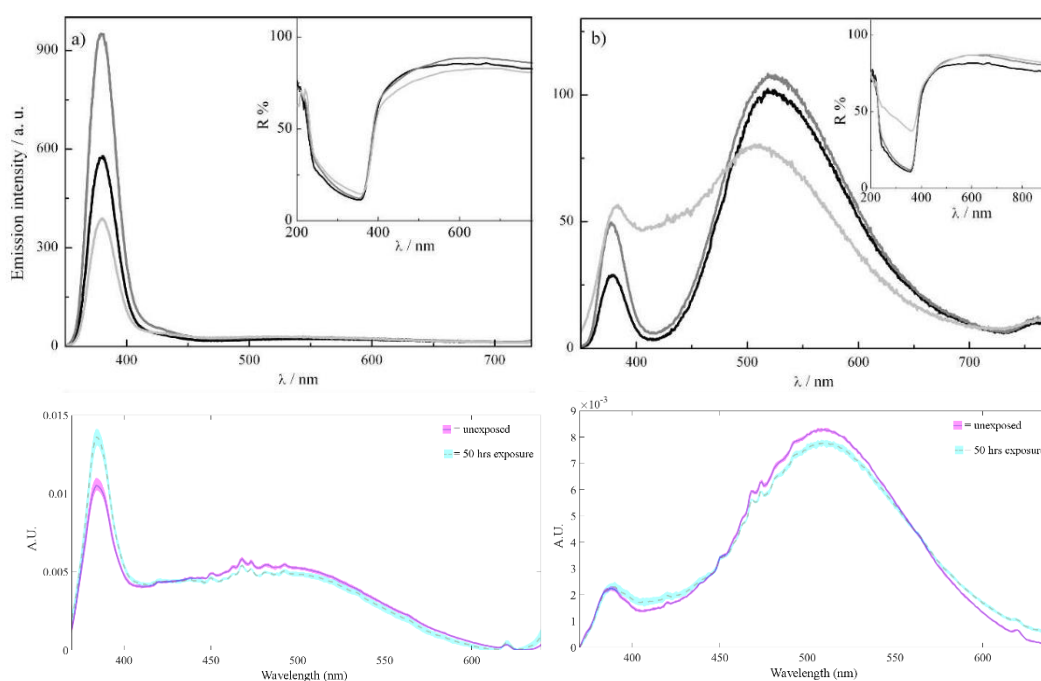
Figure 5.34 Upper left: Emission spectra of zinc oxide in alkyd medium from Clementi *et al.* (2012) **Upper right:** emission spectra of historic zinc white pigment from Clementi *et al.* **Lower left:** emission spectra from commercial sample 15 on Whatman paper and **lower right:** emission spectra from *indirect* sample 1 on Whatman paper.

5.6.3 COMPARING ANALYTICAL METHODS

Type 1 pigments, specifically *indirect* samples 3 and 4 and commercial sample 15, consistently had the smallest green-to-blue ratios across all analytical methods, with the greatest difference between their ratios and all other pigments observed in fluorescence spectra. Photographs and micrographs of type 1 pigments on Whatman

paper also had lower ratios compared to others pigments on Whatman paper. In all photographs, type 1 pigments had ratios below 1.5 before light exposure.

Commercial pigment 16 and *direct* method pigment 9 were unusual in that they sometimes compared well with type 1 pigments and other times compared more favourably with type 2 pigments. The former is true of photographs on Whatman paper when both pigments have relatively low ratios around 1.5. In photographs of the two pigments on Fabriano and Folio papers, the green-to-blue ratio for sample 16 is closer to type 2 pigments while sample 9's ratio is closer to type 1. Ratios from micrographs of the two pigments group them more easily with type 2 pigments, however.

Trends in percent changes for all samples on Whatman paper were consistent across photographs and micrographs; however, trends in samples on Fabriano and Folio paper varied widely from one technique to another. Additionally, percent changes in peak ratios from fluorimetry spectra did not agree with photographs or micrographs. This likely stems from influences by gum and paper fluorescent contributions which would be more prominent at different scales and paint thicknesses, a quality which is not consistent across paint surfaces or samples despite attempts to regulate paint application procedures.

5.6.4 CASE STUDIES

Case study pigments were most comparable when photographed in the same conditions. Samples from *General View of St. Mary's Cathedral, Iona* were photographed with a different camera and in very different light than the other four samples analysed and appear much brighter as a result. The green/blue intensity ratios are lower than the other samples but it is difficult to determine if this is an

accurate characterisation given the very different light sources and camera type used to capture the images.

Of the four samples which were photographed in a photo studio, imaging distances and camera settings varied somewhat. The colour ratios seemed to relate to the level of conservation treatment that had been carried out due to deterioration and damage by pigments. Samples IK and SSB_A had the lowest ratios, both under 1.2 and both samples came from pieces which had extremely degraded pigment areas. Samples RD and TH had much higher green/blue ratios. They appear very different on paper, one fluorescing very bright green and the other a yellow-khaki but their green/blue ratios are similar. The yellow colour of the pigment from the ruin drawing appears to fit the description by Cosentino of zinc white fluorescence as yellow.

5.6.5 INFLUENCE OF PAPER AND GUM ON FLUORESCENT SPECTRA

Several small peaks are visible in all fluorimetry spectra which, when compared with normalised spectra of gum arabic on the same paper type, can be attributed to the paper and gum fluorescence (Figure 5.35). Additionally, the dual peaks observed at 410 and 450 nm by Artesani *et al.* (2018) were not observed in this study. They may be present but are not detectable in that wavelength range.
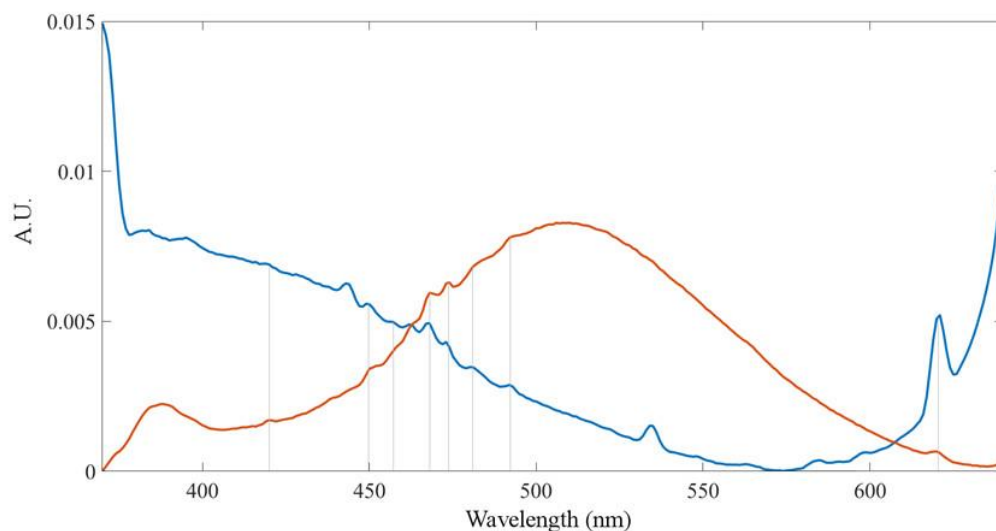
Figure 5.35 Spectra of *indirect* sample 1 on Whatman paper (orange) and gum arabic on Whatman paper (blue). Grey lines indicate where small peaks can be attributed to fluorescent contributions by paper and gum medium.

Increasing contributions by gum arabic fluorescence after light exposure could explain the heightened NBE peak in some samples which seems to run counter to the theory that degradation would increase crystal defects, increasing the green band and reducing the NBE peak by eliminating band-gap jumps. Dhenadhayalan, Mythily and Kumaran (2014) describe the increased fluorescent contributions by the amino acids present in gum arabic with decreased pH. These precipitate out of the material at these low pH values and cause the maximum of fluorescence to shift from around 300 nm to the near UV and visible region. These amino acids derive from the natural protein content of gum arabic, estimated to be between 1-5% (Anderson, Howlett and McNab, 1985). The increased fluorescence was observed with an excitation wavelength of 270 nm. While the excitation wavelength used in this study was longer at 325 nm, it would still be sufficient to cause emissions in the NBE region. Some additional fluorescence is expected with a shorter excitation wavelength, however, and a less significant amplification of the NBE peak is expected with a longer excitation wavelength.

Another source for an increase in the NBE peak after ageing are hydroxyls from gum media which are known to adsorb onto the surface of zinc oxides, providing potential oxygen ions for band-gap jumps. With the deterioration of the binding medium and introduction of water, the availability of hydroxyl groups would increase, increasing adsorption as well as the NBE emission. An increase in this emission was observed with the addition of water to zinc white pigments (Artesani *et al.*, 2018).

5.6.6 ELIMINATING GUM/PAPER CONTRIBUTIONS

A correction methodology has been modified by Verri *et al.* (2008) and later published by the British Museum (Dyer, Verri and Cupitt, 2013) to account for pigment-binder interactions and correct for contributions outside of the desired study material. The procedure involves obtaining fluorescent images similar to the methodology used in this study and then capturing a UV reflected image of reference greyscales at set reflectance intensity values. These reference images are used to extract reflectance and absorbance values which are input into a modified Kubelka-Munk equation. Each pixel is corrected using a correction factor calculated in this way to obtain a corrected UV fluorescence image.

The resultant images created using this correction methodology are only qualitative and cannot reliably provide quantitative fluorescence data from photographs. Future work could involve carrying out this correction and comparing results again with fluorimetry results to determine if information extracted from digital images is reliable enough for conservation recommendations. Complications could arise, however, from paint layers on paper not being entirely opaque. Previous attempts at calculating opacity and absorption coefficients in this study have been unsuccessful owing to the tendency of watercolours to permeate into unsized paper fibres rather

than sitting on top. Future work which uses this correction will have to modify it slightly to account for contributions by the paper, a factor which was not accounted for in the original. Perhaps a correction image using a control sample of gum on paper could be used in such a correction.

5.6.7 COMPARING UV FLUORESCENT IMAGES ACROSS CAMERAS

As ideal as a simple processing methodology is for the study of fluorescing pigments, problems arise when data from one camera and imaging setup are compared with other pigments in slightly different setups. To do this, a few factors must be accounted for.

The easiest first step towards using digital imaging as a diagnostic tool is maintaining similar lighting equipment and conditions. Many UV lamps emit at 365 nm. Keeping this as a standard could reduce both variability in reflected light and fluoresced light from papers, media and other pigments.

Additionally, corrections for uneven distribution of light on a surface due to varying distances from a light source can be carried out by imaging an evenly reflecting surface in the same position as the study object. Then the UV fluorescent image of the artwork is divided by the image of the evenly reflected surface to even out the illumination of the surface. A similar correction can be carried out for stray radiation. The fluorescent image is multiplied by an image of the ambient radiation on a 99% reflectance standard (Verri *et al.*, 2008; Dyer, Verri and Cupitt, 2013).

Spectral response of cameras differs considerably. The imaging chip will have slightly more or less sensitivity in the red, green and blue channels than a camera by a different maker. This is accounted for by colour correcting a visible image of the

artwork using a Macbeth colour chart, then applying these corrections to the UV image (Dyer, Verri and Cupitt, 2013).

The ideal workflow for this process is outlined as follows by Dyer, Verri and Cupitt (2013):

1) image capture

2) flat fielding to correct for uneven illumination of surface

3) Camera response correction using Macbeth colour chart in visible light

4) Ambient light correction

5) Pigment-binder interaction correction

Digital images of artworks which aim to capture the entire work benefit from this methodology as it corrects for most confounding influences. Data collected in this study was not corrected in this way; rather, images were taken of mock-ups at very close distance and covering a small area to reduce uneven distribution of light. The dark room reduced some of the influence of ambient light. Grey standards could not be obtained before the completion of this work, but future work would benefit greatly from a pigment-binder interaction correction with an expanded methodology which corrects for paper contributions. Additionally, use of a free program such as Nip2 for image calculations, rather than MATLAB, a prohibitively expensive program requiring a license, would broaden the reach of further research into zinc oxide's fluorescence on paper.

5.6.8 PROBLEMS WITH MIXED PIGMENTS

Even with a pigment-binder interaction correction, mixed pigments present an issue as they could radically change the appearance of zinc oxide's fluorescence. Current

image processing methods do not account well for this and it is a potential source of further study. Currently, time-resolved photoluminescence imaging is promising for differentiating between pigments in a mixed pigment area, though the technique may be out of reach for conservators and is beyond the scope of this study (Nevin *et al.*, 2014).

5.7 CONCLUSIONS

- The ratios of green-to-blue channels and the ratios of green-to-NBE peak intensities and areas were always less for *indirect* samples 3 and 4 and commercial sample 15 than for all other pigment samples on all paper types.

- All pigment samples were grouped into two types: type 1 had a stronger blue contribution and a sharp NBE emission peak while type 2 had a stronger green contribution and a less-intense NBE emission peak. Both types were present in *indirect* and commercial pigments, but only type 2 was represented in *direct* method pigments.

- Light exposure lessened the differences between type 1 and type 2 ratios of green and blue colour channels in digital images and micrographs.

- Paper and gum contributions to fluorescence were most significant in the naturally aged Fabriano and Folio papers. Trends in their fluorescent intensities dictated the fluorescent trends in the pigments painted onto them.

- Type 2 pigments with a strong green band were consistent with historic pigments studied by Clementi *et al.* (2012). Modern commercial pigment sample 15 was conversely grouped into type 1 pigments, a group Clementi *et al.* associated with analytical-grade zinc oxides.

- The literature suggests that the consistent increases in green-to-blue ratios observed in samples on Whatman paper indicate that additional crystal defects may form with prolonged exposure to daylight and moisture.

- The green/blue ratios of RGB values from case study images appear to fall into two types upon preliminary analysis but variations in image capture set-up and inadequate post-processing procedures prompt scepticism. Future work on case study paintings should involve the implementation of post-processing procedures which account for variations in lighting, camera response and pigment-binder interactions as well as contributions by paper fluorescence.

6 DISCUSSION AND CONCLUSIONS

The aim of this study was to determine whether ultraviolet-induced fluorescence could indicate previous or future photocatalytic behaviour and thereby inform conservators who wish to safely store, display or treat watercolours with zinc oxide pigments. Of interest was whether a new imaging method could act as a predictive tool for potentially higher rates of peroxide formation. The second chapter dealt with zinc oxide's history as a watercolour pigment and each subsequent chapter covered one aspect of zinc oxide's physical, chemical and optical properties. The following sections will compare across chapters to determine what relationship these three properties have. Implications of these results for the field of conservation will be discussed along with future work stemming from this study and the work of others studying zinc oxide pigments.

6.1 RELATING FLUORESCENCE TO PHYSICAL CHARACTERISTICS

Fluorescence results from Chapter 5 split the types of zinc oxide pigments in two, loosely following production methods but with slight differences. Comparing these two types with results from previous chapters indicated that the fluorescence was closely tied to physical characteristics. When fluorescent peak locations were compared with impurity content from Chapter 3, strong positive correlations were found between total impurity content in parts-per-million and both NBE and green peak locations of samples on Whatman paper, with greater impurity content leading to a red-shift in peak locations. Additionally, given that impurities are so closely tied

to production method, the latter was also strongly correlated to peak locations.[123]

Peak areas, however, were less correlated to either impurity content or production

method (Table 6.1).[124]

Table 6.1 Correlations between impurity content and fluorescent data for unexposed samples on Whatman paper

	Impurities	*NBE location*	*G location*	*G area*
NBE location	**0.884**	1		
G location	**0.829**	0.785	1	
G area	0.310	0.188	0.648	1
Production method	**0.824**	**0.969**	**0.628**	-0.0483

Key: NBE = near-band-edge peak, G = green peak. **Bold** = significant correlations

Zinc oxide crystallite morphological characteristics, particularly the surface-area-to-

volume ratio (SAV) have been strongly correlated to fluorescence characteristics

(Fabbri *et al.*, 2014). Running correlations with data from this study confirmed these

results (Table 6.2).

Table 6.2 Correlations between crystallite size data and green/NBE(B) fluorescence data

	L/W	*SAV*	*% polar*	*G/NBE areas*	*G/NBE heights*	*G/B digital*
SAV	-0.882	1				
% polar	-0.982	0.809	1			
G/NBE areas	**0.672**	**-0.497**	**-0.600**	1		
G/NBE heights	**0.695**	**-0.521**	**-0.624**	0.999	1	
G/B digital	**0.458**	**-0.586**	**-0.487**	-0.0454	-0.00907	1
G/B 50x	**0.627**	**-0.688**	**-0.638**	0.225	0.262	0.923

Key: L/W = length/width, SAV = surface-area-to-volume ratio, % polar = percent of surface accounted for by polar surfaces, NBE = near-band-edge peak, G = green (peak or channel), B = blue channel, digital = data from UV fluorescence digital photos, 50x = data from UV fluorescence micrographs. **Bold** = significant correlations

---

[123] To correlate production method, *indirect* method pigments (and commercial pigments, which are assumed based on collected data to be *indirect* method pigments) were assigned a value of 0 while *direct* method pigments were assigned a value of 1.

[124] Items with high correlations which are not in bold in Table 6.1 are those factors which are likely collinear, such as G and NBE peak locations, or G area and G peak location. These correlations are not important or surprising and are therefore not in bold.

The green/blue channel ratios from UV fluorescent micrograph images correlated most strongly to SAV ratios while an even stronger correlation was found between the length-to-width ratios of crystallites and the green/NBE peak height ratios. *Indirect* sample 1 and *direct* sample 9 appear to be outliers when the two variables are plotted against one another and removing them raises the correlation between length-to-width ratios and G/NBE peak height ratios to 0.988 (Figure 6.1). A larger data set could better determine whether this correlation is as strong as 0.988 or closer to 0.695.
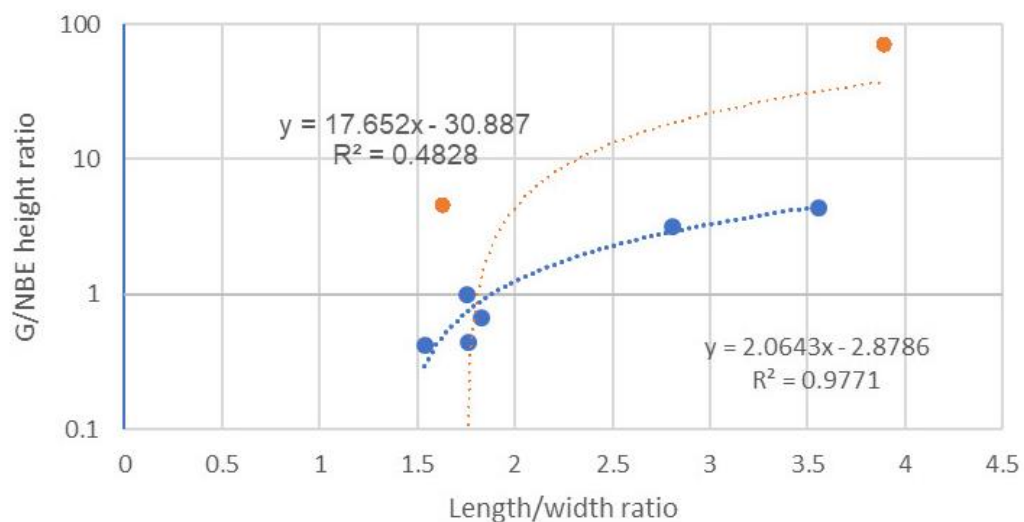
Figure 6.1 Length/width ratio vs G/NBE peak height ratio plotted on a logarithmic y-axis to facilitate visualisation. *Indirect* sample 1 (left orange point) and *direct* sample 9 (right orange point) appear to be outliers. The trend line plotted with outliers has a fairly low R^2 value of 0.4828 (orange line) while the trend line without outliers has a very high R^2 value of 0.9771 (blue line).

Fabbri *et al.* (2014) associate green fluorescence with zinc vacancies along the $(10\bar{1}0)$ plane, a crystal plane which is parallel to the long *c* axis. Additionally, they associate the NBE fluorescence with the (0001) crystal face and observe its disappearance with the removal of oxygen ions during degradation. Their results would explain the strong correlation between length/width ratios and green/NBE peak heights as a longer particle would have a greater $(10\bar{1}0)$ plane and a smaller

polar surface area as well as greater likelihood for defects on the polar surfaces due to longer grow times. As longer particles are associated with *direct* method zinc oxides grown in a reducing atmosphere, they would contain a deficiency of oxygen at the (0001) polar plane. Conversely, shorter particles associated with *indirect* method pigments would have been grown in an oxygen-rich atmosphere and maintain their 1:1 stoichiometry at the (0001) plane and its associated NBE emission. This would reduce the green/NBE ratio while increasing the percentage of the particle accounted for by polar planes.

Shalish, Temkin and Narayanamurti (2004) strongly correlated crystallite diameter to green/NBE peak heights, a result replicated in this study with a moderately strong correlation of 0.620. This value increases to 0.938 if again *indirect* sample 1 and *direct* sample 9 are excluded which again appear to be outliers when plotted against the others (Figure 6.2).
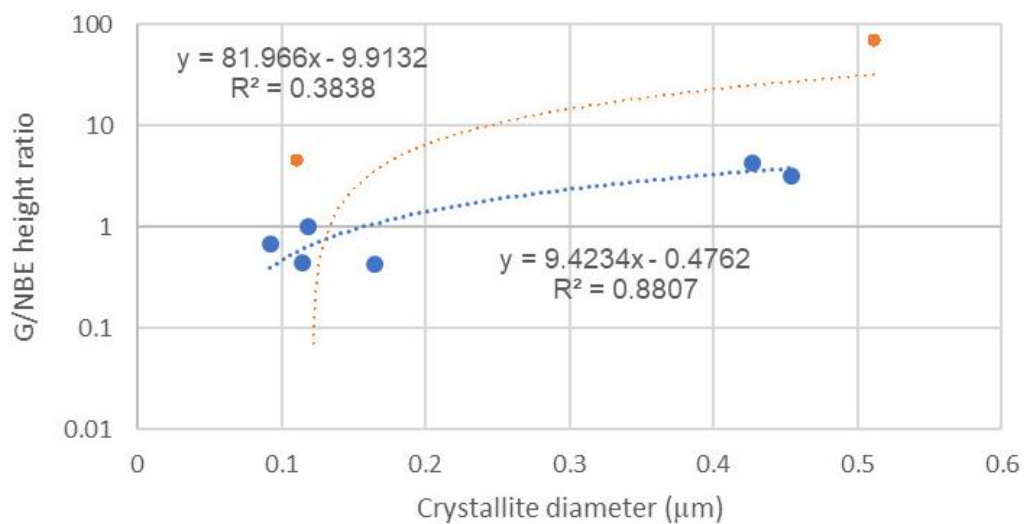
Figure 6.2 Crystallite diameters vs G/NBE peak height ratios plotted on a logarithmic y-axis to facilitate visualisation. *Indirect* sample 1 (left orange point) and *direct* sample 9 (right orange point) appear to be outliers. The trend line plotted with outliers has a low R^2 value of 0.3838 (orange line) while the trend line without outliers has a high R^2 value of 0.8807 (blue line).

6.2 FACTORS INFLUENCING PHOTOCATALYTIC BEHAVIOUR

Surface-area-to-volume (SAV) ratios derived from both crystallites and particles correlate very strongly with peroxide formation[125] as measured by Russell-grams of samples on Whatman paper (Table 6.3). A high SAV ratio is associated with smaller particles, which are in turn associated with *indirect* method pigments. No *direct* method pigments showed signs of peroxide formation, so the correlation between SAV ratios and its formation would be expected to be high.

SAV ratios were not well-correlated to browning of paper but did correlate well to increases in $L*$ and $a*$ values. Morley-Smith (1950) found that particle size and specifically surface area was the trait most closely related to chalking in oils, a result of the oxidation of the binding medium through peroxide formation.[126] The results were not linear, however, and were augmented by the ratio of blue-to-green fluorescing particles.

Table 6.3 Correlations between SAV ratios and chemical change data

	Peroxides	*Browning*	$\Delta L*$	$\Delta a*$	$\Delta b*$
Browning	-0.316	1			
$\Delta L*$	0.448	-0.459	1		
$\Delta a*$	0.527	-0.395	0.988	1	
$\Delta b*$	-0.185	0.304	-0.912	-0.896	1
SAV crystallites	**0.929**	-0.364	**0.596**	**0.677**	-0.448
SAV particles	**0.848**	-0.0568	0.273	0.358	-0.194

Key: SAV = surface-area-to-volume ratio. **Bold** = significant correlations

XRD results would have provided a good measure of crystallinity; however, results from this study were not properly corrected for instrumental line-broadening or for strain contributions. Rather, fluorescence is a better indicator of crystallinity as

---

[125] To run correlation, samples which indicated peroxide formation in Russell-grams were assigned a value of 1 while those which did not were assigned a value of 0. The same procedure was applied to browning of samples, with those which browned assigned 1, those which did not assigned 0.

[126] Refer to Appendix 10: Zinc Oxide's Use in Oil Paints for a wider discussion of degradation in zinc oxide oil paints.

strong links have been made between the strength of green fluorescence and the crystallinity of the zinc oxide.

A greater contribution by the green fluorescent band should negatively correlate to peroxides and visible browning as the strength of this band is related to the number of defects on the crystal lattice surfaces. Conversely, NBE emissions are only detected on the (0001) face when a nearly 1:1 stoichiometry is observed. When peroxide formation, browning and ratios of green-to-NBE peaks or blue channels for photographs were correlated, a strong negative correlation was found between peroxide formation and green/blue channel ratios for digital photographs (r = -0.805) and micrographs (r = -0.727), and a similarly strong correlation was found between green/NBE peak areas and browning (r = -0.796) (Table 6.4). This is in line with the expected correlation given what is known about fluorescence and crystallinity and its relationship to photocatalytic behaviour.

Table 6.4 Correlations between green-to-NBE fluorescent contributions and signs of degradation

	Peroxides	*Browning*
G/NBE area	-0.272	**-0.796**
G/NBE height	**-0.584**	**-0.557**
G/B digital	**-0.805**	-0.205
G/B 50x	**-0.727**	-0.280

Key: NBE = near-band-edge peak, G = green (peak or channel), B = blue channel, digital = data from UV fluorescence digital photos, 50x = data from UV fluorescence micrographs. **Bold** = significant correlations.

Moderately strong correlations were also found between the green/NBE peak heights and peroxide formation (r = -0.584) and with browning (r = -0.557).

Browning did not correlate well to colour channel ratios derived from photographs or micrographs.

6.3 RELATING MOCK-UP RESULTS TO CASE STUDIES

Robert Feller and many scientists before him have already made the case for honesty when studying 'accelerated ageing' in controlled scenarios (Feller, 1992). This study resists the claim that light exposure with humidification replicates natural ageing. Rather, the results of the study show ways in which typical reactions associated with zinc oxide photocatalytic behaviour affect observable properties such as fluorescence, paper colour, the structural integrity of the paint layer and so on. Comparing these properties to those observed in naturally aged paintings provides authenticity and applicability.

Three of the five case studies had visible signs of chemical change: Irene Kendall's *Bouquet of Flowers*, the watercolour *General View of St. Mary's Cathedral, Iona*, and George Thomson's *SS Buda*. The last dates from 1889 while the first two paintings were likely early 20th century. The two case studies which show little to no signs of degradation are Thomas Harper's *View of the River Coquet* from between 1856 and 1875 and an untitled ruin drawing from the late nineteenth century.

Unfortunately, useable photo paper was not available for Russell-grams of the case studies, though visible deterioration is obvious on the three pieces just named. Additionally, fluorescent photos of the case studies were all taken in slightly different light and with different camera settings. Even so, the ruin drawing and Thomas Harper watercolours had the highest green-to-blue channel ratios when fluorescing pigmented areas were cropped and analysed, both above 1.4. The lowest ratios, below 1.2, were from the remaining watercolour samples, with the lowest represented by the samples from *General View…Iona.*

Running a correlation between the green/blue channel ratios from case studies and whether visible deterioration was seen[127] returns an r value of -0.937. This seems to indicate that the green/blue channel ratio is very indicative of likelihood to degrade, however the sample set is quite small. Analysis of additional case studies is required to obtain a more accurate value. Conditions and camera settings would also need to be standardised to determine if this correlation holds.

6.4 RELATING RESULTS TO CURRENT PIGMENT TRENDS

Of the commercial pigments analysed in this study, including the Winsor and Newton sample which was abandoned early on, all three appeared to be produced by the *indirect* method. Given what is already known about the photocatalytic properties of that method, particularly the work by Morley-Smith (1950, 1958), it would seem logical to switch to using *direct* method pigments instead. However, these pigments are always slightly greenish or grey and do not produce a pure white in the same way that *indirect* pigments do.

Not a lot of warnings exist online about zinc oxide in watercolours. Winsor and Newton's website gives it a permanence rating of AA, meaning Extremely Permanent[128]. No mention is made of its potential for deterioration, which is understandable. It is also difficult to know if pigment manufacturers are aware of problems with zinc oxide as any improvements to their pigments would not be made

---

[127] Those samples which had visible deterioration were assigned 1, while those which did not were assigned 0. Samples from *General View…Iona* were assigned 1 although they themselves were not deteriorating as they were adjacent to or associated with deteriorating areas. This is particularly true of JC4, which was protected by the frame from light exposure and did not totally convert to zinc sulphate salts as those pigments adjacent to it had.

[128] Defined by W&N as 'its durability when laid with a brush on paper or canvas, graded appropriately and displayed under a glass frame in a dry room freely exposed to ordinary daylight and an ordinary town atmosphere' (*Spotlight on Chinese white*, 2011)

available as public knowledge. It would seem, however, that those tested for this work do indeed produce peroxides at a rate which can induce browning of paper and cracking of watercolour paint films.

Golden, a renowned manufacturer of acrylic paints, sells a type of watercolour with Aquazol® binding medium as an improvement over gum arabic in optical properties, vibrancy, re-wetting characteristics and luminosity. Their pigment rating system is still based exclusively on fading, however, a quality which does not apply to zinc oxide pigments and leaves out any information about other potentially damaging changes over time such as embrittlement of the binding medium or browning of paper. Future systems of pigment categorisation could benefit from a rating which accounts for these photocatalytic properties, particularly since pigments such as titanium white and Prussian blue are photocatalytic in the former case and fade when mixed with photocatalytic pigments in the latter.

Indirect sample 1, an analytical red seal zinc oxide from Norkem, a chemical supplier, fluoresced very similarly to *direct* method zinc oxides and was the only pigment to not brown on Whatman paper. It also had a comparably high impurity content when compared with *direct* method pigments. It was also, importantly, very white in colour. Perhaps a viable approach to future manufacture of Chinese white watercolour pigments could involve using lower-purity *indirect* method pigments which maintain their brilliance and workability in colloidal solutions while reducing their tendency to degrade surrounding paper or pigments. Thickly-painted zinc oxide watercolours tend to crack regardless of composition or crystal structure, unfortunately, and more work is needed to find a way to reduce this tendency.

6.5 CURRENT PREVENTIVE CONSERVATION PRACTICE

Museum professionals tend to select lighting which does not include UV and infrared wavelengths. However, museums still prefer to use illuminance, measured in lux, as their primary unit of light level measurements (Smith, 2010; Garside *et al.*, 2017) and cite Thomson's *The Museum Environment* (reprinted 1986) as the source for their recommendations.[129] Thomson recommended what are now the standard values of 200 lux for paintings and 50 lux for paper, values he derived from a survey of visual preferences by Loe, Rowlands and Watson (1982). The only conservation he discussed regarded whether to allow natural light in a gallery or whether all lighting should be artificial. UV recommendations were made in microwatts per lumen to accommodate the lux unit and were based on the UV emissions from once-ubiquitous incandescent lamps (Hill and Bouwmeester, 2005; *Advice sheet: caring for paper collections in museums*, 2009). However, Michalski states that even with these recommendations, most museums do not directly measure UV emissions from their light sources (Michalski, 2017). Matters are further complicated by the inconsistency with which lighting manufacturers release SPDs. A general correlation was made between lux levels and 'damage indices' or DI which relied on a narrow range of typical SPDs for lighting technologies; however, the wider variety of lighting and associated SPDs available today breaks down this correlation and makes the lux measurement less reliable (Garside *et al.*, 2017).

Lighting is complicated and must be selected on a case-by-case basis and given that visible light tends to bleach and fade colours, it will be inherently damaging. However, the extent to which violets and blues are filtered out will depend on the

---

[129] Illuminance meters also tend to be less expensive than irradiance meters, further prompting the use of illuminance over irradiance.

sensitivity of materials in an artwork to be illuminated. Given that zinc oxide's

proximity to carbon-containing gas molecules promotes photocatalytic activity by

wavelengths of light up to 650 nm (Gurwitz, Cohen and Shalish, 2014; Kumar and

Rao, 2015), cutting out UV wavelengths is particularly important, as is reducing total exposure to visible wavelengths (Figure 6.3).

Fortunately, LEDs present an excellent alternative to fluorescent or incandescent lighting
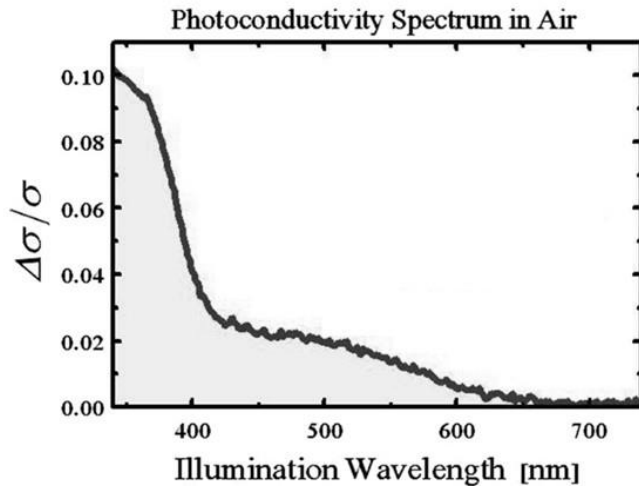
Figure 6.3 Change in photoconductance in air per illumination wavelength for zinc oxide in the presence of carbon molecules. Conductance is increased beginning at 650 nm, well into the visible wavelength range. Image credit Gurwitz Cohen and Shalish (2014).

which both contained IR and UV contributions. They can also be tuned to a

particular colour temperature by using tuneable red, green and blue LEDs, allowing

for blue wavelengths to be reduced if appropriate. Additionally, lux values may

correlate better with fading when using LEDs as they only emit in visible

wavelength ranges, allowing for current lux level guidelines to be maintained.

Guides written for the proper implementation of LED lighting are prolific (e.g.

Weintraub, 2010; Druzik and Michalski, 2012; Perrin, Druzik and Miller, 2014) as

are guidelines for tuning LEDs to be aesthetically pleasing or even to replicate initial

illumination conditions in which artworks were made for more accurate viewing

(e.g. Cuttle, 2000; Schanda, Csuti and Szabó, 2015). Both have the benefit of

tending towards warmer colour temperatures which reduce the contributions by blue

wavelengths. Additionally, as discussed in Chapter 4 and demonstrated by Gurwitz,

Cohen and Shalish (2014) in Figure 6.3, visible wavelengths of light as long as 650 nm can increase the conductivity of zinc oxide surfaces with the shorter wavelengths having a more pronounced effect. Cutting out some violet or blue light would reduce zinc oxide's conductivity. This decision must be tempered by aesthetic considerations, however, and made with knowledge and implementation of lighting that preserves the artwork physically but also the intent and palette of the artist.

Artworks are stored ideally in the dark and most museums maintain dark storage for works of art on paper. Moisture is also controlled and generally kept at near 50% relative humidity. Light appears to be the main source of energy for peroxide formation, though the results from Chapter 4 of the Russell-grams carried out six months after light exposure indicate that it can continue in the dark. While relative humidity levels must be maintained at around 50% to prevent embrittlement of paper, aggressive lighting may cause surface reactions for a period after storage. For this reason, low lighting or intermittent moderate lighting are preferable to prolonged, strong lighting for zinc oxides on paper.

An interesting effect of dark storage in oxygen is the re-oxygenation of zinc oxide surfaces. Atmospheric oxygen is absorbed into the lattice and takes up the position of the surface oxygen vacancies, effectively replenishing lost electrons in the valence band and reducing trap states, increasing the time that electrons spend in the conductance band after excitation (Bao *et al.*, 2011; Gurwitz, Cohen and Shalish, 2014). This higher oxygen content is associated with a greater NBE or blue fluorescence, a quality which reduces the green/NBE ratio and which was observed in more photocatalytic pigments in this study. However, while the extent of this neutralising of vacancies is not known, it does not appear to be a total replenishment of oxygen and does not convert those pigments with an excess of defects and

impurities into highly-reactive pigments. It is likely that dark storage does more good than harm by halting peroxide formation.

An intuitive solution to the replenishment of oxygen in zinc oxide's lattice would be to store and display artworks containing it in anoxic housing. However, anoxia removes adsorbed moisture and oxygen from zinc oxide pigment surfaces, promoting the surface accumulation of electrons (Brown, 1957; Gurwitz, Cohen and Shalish, 2014). There is also record of fluorescent and conducting pigments accelerating the yellowing and embrittlement of paper in anoxia (Townsend *et al.*, 2008), an effect which would surely be initiated by highly-conductive zinc oxide surfaces. Additionally, an aggressive reduction of moisture in the air through anoxic enclosures or display units could also weaken and embrittle the paper substrate by breaking hydrogen bonds between cellulose fibres formed via absorbed water molecules.

Anoxic environments also promote colour change and fading in a variety of pigments. Prussian blue fades readily in anoxic displays, as does vermilion, purple madder and sepia (Russell & Abney, 1888) while several other pigments have been reported to fade or deteriorate outside of the presence of air (Townsend *et al.*, 2008; Thomas, 2012; Ford, 2014; Lerwill *et al.*, 2015) making the anoxic display of non-analysed artworks contentious. More research is needed into the benefits and risks of anoxic storage and display, particularly as it pertains to pigment fading and conductivity. Given present knowledge, the risk of zinc oxide's re-oxygenation in the dark does not seem to be great enough to justify the risks posed by anoxic housing.

6.6 CURRENT INTERVENTIVE PAPER CONSERVATION PRACTICE

Several difficulties arise when treating watercolour paintings containing zinc oxide. Some are simple to circumvent, like the potential sensitivity of zinc oxide to chelating agents, which can be mitigated with local application in pigment-free areas (Liddie, 1998). Others can be more complicated in their treatment or diagnosis.

Efflorescence in watercolours can be difficult to detect in its early stages as it appears very similar to powdering effects typical of paints with a high pigment-to-volume concentration. Early detection and proper treatment can prevent further pigment loss, though misdiagnosis and consolidation of the zinc sulphate salts will only bind the crystals to the paper and allow them to dissolve and spread through the substrate, causing further visual disruption. The pale halos surrounding pigment areas typical of solubilised zinc sulphate only appear late in the degradation process and can be difficult to reverse. Zinc sulphate salts may be effectively removed by floating the artwork in a bath or supporting it on a screen during a wash, but only if the remaining white pigment is well-adhered (Colbourne, 2006) (Fig 6.4). In treating *S.S. Buda*, Liddie (1998) was able to reduce the effect of the halos around white paint areas by administering a bleaching treatment with dilute hydrogen peroxide and IMS brushed into dark paper areas. Additionally, a screen provided support during the wash for the fragile paper and minimised disruption of the paint. The treatment was effective in reducing the appearance of the halos but was more aggressive than many conservators are willing to carry out. Rather, early detection is best for avoiding such extensive pigment loss.

Figure 6.4 Example of float (left) and screen-supported (right) washing of a watercolour undertaken by the author. Washing is the best method for removing zinc sulphate salts if all other pigments are not water-sensitive.

Sulphate salts can be detected via microscopy if available, although the plate-like crystal habit of zinc sulphate may only be visible at very high magnification. Additional research into the fluorescence of zinc sulphate when forming in zinc oxide pigments may allow for detection via fluorescence analysis. White pigmented areas remaining in *SS Buda* fluoresced a rather orange colour and contained both zinc oxide and zinc sulphate particles, but these two qualities cannot be linked based on one example. The dull blue appearance of zinc sulphate in UV light can be useful in its detection microscopically, however, which may provide justification for treatment in cases where micro-sampling is permissible (Figure 6.5).
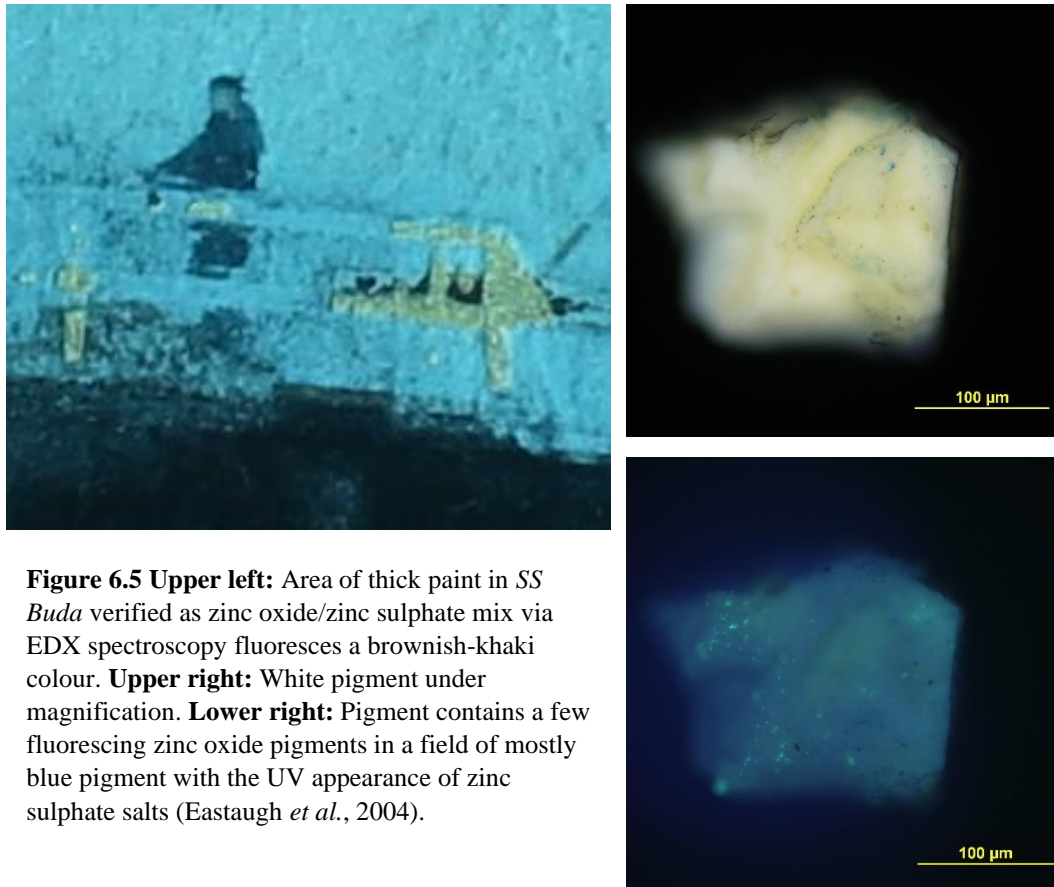
Figure 6.5 Upper left: Area of thick paint in *SS Buda* verified as zinc oxide/zinc sulphate mix via EDX spectroscopy fluoresces a brownish-khaki colour. **Upper right:** White pigment under magnification. **Lower right:** Pigment contains a few fluorescing zinc oxide pigments in a field of mostly blue pigment with the UV appearance of zinc sulphate salts (Eastaugh *et al.*, 2004).

Alkalisation treatments of works of art on paper are standard practice and involve neutralising acids and depositing a reserve of alkali into the paper for neutralisation of future acidic deterioration products. Brown (1957) found that zinc oxide was highly soluble in concentrated alkali solutions. While most bath water used for washing works of art on paper is kept at a pH between 7 and 8, raising the pH is sometimes deemed necessary to facilitate the removal of discolouration and acidic reaction products. While this poses a risk to zinc oxides, the common practice of spot testing colorants before treatment with alkalis ensures that zinc oxides in an artwork are not prone to dissolution in the water bath. This is especially important if using ammonium hydroxide as zinc oxide is particularly soluble in this reagent (Kühn, 1986). A conservator opting for a more aggressive alkalisation will test for sensitivity while any normal alkalisation should maintain a pH within a safe range for zinc oxide pigments.

Several studies have recently attempted to use zinc oxide nanoparticles as a UV screen on paper, either over an oil paint layer or embedded into the paper itself. El-Feky *et al.* (2014) created a coating to paint over a varnish layer containing 2% zinc oxide which acts to protect oil paints on paper from UV damage and fading. While their results seem promising, their ageing tests are primarily thermal ageing with tensile tests and UV exposure with subsequent measurements of colour change. While their results indicate effective screening of oils and reduction in colour change with light exposure along with maintained tensile strength, the complexity of zinc oxide's electrical properties necessitate wider research into these methods before the technique can be safely and widely applied.

Similar work was carried out by Afsharpour and Imani (2017) who carried out very similar ageing tests and fading-based measurements after UV light exposure, but in their case zinc oxide nanoparticles were impregnated in paper over a layer of Klucel G with the aim of protecting the paper from fungal attack and UV-related deterioration. Again, tests are only preliminary and do not consider the photocatalytic properties of the pigment or its peroxide formation in the presence of moisture. Promising early results need to be tempered with further research to ensure the safety of the method.

Two qualities which must be balanced for zinc oxide to be effectively used as a protectant are its antifungal properties and its UV absorption characteristics. Luo *et al,* (2018) had some success mixing zinc oxide into starches which were then used to impregnate paper with zinc oxide nanoparticles for use as a residual antifungal treatment. They identified zinc oxide's oxygen vacancies as the source of its antifungal properties. The proliferation of these defects would have also reduced photocatalytic activity in the pigment but would also theoretically reduce its UV

absorption properties as was observed in the results from Chapter 4 of this study. A targeted approach such as that used by Luo *et al.* may be the most advisable as it utilises a less-reactive pigment which still retains a useful property for conservators. Conversely, using zinc oxide as a UV protectant could be hindered by the relationship between UV absorption and higher photocatalytic activity.

6.7 FUTURE WORK

The results from this study are promising and show some consistent trends in zinc oxide behaviour related to its physical and electrical properties but more work is needed to verify and replicate these results. Specifically, peroxide formation on pigment particles can be verified with experiments modelled after those carried out by Barruah *et al.* (2010) and Singh, Saha and Pal (2015) which measure colour change in dyes in solution to measure the rate of peroxide formation on zinc oxide particles suspended in the same solution.

Additionally, more incremental light exposure tests could form a better picture of the rate of deterioration over time and assess whether there is a point at which peroxide formation will slow or stop. Further testing after prolonged dark storage would allow for comparisons with rates of peroxide formation before dark storage to determine if the theoretical replenishment of oxygen ions in the surface correlates with an increased rate of peroxide formation. Finally, constant light exposure involving concurrent humidification will allow for better study of peroxide-binder interactions as the current method introduces a wet-dry cycle which may have contributed significantly to paint cracking observed after light and moisture exposure. A constant humidification will reduce the likelihood of cracking from

expansion and contraction cycles and allow for any observed cracking to be attributed more certainly to peroxides breaking down gum arabic macromolecules.

Image processing procedures can be expanded upon, particularly those which mitigate contributions by the pigment-binder interactions as outlined by Dyer, Verri and Cupitt (2013). A further assessment of the modified Kubelka-Munk function used for this correction will need to account for additional contributions by the paper substrate given that watercolour paints are rarely opaque. Additionally, calculations and procedures will have to be streamlined for ease of use, particularly the matrix manipulations necessary for corrections of erroneous contributions by lighting, camera response and surrounding fluorescent materials. Open source software will be used exclusively, and MATLAB code converted to Nip2 procedures.

This study dealt primarily with pure zinc oxide pigments. However, many historic pigments containing zinc oxide were mixed with other pigments such as lead white, barium sulphate, zinc carbonate, or zinc sulphide in lithopone. The fluorescence and ageing of these pigments will be much different than the pure zinc oxide. Future studies could expand upon this work by characterising these qualities for mixed pigments and determining if they can be differentiated based on simple analytical techniques such as image processing or multispectral analysis.

More work regarding mixed pigments could be carried out on zinc oxide mixed with other colours, particularly since this was commonly done in gouache painting in the nineteenth century. A methodology similar to that used by Clementi *et al.* (2009) in which varying concentrations of a study pigment are mixed with another pigment and the fluorescent peak intensities and locations characterised at varying concentrations. A good starting point could be to study pigments which are often substituted with mixtures such as Naples yellow which was found to be a

combination of zinc white and cadmium yellow in watercolour form (Townsend *et al.*, 1995). As transparent watercolour painting traditionally involves less colour mixing, these mixed pigments could go under the radar as problematic. Characterising their fluorescent and photocatalytic properties could shed light on potential problems with these overlooked paints.

Most pigments analysed in this study were contemporary. This was due to the difficulties in obtaining large quantities of historic zinc oxide powders. With access to such materials, many of the analysis from this investigation could be applied to historic pigments to potentially verify the applicability of this work to historic examples. This could also shed light on changes in production method or impurity content, indicating a change in starter materials or defect concentration which would have implications for ageing properties of watercolours which contain the zinc oxide pigments. Furthermore, with additional research and corrections, XRD could be better utilised to determine the defect density of historic pigments and provide further insight into how nineteenth century pigments were produced and why differences in rates of degradation have been observed.

6.8 CONCLUSIONS

This study aimed to link zinc oxide's varying ultraviolet fluorescence with rates of deterioration and determine whether such a link could be used by conservators to predict or diagnose existing deterioration of papers containing zinc oxide watercolour pigments. As the rates of deterioration vary significantly among zinc oxides and the UV-induced visible fluorescence can similarly vary from one pigment to another, establishing the link between these two qualities allows paper conservators to make more informed decisions about display and treatment of

watercolours on paper containing zinc oxides. Prior attitudes were detailed in a historic literature review, then a range of representative zinc oxide mock-up pigments and case studies were studied to relate their physical, optical and chemical properties.

In chapter 2, a literature review of artist manuals and pigment guides published during the nineteenth century in Great Britain suggested that while zinc oxide was known to be a problematic pigment in oil paints, the watercolour pigment Chinese White, sold exclusively by Winsor and Newton, was deemed permanent and unchanging throughout the nineteenth century even as doubt was cast on the stability of watercolours as a whole. It was widely used and grew in popularity due to recommendations in artists' manuals and was heavily promoted by influential figures such as John Ruskin. No other English colourman sold a zinc oxide watercolour pigment due to its lack of body and poor working properties. Chinese White by Winsor and Newton was secretly annealed at the time to modify its qualities for better workability and stability, making their product the best on the market. A distinction was made between zinc white, which was described as thin, pasty, tending to clog and with a lack of body, and Winsor and Newton's Chinese White which did not contain any of these unpleasant qualities.

Russell and Abney wrote in their study on the fading of watercolour pigments that zinc oxide accelerated the fading of certain other pigments when mixed but they did not emphasise this or zinc oxide's role in the deterioration of surrounding materials. As a result, this failed to percolate out into the wider scientific literature until decades into the twentieth century. Other early warnings of zinc oxide's reactive potential were also found which suggested it was prone to changing colour when exposed to the industrial pollutant sulphur dioxide. Given what was known

scientifically about metal oxides at the time, and that French industrial zinc oxide pigments were highly damaging to all colours they contacted, it was curious that these concerns were not repeated beyond the confines of a few publications.

In chapter 3, the physical properties of contemporary commercial pigments, *indirect* and *direct* pigments and case study pigments were compared to determine which production method has dominated in pigment manufacturing and what the implications are for the chemical stability of historic watercolour pigments. Average crystallite sizes for modern commercial pigments compared well with *indirect* method zinc oxides (commercial = 0.105 – 0.131 µm, *indirect* = 0.121 – 0.170 µm) as did agglomerate particle sizes (commercial = 0.887 – 0.957 µm, *indirect* = 1.00 – 1.08 µm). Crystallite sizes for three of the case study pigments were also indicative of *indirect* method pigments (TH = 0.159 µm, SSB = 0.193 µm, RD = 0.271 µm). All three groups also consisted mainly of nodular crystallites with small average length-to-width ratios (commercial = 1.72, *indirect* = 1.64, case studies = 1.67) and high percentages of reactive polar surfaces were calculated for all groups (commercial = 23%, *indirect* = 24%, case studies = 24%) while *direct* method pigments consisted solely of rod-like, acicular particles (average length-to-width ratio = 3.42, average % polar surfaces = 13%) suggesting the potential for high photocatalytic activity among modern pigments and historic case studies.

The total impurity content measured in mock-up pigments using XRF was greatest for *direct* method pigments (average of 0.39%) and *indirect* method pigment 1 (0.38%) and least for the remaining *indirect* method pigments (0.27%) and commercial pigments (0.26%), further indicating that commercial pigments are produced by the *indirect* method. The presence of cadmium in *indirect* pigment 1 indicates it may have been produced from a sphalerite ore, historically a common

source of *direct* method zinc oxides. It similarly contained the highest amount of lead along with *direct* pigment 7, again suggesting a common origin. Conclusions could not be made regarding the effects of specific impurities on electrical properties as their presence in the crystal lattice could not be determined via XRD.

Chapter 4 detailed the interactions of peroxides and radicals with surrounding paper and the gum arabic binding medium after exposing mock-ups to light and moisture for 50 hours. After six months in dark storage, peroxides were detected using Russell-grams on all *indirect* and commercial mock-up pigments but none were detected on *direct* method pigments, indicating that peroxide formation is strong and persistent even in dark storage for *indirect* method zinc oxides. All pigments except for *indirect* pigment 1 on Whatman #1 filter paper induced visible browning, indicating likely deterioration of cellulose via oxidation of side chains by peroxides. All paint films except that which contained commercial pigment 15 cracked on highly-sized Fabriano paper and all cracked on mixed-fibre sized folio paper, suggesting that the paper size restricted interactions between peroxides and the paper, instead confining degradation to the binding medium.

The band gaps calculated from the absorption spectra of samples on Whatman paper was widest for *indirect* method and commercial pigments (3.02 – 3.12 eV) resulting from the steep slopes of the absorption edges (average slopes = 393 – 459). Wider band gaps are associated with slower recombination rates and greater reactivity and peroxide formation. The band gap was narrowest for *direct* method pigments (2.42 – 3.02 eV) which also had shallow absorption edges (average slopes = 154 – 293). *Indirect* pigment 1 accounted for the narrowest band and shallowest absorption edge for *indirect* and commercial pigments and was the only pigment to not cause

browning on Whatman paper. It did, however, image in Russell-grams, meaning peroxides were being formed on pigment surfaces.

Two defect gradients were found in elemental maps of pigment particles: one along the *c* axis and one perpendicular to it. That which was perpendicular to the *c* axis is known to readily adsorb hydroxyls yet is not associated with photocatalytic activity, being prominent in *direct* method pigments. The lack of paper discolouration by detected peroxides on *indirect* pigment 1's surface is notable and could indicate that these perhaps remain adsorbed onto the pigment's surface rather than migrate out into the paper substrate yet are able to image on a photographic film with long exposure.

In chapter 5, the fluorescence of mock-up samples was characterised by dividing the green fluorescence by the blue or near-band-edge fluorescence as measured by both fluorimetry and digital photography. Two fluorescence types were observed: type 1 pigments (*indirect* pigments 3 and 4 and commercial pigments) had low green/blue ratios and a green peak centred at 460-485 nm. A green peak at this location was associated with production or annealing in an oxygen atmosphere, implying few surface defects and higher reactivity. Type 1 pigments had the highest green/blue ratio increase on Whatman paper after light exposure, implying increase in defects due to photocatalytic processes. Type 2 pigments (*indirect* pigment 1, all *direct* method pigments) had high green/blue ratios and a green peak centred at 500-515 nm. This green peak location was associated with zinc oxides annealed in an anoxic atmosphere, increasing surface defect concentration and reducing photocatalytic activity. No fluorescence changes were observed in type 2 pigments on Whatman paper after light exposure, implying chemical stability and little to no change to defect concentrations. When compared with fluorescent spectra of historic and

analytical pigments in the literature, pigment 1 was most like historic paint analysed by Clementi *et al.* (2012) while contemporary pigments were most similar to Clementi *et al.*'s analytical sample. This further confirms that at least some historic pigments may be *indirect* method pigments annealed in an anoxic atmosphere to impart greater chemical stability.

Case studies photographed in different lighting with different cameras still contained green/blue ratios which were in line with findings from the mock-up samples. The lowest ratios were calculated for the three case studies which had visible degradation while case studies in good condition accounted for the highest ratios. Contributions by paper fluorescence dominated fluorescence changes measured on Fabriano and Folio papers, rendering comparisons of these samples before and after light exposure difficult.

In chapter 6, results were compared across chapters to determine if fluorescence or any other observable qualities can be used for diagnostic or predictive purposes. The green/blue colour channel ratios from digital photographs and micrographs correlated very strongly with peroxide formation (r = -0.805 and r = -0.727 respectively) while the ratio of green/NBE peak areas correlated strongly with browning on Whatman paper (r = -0.796). Even without correcting for lighting, contributions from paper fluorescence or differences in camera types, the green/blue colour channel ratios for case studies were lowest for pigments which had caused visible degradation and highest for those which appeared undamaged. While Russell-grams could not be collected for case studies due to a limited supply of the lithographic film, it appears that even after a century, photoactive pigments still fluoresce with a low green/blue ratio implying high levels of photoactivity. This green/blue channel ratio appears effective in indicating peroxide formation in

pigments and results from case studies imply that the surface defect concentration increases very slowly over time. This study was unable to determine an endpoint for peroxide formation reactions on zinc oxide watercolour pigments and implies that such an end may not be reached for over a century of natural ageing, even in extreme display environments.

The green/blue ratio was relative within a data set and not representative of absolute reference values. Standardising the image acquisition and processing procedure could provide a more definite ratio value associated with high photocatalytic activity. Corrections for uneven illumination, erroneous light sources, pigment-binder interactions, and fluorescent contributions by the paper substrates would further produce more consistent results. Automating the process and using freeware programs such as Nip2 for matrix processing will make the method more accessible to practicing conservators and allow them to relate fluorescence more easily to potential photocatalysis.

Paper conservators must keep in mind the photoactivity of zinc oxide pigments when making display and storage recommendations. Most pigments used historically and currently are produced by the *indirect* method and are therefore photoactive to some degree. Literature also suggests that gaseous carbon-containing molecules can increase surface conductivity when zinc oxide is illuminated by a range of visible wavelengths of light. Therefore, overall reduction in light exposure is recommended. Intermittent exposure via a covering cloth or button which turns on a light for a short period is a viable solution as it allows for viewing in a full spectrum of visible light without creating difficult viewing conditions with reduced light levels. The conversion of many museum lighting systems to LED technology ensures that UV and IR wavelengths are eliminated and tuneable LEDs allow for

reduction of the blue component of light when appropriate for management of light sensitivities. Anoxic display scenarios should be avoided as zinc oxide's conductivity increases substantially in vacuum, putting surrounding pigments and paper at risk of deterioration and fading. Storage in the dark is recommended even though lost oxygen ions may replenish in the dark, simultaneously replenishing electrons for reactions. The extent of this effect is not known, however, and should be considered an acceptable risk.

Paper conservators treating artworks containing zinc oxide pigments should remain cautious of overly interventive approaches. While bleaching is the only known treatment for eliminating browning and evening out paper tone, alkalis higher than pH 8 must be avoided to reduce the chance of dissolving any remaining zinc oxide pigments. Sulphate salts can easily be washed out with water in a float or screen wash while leaving behind zinc oxides and is recommended if zinc sulphate salts are present. Consolidation is safe and recommended if pigments have cracked, although sulphates must not be consolidated and must be removed first. Consolidation itself may provide a physical barrier between electrons on pigment surfaces and surrounding paper if the paint is not too embedded and serves a preventive as well as interventive purpose. There is not presently a method of reducing zinc oxide conductivity once it has been used as a pigment, instead paper conservators should focus on stabilization and prevention. Additionally, zinc oxide pigments are not recommended for retouching until further work can be done to verify their long-term stability on paper. As current pigment permanence classifications only account for tendency towards fading, they cannot be relied on to reflect the reactivity of photoactive pigments.

Future work will involve expanding on photocatalytic experiments in this study by testing for physical, chemical and optical properties at multiple light exposure durations to model the reaction curve of peroxide formation and zinc oxide defect creation. Additionally, a constant light and moisture exposure along with a control which is only humidified will allow for cracking of paint pigments to be assigned to gum arabic macromolecule deterioration rather than mechanical breakage by wet-dry cycles. Other methods for modelling peroxide formation can also be carried out which involve irradiation of pigments in water in the presence of organic dyes which will fade upon reacting with peroxides. Additionally, surface analysis using x-ray photoelectron spectroscopy (XPS) will allow for quantitative measurements of electronic surface states and verify photoactivity of pigment samples.

Expanding these studies to mixed pigments could allow for greater understanding of the fluorescence and deterioration of zinc oxides when mixed with other pigments, particularly in the cases of lithopone and leaded zincs as well as gouaches which used zinc oxide to make opaque colours. Studying larger samples of nineteenth century pigments could also allow them to be characterised using a wider range of analytical tools in a similar mode as the mock-up samples and verify whether findings using contemporary pigments are widely applicable to those produced in the nineteenth century. Finally, given the consistency of results in this study and the promise of fluorescence as a diagnostic tool, an image processing procedure which accounts for fluorescence contributions by paper and gum is essential for the effective utilisation of ultraviolet-induced fluorescence by conservators.

Appendix 1: Case Study and Mock-Up Sample Reference Tables

Table A1.1 Case studies with associated artists, dates and sample codes

Title	Artist	Date	Code
Bouquet of Flowers	Irene Kendal	Early 20th century	IK
S.S. Buda	George Thomson	1889	SSB
View of the River Coquet	Thomas Harper	Mid 19th century	TH
Ruin drawing	Unknown	Late 19th century	RD
General View of St. Mary's Cathedral, Iona	Unknown	Unknown	JK

Table A1.2 Mock-up pigment numbers with descriptions

Sample number	Description
1	Zinc oxide red seal (*indirect*), Norkem chemical suppliers
3	Zinc oxide high purity (*indirect*), Norkem chemical suppliers
4	Zinc oxide white seal (*indirect*), Brüggemann Chemical
6	Zinc oxide American Process (*direct*), Norkem chemical suppliers
7	Zinc oxide 2011 (*direct*), Grillo-Werke AG
9	Zinc oxide spezial (*direct*), Brüggemann Chemical
14	Winsor and Newton Chinese White
15	Zinc white 46300, Kremer Pigments
16	Zinc white, Cornelissen

Table A1.3 Mock-up substrate types with associated codes

Substrate code	Description
P	None, P delineates only pigment present
W	Whatman #1 filter paper, 100% cotton fibres, no size or fillers
B	Mid-nineteenth century wove, wood pulp and cotton fibre Folio paper
F	Highly sized (alum and rosin) Fabriano cotton rag watercolour paper potentially with calcium carbonate filler

All mock-up samples are mixed with Cornelissen gum arabic, mixed by combining 1.4 grams solid gum arabic with 6 grams boiling water and straining after leaving overnight. Sample codes are formatted W1C, with W indicating substrate, 1 pigment number and C the Cornelissen gum arabic. All mock-ups used this binding medium.

Appendix 2: Supplemental Information on Zinc Oxide Production

A2.1 WET PROCESS/PRECIPITATED ZINC OXIDE PRODUCTION

Precipitated or *wet* process zinc oxide has been available on the market for at least 100 years, though its use in paint manufacture is not well-documented. Kühn (1986) describes a process in which sulphuric acid is added to zinc waste products or ores to leach out zinc carbonates which are then roasted to obtain zinc oxide. Zinc carbonate can also precipitate from purified zinc sulphate or chloride solutions, then calcine to a zinc oxide with a high specific surface area (Auer, Griebler and Jahn, 2005). Fleury (1912) described the process as producing a white material of superior whiteness to other methods and one which absorbed oil similarly to lead white. His enthusiasm for the process was tempered by its enormous cost at the time of writing although Auer *et al* in 2005 claimed that the process was still being used but less so than the *indirect* or *direct* methods of production. Morgan was less impressed, reporting that the zinc oxide was not of the right 'crystalline form' to be used as a pigment without mentioning what this ideal form might be (Morgan, 1985, p. 223).

A2.2 ZINC ORES AND THEIR COMPOSITION

Most zinc oxide used by European and American artists in the nineteenth century were produced industrially in France (*indirect* or French process) and New Jersey (*direct* or American process). Great Britain attempted to produce zinc oxide in the early part of the century but found the local ores to be very difficult to process (Downs Jr, 1976).

By far the largest manufacturer of zinc oxide at this period was the Société Anonymé de la Vieille Montagne in Belgium (Boni, 2011). The company was founded to process the large calamine deposits in Belgium (Downs, 1976). Calamine is a zinc ore also known as smithsonite composed of zinc carbonate with a small concentration of lead. Additional deposits of calamine were found in southwest Sardinia alongside sphalerite and hemimorphite (a zinc carbonate silicate). These were mined and processed in three plants on the island then exported to La Vieille Montagne.

Table A2.1 compiled by Holley (1909) details La Vieille Montagne percentage composition of zinc oxide c. 1909.

Table A2.1 Composition of zinc oxide produced at La Vieille Montagne

Compound	Percent composition
Zinc oxide	99.695 to 99.995%
Lead oxide	0.200 to 0.002%
Cadmium oxide	0.100 to 0.000%
Ferric oxide	0.005 to 0.003%

In the United States, a large deposit of franklinite was discovered in New Jersey and led to the development the direct method of zinc oxide production at the New Jersey Zinc Company in 1850 (Auer, Griebler and Jahn, 2005). Over time, franklinite was slowly replaced by sphalerite, an ore composed mainly of zinc sulphide (Gettens & Stout, 2011; Holley, 1909). Morgan (1985) writes that a mixture of calcine blende, or sphalerite with high calcium content, and anthracite,[130] were used as raw materials for the *direct* process in a ratio of 60-70% sphalerite to 40-30% anthracite. Later, more commonly smithsonite, hemimorphite, willemite, and zincite were

---

[130] A type of coal with high carbon content

combined in direct method production. Table A2.2 catalogues the compositions of the ores used by the New Jersey Zinc Company (Remington & Francis, 1954).

Table A2.2 Common ores used in zinc oxide manufacture

Sphalerite	Franklinite	Smithsonite	Hemimorphite	Willemite
67% zinc	19.40% ZnO	64.80% ZnO	67.50% ZnO	73.00% ZnO
33% sulphur	60.50% Fe_2O_2	35.20% CO_2	25.00% silica	27.00% silica
	0.50% FeO		7.50% combined water	
	6.80% Mn_2O_2			
	12.80% MnO			

A2.3 CONTEMPORARY PRODUCTION PROCESSES

Today, more than 81% of all zinc oxide in Europe is produced by the *indirect* method, compared with 10-20% produced by the *direct* method[131] (Auer, Griebler and Jahn, 2005). The ASTM[132] international standard D79-86 for producing zinc oxide outlines the necessary composition and qualities for pigments (Table A2.3).

Table A2.3 Zinc oxide composition standard from ASTM international standard D79-86

	French Process	American Process
Zinc oxide, min, %	99	98.5
Total sulphur, max, %	0.1	0.2
Moisture and other volatile matter, max, %	0.5	0.5
Total impurities, including moisture and other volatile matter, max, %	1.0	1.5
Coarse particles (total residue retained on a No. 325 (45-µm) sieve), max, %	0.10	0.25

[131] The remaining 5-7% of zinc oxide are produced by another production process called the wet process, used for creating zinc oxides for the rubber industry, but never for pigment manufacture. This is because the wet process tends to retain more moisture and surface hydroxyl groups in the finished product and is much more reactive than other methods.

[132] American Society for Testing and Materials, an international organization which releases production standards for a range of materials.

A2.4 GRADES AND QUALITY OF COMMERCIALLY AVAILABLE ZINC OXIDE

Zinc oxide suppliers retail their product in a series of grades based on purity, particle size and colour. Generally, *indirect* method zinc oxides have smaller average particles when compared with *direct* zinc oxides (Remington & Francis, 1954). Both forms are then classified according to composition. It is worth detailing the various systems of classification as they evolved since they provide valuable information regarding likely method of production, resultant composition and probable ageing behaviour.

In the nineteenth century, zinc oxides sold in dry powder form were characterised by 'seal', a purity classification generally denoted by a colour. White seal was designated as the zinc oxide with the highest purity, though Green seal was of similar purity and had greater hiding power due to its larger particle size (Gettens & Stout, 1966) making it ideal for oil paints (Kühn, 1986). Red and Gold seal were widely claimed to be less pure than White or Green seal (Gettens & Stout, 1966; Kühn, 1986) although Holley (1909) argued Red seal manufactured at the Florence, Pennsylvania plant of the New Jersey Zinc Company was of a very high and comparable purity to the Green seal produced there. Grey seal is the last designation under this system and usually denotes a zinc oxide containing a significant percentage of metallic zinc (Gettens & Stout, 1966).

There was some deviation however from this classification system. For example, the New Jersey Zinc Company, producers of the *direct* method pigments until the twentieth century, produced zinc oxides from materials other than the ore. These were designated according to the classifications listed in Table A2.4 (Holley, 1909).

Table A2.4 Grades of ZnO Sold by the New Jersey Zinc Company

Name	Zinc oxide %
Spezial	99.121
xx Red	98.796
Selected	99.227
Xx	99.051

Two other grades of zinc oxide were named by Auer, Griebler and Jahn (2005) as Pharmaceutical grade and Chemical pure grade. Chemical grade ZnO is again subdivided into *direct* process Chemical pure grade, *indirect* process Chemical pure grade, and *wet* process Chemical pure grade with the latter being the least pure, 93% zinc oxide content as opposed to 98.5 – 99.5 for all other grades. Zinc oxide is still classified by seal in Europe; however, manufacturers often have their own standards, increasing the variability in composition among zinc oxide powders.

Another anomaly extensively manufactured until the late twentieth century was a leaded zinc white. This was discontinued in the United States due to health concerns at which point the phrase 'lead free' was applied to *indirect* pigments composed of 99% zinc oxide and 98% zinc oxide for *direct* pigments (Kühn, 1986). Germany from 1986 also produced a variety of leaded pigments which in turn were classified by name based on the pigment's lead content (see Table A2.5) (Kühn, 1986).

Table A2.5 German Zinc Oxide Nomenclature

Name	Composition
"Zinc white" or "metallic zinc white"	99% zinc oxide (minimum) 0.4% lead (maximum)
"Plumbing zinc oxide"	75% zinc oxide minimum Variable lead content
"Leaded zinc oxide"	12-70% lead sulphate

Appendix 3: Relationship Between Energy and Wavelength of Light

Each particle of light in the form of a photon[133] has an associated energy level (eV).

Equation A3.1 can convert the wavelength of light to energy in electron volts:

$$E \text{ (eV)} = \frac{hc}{\lambda} \tag{A3.1}$$

where E is the energy of a photon in eV, h is Planck's constant (which has a value of approximately 4.135×10^{-15} eV·s), c is the speed of light (3.0×10^8 m/s) and λ is the wavelength of the photon in metres. Given that h and c are both constants and given that input values for wavelength in the UV to visible range will be in nanometres, this equation can be rewritten as Equation A3.2:

$$E \text{ (eV)} = \frac{1240.5 \text{ eV·nm}}{\lambda \text{(nm)}} \tag{A3.2}$$

To solve for λ, Equation A2.2 is rearranged as Equation A3.3:

$$\lambda \text{ (nm)} = \frac{1240.5 \text{ eV·nm}}{E \text{(eV)}} \tag{A3.3}$$

Equation A3.2 can be used to solve for energy if wavelength is known.

---

[133] Light has both a particle and a wave nature. The light particle can be described as having a specific energy while the light wave can be described by its length. This wave-particle duality is fundamental to the physics of light and matter, and is the principle behind spectroscopy, or the analysis of materials by examining how light is altered by electronic structures such as bonds and electron orbitals of a material.

Appendix 4: Miller Indexing and Miller-Bravais Indexing

A4.1 MILLER INDEXING

Miller Indexing, a method of describing planes in a crystal lattice, works simply and describes the orientation of a plane in relation to three reference axes, *a, b,* and *c*. These relations are noted by three numbers which correspond to the three planes and are referred to as *h, k,* and *l*. This Miller notation can describe cubic crystal systems, but also describes systems in which the axes are not 90 degrees to one another.
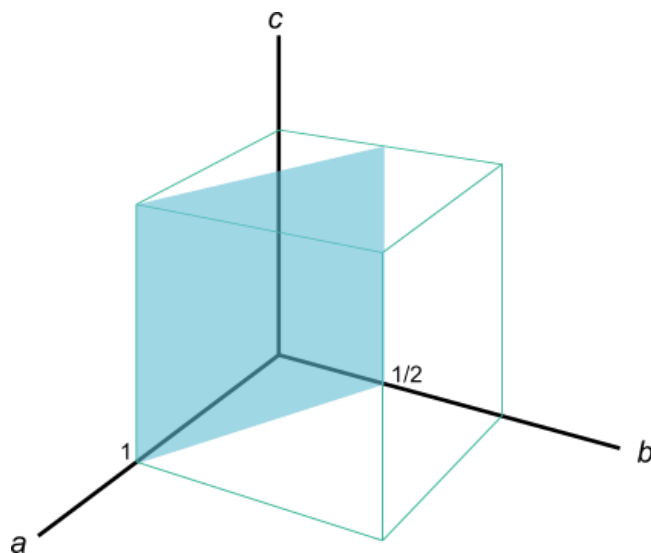
Figure A4.1 A plane in blue and its relationship to the *abc* coordinate plane. Given its intercepts of 1, ½, and infinity on the *a, b,* and *c* planes respectively, this plane is notated as the (1 2 0) plane using Miller Indexing.

Miller indices do not indicate specific distances but are ratios within axes. To describe a plane using the Miller indexing system, an origin is selected. This origin can be translated according to the rules of Miller indexing. Most often, the origin is at the xyz coordinate (0, 0, 0). A plane is described as the reciprocal of the intercepts between each axis. For example, in Figure A4.1 a plane is shown which intercepts the *a* axis at 1, the *b* axis at $\frac{1}{2}$, and the *c* axis not at all. To describe this plane, *h*, the first coordinate, is obtained by taking the reciprocal of 1, which is 1. *k* is obtained in the same way, and would be notated as 2, the reciprocal of $\frac{1}{2}$. The

third l coordinate has an intercept of infinity, and in this indexing system, the reciprocal of infinity is 0. Therefore, the Miller notation for this plane is (1 2 0). If the plane intercepted the c axis at any point, tilting it, then this intercept would be written as the reciprocal of that number.

If a plane intercepts an axis at a negative point, or if a negative direction needs to be indicated, this is done by placing the negative sign above the number rather than to the side. So if a plane intercepts at -1, $\frac{1}{2}$, and infinity, the notation would read $(\bar{1}, 2, 0)$.

A4.2 MILLER-BRAVAIS INDEXING

Miller Indexing was expanded upon to better reflect symmetry relationships in hexagonal and rhombohedral systems. The reasons for this are beyond the scope of this study, but this expansion, called Miller-Bravais Indexing, adds a fourth coordinate i placed just before the l coordinate. In this system, $h + k + i = 0$. What this means is that the value for i is assigned as the negative sum of h and k. In the example given in Figure A4.1, the Miller-Bravais indices would be (1 2 $\bar{3}$ 0).

As a hexagonal crystal, zinc oxide can be notated using Miller-Bravais indexing. Some literature reports zinc oxide planes as Miller indices but these can be easily converted to Miller-Bravais indices for comparison or vice versa by either taking out the third index to convert from Miller-Bravais to Miller or by adding the negative sum of the first two indices to convert from Miller to Miller-Bravais.

To understand more fully how Miller-Bravais indexing relates to the zinc oxide crystal structure and the atomic distribution within it, Figure A4.2 illustrates a unit cell for zinc oxide within the coordinate system. For hexagonal systems, the b axis is

replaced by an *a* axis as the *a* and *b* axes are the same length. a_1 corresponds to the usual *a* axis and *h* index, a_2 corresponds to the *b* axis and *k* index, a_3 is the fourth axis in the Miller-Bravais system and corresponds to the *i* index, and the *c* axis is normal, corresponding to the *l* index. In this system though, the *c* axis is longer than the *a* axis, so the distance denoted by an *h* value of 1 will appear shorter than an *l* value of 1.

The plane illustrated in Figure A4.2 is the (1 1 $\bar{2}$ 1) plane. This plane intercepts the a_1 axis at 1, the a_2 axis at 1, the a_3 axis at $-\frac{1}{2}$, and the c axis at 1. The positive direction of the a_3 axis is facing away from the front of Figure A4.2, meaning the intercept is negative. When the reciprocal for all intercepts is taken, it is shown that the a_3 intercept is the negative sum of the other reciprocals.
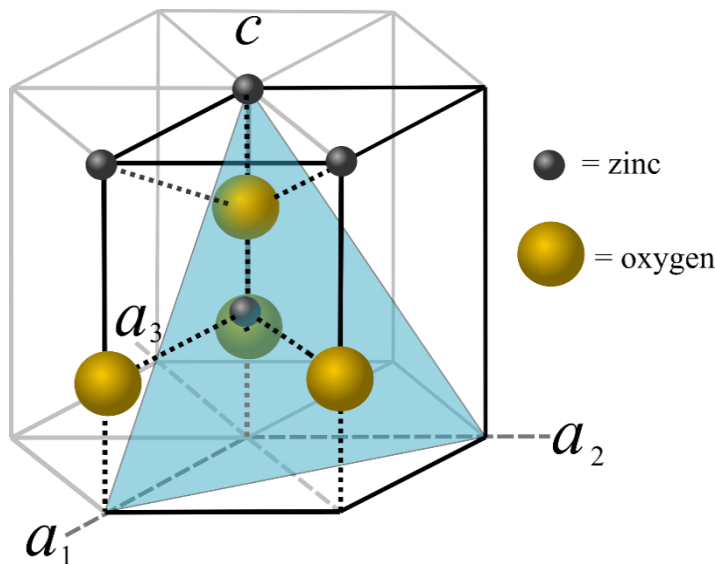
Figure A4.2 Miller-Bravais indexing illustrated by the the (11$\bar{2}$1) plane. The first three numbers correspond to a_1, a_2, and a_3 axes, while the fourth corresponds to the *c* axis.

Appendix 5: Diffractogram Processing Methodology in MATLAB

First, x and y vectors were created in MATLAB. These were for each peak. The x vectors contained values for angle of beam, and the y vectors, named after samples and beginning with P, contained intensity values. The purple n in the following code refers to a number. So for a y variable `Pn_peak1`, the actual code may read `P1_peak1`. The n is replaced in each case with the appropriate number. The following code reduces the range of values for each x and y variable to only contain values beginning before a peak and ending just after a peak.

```
Pn_peak1=Pn(1:659);
xn_peak1=xn(1:659);
Pn_peak2=Pn(660:774);
xn_peak2=xn(660:774);
Pn_peak3=Pn(775:958);
xn_peak3=xn(775:958);
Pn_peak4=Pn(959:1613);
xn_peak4=xn(959:1613);
Pn_peak5=Pn(1614:1986);
xn_peak5=xn(1614:1986);
Pn_peak6=Pn(1987:2290);
xn_peak6=xn(1987:2290);
Pn_peak7=Pn(2291:2352);
xn_peak7=xn(2291:2352);
Pn_peak8=Pn(2353:2437);
xn_peak8=xn(2353:2437);
Pn_peak9=Pn(2438:2535);
xn_peak9=xn(2438:2535);
Pn_peak10=Pn(2536:2754);
xn_peak10=xn(2536:2754);
Pn_peak11=Pn(2755:3000);
xn_peak11=xn(2755:3001);
```

A baseline value was obtained from all baseline values using a mean. This was because the baseline was noisy and correcting using a single point would have been inaccurate. These mean baselines would be used as minimums for FWHM calculations. Each FWHM calculation was completed immediately after the mean

was obtained, meaning the same mean was not used for all calculations, even though every mean has the same name.

```
mean(Pn_peak1(1:501));
mean(Pn_peak2([1:45,84:115]));
mean(Pn_peak3(77:184));
mean(Pn_peak4([1:377,454:655]));
mean(Pn_peak5([1:188,238:373]));
mean(Pn_peak6([1:115,180:304]));
mean(Pn_peak7([1:19,45:62]));
mean(Pn_peak8([1:22,68:85]));
mean(Pn_peak9(40:98));
mean(Pn_peak10([1:82,107:219]));
mean(Pn_peak11([1:70,120:247]));
```

The half-height of the peak was found by adding the maximum value (peak height) to the baseline (non-zero mean value) and dividing by 2.

```
h=(mean + max(y)) / 2;
```

`idx1` and `idx2` each returned two points, one before and one after the desired point at half the y value. Then these points were used to interpolate values for `x1` and `x2` at half of `y` and subtracted from one another to get the width of the peak (the full-width at half maximum value), delineated here by `w`. This was carried out for all peaks (1-11) and for all XRD samples.

```
idx1=find(y>h,1) +[-1 0];
idx2=find(y>h,1,'last') +[0 1];
x1 = interp1(y(idx1),x(idx1),h);
x2 = interp1(y(idx2),x(idx2),h);
w = x2 - x1;
```

Appendix 6: Sample Masses for XRF Analysis

Table A6.1 Masses of samples analysed by X-Ray Fluorescence spectroscopy

Sample number	Mass (grams)
1	1.8454
3	2.5786
4	2.1339
6	5.6046
7	2.7845
9	1.5277
14	2.1600
15	2.6271
16	1.7218

Appendix 7: XRF Correction Factors

Elemental data from XRF analysis was multiplied by the following values to correct for instrumental effects. These include absorption and amplification effects which would give inaccurate results. XRF correction factors were calculated by the lab technician for powder samples by collecting data from standard reference materials, checking the results against known quantities in these samples and calculating correction factors to adjust for instrumental effects.

Table A7.1 Correction factors applied to XRF data

Element	Correction factor
Al	1.0000
Si	1.0000
p	1.0000
S	1.0000
Cl	1.0000
K	1.1442
Ca	1.2579
Ti	1.2225
V	1.0638
Cr	1.6779
Mn	1.4006
Fe	1.0070
Co	1.0000
Ni	0.9930
Cu	1.1364
Zn	1.1364
Ga	1.0695
Ge	1.8727
As	1.0684
Se	1.0000
Br	1.0000
Rb	1.0152
Sr	1.0741
Y	0.8850
Zr	0.8905
Nb	0.6515
Mo	1.0000
Ag	0.7740
Cd	0.8711

In	1.0000
Sn	0.8445
Sb	0.7363
Te	1.0000
I	0.7257
Cs	0.5235
Ba	0.7689
La	0.6169
Ce	1.0000
Pr	1.0000
Nd	1.0000
Ta	1.0000
W	1.0010
Hg	1.0000
TL	1.0000
Pb	0.8756
Bi	1.0000
Th	1.0000
U	1.0000

Appendix 8: Particle and Crystallite Analysis: Procedure, Code and Graphs

The following appendix outlines the data processing method for particle and crystallite analysis from acquisition to graphing. Included are images used and data acquired.

A8.1 PARTICLE SIZE ANALYSIS (MEASURING AGGLOMERATES)

A8.1.1 SLIDE PREPARATION AND IMAGE ACQUISITION

Pigments were mounted onto glass slides in Meltmount™ medium with a refractive index of 1.662 (zinc oxide = 2.008). While still melted, a cover slip was applied to create a thin view field. Imaging was carried out using a microscope-mounted Olympus DP70 camera with CCD chip in dark field mode. The microscope used was an Olympus BX51M with 10x binocular eyepiece objective and 5x, 20x and 100x additional objectives. Images were captured at 200x magnification at an image size of 4080x3072 pixels to minimise spatial coverage per pixel, thereby reducing error associated with individual pixels. All images were saved as tiffs to avoid compression of the image and related losses of information.

Scale factors were obtained from a 200x reference image with a scale bar. By comparing the pixel length and given length of the scale bar, the length of one pixel was found to equal 0.104 μm and the area of one pixel to be 0.0108 μm^2.

A8.1.2 PARTICLE ANALYSIS IN FIJI (IMAGEJ)

Tiff images were imported into Fiji, a freeware program developed by Bankhead (2014) for a range of image processing procedures. The following steps were carried out to obtain image size data:

Set scale – after drawing a line, Set Scale was selected in the Analyse tab. The scale was entered using the scaling factor derived from the scale bar image. A scale of 9.62 pixels/μm was returned. Pressing OK assigned the scale to the image for further processing.

RGB to Luminance and Duplicate – after scale was set, the image was converted to luminance. This converts the image pixels to intensity values only (Figure A8.1). The resulting image was then duplicated.
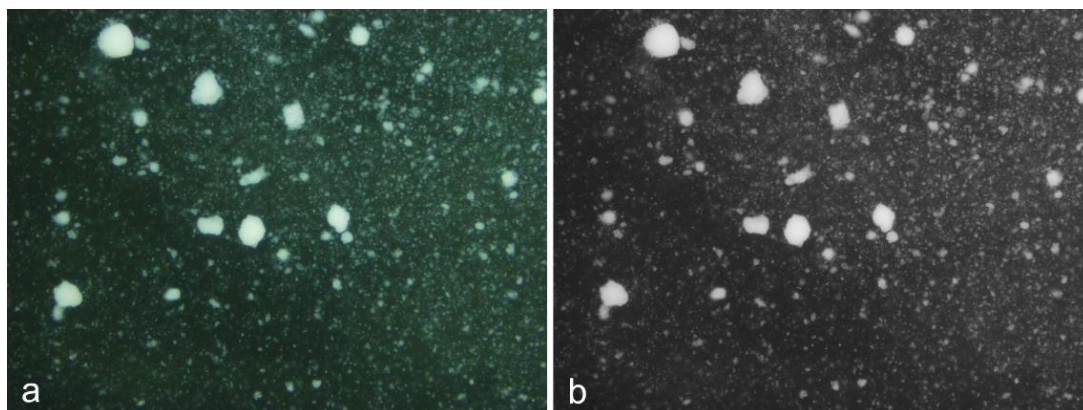
Figure A8.1 Original image of particles on left and image after conversion to luminance on right. Images taken as described in section A8.1.1.

Manual Background Subtraction: To subtract the background tone as well as any ill-defined particles, a Gaussian blur was applied to the duplicated luminance image. The degree to which the original image is maintained is a function of the standard deviation σ, assigned a value depending on the intensity of the blur. Equation A8.1 describes the Gaussian blur function in two dimensions:

$$G(x,y) = \frac{1}{2\pi\sigma^2} e^{-\frac{x^2+y^2}{2\sigma^2}} \tag{A8.1}$$
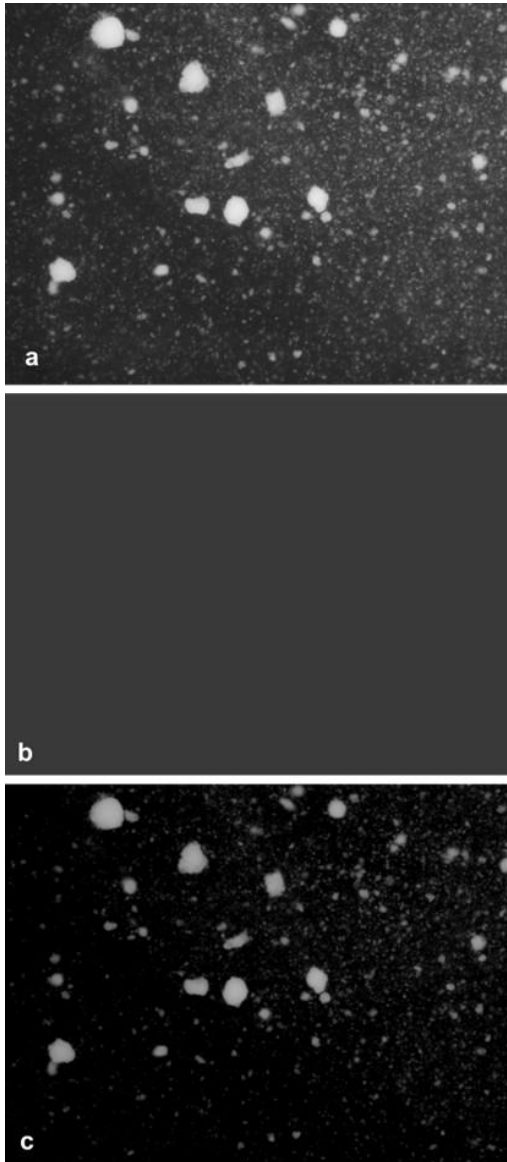
Figure A8.2 a: Luminance image of particles **b:** image after Gaussian blur applied **c:** result after Gaussian blur image subtracted from luminance image

where σ is the standard deviation assigned by the programmer and x and y delineate the position of a central pixel. A weighted average is applied based on the above formula which gives the most weight to the central pixel (that described by x and y) and less weight with increasing distance, dependent on the σ value. For a background subtraction, a very high σ value of 2,000,000 was used which resulted in a uniform grey image as similar weight was given to the pixels. Then the blurred duplicate image was subtracted from the original image, leaving only well-defined particles. This completed the manual background subtraction (Figure A8.2).

Auto Brightness/Contrast and Threshold – In the Image → Auto brightness/contrast was applied to the image resulting from the manual subtraction, then auto threshold (Figure A8.3). Occasionally, auto thresholding values were shifted manually to achieve a closer approximation of particle areas to those seen in the original image. This was often necessary when bubbles in the Meltmount™

created false continuity between particles, which had to be broken up by adjusting the sensitivity of the threshold, or when the threshold did not detect most particle areas. Visual confirmation of fit was sufficient for this type of processing.
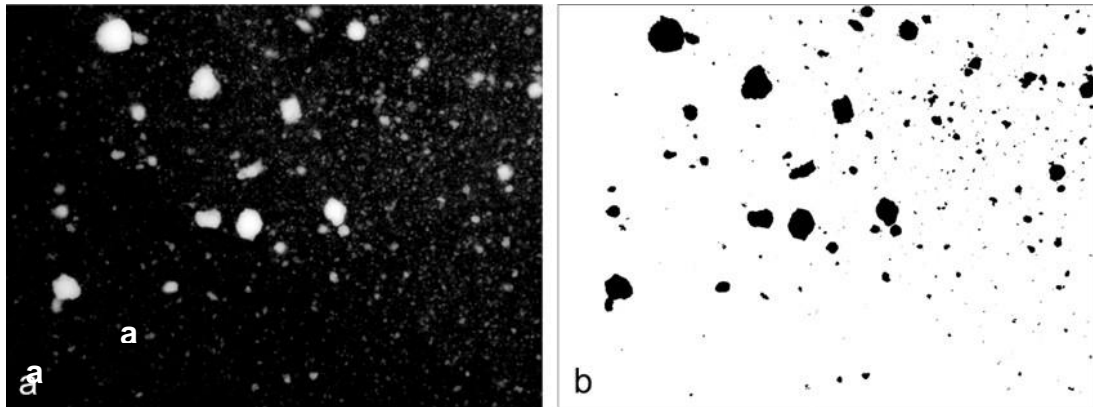
Figure A8.3 a: image after auto brightness/contrast **b:** image after applying threshold

Watershed –A Watershed algorithm was sometimes utilised to break up particles which were adjacent and would be interpreted as one particle by the Analyse Particles algorithm. The watershed algorithm was used when particles were only slightly overlapping, making the estimation more accurate, or when many particles were bordering each other, creating a large net which would have been interpreted as one particle rather than many smaller ones. In all cases, images were processed with Fiji's watershed algorithm when overlap between particles was minimal (Figure A8.4). As with thresholding, images with watershed applied were compared with the original to ensure accuracy.
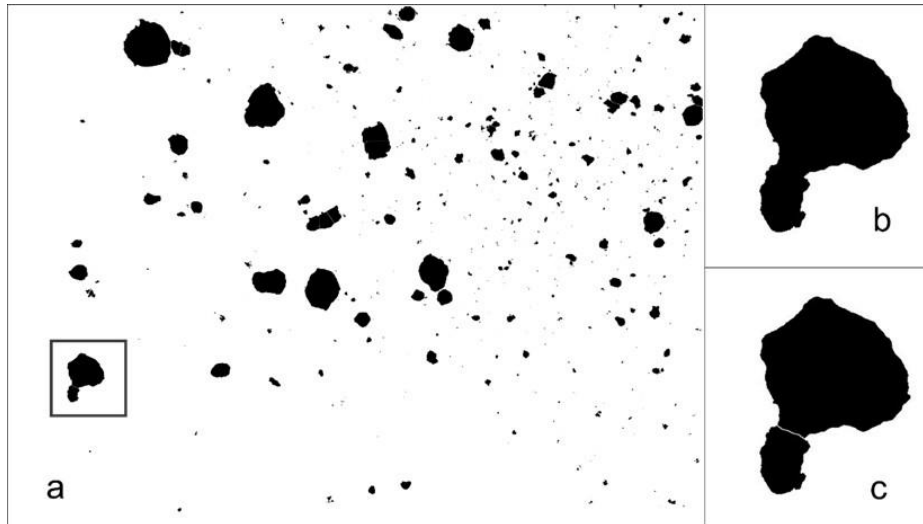
Figure A8.4 a: threshold image before watershed applied, detail outlined in red **b:** detail of particle in threshold image before watershed applied **c:** detail of particle after watershed applied showing splitting of particle into two.

Analyse Particles – The Analyse Particles function was used to obtain projected area values of particles in the final processed image. A lower limit of 0.1 μm^2 was applied as this is the calculated area of a particle containing 10 pixels. Restricting the range in this way reduced the error of the estimation to less than 10% per pixel (Mora et al., 1998). An outline map of particles was selected as the output format (Figure A8.5) along with a spreadsheet of particle area values associated to each particle in the map. Both images and the spreadsheet were saved and the entire process repeated for each image.
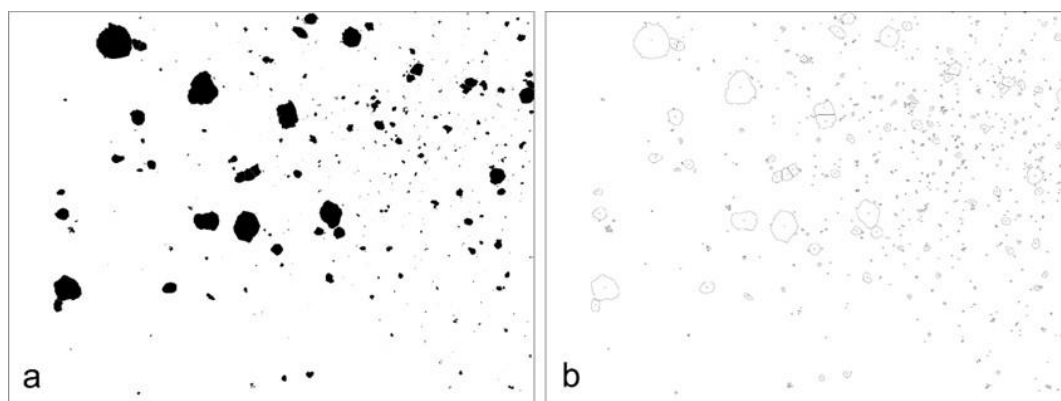
Figure A8.5 a: Image after watershed applied **b:** Outlines of particles created by Fiji during analyse particles process. Inside each outline is a value for the area of that particle.

Images were captured and analysed until 5000 particles were measured for each pigment. If the number measured by ImageJ was over 5000, the list order was randomised[134] and particle measurements were removed from the end of the list until 5000 particles remained. Area values were interpreted as the projected area of a sphere, given the approximately spherical nature of pigment clumps. Other diameter and size values were derived for calculations by assuming a spherical geometry.

A8.1.3 PROCESSING AREA VALUES IN EXCEL AND MATLAB

Excel data processing: 5000 area values for each pigment sample were imported into Excel and ordered from smallest to largest. The first and last 500 cells were then deleted eliminating potential outliers. The remaining values fall between 10% and 90% of all measured areas. In this way, 4000 particles remain for analysis.

Assuming spherical geometry, area values are converted to diameters via Equation A8.2:

---

[134] To randomize, another column was set up to the left of the column containing area values. In the first cell was input =RAND(), then the box double-clicked to create random values in all cells to the left of input values in the measurements column. The random values were then arranged in reverse order, expanding the selection to arrange the measured values in the same order as the random inputs. Finally, any measured values in cells past the 5000th cell were deleted. This process ensured that measurements were deleted at random and that remaining values represented the full range of projected areas measured.

$$D = 2\sqrt{\frac{A}{\pi}} \qquad\qquad (A8.2)$$

Where D is the diameter and A the projected area of the particle. D was divided in half to get radius, r. To obtain particle volume, Equation A8.3 was used:

$$V = \frac{4\pi r^3}{3} \qquad\qquad (A8.3)$$

To allow for comparisons between agglomerates and crystallites measured using image processing methods and crystallites measured using the Scherrer equation with XRD data, the cube root of volume was calculated for all particles. This value was delineated as the size of the particle.

Finally, surface area was derived from the radius assuming spherical geometry using Equation A8.4:

$$SA = 4\pi r^2 \qquad\qquad (A8.4)$$

From these calculations, average size and diameter were calculated as were the median size and diameter values. The total surface area was divided by the total volume to obtain a value for this ratio which could be compared between samples. A higher value would indicate greater overall surface area and possibly greater potential for degradation.

MATLAB data processing for particle size distribution: Particle size distribution for agglomerates were analysed and reported in two ways: first as the number of particles per size, then as the percent volume per size. This latter reporting method can reveal more about the contribution of very large clumping behaviour, particularly if the number of large clumps is not great when compared with the number of smaller particles. Particle sizes obtained through image processing methods are often reported in these two ways (Horiba, 2014).

To obtain the distribution of size by counting the number of particles per size, variables were imported into MATLAB under the naming convention sPn. Whenever a purple n is mentioned in the following section, it is assumed that it will be replaced with the sample number when running the code in MATLAB. This was done manually.

First, minimum and maximum values were manually assigned for sizes. These were different for different data sets and were assigned as follows:

- **Indirect method samples and pigments**:

  - min= 0.378277914

  - max= 2.36356996

- **Direct method samples**:

  - min= 0.378278

  - max= 3.833172

- **P14:**

  - min= 0.378278

  - max= 10.36316

The following variables were created. The words in brown were replaced with the values they describe from above:

```
minsP=minimum particle value;
maxsP=maximum particle value;
n=maxsP-minsP;
m=n/18;
maxsP=maxsP+m;
n=maxsP-minsP;
m=n/18;
```

Then the following program named size_edges_script is run to create bin boundaries
(one value to either side of the bin, resulting in one more value than will be included
in the final graph):

```matlab
%assign variable to be increased stepwise in while loop135
k=2;
%create empty variable named 'edges'
edges=[];
while (k>0)
    for i = k
        %assign variable minsP to first edges cell
        edges(1)=minsP;
        %assign value to the a variable using variable m
        a=edges(k-1)+m;
        %assign the kth cell the value of a
        edges(k)=a;
        %increase k by 1 before repeating loop
        k=k+1;
    end
    %break the loop when k reaches 20, will result in vector of
    length 19
    if k==20
        break;
    end
    %transpose edges
    edges=transpose(edges);
end
```

Using the variable containing size data (sPn), the data_parsing_size program parsed
data into bins delineated by the edges variable. The result was a vector composed of
the number of data points in each bin or range of values.

```matlab
%assign variable to be increased stepwise in while loop
k=1;
%create empty variable named 'sPnval'
sPnval=[];
while (k>0)
    for i = k
        %create c variable which is a vector of cells in sPn which
        are greater than or equal to the ith cell in edges and less
        than the i+1 cell in edges
        c=find(sPn>=(edges(i)) & sPn<(edges(i+1)));
        %assign variable z the values of the cth cells in sPn
        z=sPn(c);
        %assign variable d the value of the length of z
        d=length(z);
        %assign the kth cell in sPnval the value of d
```

---

135 In MATLAB programming, informational text is added by preceding with a % sign. This text is
green and does not contribute to the program but merely aids the programmer or reader in
understanding the program. It typically gives information on the line or lines following it. All non-
green text is part of the program.

```
        sPnval(k)=d;
        %increase value of k by 1
        k=k+1;
    end
    %break loop when k reaches 20
    if (k==20)
        break;
    end
    %transpose sPnval
    sPnval=transpose(sPnval);
end
```

Finally, the last cell in the edges variable was deleted to reduce its length to 50 cells. Size data was plotted against the minimum values in edges (i.e. a bar over 0.3 μm and before 0.6 μm represents particles which are as large as or larger than 0.3 μm and smaller than 0.6 μm).

```
edges=edges(1:end-1);
```

vPnval variables and edges were imported into Excel and graphed there using the bar graph function.

MATLAB data processing for percent volume per size: Methodology for processing volume data in MATLAB was very similar to size data. First, variables were imported under naming the convention vPn. Minimum and maximum volume values were varied according to sample type:

- **Indirect method samples and pigments**:

    o min= 0.054129

    o max= 2.36356996

- **Direct method samples**:

    o min= 0.081358435

    o max= 56.32159522

- **P14:**

  - min= 0.054129

  - max= 1112.952324

The following code was run with the words in brown replaced with the values described:

```
minvP= minimum volume value;
maxvP= maximum volume value;
n=maxvP-minvP;
m=n/18;
maxvP=maxvP+m
n=maxvP-minvP;
m=n/18;
```

Then the program volume_edges_script was run:

```
%assign variable to be increased stepwise in while loop
k=2;
%create empty variable named 'edges'
edges=[];
while (k>0)
    for i = k
        %assign variable minvP to first edges cell
        edges(1)=minvP;
        %assign value to the a variable using variable m
        a=edges(k-1)+m;
        %assign the kth cell the value of a
        edges(k)=a;
        %increase k by 1 before repeating loop
        k=k+1;
    end
    %break the loop when k reaches 20, will result in vector of
    length 19
    if k==20
        break;
    end
    %transpose edges
    edges=transpose(edges);
end
```

The data_parsing_volume program parsed data into bins delineated by the edges variable.

```
%assign variable to be increased stepwise in while loop
```

```
k=1;
%create empty variable named 'vPnval'
vPnval=[];
while (k>0)
    for i = k
        %create c variable which is a vector of cells in vPn which
        are greater than or equal to the ith cell in edges and less
        than the i+1 cell in edges
        c=find(vPn>=(edges(i)) & vPn<(edges(i+1)));
        %assign variable z the values of the cth cells in vPn
        z=vPn(c);
        %assign variable d the value of the sum of z to obtain a sum
        of volumes
        d=sum(z);
        %assign the kth cell in vPnval the value of d
        vPnval(k)=d;
        %increase value of k by 1
        k=k+1;
    end
    %break loop when k reaches 20
    if (k==20)
       break;
    end
    %transpose vPnval
    vPnval=transpose(vPnval);
end
```

The last cell in the edges vector was deleted to reduce its length to 18 cells long.

```
edges=edges(1:end-1);
```

Edges were then converted to sizes. As the edges for volume were created using

volume data, then they can be converted to size values by taking the cube root.

```
edges=edges.^(1/3);
```

The elements of the vPnval variables were then converted to percentages by dividing

them by the total volume of particles and multiplying the result by 100.

```
%assign variable sumv to the value of the sum of the volume data
sumv=sum(vPn);
%create new variable vPnper which converts the result of the data
parsing program to percentages
vPnper=(vPnval./sumv)*100;
```

vPnper variables were imported into Excel and plotted there using the bar function.

A8.2 CRYSTALLITE SIZE ANALYSIS

Crystallite sizes were reported similarly to particle agglomerate sizes: as the number of particles per size. Percent volume per particle was not reported for crystallites as this value gave a good indication of clumping behaviour but is not helpful as a visualisation tool for crystallite sizes.

First, minimum and maximum size values were assigned for different data sets and were as follows:

- **Indirect method samples, pigments and case studies (not Lore or Ruin)**:
  - min= 0.067875198
  - max= 0.391577353

- **Direct method samples**:
  - min= 0.195829801
  - max= 1.480990336

- **Ruin sample**
  - min=0.155371828
  - max= 0.53820066

- **SS Buda and Thomas Harper painting, site 3 (TH3)**
  - min= 0.094002832
  - max= 0.391577352

Histogram of crystallite sizes

Variables were imported under the naming convention sSEMn.

- Case studies were sBuda, sRuin and sTH3

All sSEM variables in following code sets were replaced with case study variable names listed above

Bin sizes created:

```
minsSEM= minimum size value;
maxsSEM= maximum size value;
n=maxsSEM-minsSEM;
m=n/18;
maxsSEM=maxsSEM+m
n=maxsSEM-minsSEM;
m=n/18;
```

Then size_edges_script_SEM code was run

- Variable names were not replaced if numbered powder samples were analysed. Case studies used case study min and max variables such as minsBuda instead of minsSEM.

```
%assign variable to be increased stepwise in while loop
k=2;
%create empty variable named 'edges'
edges=[];
while (k>0)
    for i = k
        %assign variable minssSEM to first edges cell
        edges(1)=minsSEM;
        %assign value to the a variable using variable m
        a=edges(k-1)+m;
        %assign the kth cell the value of a
        edges(k)=a;
        %increase k by 1 before repeating loop
        k=k+1;
    end
    %break the loop when k reaches 20, will result in vector of
    length 19
    if k==20
        break;
    end
    %transpose edges
    edges=transpose(edges);
end
```

Then data_parsing_size_SEM.m shown below parsed data into bins delineated by the edges variable.

```
%assign variable to be increased stepwise in while loop
k=1;
%create empty variable named 'sSEMnval'
sSEMnval=[];
while (k>0)
    for i = k
        %create c variable which is a vector of cells in sSEMn which
        are greater than or equal to the ith cell in edges and less
        than the i+1 cell in edges
        c=find(sSEMn>=(edges(i)) & sSEMn<(edges(i+1)));
        %assign variable z the values of the cth cells in sSEMn
        z=sSEMn(c);
        %assign variable d the value of the length of z
        d=length(z);
        %assign the kth cell in sSEMnval the value of d
        sSEMnval(k)=d;
        %increase value of k by 1
        k=k+1;
    end
    %break loop when k reaches 20
    if (k==20)
       break;
    end
    %transpose sSEMnval
    sSEMnval=transpose(sSEMnval);
end
```

The last cell in edges vector was deleted, reducing its length to 50 cells.

```
edges=edges(1:end-1);
```

sSEMnval variables and edges were imported into Excel and graphed there using the bar graph function. Data was plotted against minimum values (i.e. a bar over 0.3 µm and before 0.6 µm represents particles which are as large as or larger than 0.3 µm and smaller than 0.6 µm).

Appendix 9: Additional EDX Data and Sample Locations for Case Studies

A9.1 RESULT SUMMARIES AND SAMPLE LOCATIONS

A9.1.1 RUIN DRAWING

The white pigment sample taken from the nineteenth-century ruin drawing contained mostly zinc and oxygen with traces of aluminium, sulphur and silicon. The paint itself appears white, also indicating only trace amounts of other pigments. Given the similar behaviour of all white pigments under various wavelengths of light, the EDX results for RD2 are assumed to be representative of all white pigments in the drawing (Figure A9.1).
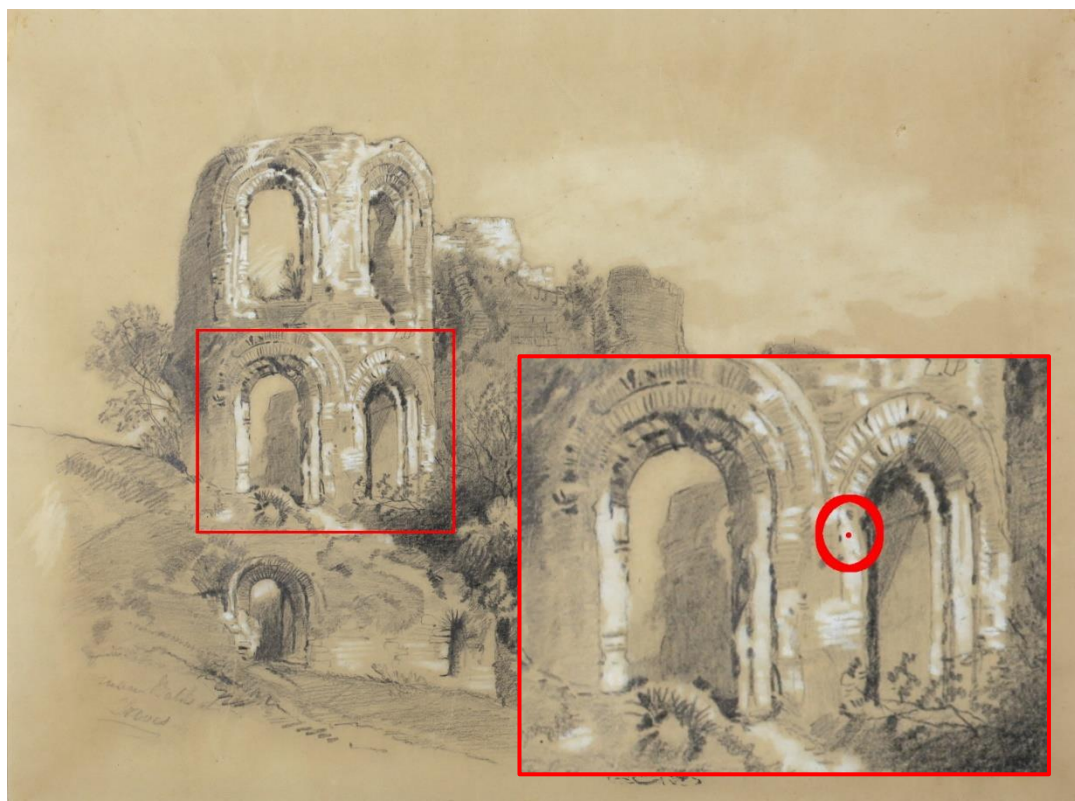
Figure A9.1 Inset detail showing location of RD2 EDX pigment sample from nineteenth-century ruin drawing.

A9.1.2 *VIEW OF THE RIVER COQUET* BY THOMAS HARPER

Three samples analysed from Thomas Harper's *View of the River Coquet* contained

mostly zinc oxide with larger amounts of aluminium, sulphur, and silicon. Some

potassium was detected, which could indicate that much of the aluminium and

sulphur is attributed to alum sizing[136], though the presence of silicon and the blue

surrounding the white areas suggests some of the elements could be components of

an ultramarine blue pigment. The three samples were taken from two different areas

of the painting (Figure A9.2).
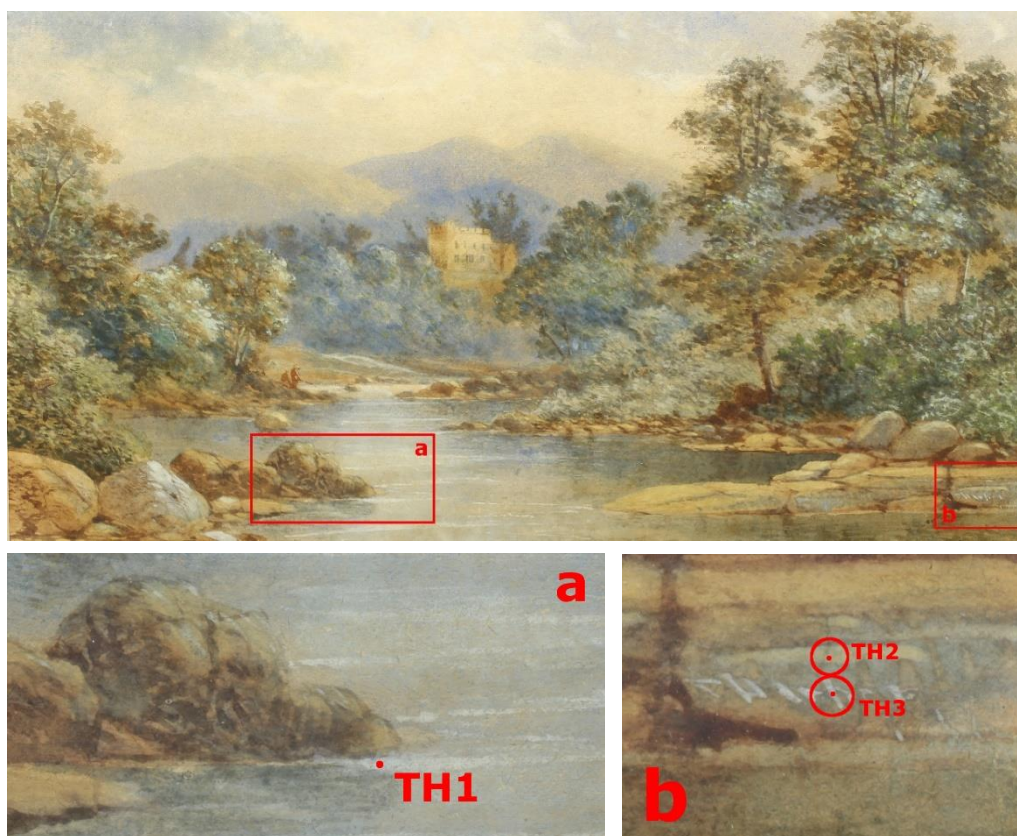
Figure A9.2 Thomas Harper's *View of the River Coquet* with details showing location of EDX pigment samples **a)** TH1 and **b)** TH2 and TH3.

---

[136] This would take the form of potassium alum with chemical formula $KAl_2 \cdot 12H_2O$.

A9.1.3 *BOUQUET OF FLOWERS* BY IRENE KENDALL

Irene Kendall's *Bouquet of Flowers* contained three different types of white pigments. Two samples, IK1 and IK5, were composed mostly of zinc oxide, with traces of silicon, sulphur, chlorine and calcium detected, while IK5 also contained aluminium and arsenic, suggesting other trace pigments. Samples IK2 and IK4 contained both zinc and titanium, suggesting both zinc oxide and titanium oxide pigments. The presence of titanium dioxide is explained by conservation work carried out in 2007 where the pigment was used to discretely infill lost areas of the design. Sample IK3 contained lead, barium and sulphur, indicating possibly lead white and barium sulphate. Both could be results of previous conservation work or later additions by the artist. Locations of all EDX samples are shown in Figure A9.3.

Figure A9.3 Irene Kendall's *Bouquet of Flowers* (top) with locations of details.
Below a) shows the location of EDX samples IK3 and IK5, **b)** shows locations of IK1 and IK4, and **c)** shows location of IK2.

A9.1.4 *S.S. BUDA* BY GEORGE THOMAS

The white pigments labelled samples A and E from *S.S. Buda*[137], collected from thick accretions of paint on the railing, and sample J from a thick white paint on the smokestack of the ship, were mostly zinc oxide with traces of elements found in ultramarine. Sample G, a brownish accretion on the ship's sails, contained zinc oxide but also a significant sulphur component. Sample H, a mixed pigment from the waves, contained mostly zinc oxide but the spectra collected for this sample were unfortunately weak and inconclusive.

Samples D, I, K, and L were of mixed composition and not majority zinc oxide. Sample D, a later addition by Colin Liddie during conservation, was complex and clearly a mixed paint. Sample I contained mostly calcium, either from a filler or from remnants of an alkaline treatment. Sample K contained aluminium, iron, sulphur, potassium, magnesium, calcium and silicon, indicating that it may have ultramarine pigment (due to the blue colour) and have traces of alum sizing or calcium and magnesium salts. Sample L contained some zinc and sulphur in high ratios to one another (sulphur to zinc approximating 0.58), indicating solubilised zinc sulphate salts. All sample locations are shown in Figure A9.4.

---

[137] Delineated in data as SSB-A, SSB-E, etc., but referred to here only by their last letter.
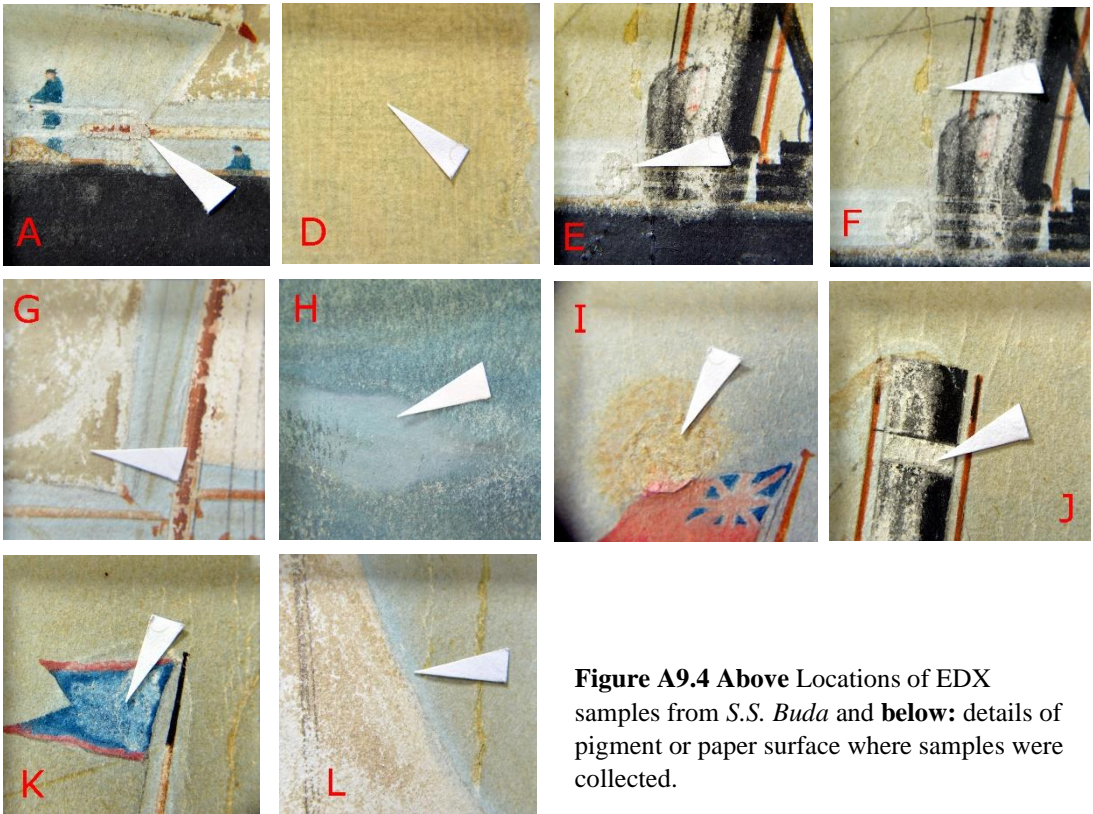
Figure A9.4 Above Locations of EDX samples from *S.S. Buda* and **below:** details of pigment or paper surface where samples were collected.

A9.1.5 *GENERAL VIEW OF ST. MARY'S CATHEDRAL, IONA*

All samples from *Iona* contained high levels of zinc, over 10% in all cases. Samples 3 and 5 also had high levels of sulphur relative to zinc, indicating these are likely zinc sulphate salts. This conclusion agrees with visual evidence of salts. Samples 1, 2, and 6 contained the highest percentage of zinc ions, while sample 7 had the highest percentage of zinc of all samples (at around 20%). Locations of all samples are shown in Figure A9.5.
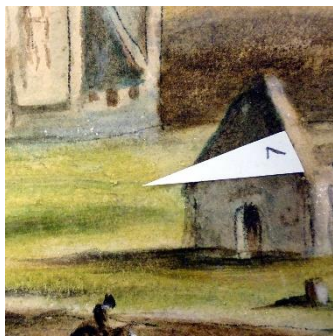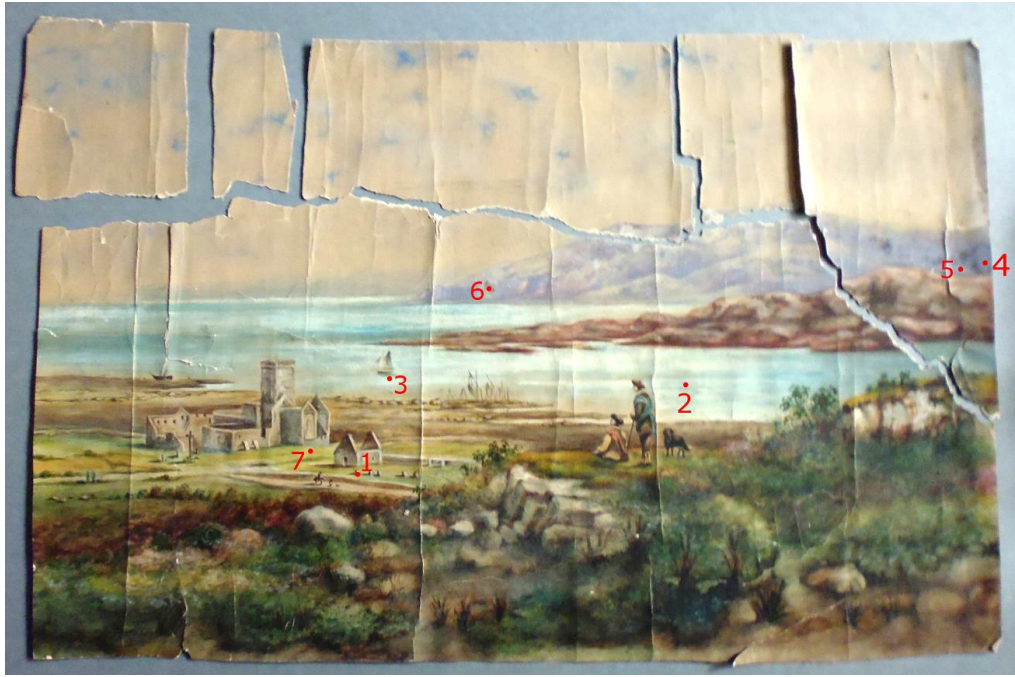
Figure A9.5 Above: locations of EDX samples from *General View of St. Mary's Cathedral, Iona* and **below:** details showing pigment or paper surfaces where samples were collected.

Appendix 10: Zinc Oxide's Use in Oil Paints

A10.1 HISTORY OF ZINC OXIDE AS A PIGMENT IN OILS

Zinc oxide powders were first proposed as a pigment for oil paints. Basic lead carbonate (called lead white) dominated among white oil paint pigments until concerns about lead's toxicity arose in the late 18th century, prompting some scientists to consider alternate white pigments (Kühn, 1986). Guyton de Morveau responded to these concerns in 1782 by promoting zinc oxide as a safe and inert alternative to lead white. That same year, Courtois of the Dijon Academy began to manufacture zinc oxide commercially but found that the pigment retarded the drying of oils. The zinc oxide paint was subsequently mixed with zinc sulphate to increase the paint's drying rate (Harley, 2001). However, the pigment still suffered from a reputation as being difficult to work with and lacking body due to the small particle size of the pigment. As a result, lead white remained the predominant white pigment well into the nineteenth century (Downs Jr, 1976).

Zinc white's popularity in oil paints increased slightly with the development of the indirect or French production method in 1849 by Leclaire in France (Colbourne, 2006) who improved the drying qualities of the pigment by grinding it in a poppy seed oil boiled in pyrolusite (manganese dioxide). This modified oil was more quick-drying and yellowed less than linseed oils (Picollo et al., 2006). Leclaire campaigned for zinc white's use in French government building projects, greatly increasing demand within his country (Remington & Francis, 1954), though use outside of France remained limited.

Zinc white had a similar surge in popularity as a house paint in the United States with the invention and refinement of the direct or American manufacturing process in 1850 by Samuel Jones and Samuel Wetherill (Holley, 1909). The invention of the direct manufacturing process for producing zinc oxide was likely catalysed by the discovery of a large deposit of zinc-containing Franklinite ore in New Jersey (Morley-Smith, 1958). The direct process was much less costly than the indirect process and provided a cheap alternative to imported French zinc oxide (Holley, 1909) as well as providing a non-toxic alternative to lead white. As the French zinc oxide was generally whiter and contained fewer impurities than the American alternative, its importation continued through the nineteenth century (Sons, 1901).

Some early examples of "zinc white" in oil paintings have been found in England and in Germany dating from the early nineteenth century before Leclaire's improvements (Kühn, 1986). Beginning in the 1850s, Pre-Raphaelite painters found zinc oxide oil paints useful as a ground layer (Townsend, Ridge and Hackney, 2004; Osmond, 2019). Chemical analysis suggests that zinc white was mostly present in pigment mixtures found in many oil paintings. In a study cited by Kühn (1986) of oil paintings in the Schack-Galerie, he found that "[i]n the majority of the works investigated the whites do not contain zinc white, whereas the colored [sic] paints often do," (Kühn, 1986, p. 172) implying that colourists often mixed the pigment in as a lightening agent. In this way, the pigment was more widely used in oil paintings than previously thought.

Zinc white's use and popularity steadily increased after 1850, eventually being favoured by a number of successful artists including Cezanne, Picasso, and Van Gogh (Bertrand et al., 2013). It has continued to be an important and widely-used pigment in oil painting through the twentieth century (Picollo et al., 2006), though

titanium white has become the most popular pigment in the last half of the century given its greater hiding strength and lack of toxicity when compared with zinc white and lead white, respectively.

A10.2 DEGRADATION IN OIL PAINTINGS LINKED TO ZINC OXIDE

A10.2.1 CHALKING

Oil paintings containing zinc oxide undergo many of the same degradative processes as works of art on paper containing the pigment. They are known to experience a unique phenomenon called 'chalking'. The term chalking refers to the breakdown of the binding medium in oil paint films resulting in the pigment coming loose from the paint film and appearing as a chalky dust sitting on the surface. Morley-Smith (1950) compared rates of chalking between zinc oxides produced by indirect and direct methods in raw linseed oil and found that indirect zinc oxides chalked much faster than direct process pigments and that this accelerated degradation was largely correlated to a larger surface-area-to-particle-size ratio of the zinc white pigment produced by the indirect method. Rischbieth (1950) found that chalking in paints containing zinc oxide was greatly accelerated by applying a water spray to an ageing sample. Chalking appears to be the oxidation of the binding medium by the hydrogen peroxide formed on the surface of zinc oxide particles. Some painting media are more prone to oxidation by zinc oxide. Feller (1966) has suggested that dammar varnish is especially prone to oxidation by zinc oxide while polyvinyl acetate (PVA) is highly resistant to chemical changes by zinc oxide.

A10.2.2 METAL SOAP FORMATION

In addition to chalking, soap formation has been a long-standing problem in oil paintings containing zinc white. Soaps are formed when metals form complexes

with fatty acids by bonding with their carboxyl groups, often forming large masses which break through the surface of paintings and disrupt the colour and texture of painted surfaces. While zinc oxide particles are not birefringent, zinc soaps can be differentiated from pure pigment by their high birefringence (Kühn, 1986). Zinc and lead soap formation was mentioned as early as 1912 by Fleury (1912) in his treatise on the uses and preparation of zinc oxide paints. It is the most thoroughly-investigated phenomenon associated with the degradation of paintings containing zinc oxide pigments. While carboxyl groups are present in some acids found in gum arabic such as glucuronic acid, soap formation has not been observed in aqueous binding media (Noble et al., 2005).

Jacobsen and Gardner (1941) were the first who determined the structure of zinc oleates and the bonding which occurs between zinc and the carboxyl groups of oleic acids. Morley-Smith (1958) expanded the study by observing that the rates of reactions which produced soaps was slower for acids with long chain lengths such as stearic acid as opposed to shorter acids such as oleic, linoleic and linseed acids. Saturated acids such as stearic acids were also found to have a much longer reaction time than unsaturated acids which reacted quickly and soon levelled off. Finally, Morley-Smith found that zinc oxides with a large surface-area-to-volume ratio were the most prone to react with surrounding materials and readily saponified.

Van der Weerd *et al.* (2003) observed soap formation consisting of zinc oxide and saturated fatty acids in the 1888 painting *Falling Leaves* by Vincent Van Gogh, reaffirming Morley-Smith's findings that saturated acids seem to have the longest period of reactivity with surrounding pigments. Osmond et al. (2005) emphasized the role which slow-drying of oils may have in zinc carboxylate formation and mobility within the paint layer. They also highlighted the frequent presence of

magnesium and cobalt in zinc soap complexes. Osmond, Ebert and Drennan (2014) later found that high humidity and the presence of sulphur compounds in the paint prior to application may also have accelerated the formation of zinc soaps found in the 1963 painting *Portrait of my wife* by artist Nguyên Trong Kiêm.

Recently, Hermans *et al.* (Hermans *et al.,* 2014; Hermans *et al.,* 2015; Hermans *et al.,* 2016) conducted a series of experiments on the structural nature of zinc soaps using Fourier-transform infrared (FTIR) spectroscopy. Typical carboxylates were isolated including zinc palmitate and zinc alkanoates, a metal coordinated structure known to cause transparency in paint layers which in time alter the appearance of the painting.

A10.2.3 CONVERSION TO SOLUBLE SULPHATES

Zinc oxide pigments in oil can again be troublesome if reacted with atmospheric sulphides, producing soluble sulphates which are easily removed with water. Holley (1909) makes note of zinc oxide's sulphide sensitivity at the turn of the century, describing the way a drop of water applied to a reactive area is seen to absorb deep into the paint layer and leave a white halo of zinc sulphate upon drying. Ebert, Singer and Grimaldi (2012), in a study to determine the usefulness of poly(2-ethyl-2-oxazoline) adhesive (Aquazol®) for consolidating flaking oil paints, found that some zinc oxide pigments in a Vietnamese painting had converted to the more soluble zinc sulphate, likely due to the high levels of air pollution in Hanoi where the painting was created. Silvester *et al.* (2014) found that zinc white oil paints became water soluble upon reaction with sulphides, although solubility remained low when mixed with certain other pigments such as cobalt blue. Cadmium yellow, which is cadmium(II) sulphide, CdS and mixed crystals of $ZnS.CdS$ and $CdS.CdSe$

in varying concentrations, was greatly affected by zinc oxide's conversion to a sulphate and was easily removed after its conversion to the sulphate salt.

A10.3 CONSERVATION ISSUES IN OIL PAINTINGS

A10.3.1 CONVERSION TO WATER-SOLUBLE ZINC SULPHATES

When zinc sulphates are formed in an oil painting, they can disrupt the surface and create large, water-soluble flakes. Ebert, Singer and Grimaldi (2012) found that reattaching flaking paint, or consolidating the flakes, was complicated by the presence of soluble zinc. A solution was found by dissolving Aquazol® in propan-2-ol instead of water. The authors used FTIR and energy-dispersive x-ray (EDX) spectroscopy to identify zinc and sulphur in the paint flakes, a vital preliminary step in this case although a technique unlikely to be available to many practicing conservators.

Soluble zinc sulphate salts also present a problem when cleaning the surface of unvarnished paintings, which is commonly undertaken using aqueous solutions or saliva (Stavroudis, Doherty and Wolbers, 2005), both of which would dissolve zinc sulphate, potentially removing paint which is embedded in the soluble material. In these cases, alternate means must be found for cleaning which do not remove excess paint; however, the problem of identifying the zinc sulphates remains as many conservators do not have access to analytical equipment needed for such an analysis.

A10.3.2 REMOVAL OF METAL SOAPS

Metal soap formation, particularly zinc and lead soap aggregates, are incredibly difficult to treat as they are insoluble in oils and in solvents commonly used to remove varnishes and surface dirt. They have previously been referred to as

irreversible (Hermans *et al.,* 2016) although in 2014 a treatment method was proposed by Sawicka *et al.* (2014) involving aqueous solutions with the chelate ethylenediaminetetraacetic acid (EDTA). The authors claimed some success at removing both lead and zinc soaps but cautioned that the chelate was strongly attracted to lead ions, making its use risky for lead-based pigments surrounding soap aggregates. This is the only claim found to date for the removal of these metal soap aggregates suggesting that successful removal is both a rare and difficult procedure.

Appendix 11: Analysis of Mock-Up Papers

A11.1 EDX RESULTS

Paper was first coated with 5 nm of platinum to facilitate SEM imaging, then compositional data was acquired using an Oxford Instruments X-Max 150 EDX detector mounted on a TESCAN MIRA3 SEM with a 10 kV beam. The secondary electron detector was used to allow for 15 mm working distance required for EDX data collection.

Fabriano paper contained calcium, aluminium, sulphur and potassium in addition to carbon and oxygen. Calcium could indicate a calcium carbonate filler, while aluminium, sulphur and potassium are all in alum sizing which has a chemical formula of $KAl(SO_4)_2 \cdot 12H_2O$.

Both Folio and Whatman papers only contained carbon and oxygen. This indicates that both likely only contain organic fibres and no alum or fillers. Gelatine might have returned a nitrogen peak but cannot be ruled out for the Folio paper. Whatman #1 filter paper is only supposed to contain cotton fibres, and the EDX results appear to confirm this.

A11.2 EXAMINATION OF FIBRES

SEM images confirmed that Whatman (Figure A11.1) and Folio (Figure A11.2) papers both contained cotton fibres with a characteristic flat fibre and twist, though Folio papers contained linen fibres as well which were identified by their segmented fibres (Carpenter, 1952).
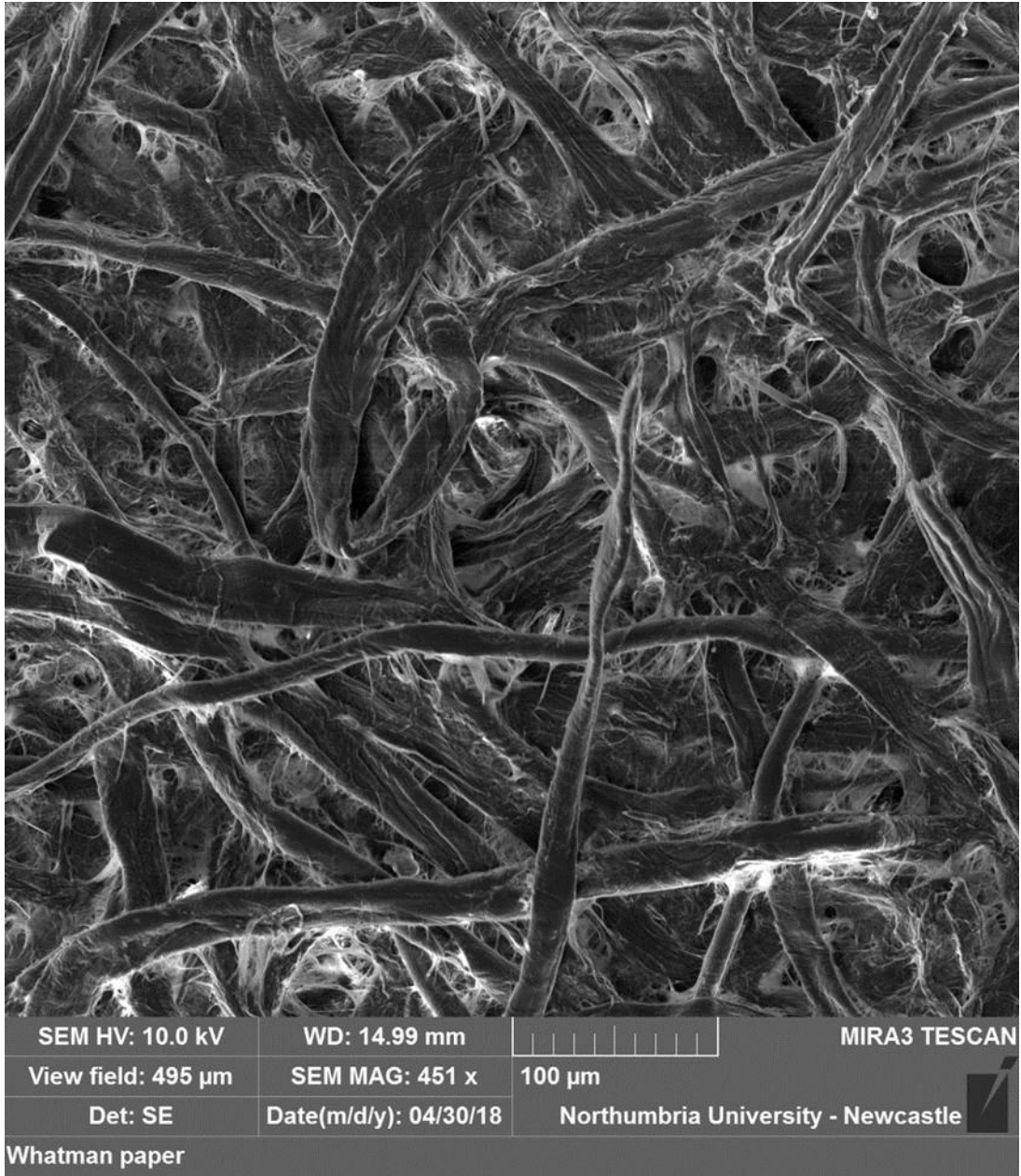
Figure A11.1 Whatman fibres imaged by SEM at 451x magnification. Image shows only cotton fibres with characteristic twist.
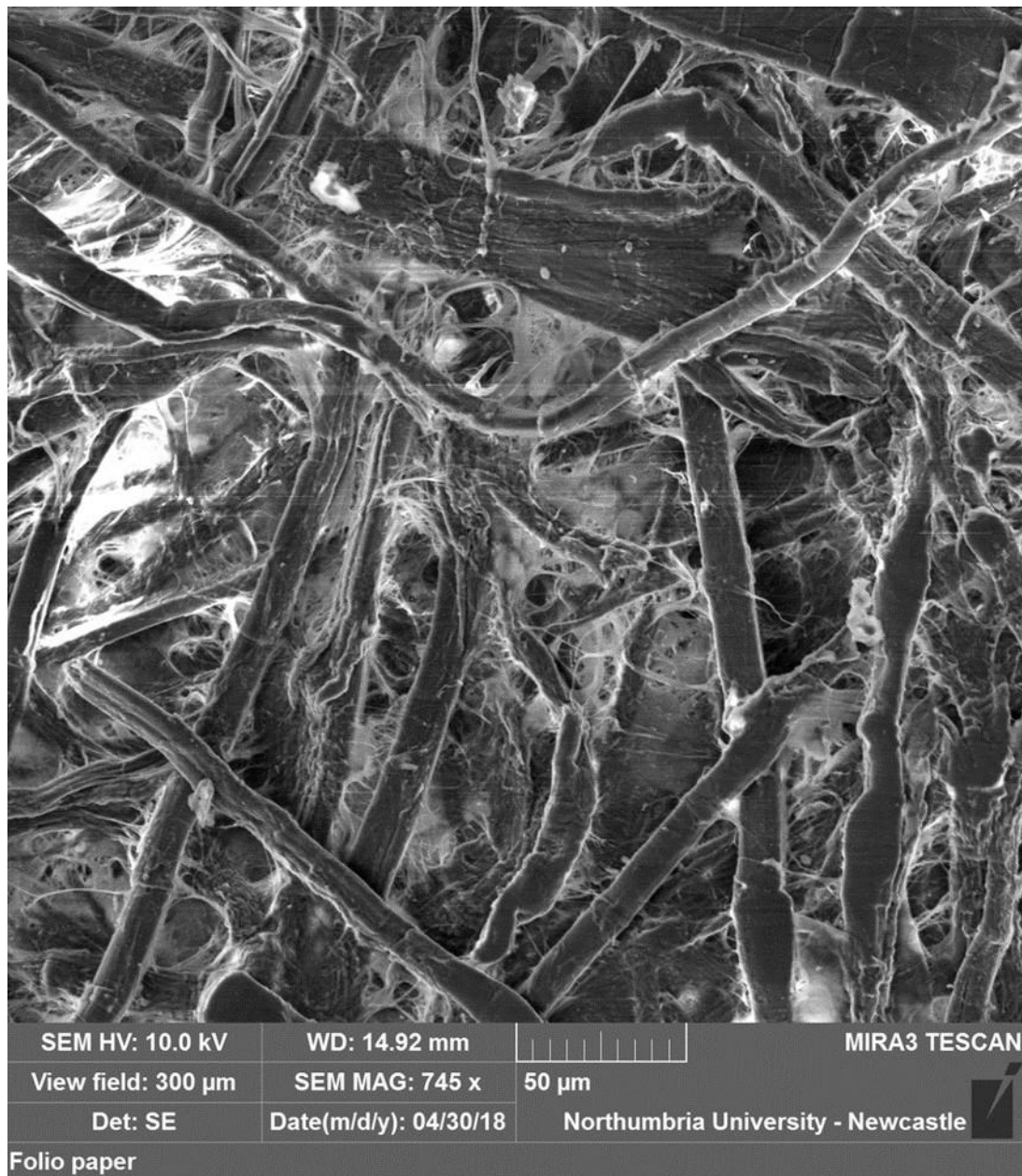
Figure A11.2 Folio fibres imaged by SEM at 745x magnification. Image shows mixed fibres appearing to be cotton and linen or flax due to their segmentation.

Micrographs of Folio papers after Hertzberg staining revealed that they contained mechanised wood pulp residues due to yellow staining of the pulp (Manente *et al.*, 2012) (Figure A11.3). The fibres from Fabriano papers were characteristic of cotton without traces of lignin or wood pulp as seen in Folio papers (Figure A11.4).
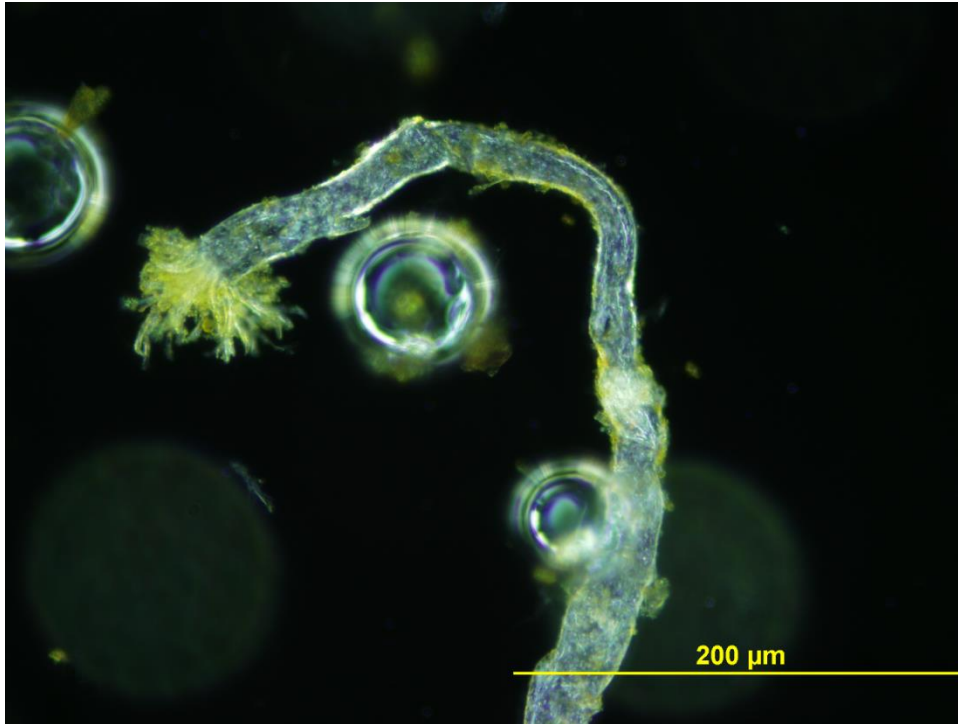
Figure A11.3 A linen fibre from Folio paper with fragments of wood pulp visible as yellow particles after Hertzberg staining. Image taken at 200x magnification in dark field mode.
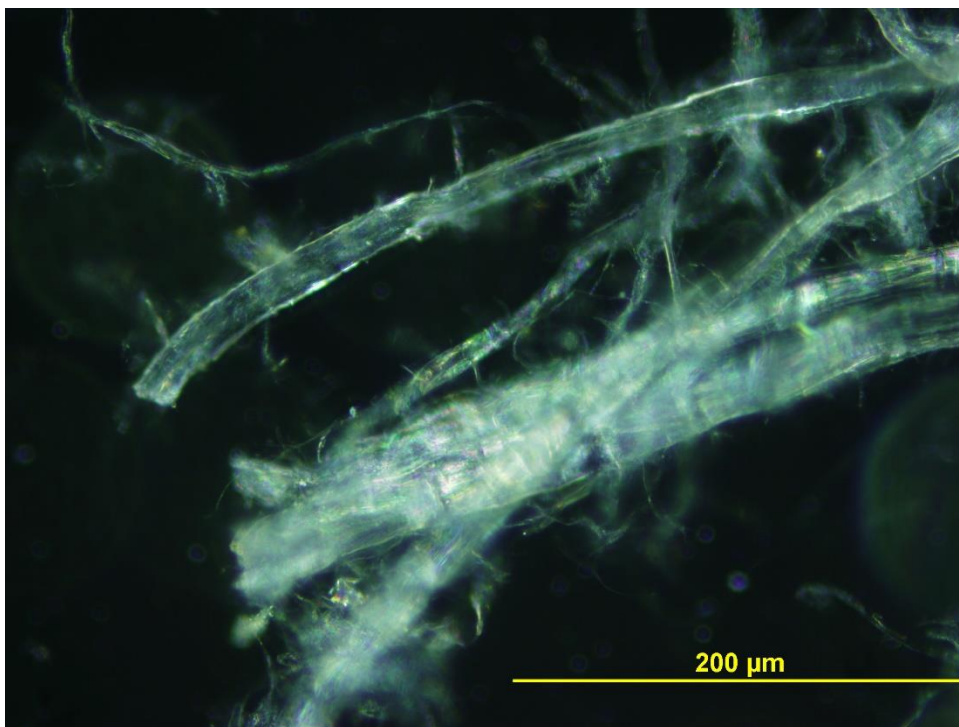
Figure A11.4 Cotton fibres from Fabriano paper after Hertzberg staining. Image taken at 200x magnification in dark field mode.

Appendix 12: Light Exposure Rationale

A light exposure duration for this study had to be short enough to be practical but long enough to ensure that a photocatalytic reaction would take place on the zinc oxide surfaces. To find an optimal duration, a photocatalysis study by Singh, Saha and Pal (2015) was analysed and converted to a comparable and practical duration in the Q-SUN Xenon Test Chamber Xe-1.

The study cited involved irradiating a solution of methyl red, water, and zinc oxide in a 500 mL beaker on a stir plate and tracking colour loss over 60 minutes of irradiation. A 25 W UV light emitting at 365 nm was placed 12.2 cm above the surface of the solution. Sasges, Robinson and Daynouri (2012) give Equation A12.1 to determine 'the distribution of irradiance I_L on a spherical surface centred on a differential lamp element of power dP' (p. 307):
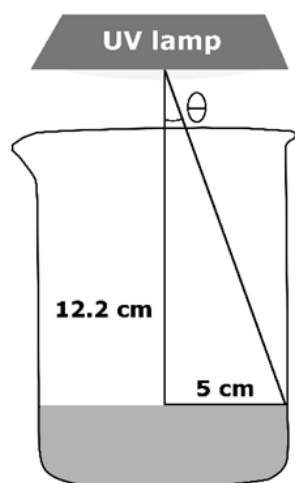
$$I_L[r,\theta] = \frac{dP cos\theta}{\pi^2 r^2} \tag{A12.1}$$

Knowing that the lamp used by Singh, Saha and Pal was 25 W and the distance from the lamp to the surface, r, was 12.2 cm or 0.122 m, the variation in irradiance due to the changing distance and angle to the bottom of the beaker can be calculated (Figure A12.1).

Figure A12.1 Singh, Saha and Pal (2015) experimental set-up

As particles moving through the liquid would pass through positions covering all distances from the lamp within the beaker, an average irradiance would approximate a wattage value over time. To obtain this, the angle θ between the normal or vertical line from the centre of the lamp to the centre of the solution and the line from the centre of the lamp to

the outer edge of the solution was calculated as 0.1826 radians. Dividing this by 9

provided an even increment from 0 to 0.1826 radians to supply 10 points. The radius

values are calculated using these angle values and solving for the unknown

hypotenuse given that the 0.122 m line always remains normal to the UV lamp. At

each angle, the following equation is solved:

$$\cos \theta = \frac{0.122 \, m}{r} \tag{A12.2}$$

Given that 10 values for theta are known, the equation is solved for r using these

values. Then values for θ and r are plugged into Equation A12.1 to obtain 10

irradiance values (Figure A12.2). These were averaged to obtain the value of 167

watts.
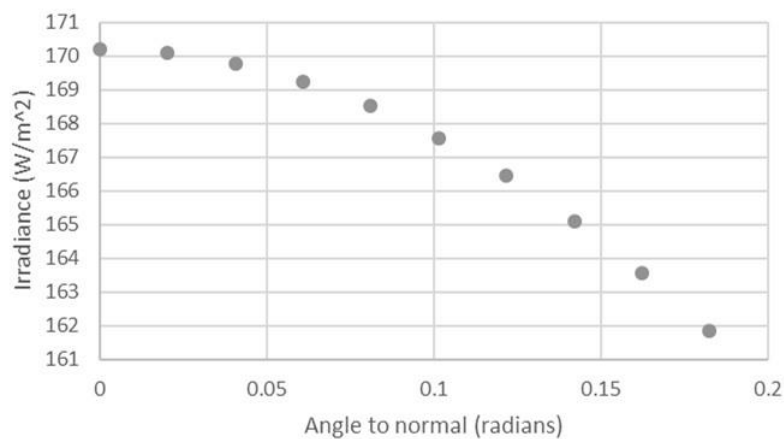
Figure A12.2 Ten irradiance values from the centre of beaker to the edge
calculated using Equation A12.1.

The duration of the experiment was 3600 seconds, so if 167 watts per metre squared,

or 167 joules per second per metre squared, is multiplied by 3600 seconds, the

resulting value is 601,200 joules per metre squared.

Then the area of liquid is calculated from the radius.

$$(0.05\text{m})^2 * \text{pi} = 0.00785 \text{ m}^2 \tag{A12.3}$$

Finally, the calculated energy per metres squared is multiplied by the liquid area to obtain total energy imparted to the liquid surface:

$$0.00785\text{m}^2 * 601{,}200 \text{ J/m}^2 = 4719 \text{ J} \qquad (A12.4)$$

This value is the total energy imparted over 60 minutes of irradiation by light in the near-UV. The photocatalytic response measured by Singh, Saha and Pal was logarithmic, with the majority of reaction occurring within the first 20 minutes (Figure A12.3).
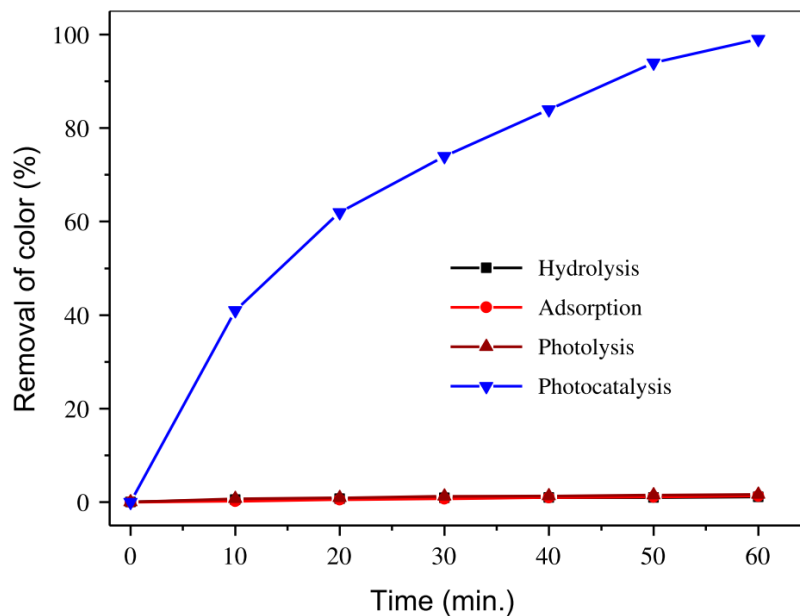
Figure A12.3 Graph reproduced from Singh, Saha and Pal (2015) exhibiting strong photocatalytic response immediately upon irradiation by UV light

Knowing this, calculations were carried out for a reasonable irradiation time using the light exposure chamber. To calculate the irradiance of the bulb, the area under the spectral power distribution (SPD) curve provided by Q-Lab had to be determined. This was done in MATLAB using the following code on spectral radiance data provided in the Q-Lab Technical Bulletin LX-5056:

```
irradiance=trapz(x,y)
```

X-values were assigned as wavelengths and y-values as spectral radiance values and the following code used to approximate the shaded area shown in Chapter 4, Figure 4.8. The total lamp irradiance was calculated to equal 496.21 W/m^2. To calculate the total energy imparted to the material, measured in Joules, the total irradiance was multiplied by the sample size to obtain a power value:

$$496.2100 \text{ W/m}^2 * 0.0002\text{m}^2 \text{ (sample size)} = 0.099242 \text{ W} \qquad \text{(A12.5)}$$

Then the power (watts, or Joules/second) was converted to Joules (energy) by multiplying the power by the total ageing time:

$$50 \text{ hours ageing} = 0.099242 \frac{Joules}{second} \text{ x } 180,000 \text{ seconds} = 17,863 \text{ Joules} \qquad \text{(A12.6)}$$

The same calculation was carried out for all wavelengths shorter than 400 nm by creating x and y vectors in MATLAB comprising only values below 400 and running the irradiance code on them to obtain a value of 48.81 W/m^2.

$$48.8100 \text{ W/m}^2 * 0.0002\text{m}^2 = 0.009762 \text{ W} \qquad \text{(A12.7)}$$

$$50 \text{ hours ageing: } 0.009762 \text{ W} * 180,000 \text{ seconds} = 1757 \text{ Joules} \qquad \text{(A12.8)}$$

While the total energy imparted to the samples over 50 hours is well in excess of that imparted by Singh, Saha and Pal (2015), the contribution by UV is most comparable and needs to be enough for a noticeable reaction to occur.

By dividing the total energy from the light exposure chamber's lamp over 50 hours by the reference study's total UV energy, a value of 0.37 is obtained, which if multiplied by 60 would indicate that ageing samples for 50 hours would be equivalent to the energy imparted by Singh, Saha and Pal after 22.3 minutes. As seen in Figure A11.3, 60% of the photocatalytic reaction has taken place by this

point, making it likely that a noticeable reaction will occur after 50 hours in the Q-Lab chamber.

A significant difference in setup which must be accounted for involves the use of saturation by liquid water during Singh, Saha and Pal's experiment versus the introduction of water via vapour in the experiment using the Q-Lab chamber. While the reduced amount of water will likely result in a slower reaction, even a reaction which is halved should cause a detectable response after 50 hours as this would account for 40% of the photocatalytic reaction measured by the reference study. In this way, 50 hours was chosen as the duration of light exposure, being both reasonable and convenient as well as likely to undergo noticeable photocatalytic reactions during that time given the data and results provided by the reference study.

Appendix 13: Lux vs. Irradiance

Museum professionals currently rely on the unit of lux for measuring visible light exposure and making recommendations for safe light levels. Lux is a measurement of lumens per square meter, a lumen being a unit of candelas (the visible light emitted by a candle) times steradians (a measurement of angle) and measures the amount of visible light reaching the human eye. It measures the appearance of light, not its energy.

Display recommendations based on these values can differ from one institution to another in quantity or specificity. The advice sheet provided by Museums Galleries Scotland for the care of paper objects recommends that light levels for paper not exceed 50 lux and that ultraviolet light wavelengths be limited to 10 micro watts per lumen (Museums Galleries Scotland, 2009) while the V&A recommends a cumulative light dose of no more than 200,000 lux hours (Smith, 2010), a unit determined by multiplying the lux level by the hours of exposure. The difficulty with using lux to measure light exposure is acknowledged in a conservation factsheet provided by the Scottish Museums Council (Hill & Bouwmeester, 2005). It rightly asserts that such a method of measuring and managing light exposure is imperfect in the information it provides. Reducing lux levels is only meant to mitigate damage to objects, though light of all wavelengths has the potential to cause damage.

A13.1 PROBLEMS WITH LUX MEASUREMENTS

Lux, being a measurement of lumens per metre squared, only measures the intensity of a light source in a predetermined wavelength range centred at 550 nm. This range

is the basis for the CIE 1931 standard for L*a*b* colour values.

The wavelengths accounted for in lux measurements, as demonstrated in Figure A13.1, do not account for UV or IR wavelengths, both of which are damaging to works of art. Additionally, a light which is comprised largely of green wavelengths near the lumen peak will have a higher lux value than one which is composed of more blue or UV wavelengths which are more energetic and damaging but would return a lower lux value using a lux meter. An extreme example is a hot stove, which has a lux value of 0 but which will incinerate any art which touches it due to its intense IR emission.
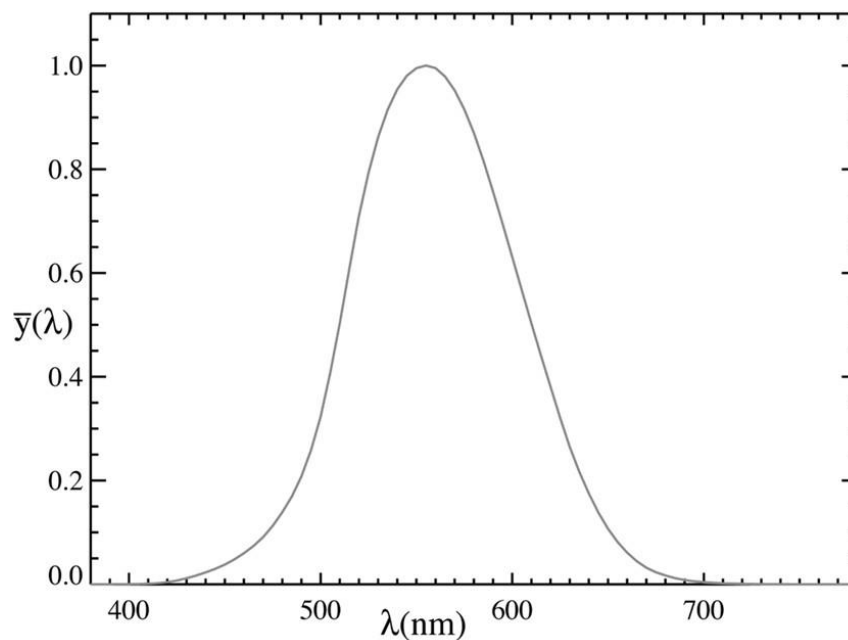
Figure A13.1 Wavelength distribution for lumens based on photopic human vision. Photopic vision relates to the intensity of wavelengths perceptible to the human eye under well-illuminated conditions. Graph of wavelengths in the public domain under a creative commons license.

A.13.2 BENEFITS OF IRRADIANCE OVER LUX

Irradiance, unlike lux, accounts for all wavelengths and describes the exact energy provided by a light over the entire electromagnetic spectrum. Irradiance gives the energy in joules per second, in watts, per metre squared. An SPD, or spectral power

distribution, gives the irradiance for every wavelength of light emitted by a lamp, allowing for exact energy values to be extracted for wavelength ranges. Additionally, SPDs can quickly inform a conservator of the presence of UV or IR wavelengths and whether the energy imparted by these wavelengths is acceptable or if another bulb is desirable which may cut these wavelengths out entirely or filtration is required.

Appendix 14: Elemental Mapping Supplemental Information

Before elemental mapping, images were acquired using the following settings:

- Input signal: SE

- Dwell time: 10 μs

- 1 frame acquired (no averaging of frames)

- Autolock set to custom to track image and make sure minute motion of the image did not affect measurements. Autolock settings were as follows:

    o Image scan size: 512

    o Measurement interval: 10 seconds

    o Autolock mode: extended field (2x – 4x zoom depending on magnification, more if higher mag)

        ▪ Maintain subject size checked

    o 'Use predictive correction' setting selected and reference interval set to 10 seconds

Mapping settings were as follows:

- Pixel Dwell time: 10,000 μs

- Process time: 3

All other settings were adjusted to obtain a map with good resolution and sufficient data for analysis. The settings used for each sample are outlined in Table A14.1.

Table A14.1 Collection parameters for elemental maps

Sample	Resolution	Frame count	Beam energy (kV)
1	1024	15	2
3	1024	10	2
4	1024	10	2
6	512	10	10
7	512	5	10
9	512	5	10
15	1024	10	2
16	1024	10	2
RD2	1024	10	2

Appendix 15: Morphological Trends in Mapping Data

A15.1 GROUPING DATA MORPHOLOGICALLY

To determine if any meaningful relationships between crystallites could be found

from mapping data, all samples were graphed by morphology, volume, and length-

to-width ratio. Morphology appeared to be the greatest predictor of oxygen gradient

and samples were easily grouped according to this criteria.

A15.1.1 HEXAGONAL PRISMS, FLAT ENDS

Crystallites which were clearly discernible as hexagonal prisms with flat polar faces

could be grouped by slope. Both W1C50 and W1C50_2 from sample 1 had nearly

identical slopes (-2.57 and -2.53 respectively); however, their gradients differed

(Figure A15.1).
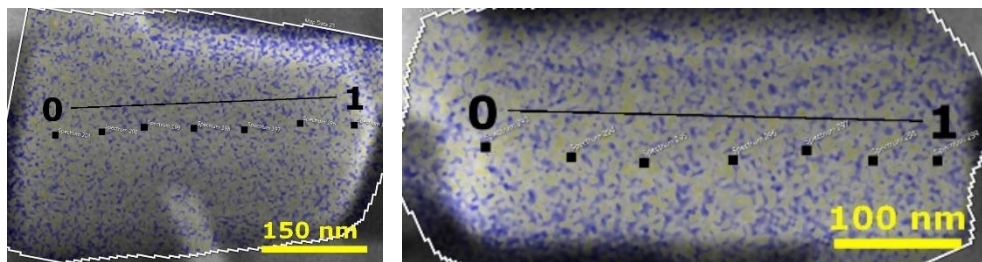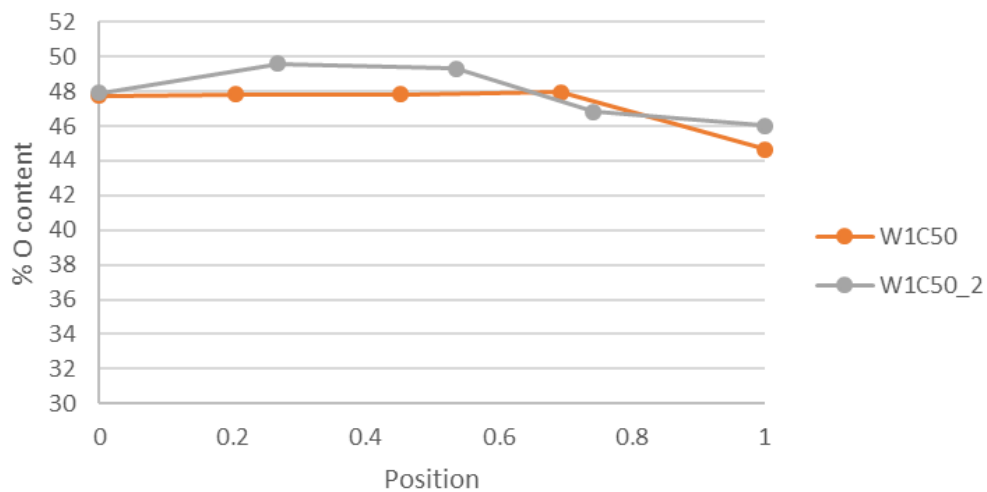
Figure A15.1 Above: Graph of oxygen content for samples W1C50 and W1C50_2, hexagonal crystallites with flat polar ends. Both have extremely similar slopes but slightly different oxygen content and shape. **Lower left:** W1C50, **lower right:** W1C50_2

Samples W3C50 and P6 both had very shallow slopes at -0.68 and -0.58 respectively (Figure A15.2). They were both measured approximately centred along the visible crystal, but their total oxygen content differed at any measured point by about 2%. This may have been due to the orientation of the crystallite in relation to the detector.
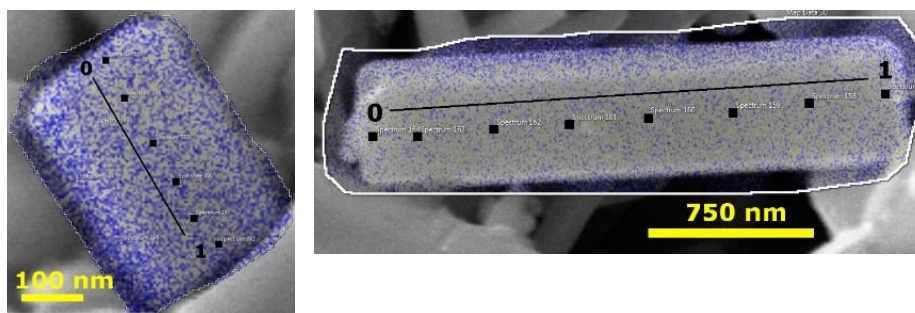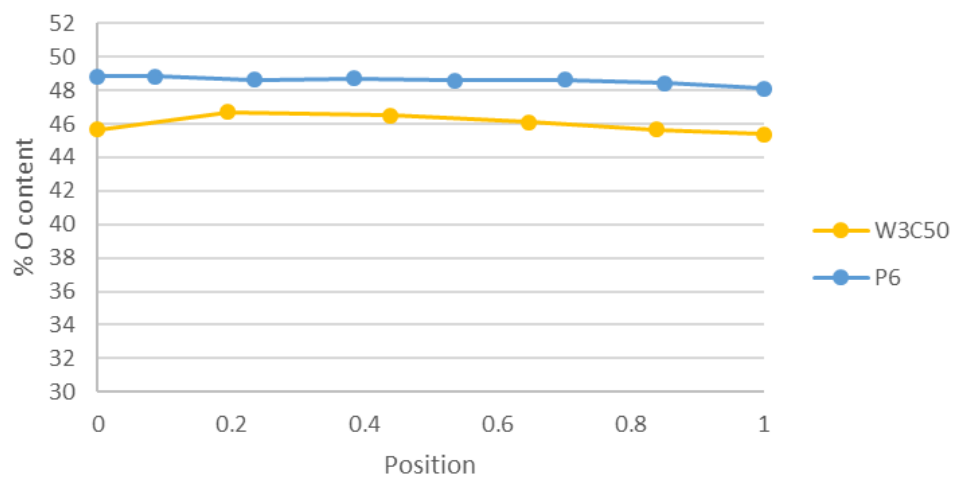
Figure A15.2 Top: Graph of oxygen content for samples W3C50 and P6, hexagonal crystallites with flat polar ends. Both have similar slopes and line shapes but slightly different oxygen content. **Bottom left:** W3C50, **bottom right:** P6.

Samples W15C50_3 and W16C50 had nearly identical graphs and similar slopes, at -4.04 and -3.73 respectively (Figure A15.3).
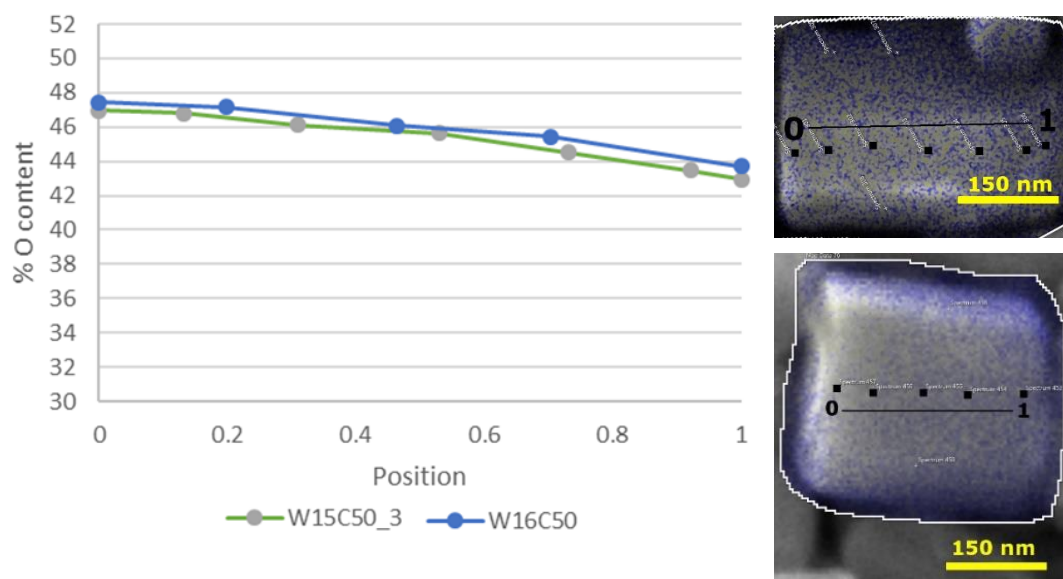
Figure A15.3 Left: Graph of oxygen content for samples W1C50_3 and W16C50, hexagonal crystallites with flat polar ends. Both have similar slopes, line shapes and oxygen content. **Upper right:** W15C50_3, **lower right:** W16C50.

A15.1.2 HEXAGONAL PRISMS, ONE CONE END

All crystallites which were hexagonal prisms with one cone end were found in direct method pigments. Samples P7, P9, W6C50 and W7C50_2 all had similar slopes at -3.94, -3.28, -4.06 and -3.98 respectively. P7 and W7C50_2 have the most similar graphs, while P9 and W6C50 likewise have similarly shaped graphs (Figure A15.4).
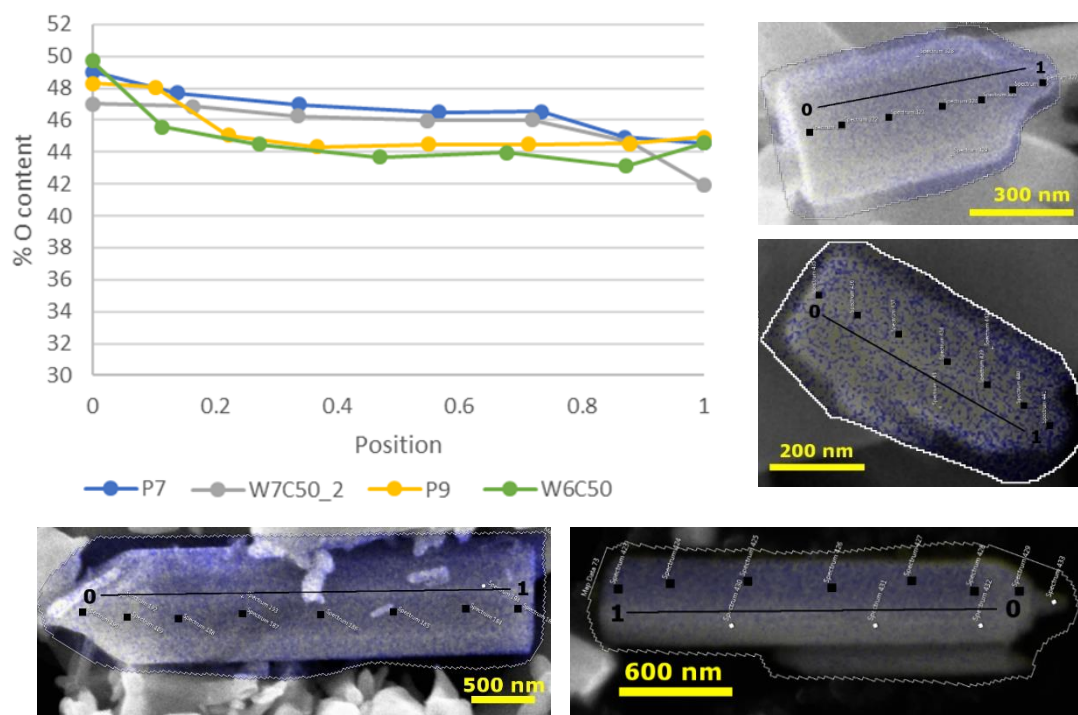
Figure A15.4 Upper left: Graph of oxygen content for samples P7, W7C50_2, P9 and W6C50, hexagonal crystallites with one cone ends. The four samples split evenly into two types of oxygen gradient. **Clockwise from upper right:** P7, W7C50_2, W6C50, P9. Top two images have similar gradient, as do bottom two images.

Samples W7C50 and W9C50 were outliers, with slopes of -15.56 and -1.59 respectively.

A15.1.3 ROUND WITH TWO FLAT POLAR ENDS

Samples P1, P3, and W15C50_2 all had similar graph shapes and slopes, at -1.60, -2.45 and -0.91 respectively[138]. Samples P3 and W15C50_2 had the most similar graph shapes of the three (Figure A15.5). Total oxygen content for all three differed, however, with P3 and W15C50_2 different by about 4% along the *c* axis.

---

[138] P15 and RD2 were also samples which fit this morphology and which graphed similarly, but the similarities between these two are covered in Chapter 2.
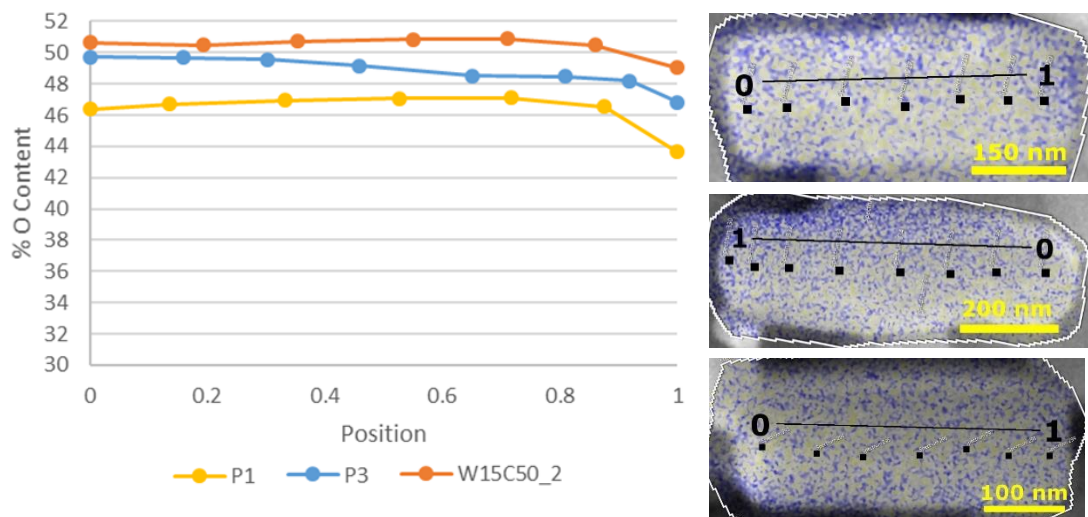
Figure A15.5 Left: Graph of oxygen content for samples P1, P3 and W15C50_2, round crystallites with two flat polar ends. **Upper right:** sample P1**, centre right:** sample P3 and **lower right:** sample W15C50_2. P1 and W15C50_2 have similar line shapes and slopes, although all three samples have slightly different oxygen contents overall.

Appendix 16: Fluorimetry Spectra

The following spectra represent the minimum and maximum values of unexposed and exposed spectra taken from all mock-up samples on Whatman and Folio paper. The range of values is represented by a band of colour, and the line in the middle of this band represents the average spectra. The top spectra have had minimum values subtracted while the bottom spectra have been normalised by area (area = 1).
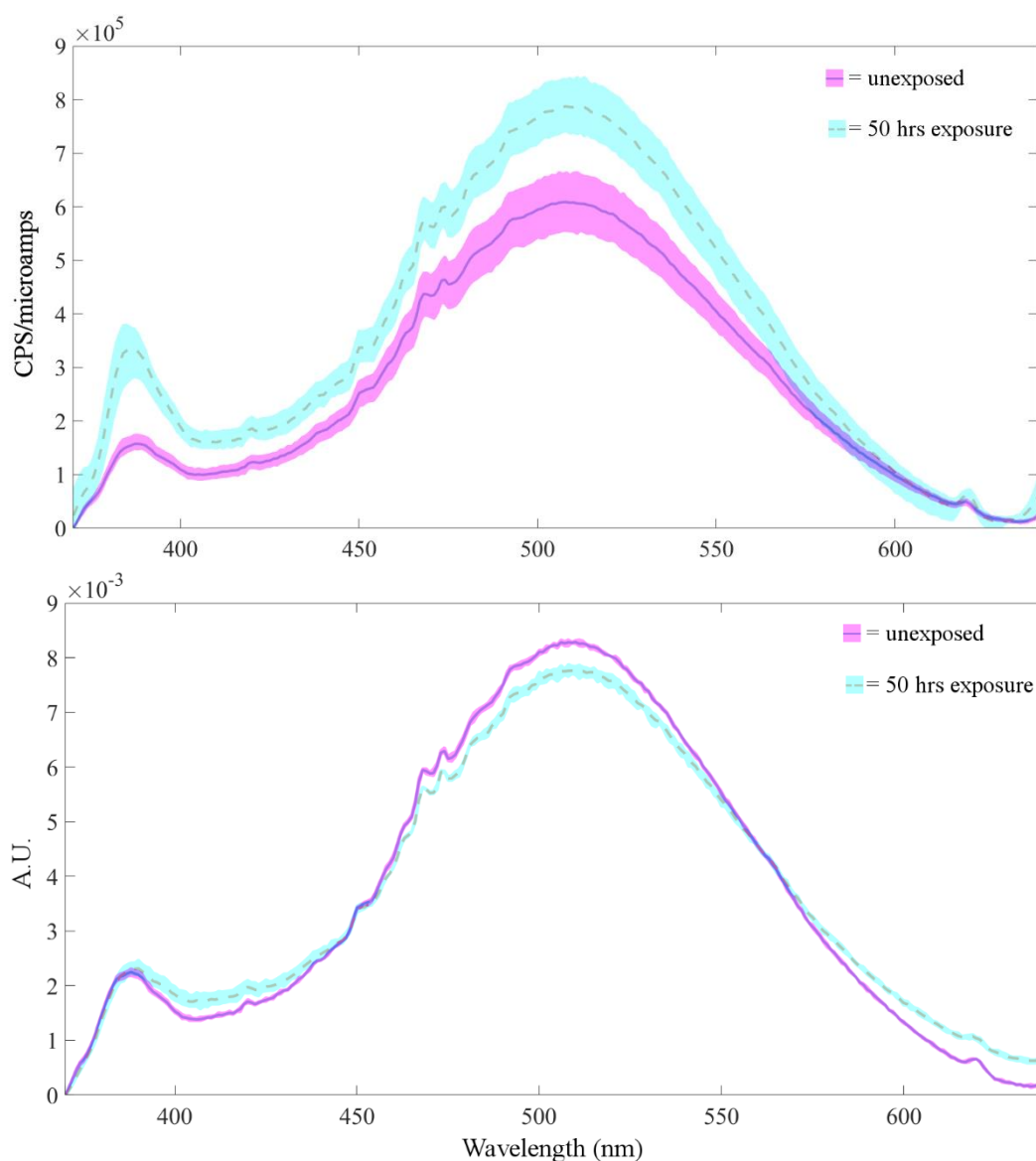
Figure A16.1 *Indirect* sample 1 on Whatman paper. **Above:** minimum value subtracted and **below:** area normalised to 1.
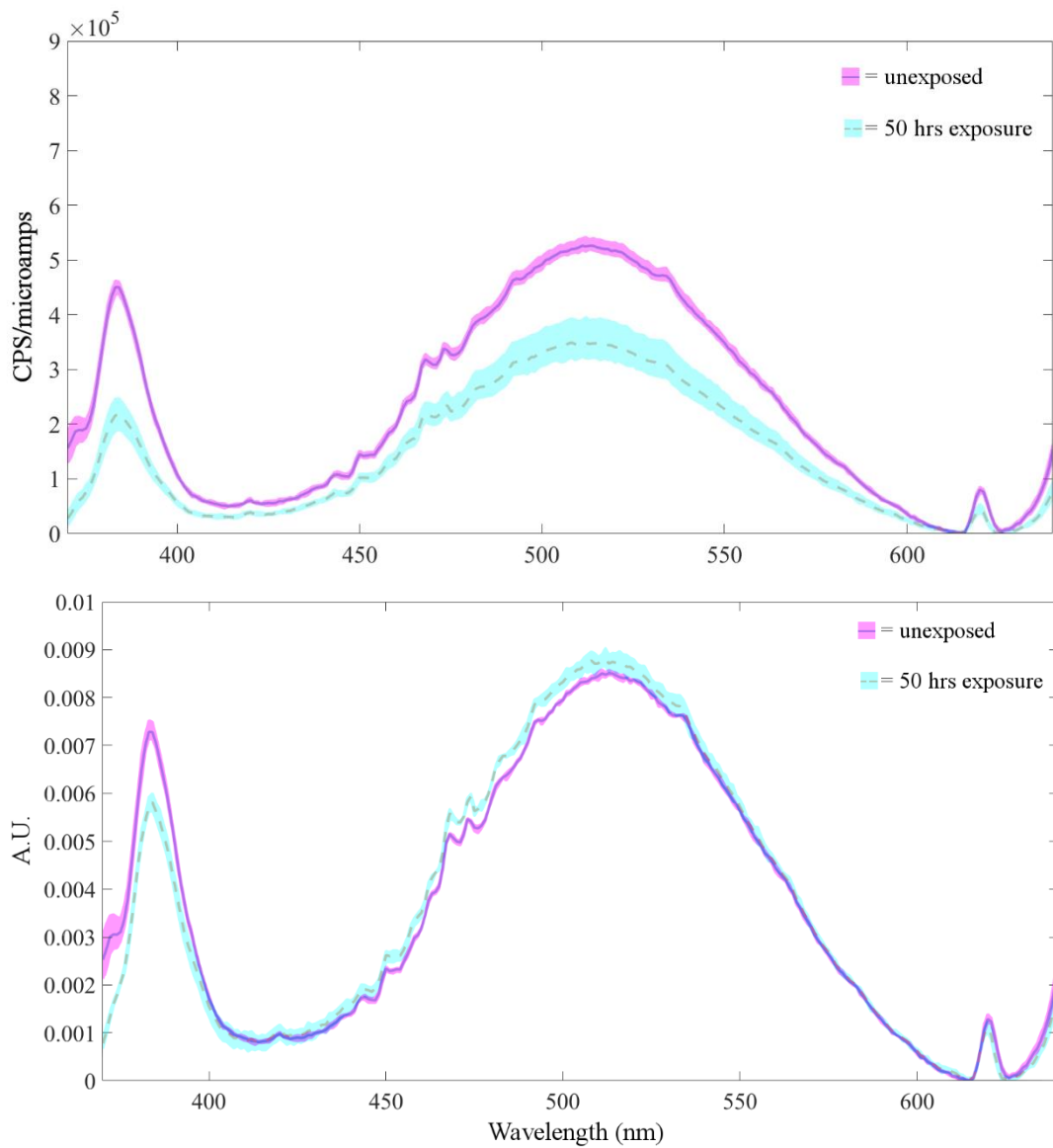
Figure A16.2 *Indirect* sample 1 on Folio paper. **Above:** minimum value subtracted and **below:** area normalised to 1.
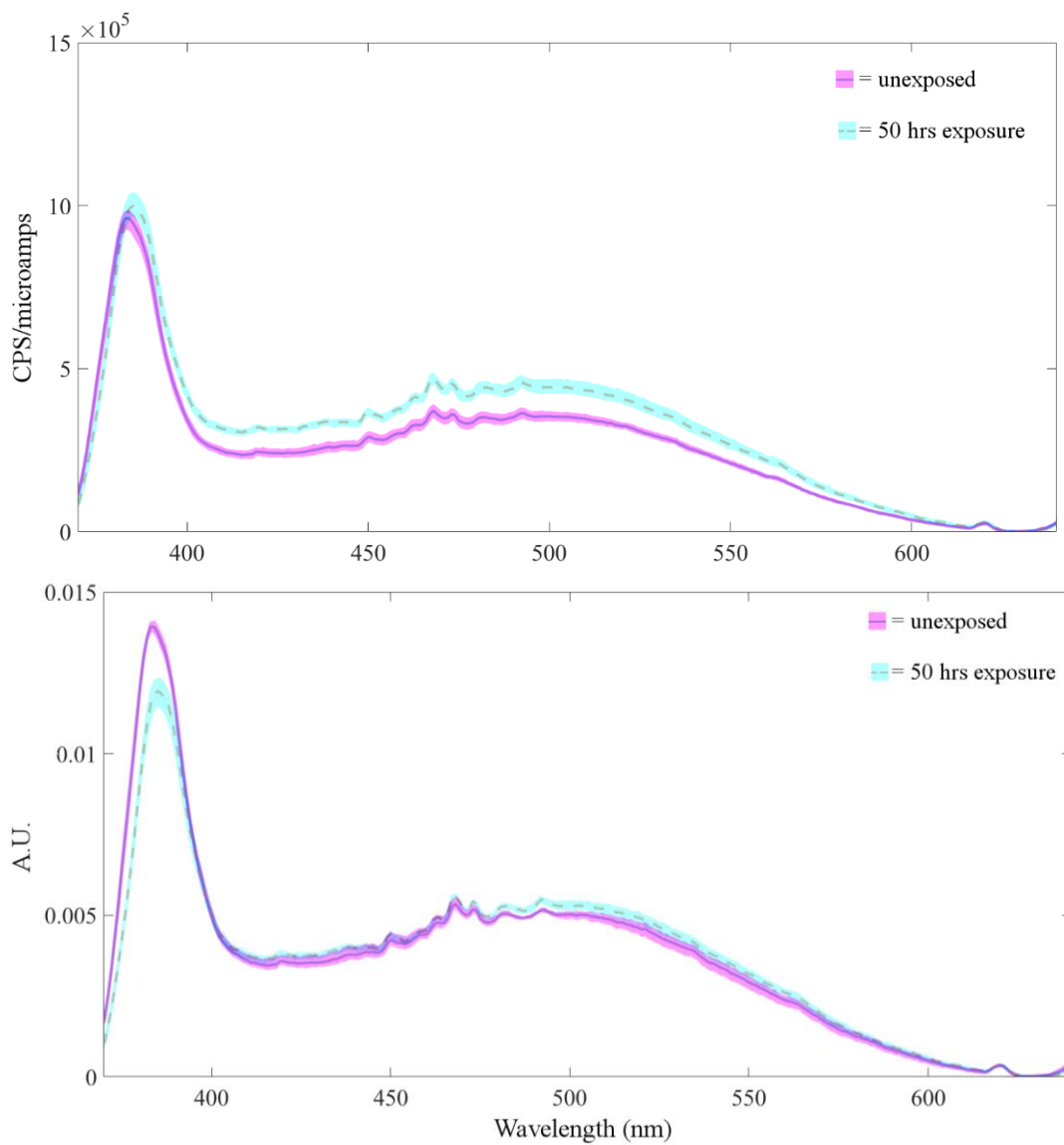
Figure A16.3 *Indirect* sample 3 on Whatman paper. **Above:** minimum value subtracted and **below:** area normalised to 1.
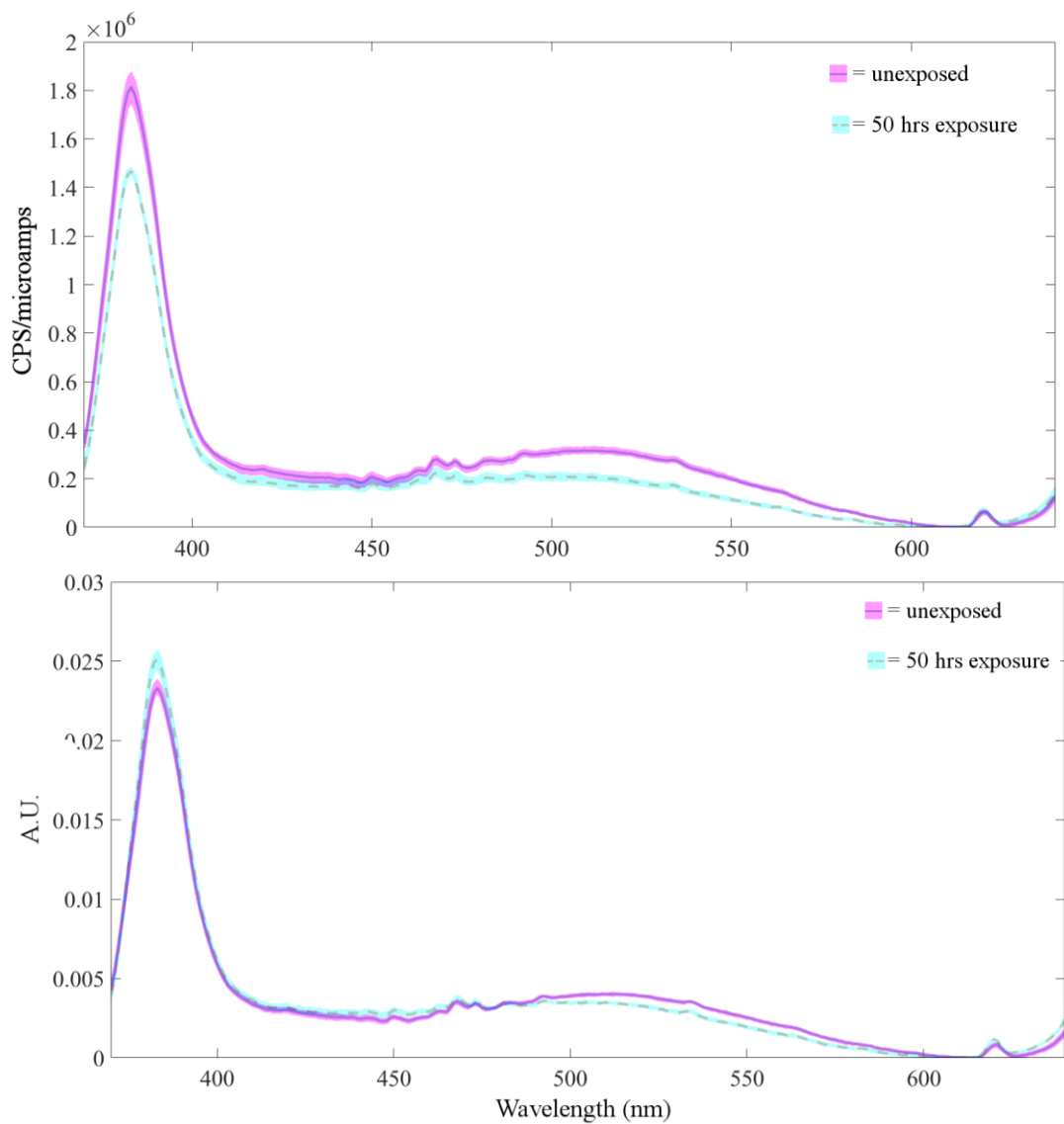
Figure A16.4 *Indirect* sample 3 on Folio paper. **Above:** minimum value subtracted and **below:** area normalised to 1.
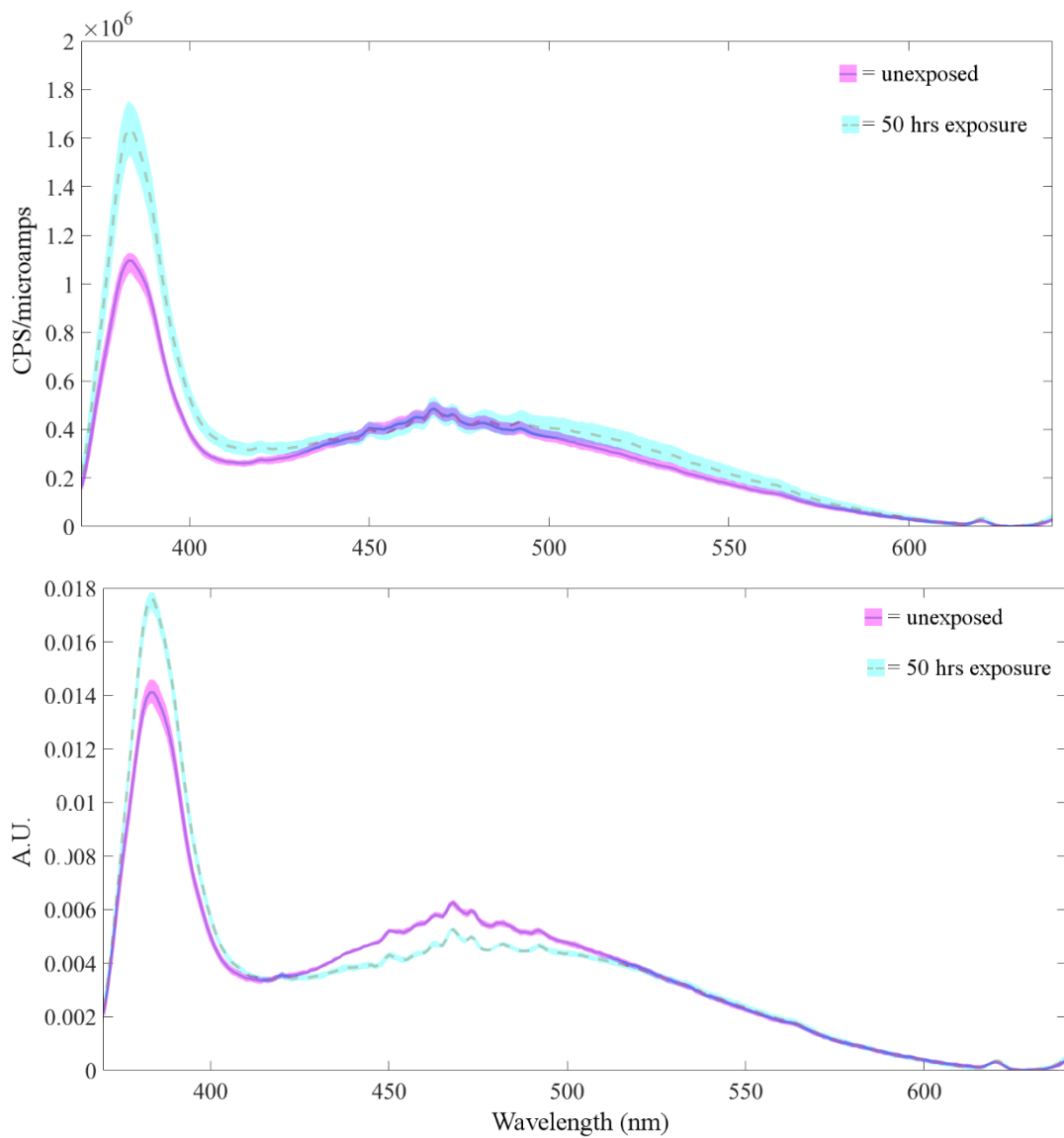
Figure A16.5 *Indirect* sample 4 on Whatman paper. **Above:** minimum value subtracted and **below:** area normalised to 1.
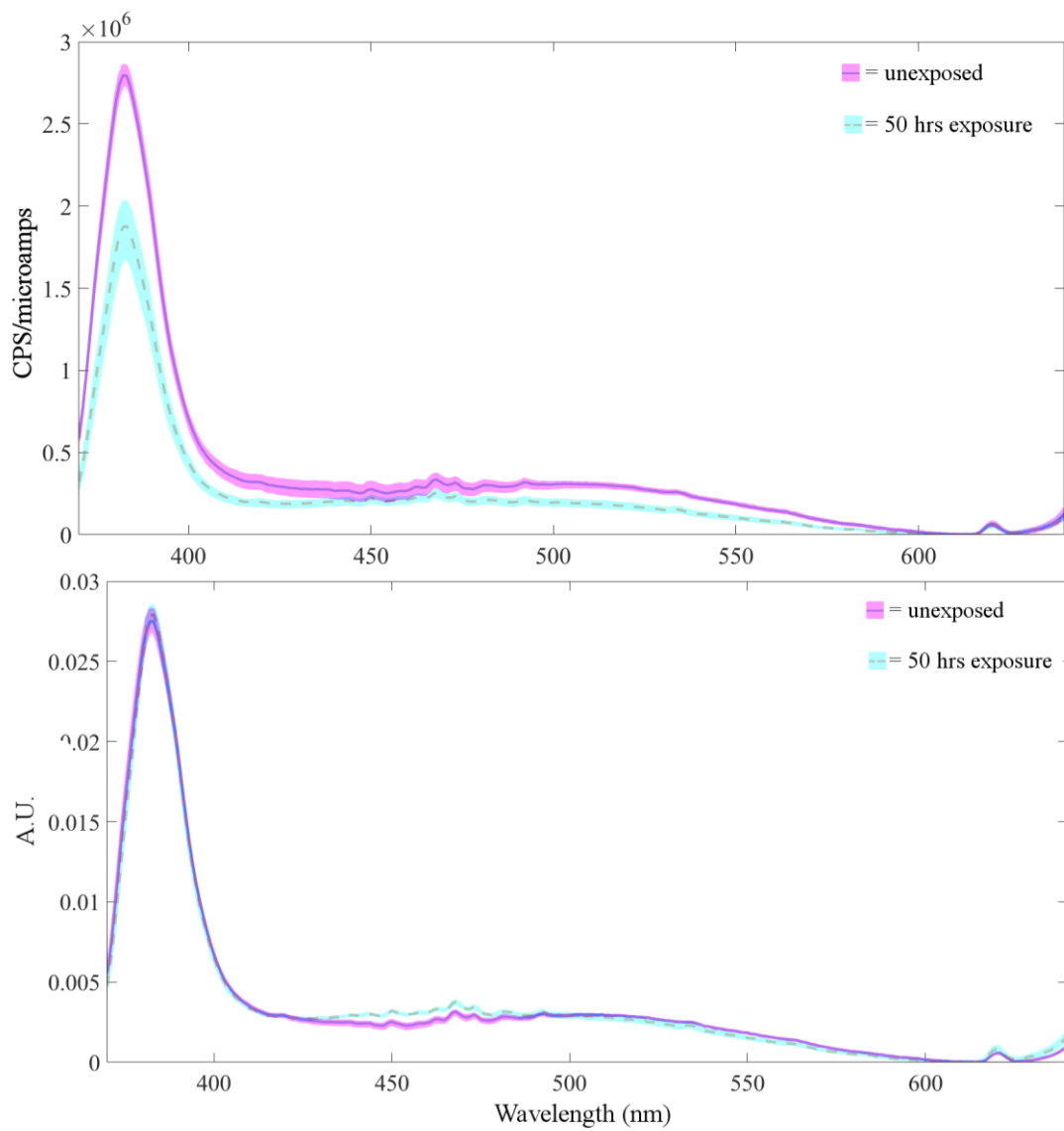
Figure A16.6 *Indirect* sample 4 on Folio paper. **Above:** minimum value subtracted and **below:** area normalised to 1.
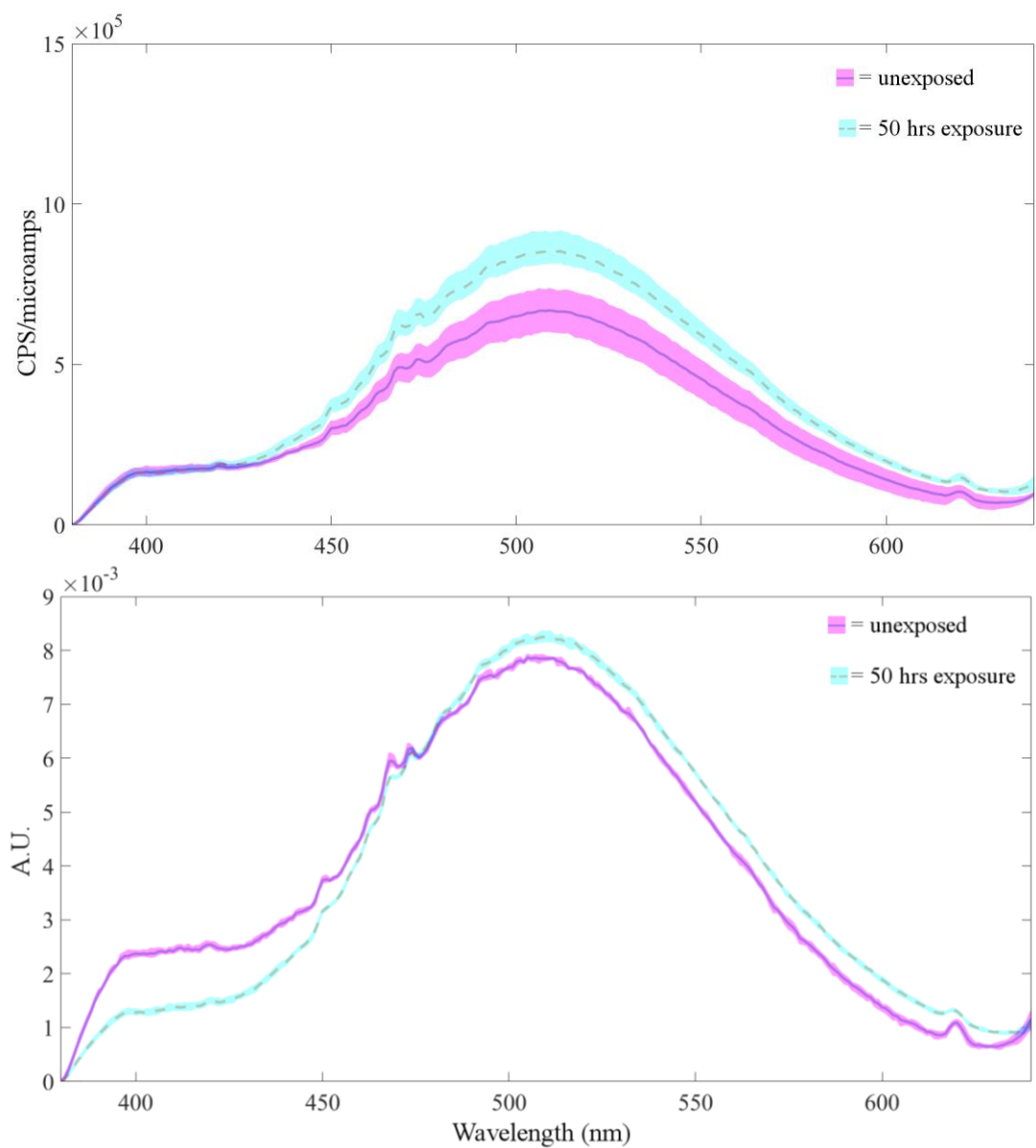
Figure A16.7 *Direct* sample 6 on Whatman paper. **Above:** minimum value subtracted and **below:** area normalised to 1.
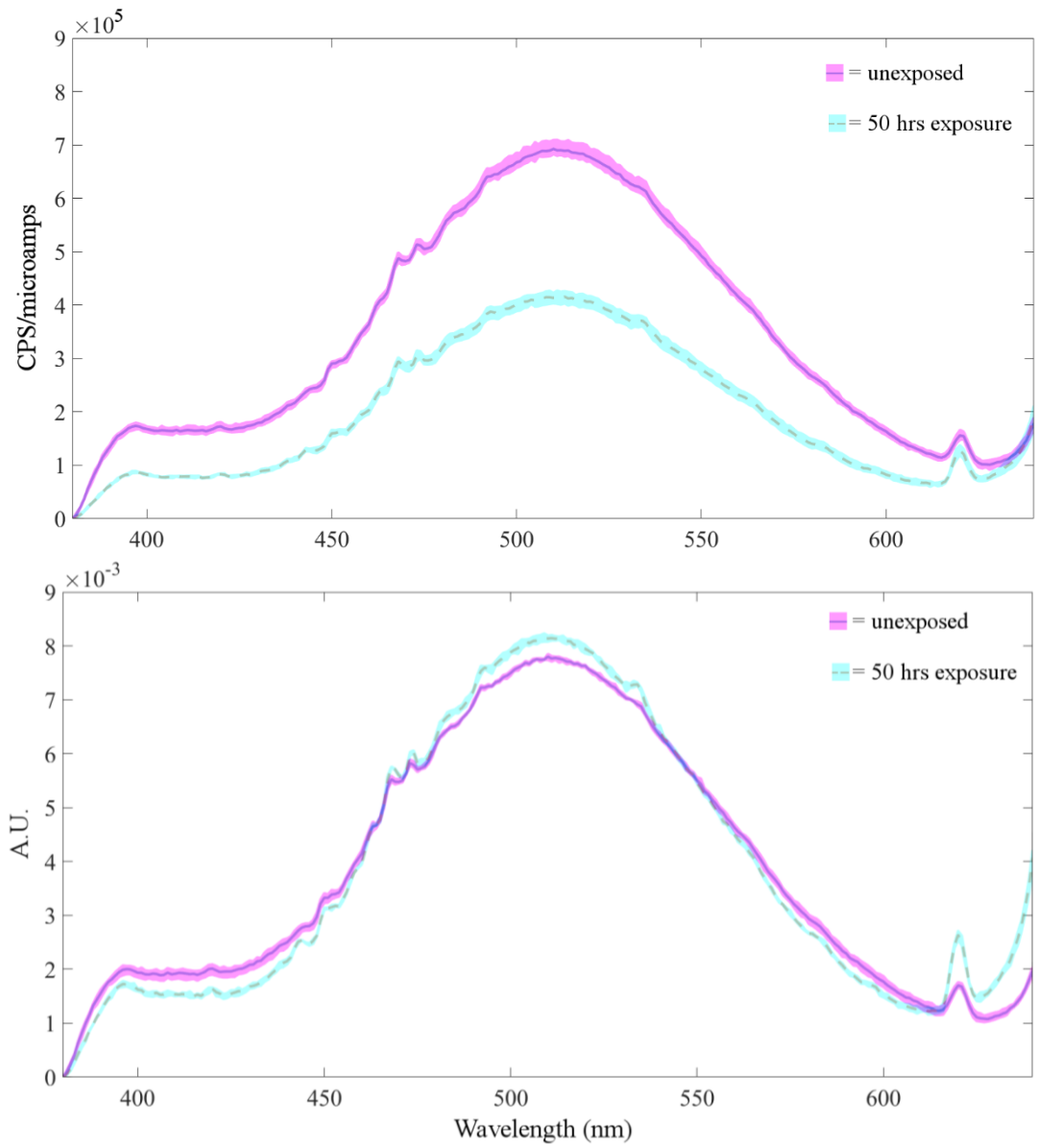
Figure A16.8 *Direct* sample 6 on Folio paper. **Above:** minimum value subtracted and **below:** area normalised to 1.
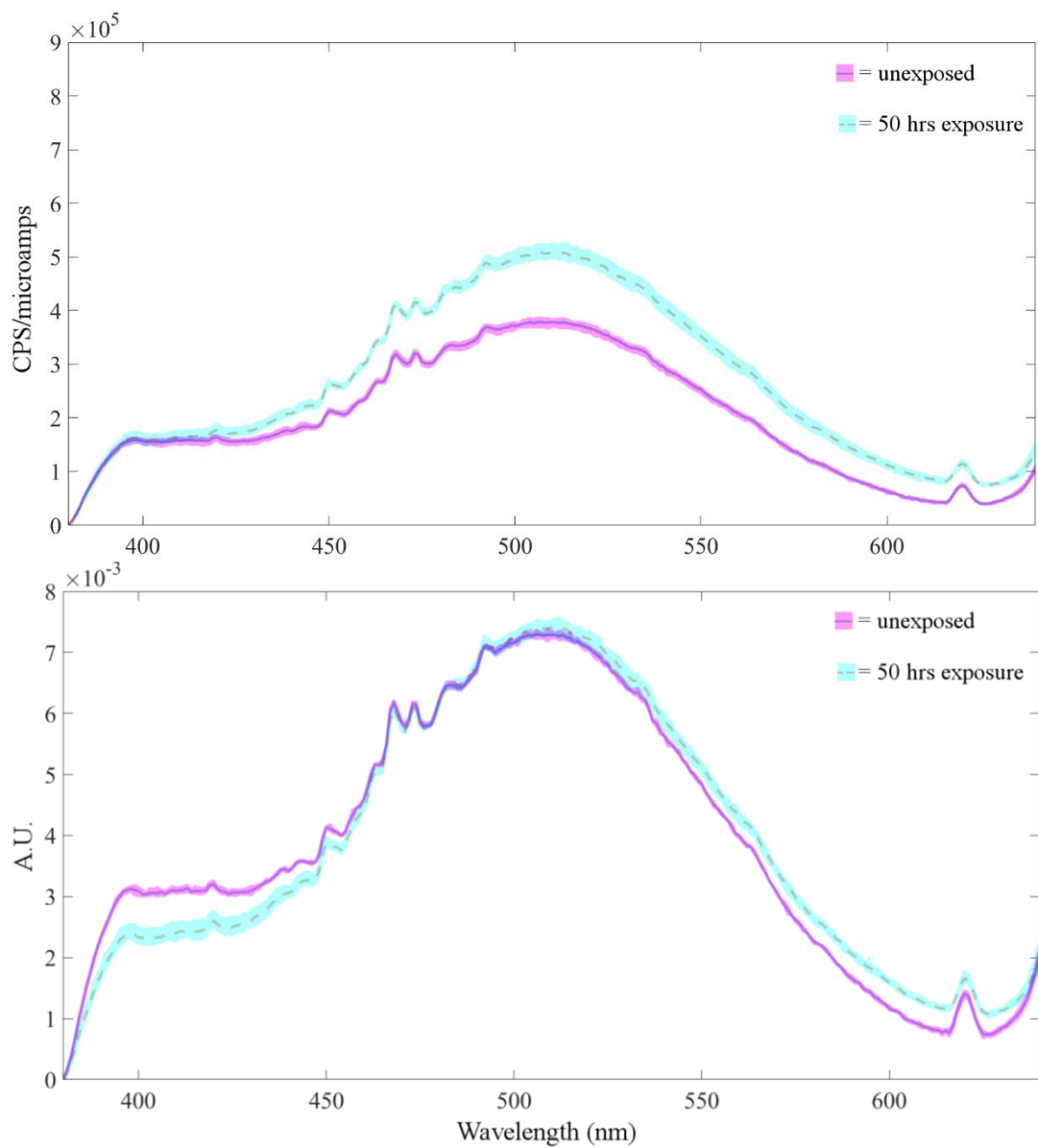
Figure A16.9 *Direct* sample 7 on Whatman paper. **Above:** minimum value subtracted and **below:** area normalised to 1.
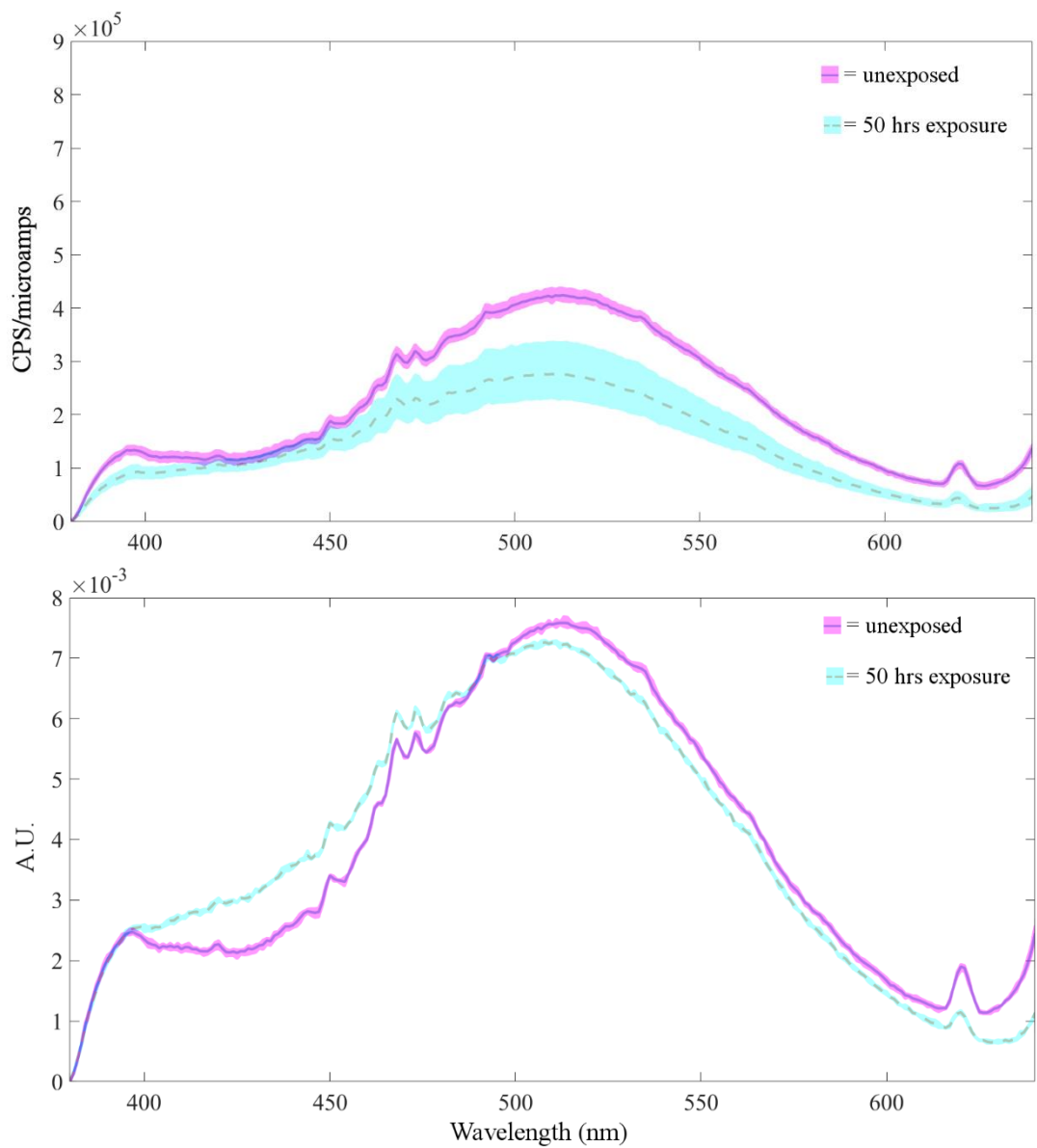
Figure A16.10 *Direct* sample 7 on Folio paper. **Above:** minimum value subtracted and **below:** area normalised to 1.
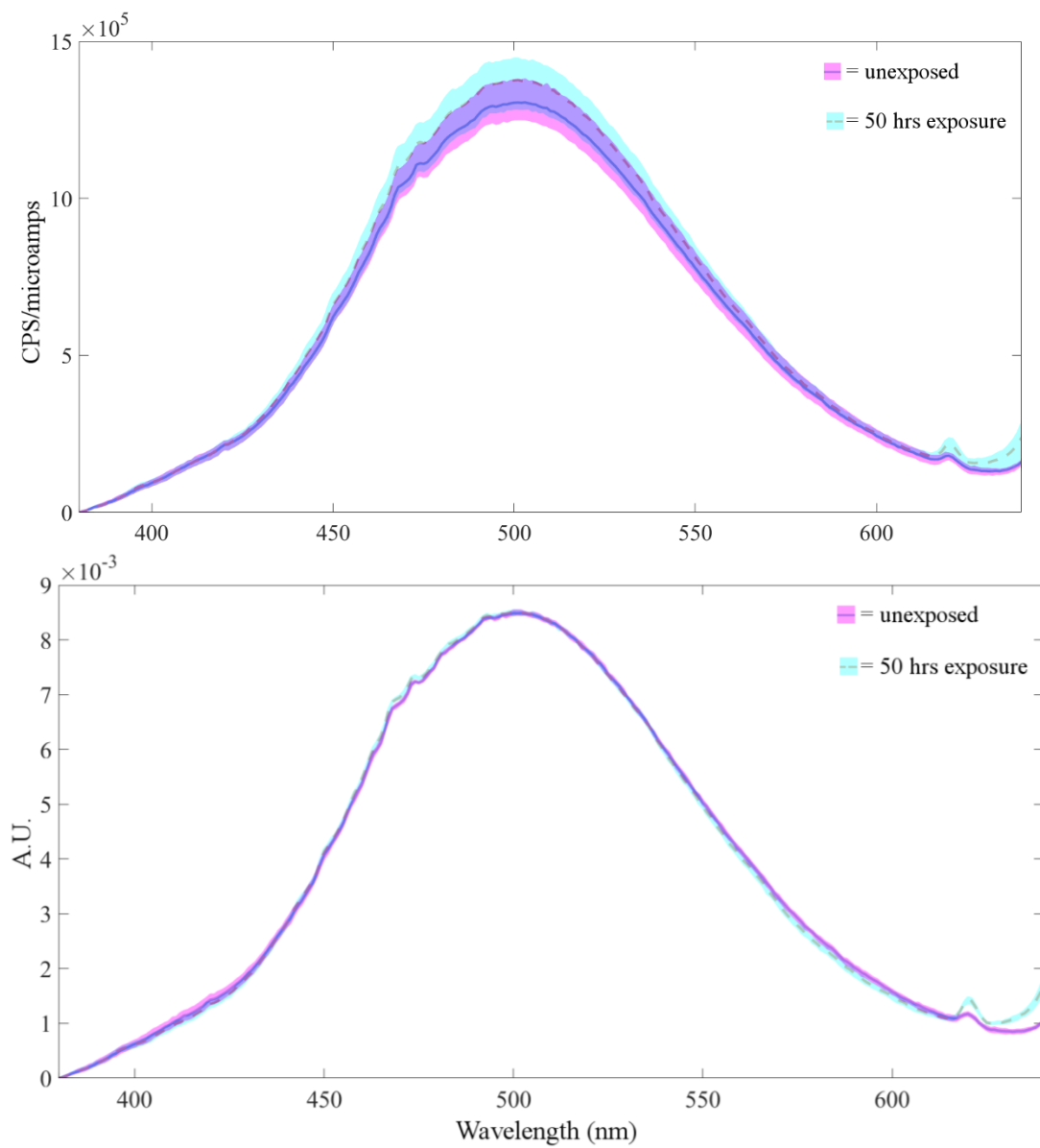
Figure A16.11 *Direct* sample 9 on Whatman paper. **Above:** minimum value subtracted and **below:** area normalised to 1.
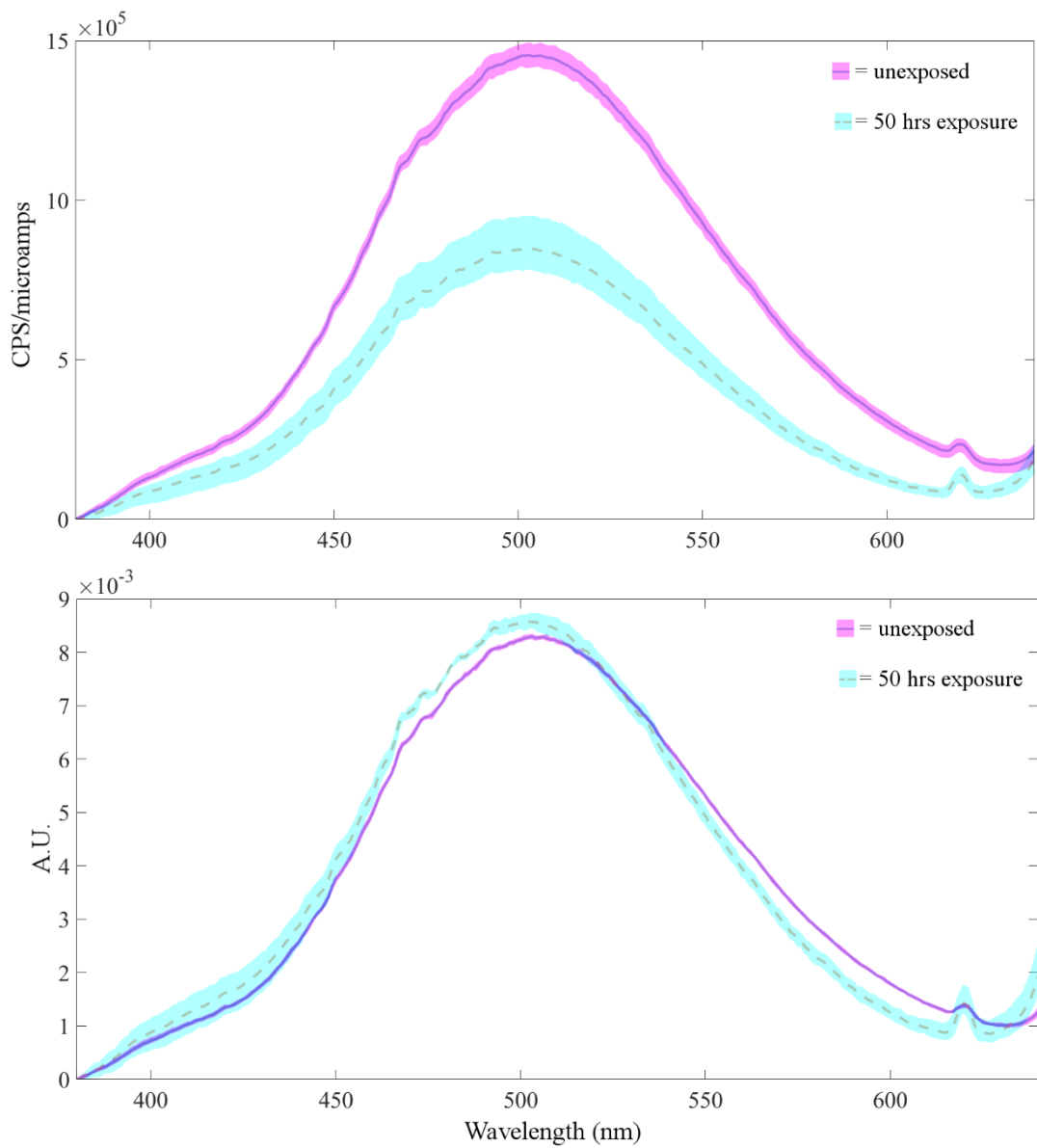
Figure A16.12 *Direct* sample 9 on Folio paper. **Above:** minimum value subtracted and **below:** area normalised to 1.
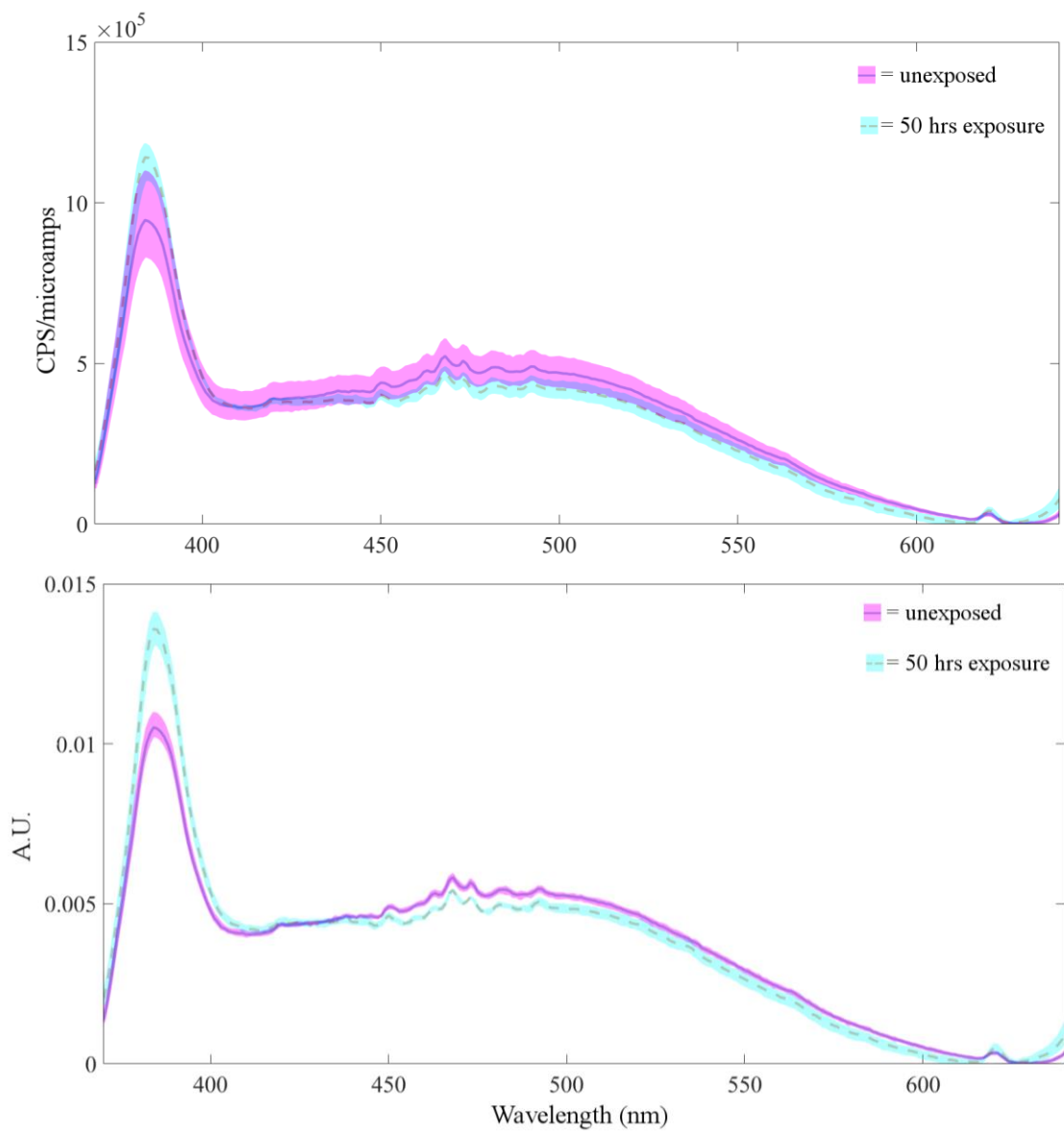
Figure A16.13 Commercial sample 15 on Whatman paper. **Above:** minimum value subtracted and **below:** area normalised to 1.
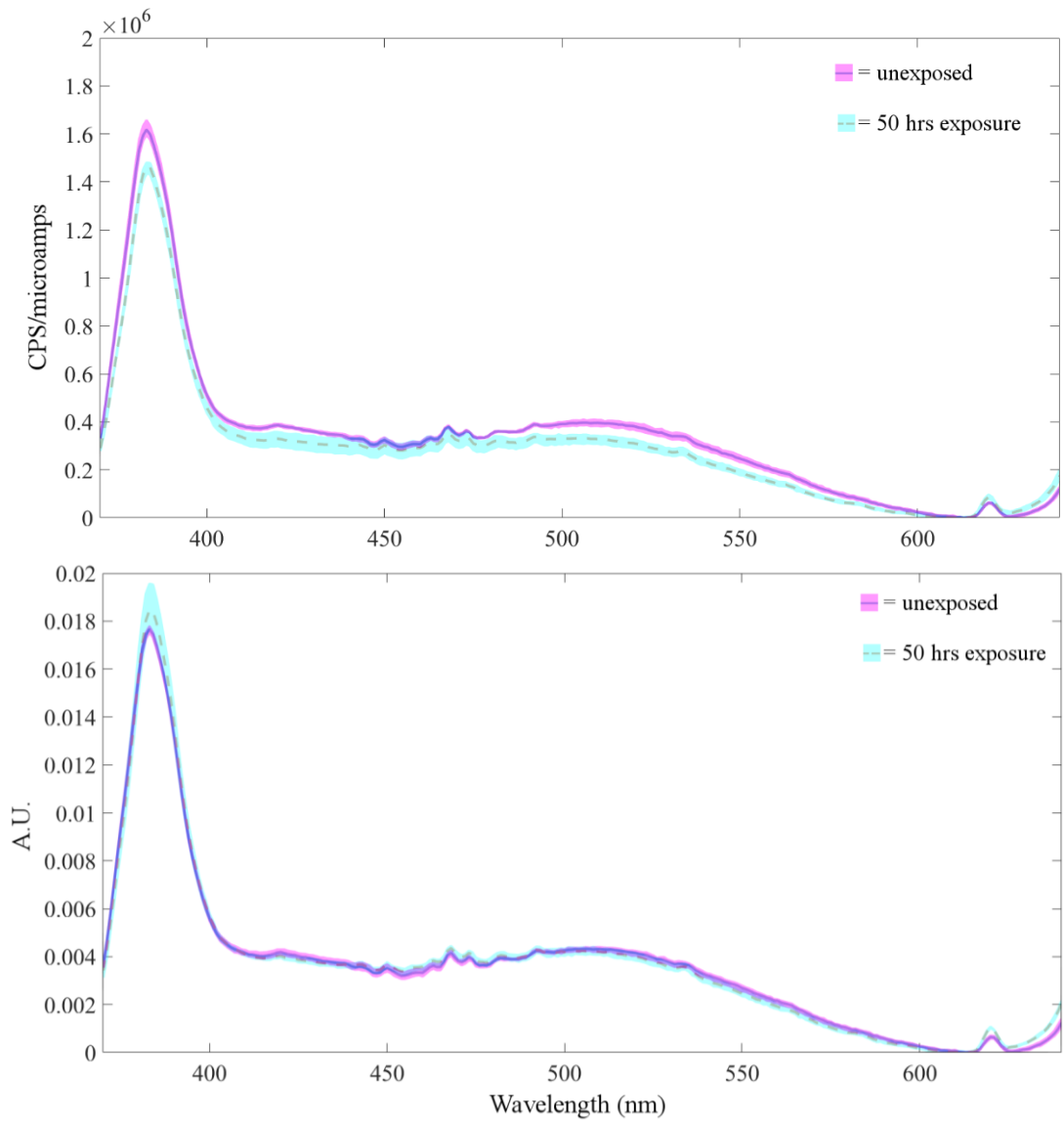
Figure A16.14 Commercial sample 15 on Folio paper. **Above:** minimum value subtracted and **below:** area normalised to 1.
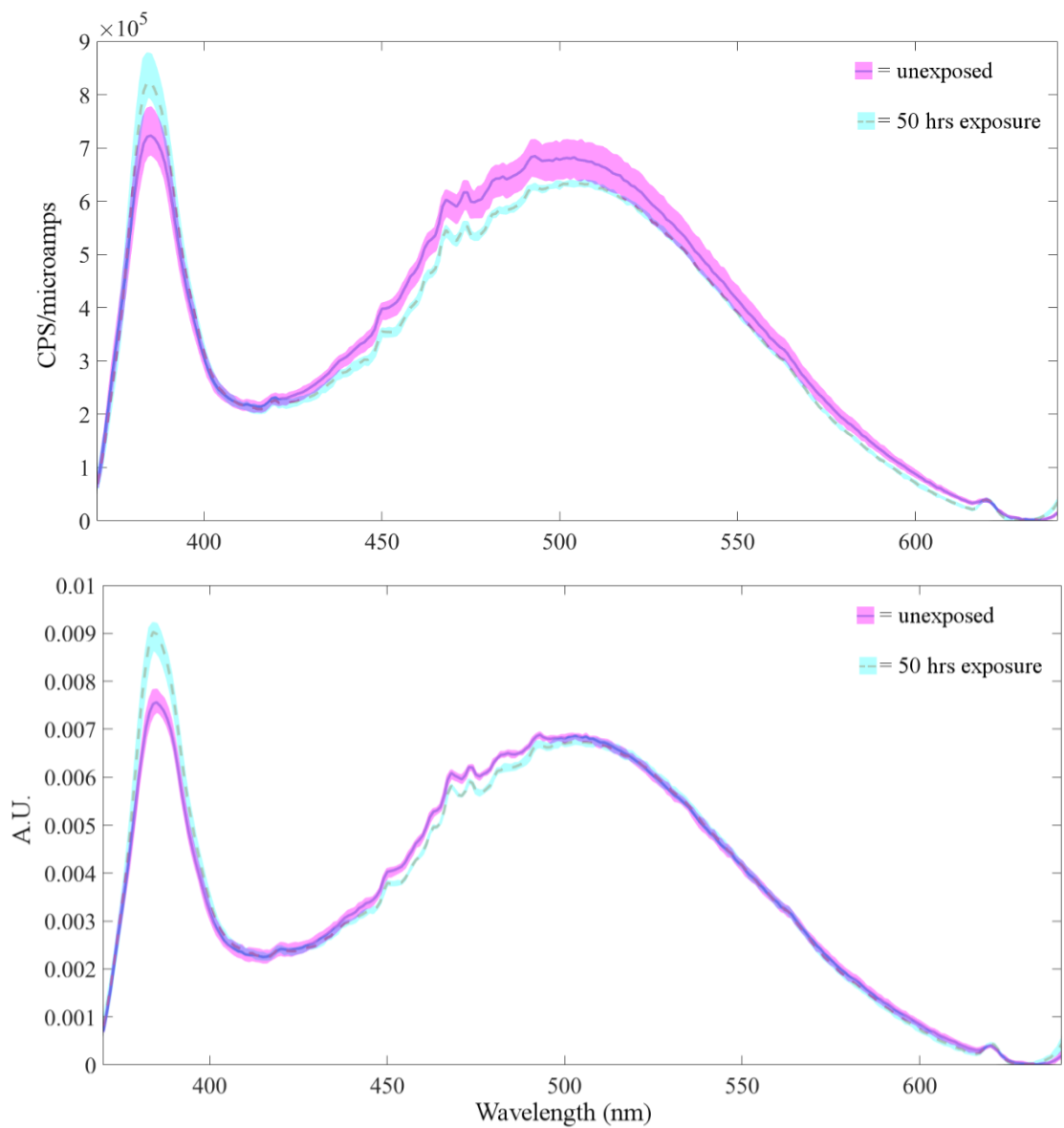
Figure A16.15 Commercial sample 16 on Whatman paper. **Above:** minimum value subtracted and **below:** area normalised to 1.
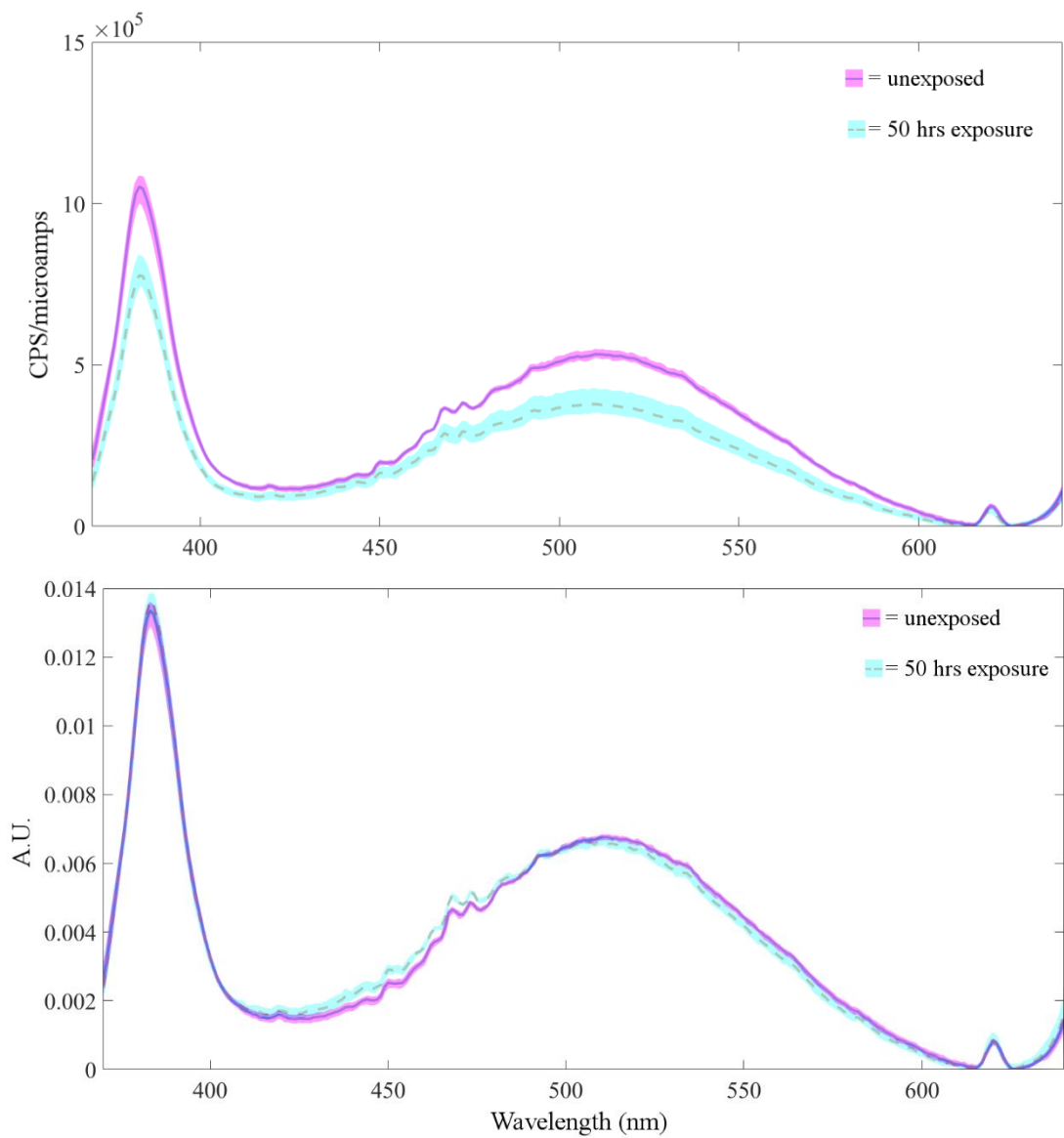
Figure A16.16 Commercial sample 16 on Folio paper. **Above:** minimum value subtracted and **below:** area normalised to 1.
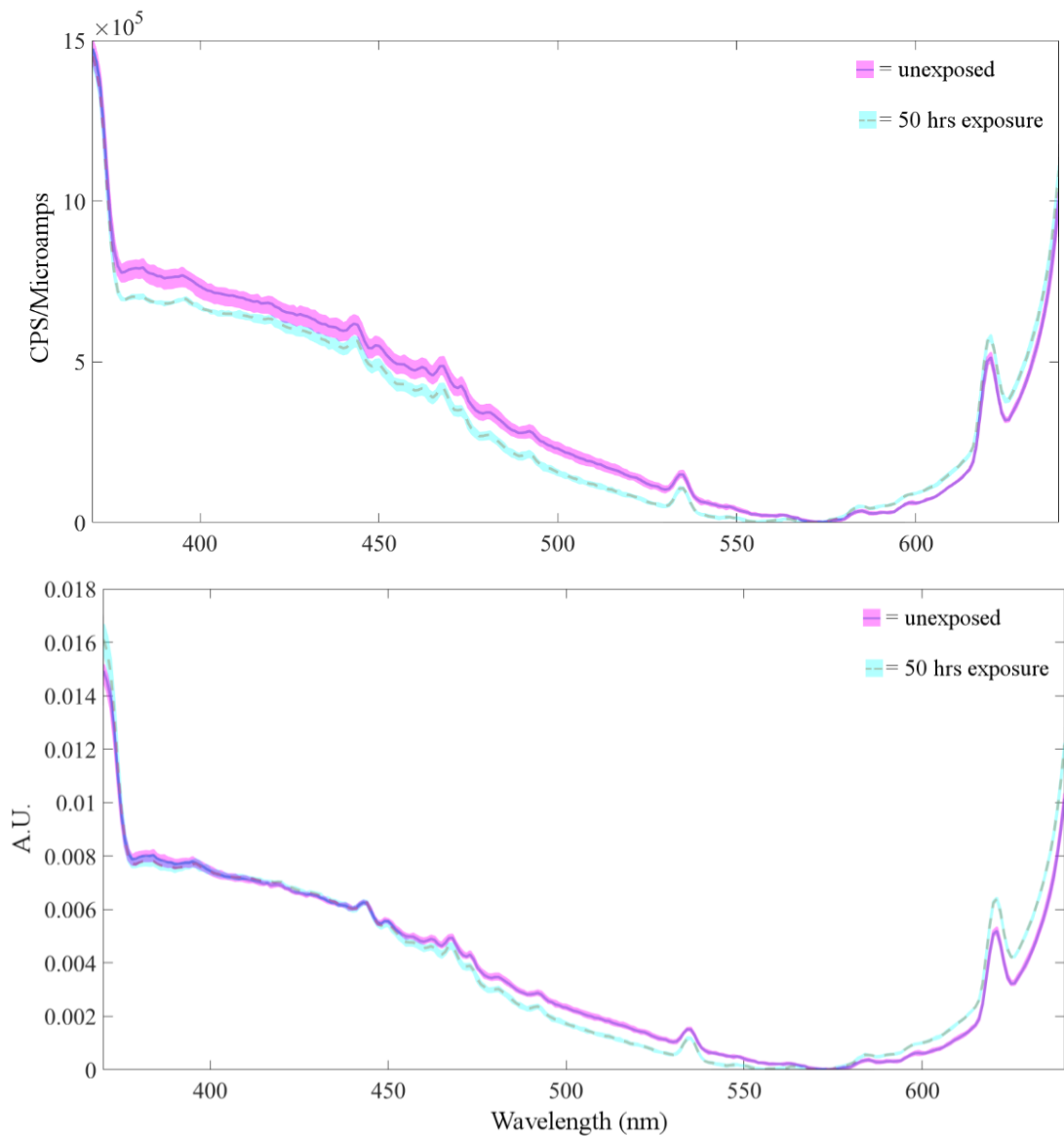
Figure A16.17 Gum arabic on Whatman paper. **Above:** minimum value subtracted and **below:** area normalised to 1.
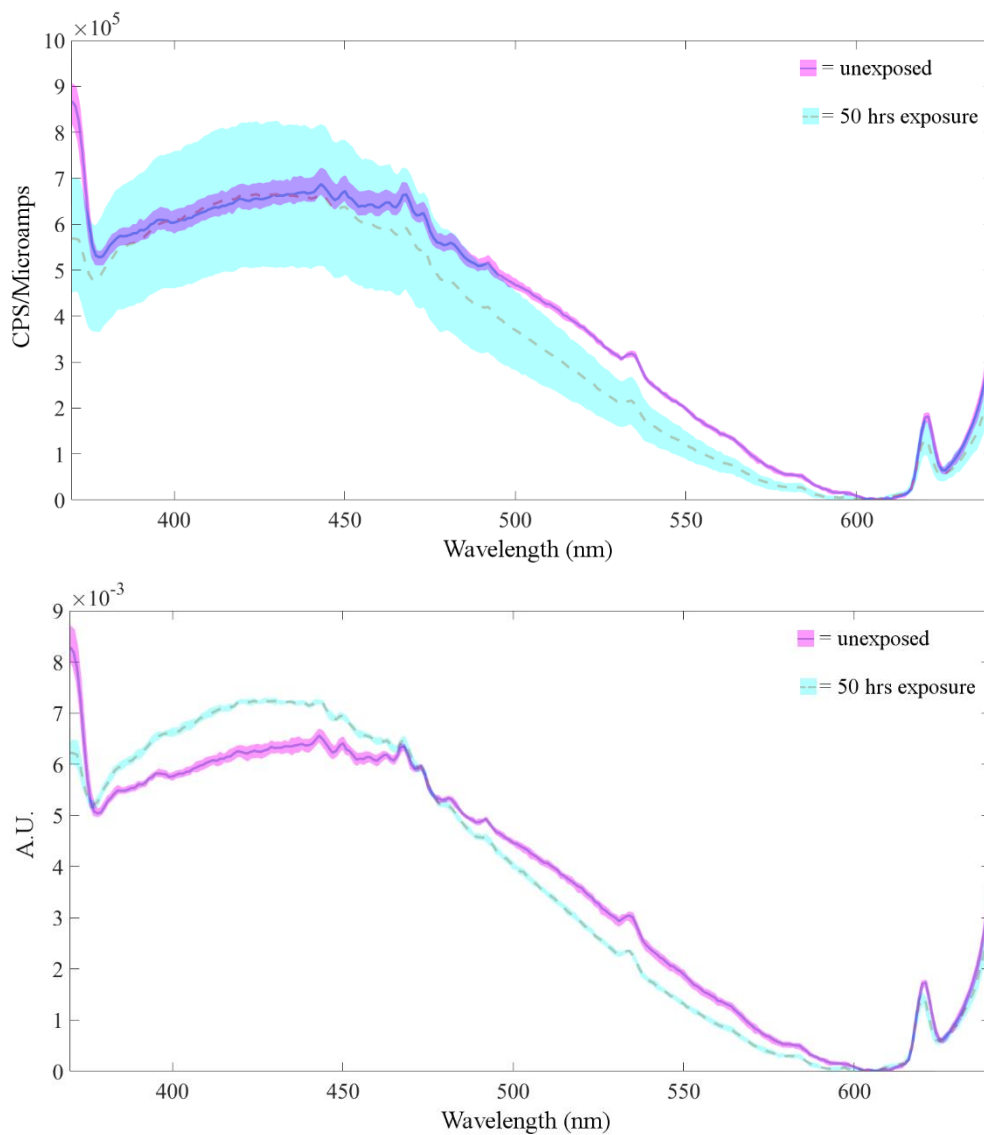
Figure A16.18 Gum arabic on Folio paper. **Above:** minimum value subtracted and **below:** area normalised to 1.

Appendix 17: Decomposition of Emission Spectra in MATLAB

The following images depict graphs from emission spectra decomposition in MATLAB using the Interactive Peak Fitter program. They detail all values derived in this method such as R^2 values, error percentages, residuals and peak data.
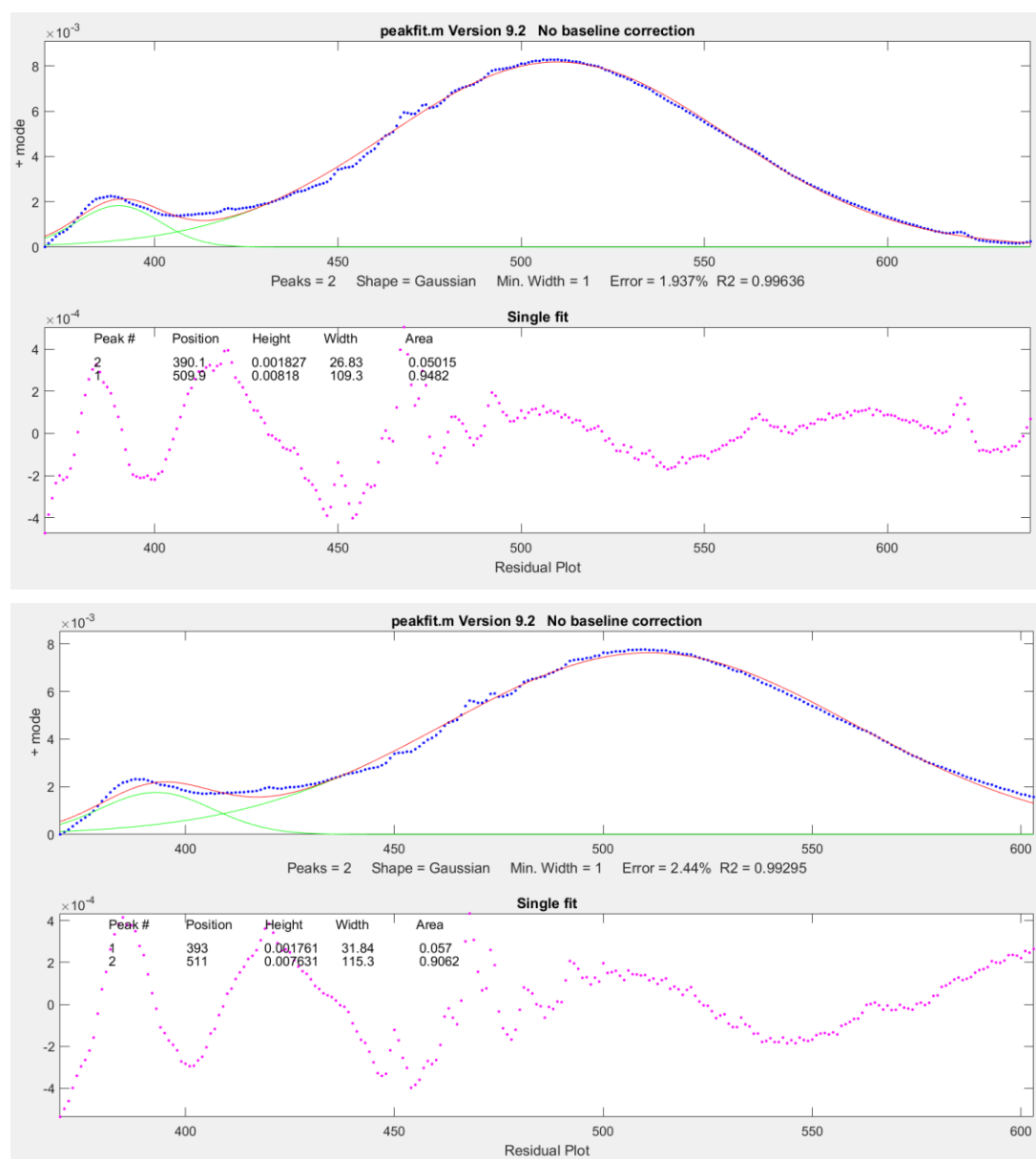
Figure A17.1 Above: Interactive Peak Fitter results for average spectra from *indirect* sample 1 on Whatman paper, **below:** Interactive Peak Fitter results for average spectra from *indirect* sample 1 on Whatman paper after 50 hours of light exposure.
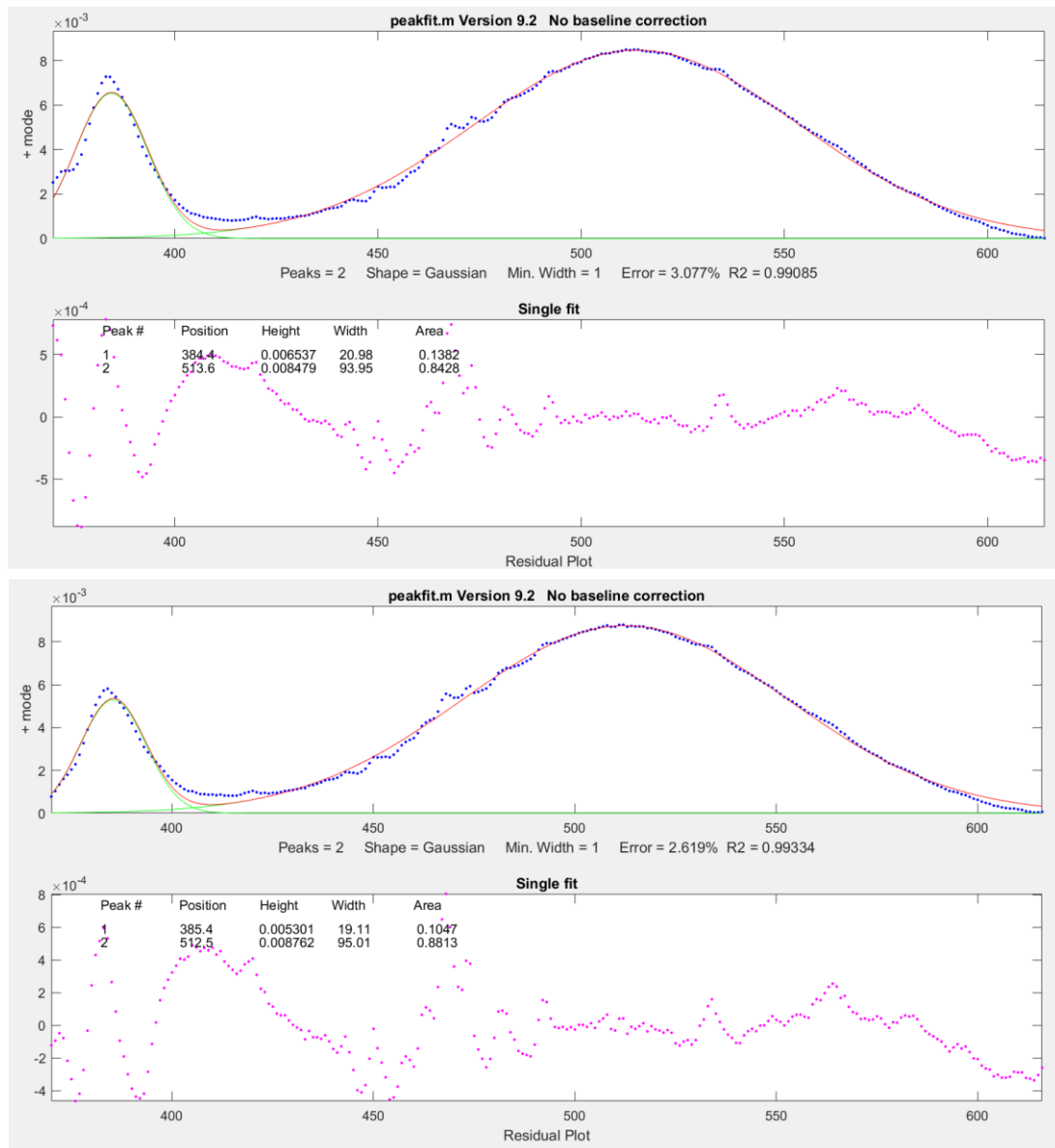
Figure A17.2 Above: Interactive Peak Fitter results for average spectra from *indirect* sample 1 on Folio paper, **below:** Interactive Peak Fitter results for average spectra from *indirect* sample 1 on Folio paper after 50 hours of light exposure.
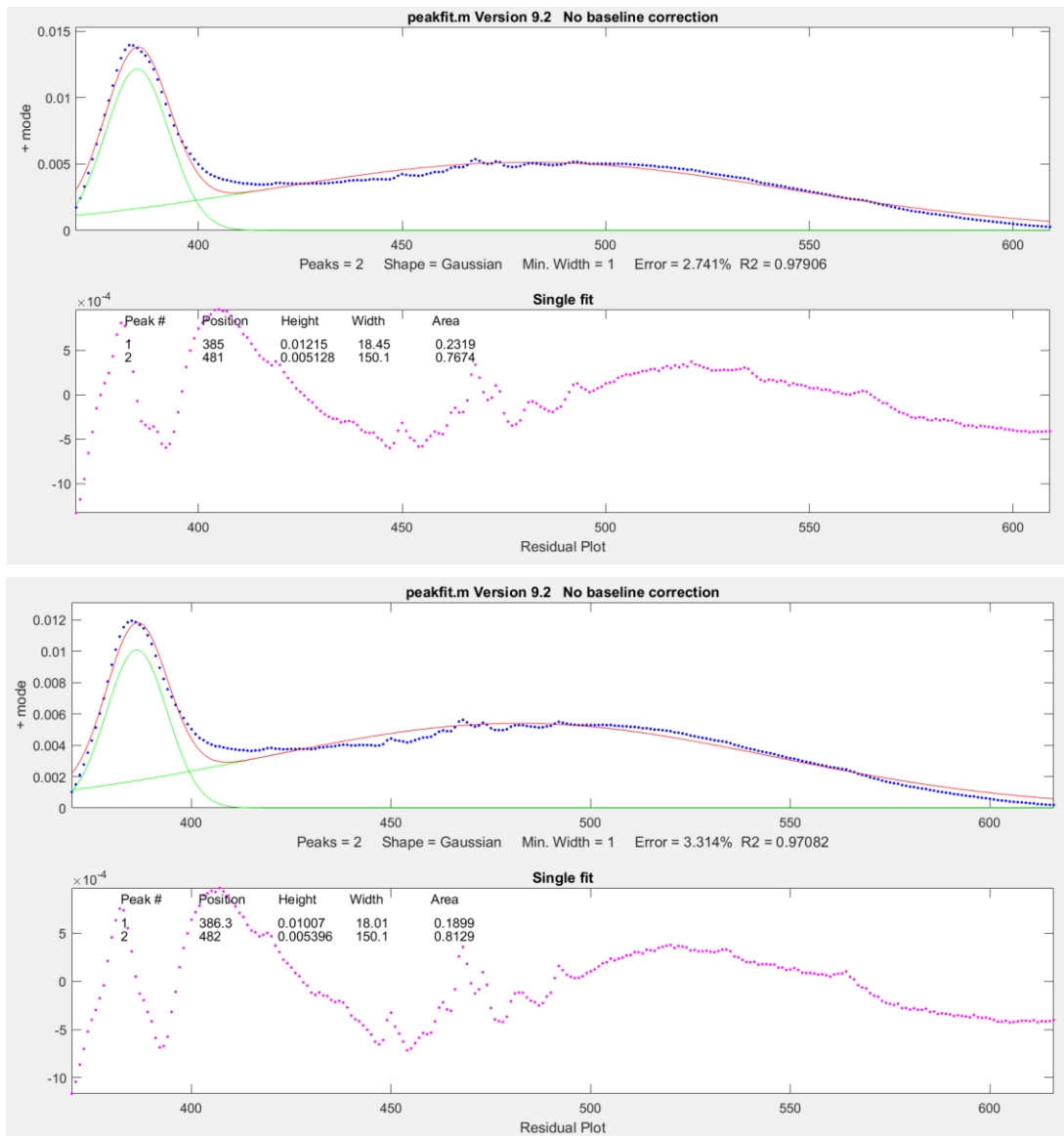
Figure A17.3 Above: Interactive Peak Fitter results for average spectra from *indirect* sample 3 on Whatman paper, **below:** Interactive Peak Fitter results for average spectra from *indirect* sample 3 on Whatman paper after 50 hours of light exposure.
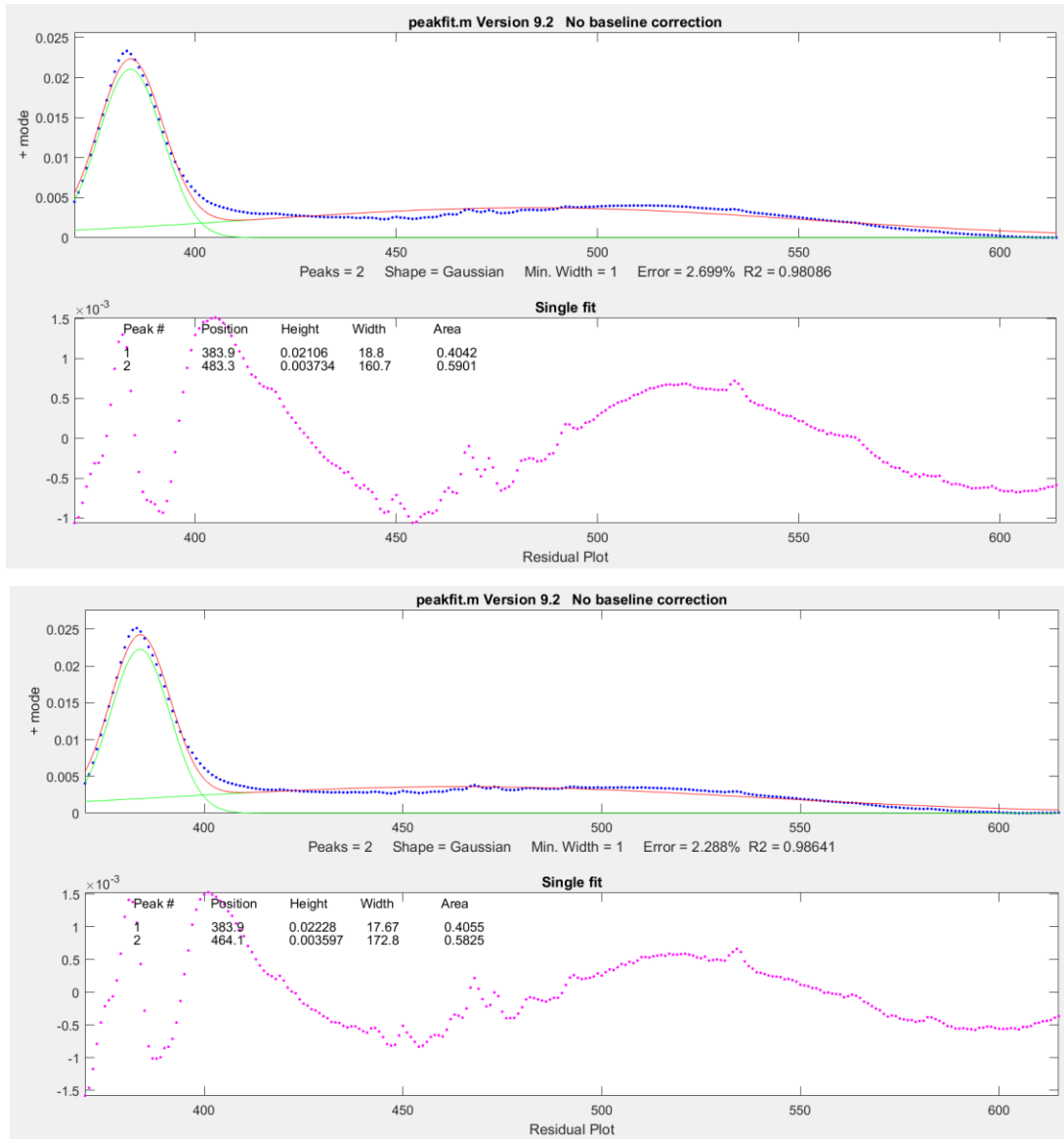
Figure A17.4 Above: Interactive Peak Fitter results for average spectra from *indirect* sample 3 on Folio paper, **below:** Interactive Peak Fitter results for average spectra from *indirect* sample 3 on Folio paper after 50 hours of light exposure.
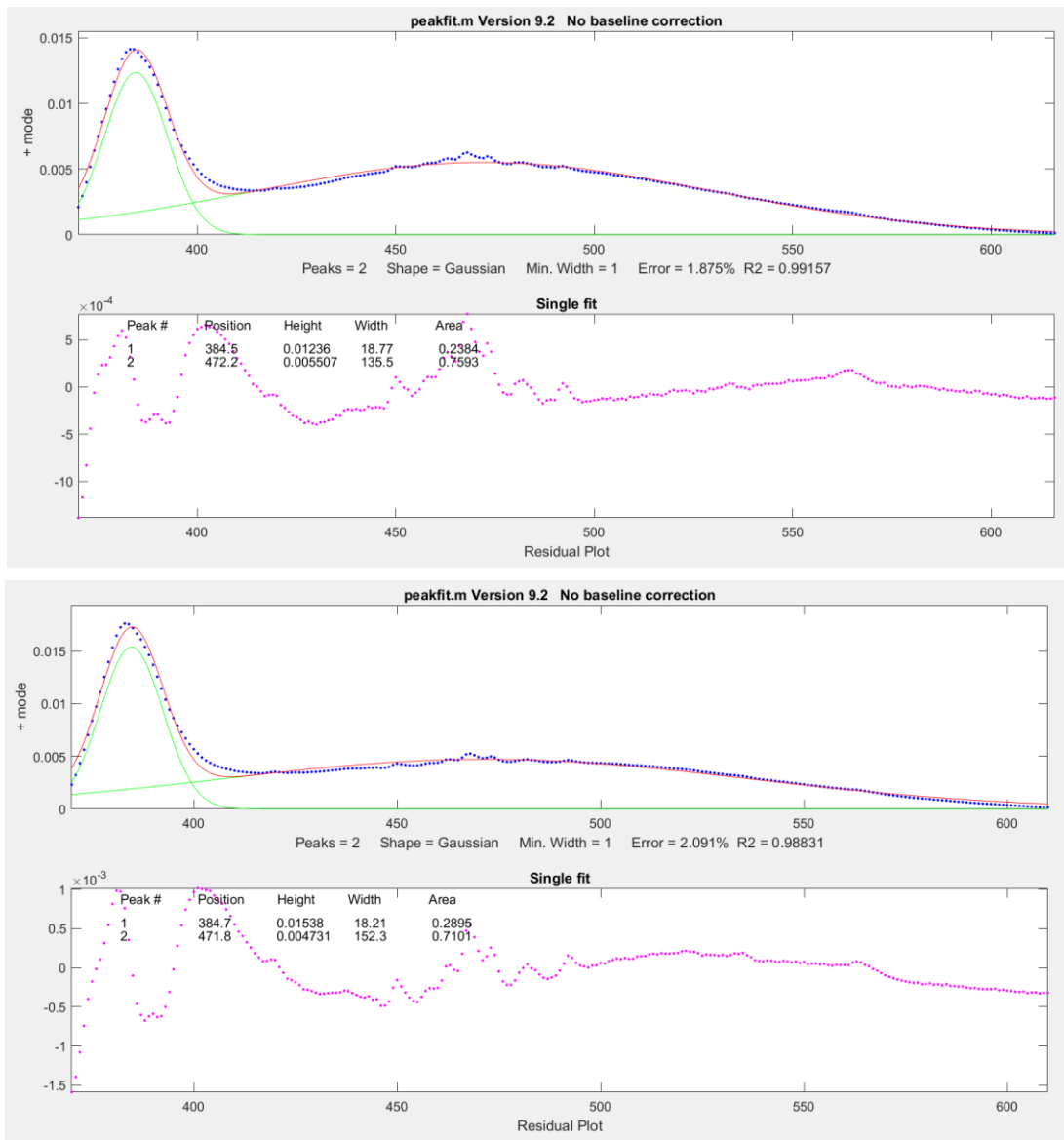
Figure A17.5 Above: Interactive Peak Fitter results for average spectra from *indirect* sample 4 on Whatman paper, **below:** Interactive Peak Fitter results for average spectra from *indirect* sample 4 on Whatman paper after 50 hours of light exposure.
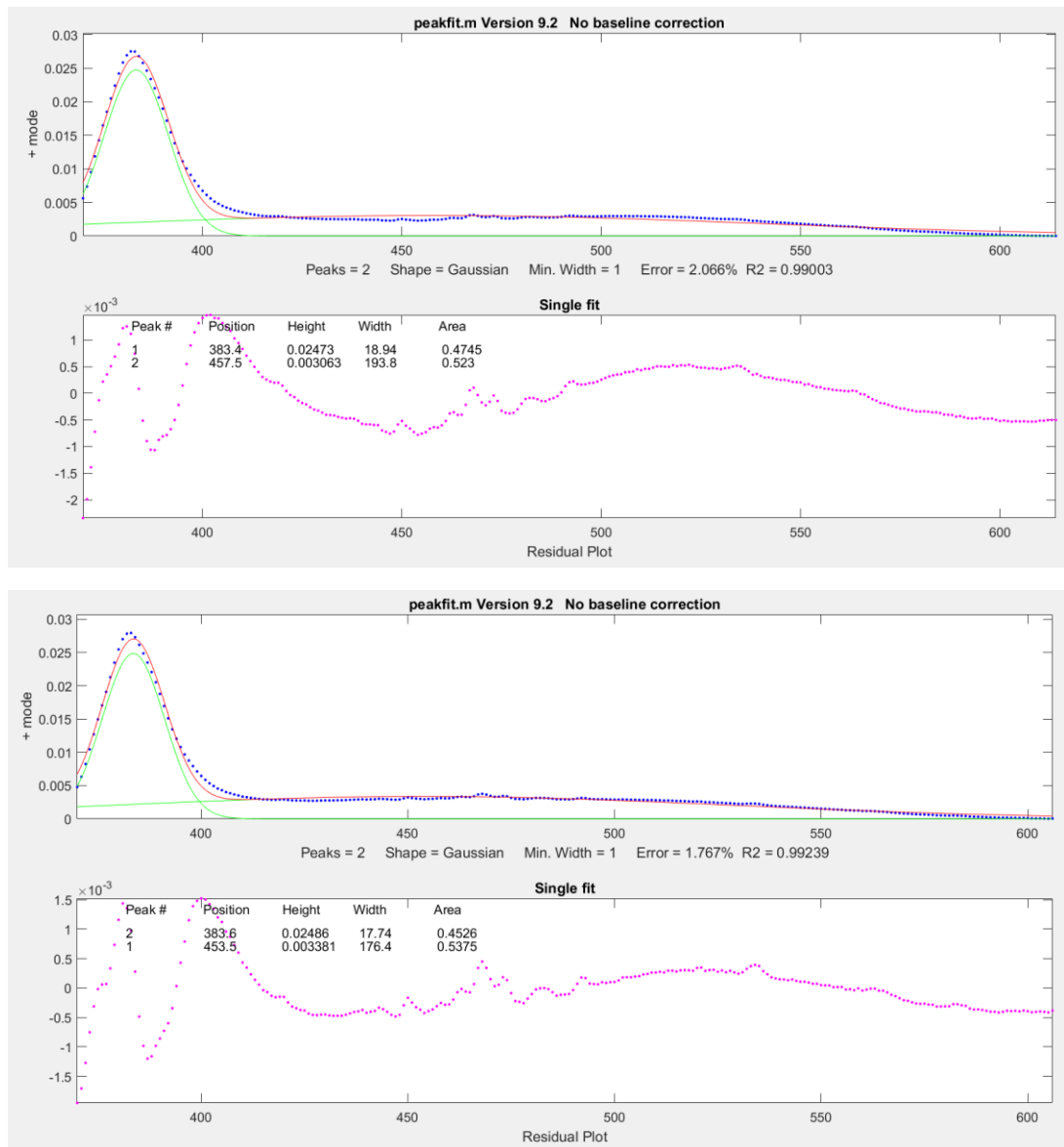
Figure A17.6 Above: Interactive Peak Fitter results for average spectra from *indirect* sample 4 on Folio paper, **below:** Interactive Peak Fitter results for average spectra from *indirect* sample 4 on Folio paper after 50 hours of light exposure.
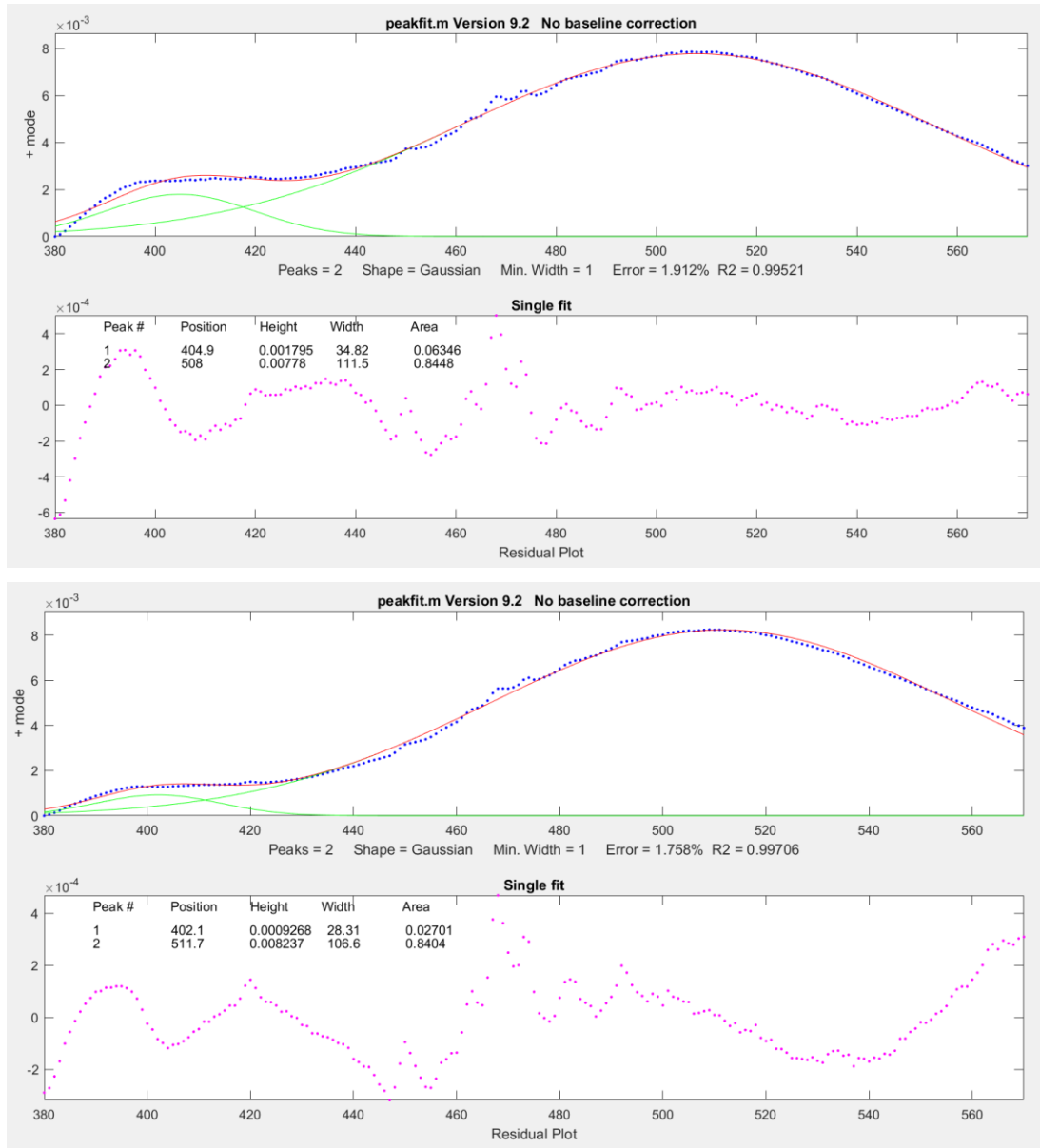
Figure A17.7 Above: Interactive Peak Fitter results for average spectra from *direct* sample 6 on Whatman paper, **below:** Interactive Peak Fitter results for average spectra from *direct* sample 6 on Whatman paper after 50 hours of light exposure.
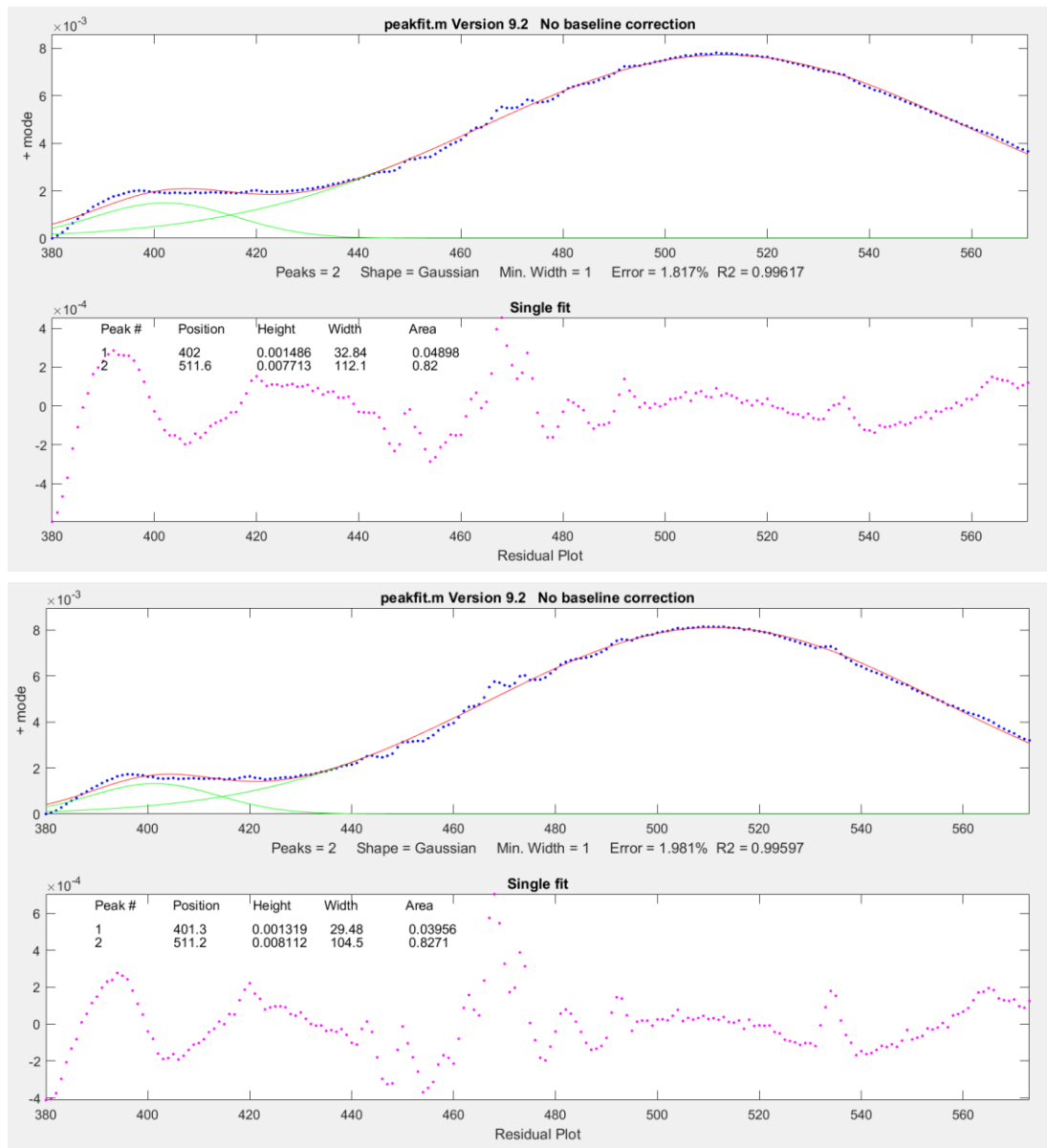
Figure A17.8 Above: Interactive Peak Fitter results for average spectra from *direct* sample 6 on Folio paper, **below:** Interactive Peak Fitter results for average spectra from *direct* sample 6 on Folio paper after 50 hours of light exposure.
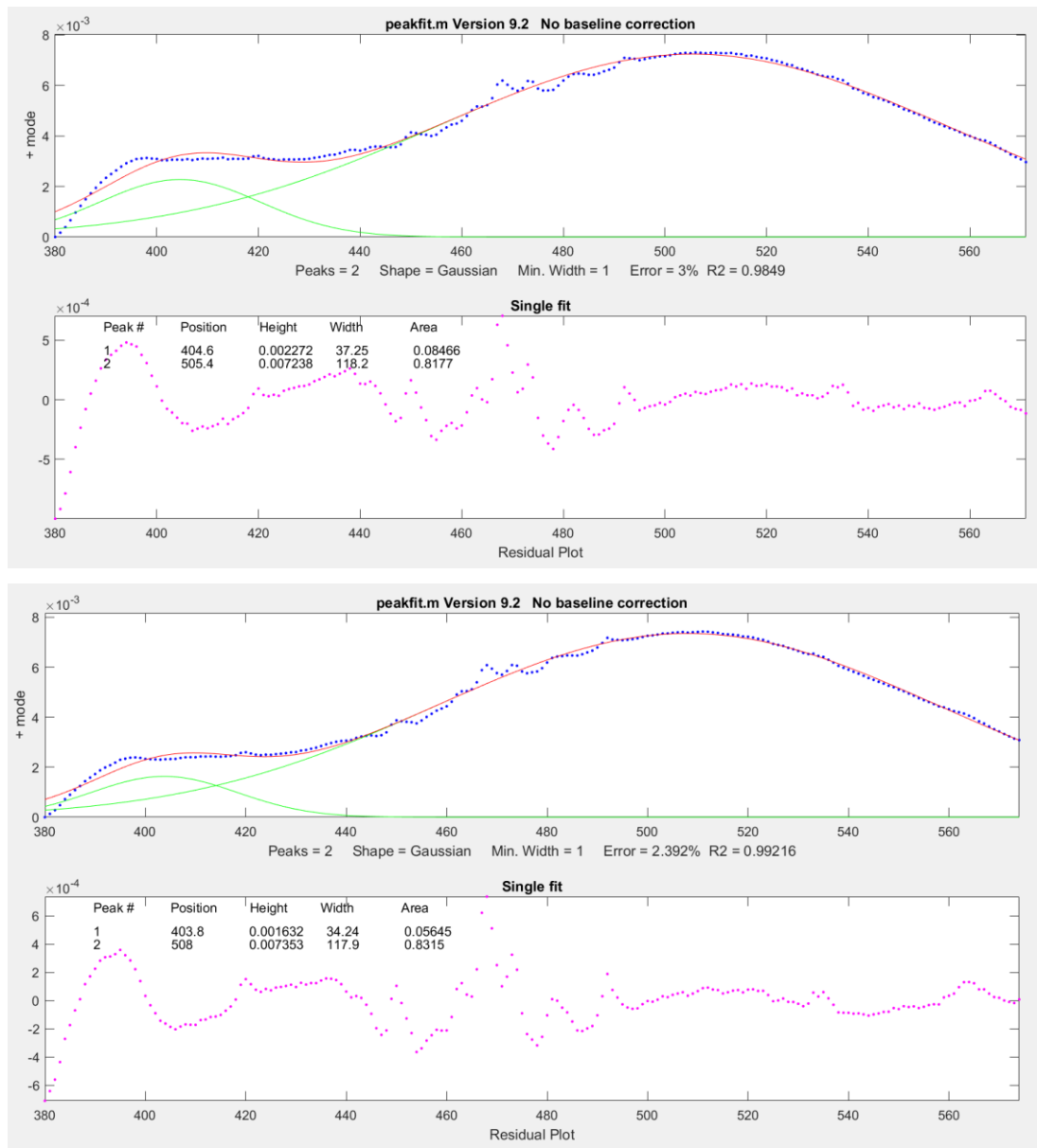
Figure A17.9 Above: Interactive Peak Fitter results for average spectra from *direct* sample 7 on Whatman paper, **below:** Interactive Peak Fitter results for average spectra from *direct* sample 7 on Whatman paper after 50 hours of light exposure.
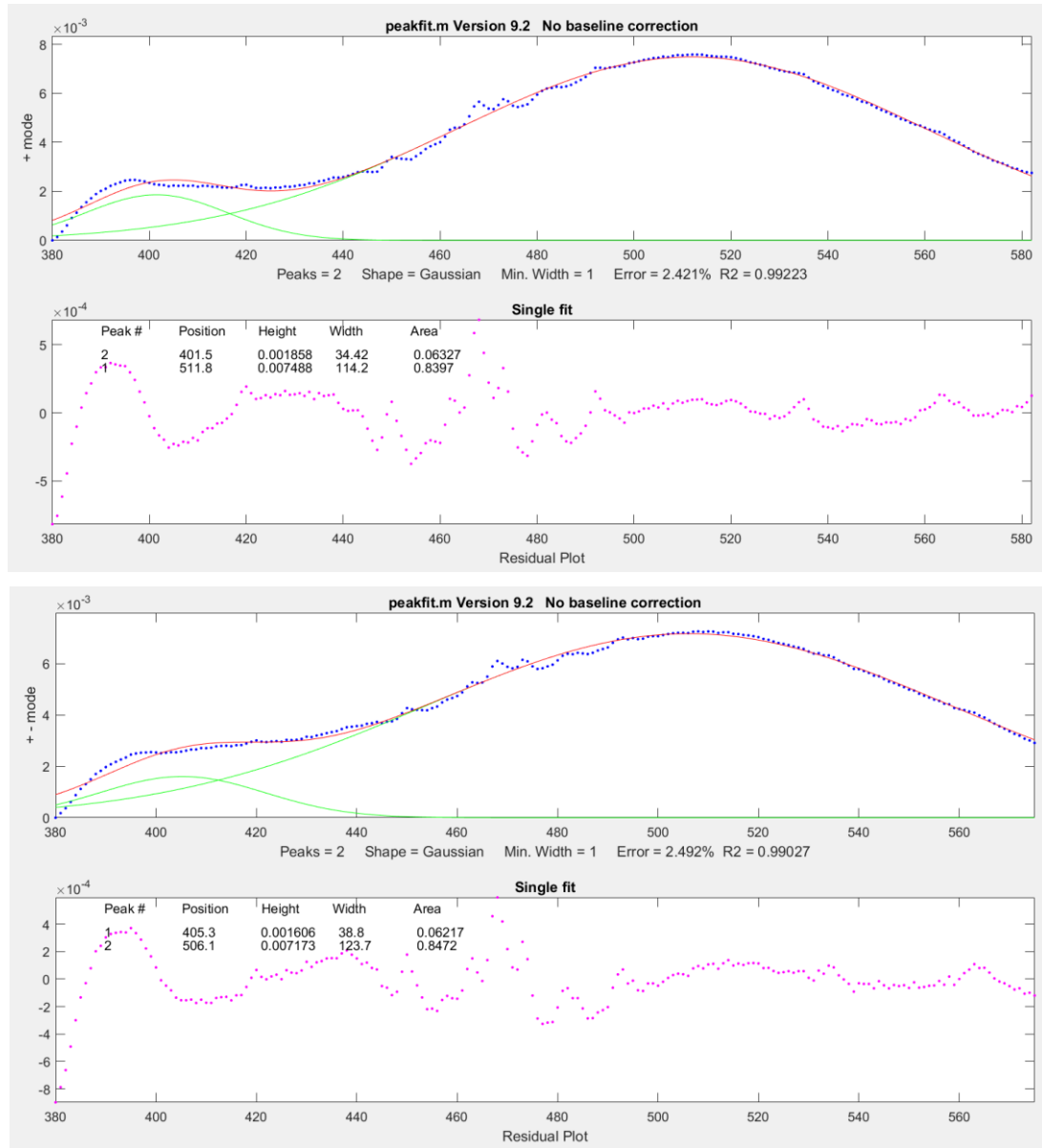
Figure A17.10 Above: Interactive Peak Fitter results for average spectra from *direct* sample 7 on Folio paper, **below:** Interactive Peak Fitter results for average spectra from *direct* sample 7 on Folio paper after 50 hours of light exposure.
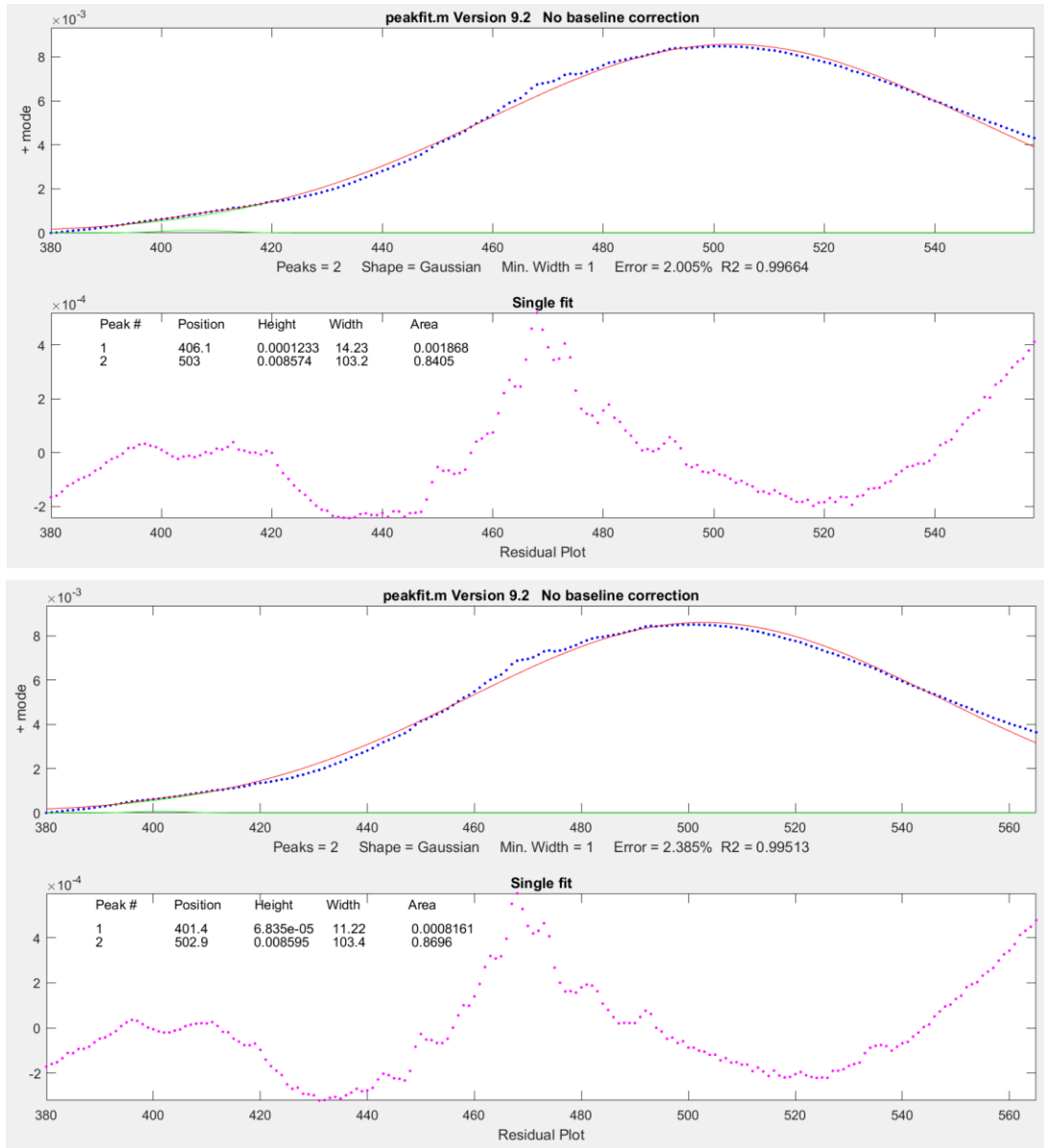
Figure A17.11 Above: Interactive Peak Fitter results for average spectra from *direct* sample 9 on Whatman paper, **below:** Interactive Peak Fitter results for average spectra from *direct* sample 9 on Whatman paper after 50 hours of light exposure.
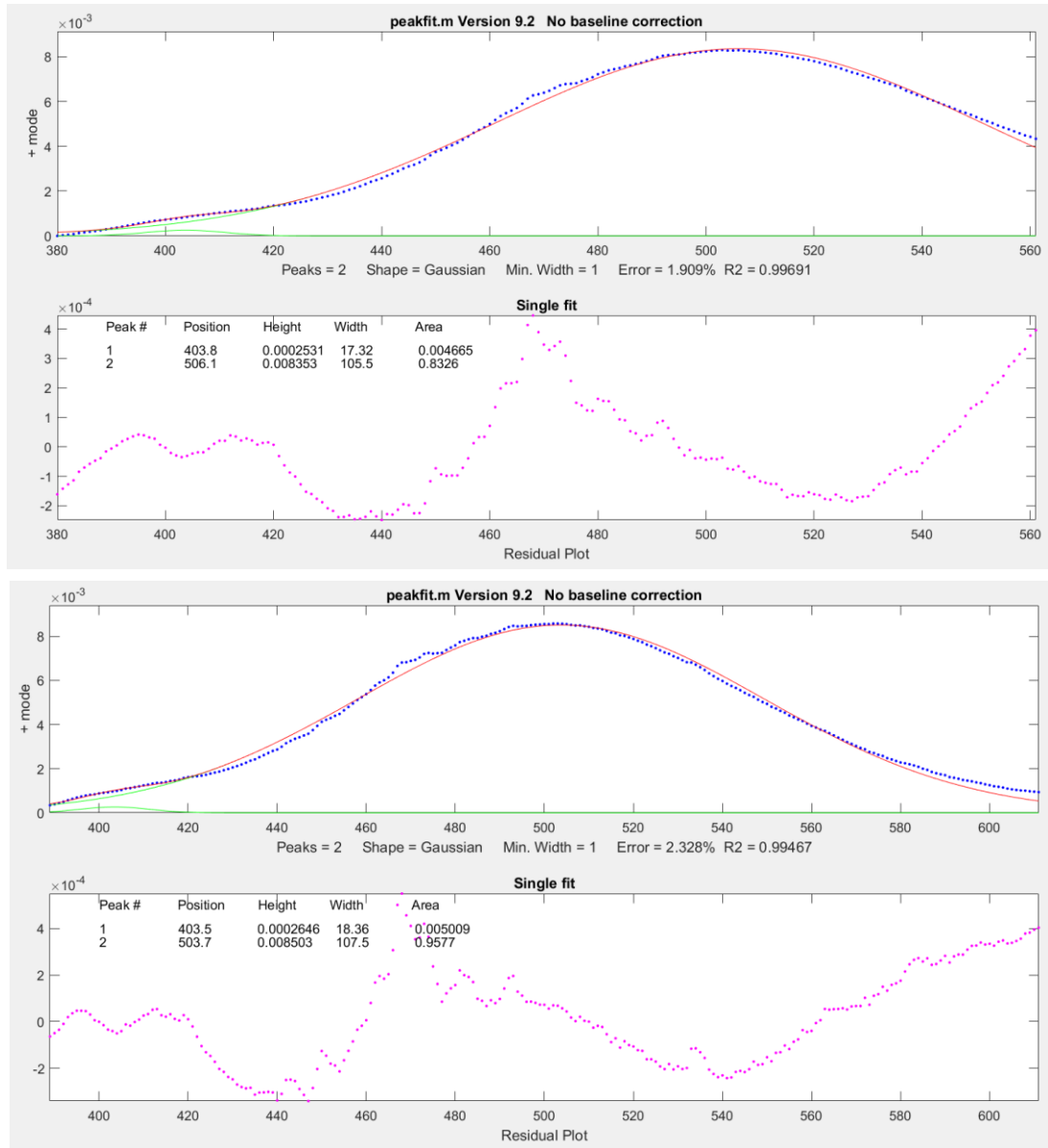
Figure A17.12 Above: Interactive Peak Fitter results for average spectra from *direct* sample 9 on Folio paper, **below:** Interactive Peak Fitter results for average spectra from *direct* sample 9 on Folio paper after 50 hours of light exposure.
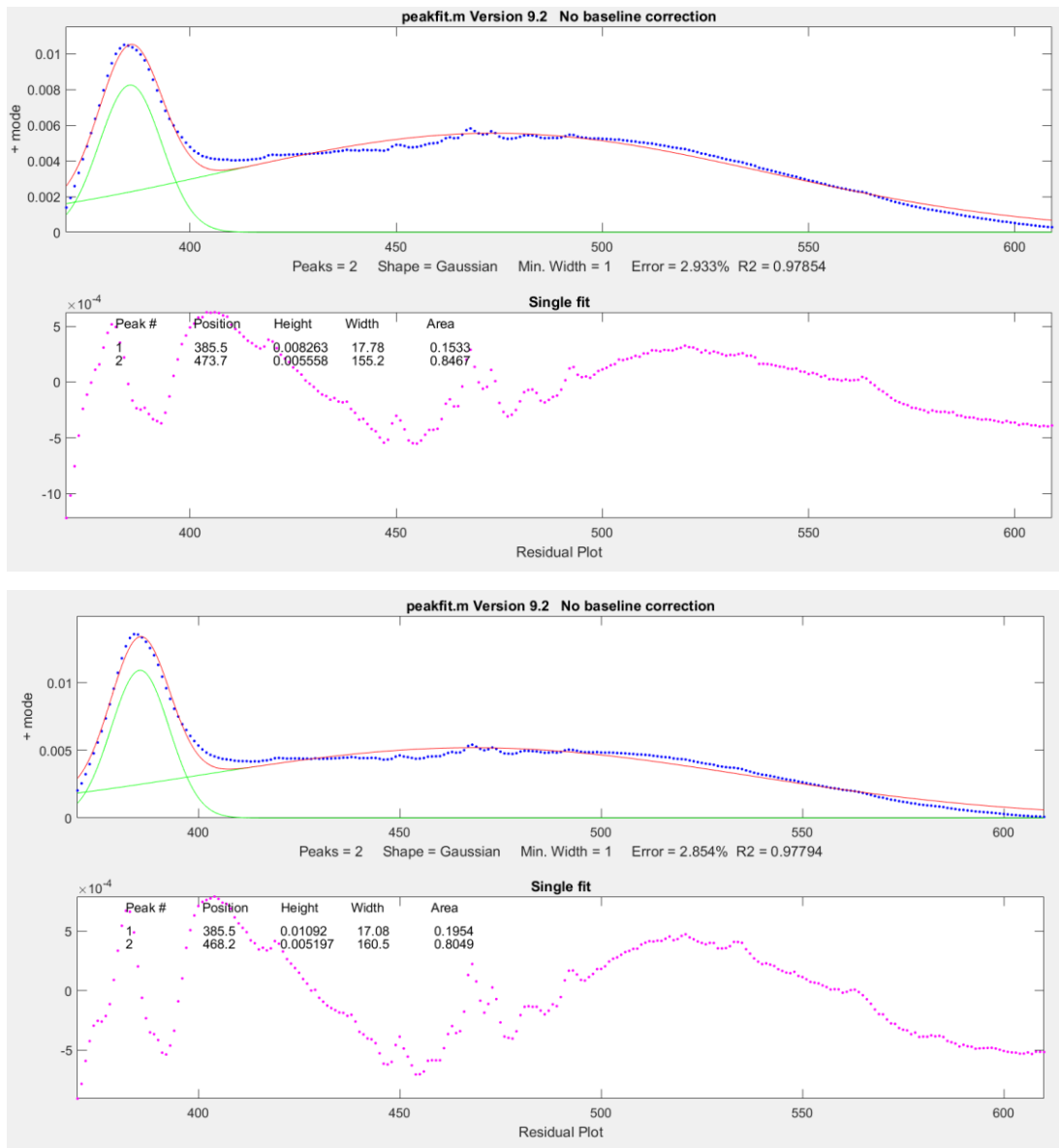
Figure A17.13 Above: Interactive Peak Fitter results for average spectra from commercial sample 15 on Whatman paper, **below:** Interactive Peak Fitter results for average spectra from commercial sample 15 on Whatman paper after 50 hours of light exposure.
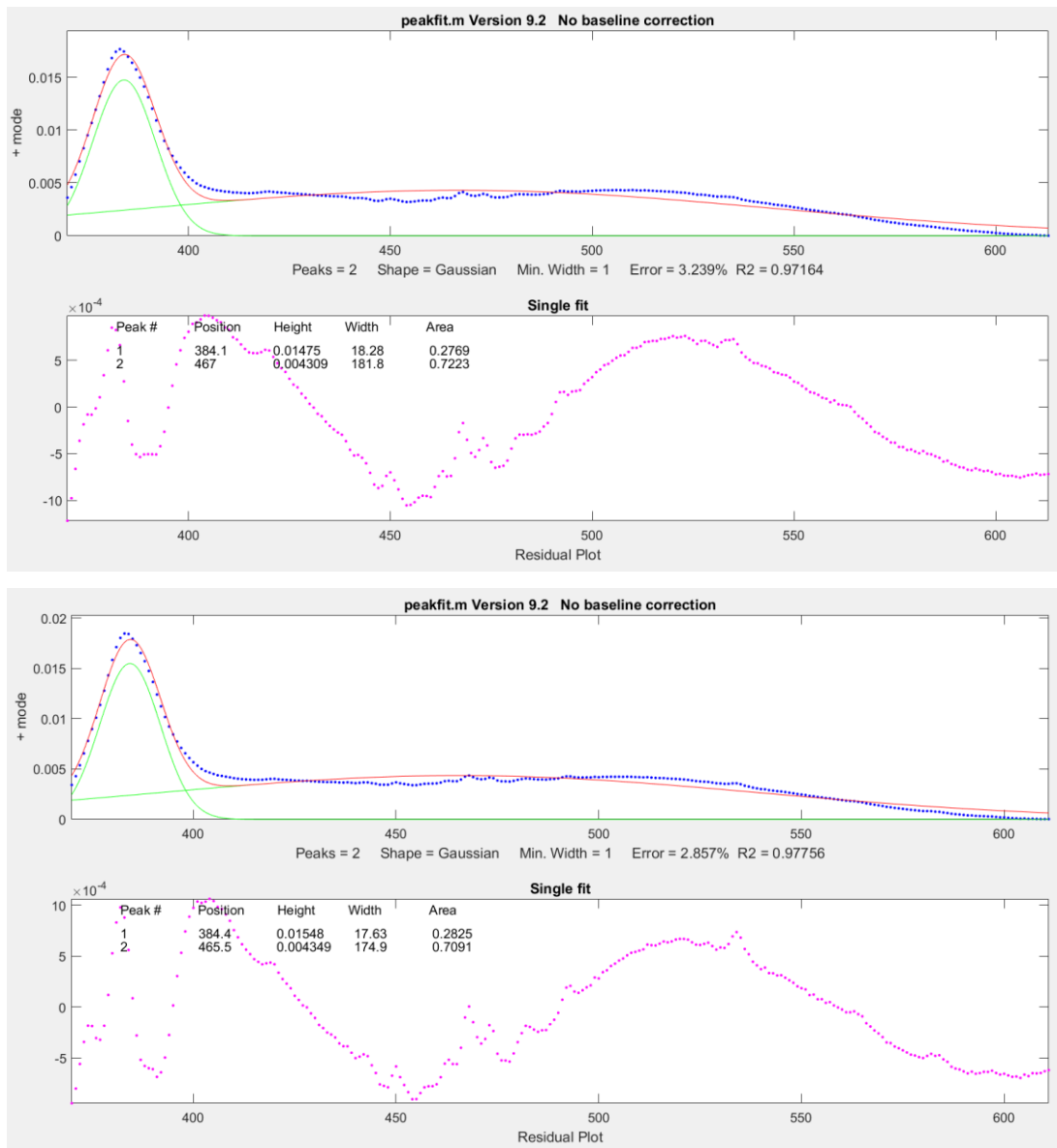
Figure A17.14 Above: Interactive Peak Fitter results for average spectra from commercial sample 15 on Folio paper, **below:** Interactive Peak Fitter results for average spectra from commercial sample 15 on Folio paper after 50 hours of light exposure.

Figure A17.15 Above: Interactive Peak Fitter results for average spectra from commercial sample 16 on Whatman paper, **below:** Interactive Peak Fitter results for average spectra from commercial sample 16 on Whatman paper after 50 hours of light exposure.
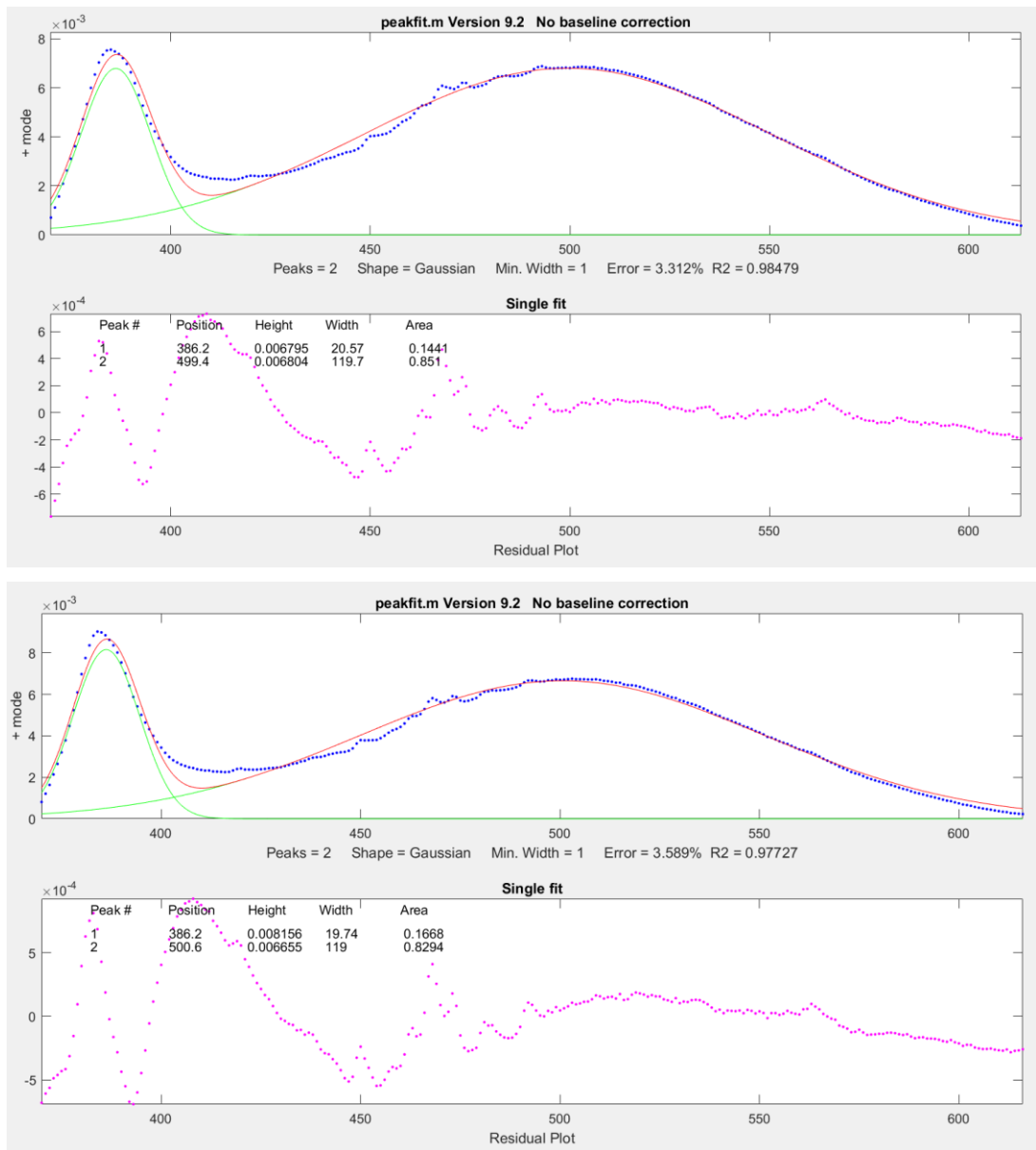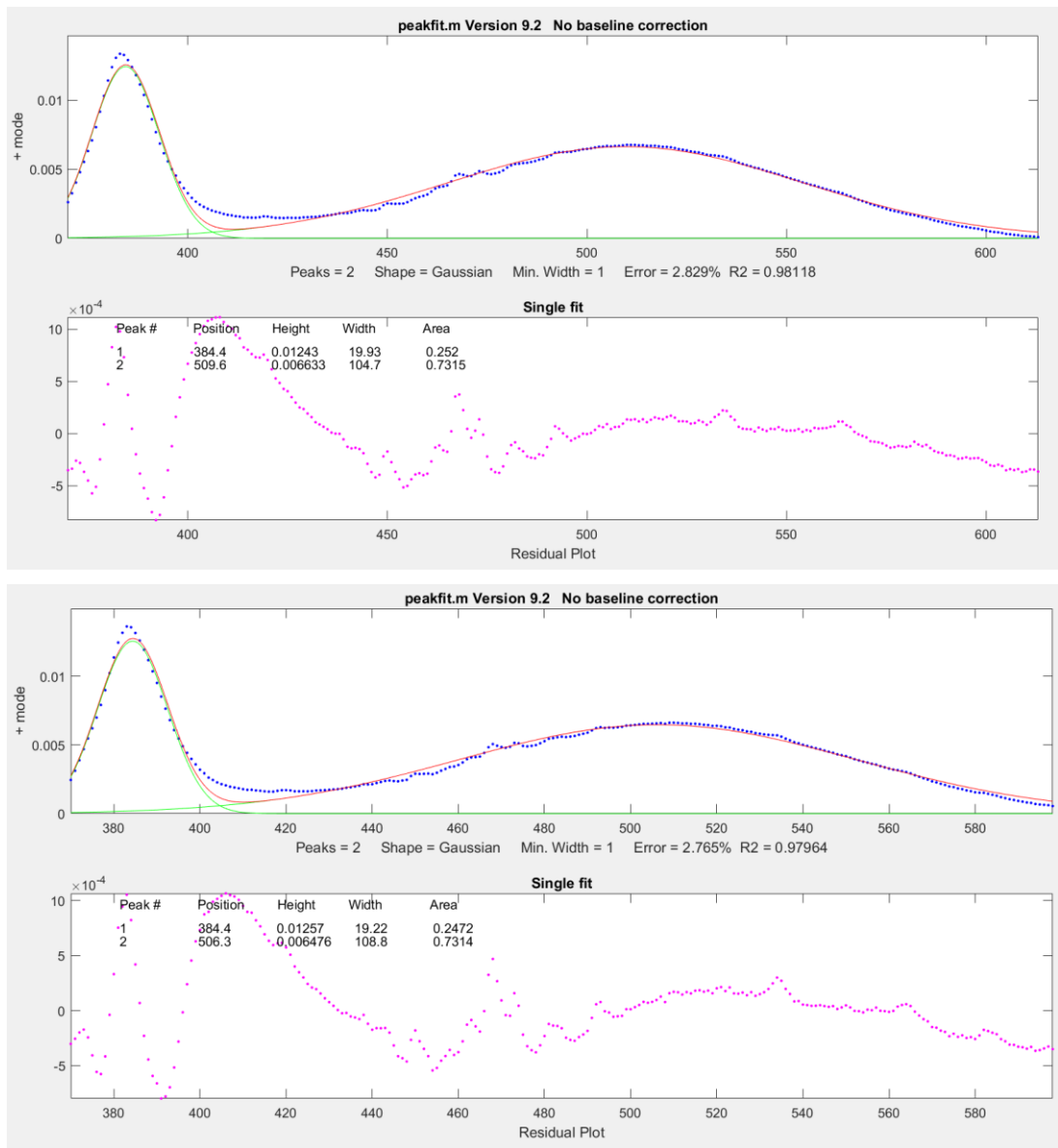
Figure A17.16 Above: Interactive Peak Fitter results for average spectra from commercial sample 16 on Folio paper, **below:** Interactive Peak Fitter results for average spectra from commercial sample 16 on Folio paper after 50 hours of light exposure.

Appendix 18: Wratten 2e Filter Diffusion Density

Figure A18.1 shows the density of diffusion for the Kodak 2e Wratten UV cut-off filter. The diffusion density is inversely related to transmission, with low values corresponding to high transmission and vice versa. The 2e Wratten filter allows transmission of wavelengths greater than approximately 410 nm.
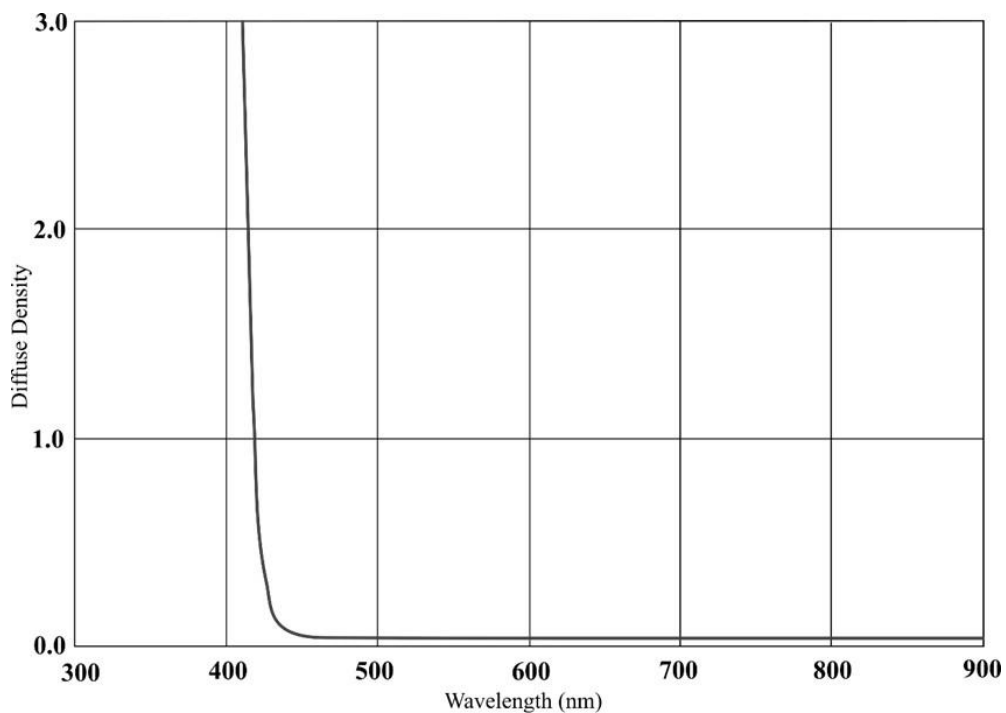
Figure A18.1 Diffuse density over wavelength for Kodak Wratten 2e filter. The higher the diffuse density, the lower the transmission of light through the material. The approximate wavelength cut-off for the 2e filter is 410 nm. Graph modified from Kodak data.

Appendix 19: Image Processing Procedure for UV-Induced Fluorescent Digital Images and Micrographs

The following details the image processing procedure for digital images followed by the background subtraction procedure undertaken for digital images in ImageJ followed by a description of RGB value processing in MATLAB for both digital images and micrographs.

A19.1 BACKGROUND SUBTRACTION IN IMAGEJ

Images taken using the Canon EOS 6D digital camera were opened in ImageJ for background subtraction. First, the image was duplicated, then with the duplicated image selected 'Subtract Background' was opened in the Process tab. In the 'Subtract Background' window, 'create background' was selected and the rolling ball radius set to 20. This radius did not remove too many features or alter the border of the fluorescing area.[139] This rolling ball algorithm removes pixels which have an intensity much higher or lower than the surrounding pixels and replaces them with pixels with more similar intensity values to their neighbours. This 'smooths' the intensity curve of the fluorescent image and remove parts of the image which are due to shadows or surface texture and facilitates later thresholding. The background subtraction was then applied.

---

[139] In the documentation for Fiji's background subtraction, it is recommended that the radius of the rolling ball be set to 'at least the size of the largest object that is not part of the background.' See Castle and Keller (2007) or go to https://imagej.net/Rolling_Ball_Background_Subtraction for documentation.

After applying the background subtraction to the duplicated image, the image was converted to luminance under Image → Color → RGB to Luminance. A threshold was then applied to the luminance image. Using auto threshold maintained consistency in processing. Dark background was selected so that the fluorescent area appeared black. If any holes remained in the fluorescing area after thresholding, Process → Binary → Fill holes was applied. Finally, Process → Image Calculator was selected. The luminance image was subtracted from the original colour image. The remaining image consisted of only fluorescing pigment with a completely black background (Figure A19.1).
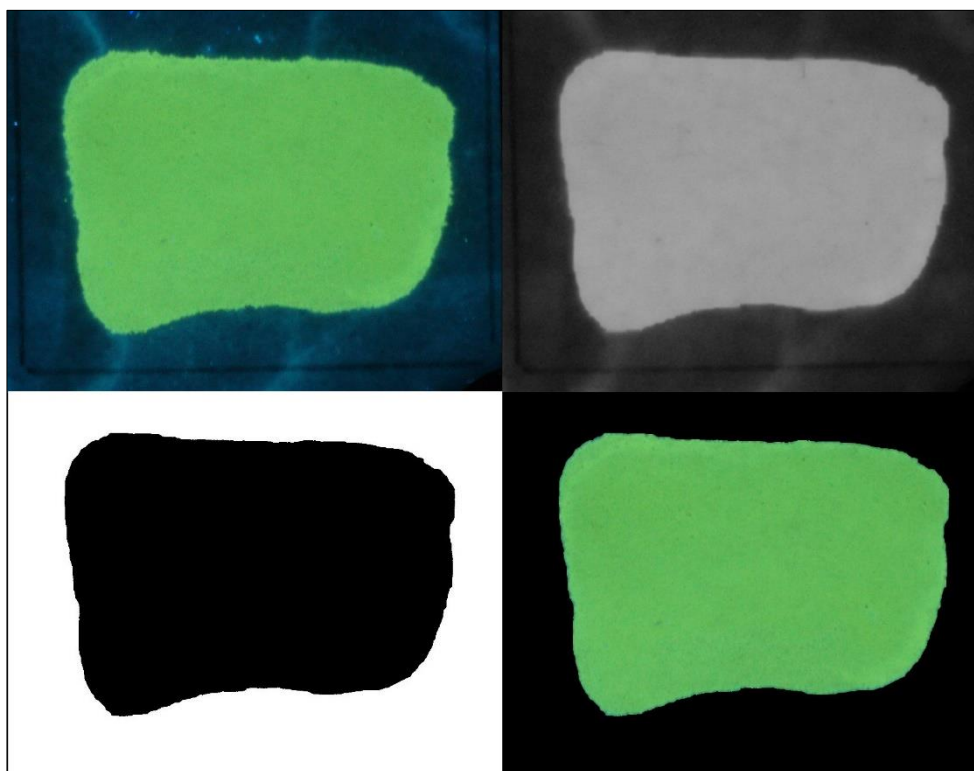
Figure A19.1 Processing of UV fluorescence images of *indirect* sample 1 on Whatman paper. **Upper left*:* original image of sample. **Upper right:** image of sample after subtract background and RGB-luminance conversion. **Lower left:** threshold of top right image. **Lower right:** threshold image subtracted from original image shows complete background removal.

A19.2 RGB MEAN AND MEDIAN PROCESSING IN MATLAB

Background subtracted images were loaded into MATLAB and separated into individual R, G and B vectors. Zero values were eliminated. Finally, average and median values were found for all vectors. The code below from file RGB_mean.m was used for this data processing.

```matlab
%Import image, change name as needed. Convert to double
Image_name= double(Image_name);

%Delineate each channel
R=Image_name(:,:,1);
G=Image_name(:,:,2);
B=Image_name(:,:,3);

%Turn each channel into vector or string of numbers
R1=R(:);
G1=G(:);
B1=B(:);

%Eliminate 0 values resulting from black background
R1=R1(R1~=0);
G1=G1(G1~=0);
B1=B1(B1~=0);

%Find mean and median values for all three channels
meanR1=mean(R1);
meanG1=mean(G1);
meanB1=mean(B1);
medianR1=median(R1);
medianG1=median(G1);
medianB1=median(B1);
```

A19.3 MICROGRAPH PROCESSING

Micrographs were cropped to 869x674 pixels to reduce processing time and maintain consistency of pixel numbers processed. While there will still be more pixels analysed for micrographs at this size as they do not have any deleted zero values, the increase in data points will not lead to significant differences in average or mean values. Cropped micrographs were processed in MATLAB using the RGB_mean.m code, then analysed in Excel similarly to digital images.

Appendix 20: Fluorescent Spectra Peak Area and Intensity Values

Table A20.1 Peak areas derived from fluorescence spectra analysed by Interactive Peak Fitter

	NBE	NBE50	G	G50	G/NBE	G50/NBE50
W1C	0.05015	0.05700	0.9482	0.9062	18.91	15.90
W3C	0.2319	0.1899	0.7674	0.8129	3.309	4.281
W4C	0.2384	0.2895	0.7593	0.7101	3.185	2.453
W6C	0.06346	0.02701	0.8448	0.8404	13.31	31.11
W7C	0.08466	0.05645	0.8177	0.8315	9.659	14.73
W9C	0.001868	0.0008161	0.8405	0.8696	449.9	1066
W15C	0.1533	0.1954	0.8467	0.8049	5.523	4.119
W16C	0.1441	0.1668	0.8510	0.8294	5.906	4.972
B1C	0.1382	0.1047	0.8428	0.8813	6.098	8.417
B3C	0.4042	0.4055	0.5901	0.5825	1.460	1.436
B4C	0.4745	0.4526	0.5230	0.5375	1.102	1.188
B6C	0.04898	0.03956	0.8200	0.8271	16.74	20.91
B7C	0.06327	0.06217	0.8397	0.8472	13.27	13.63
B9C	0.004665	0.005009	0.8326	0.9577	178.5	191.2
B15C	0.2769	0.2825	0.7223	0.7091	2.609	2.510
B16C	0.2520	0.2472	0.7315	0.7314	2.903	2.959

Key: G=green band, NBE=near band edge emission, 50 indicates 50 hours of light exposure

Table A20.2 Peak intensities derived from fluorescence spectra analysed by Interactive Peak Fitter

	NBE	NBE50	G	G50	G/NBE	G50/NBE50
W1C	0.001827	0.001761	0.008180	0.007631	4.477	4.333
W3C	0.01215	0.01007	0.005128	0.005396	0.4221	0.5358
W4C	0.01236	0.01538	0.005507	0.004731	0.4456	0.3076
W6C	0.001795	0.0009268	0.007780	0.008237	4.334	8.888
W7C	0.002272	0.001632	0.007238	0.007353	3.186	4.506
W9C	0.0001233	0.00006835	0.008574	0.008595	69.54	125.7
W15C	0.008263	0.01092	0.005558	0.005197	0.6726	0.4759
W16C	0.006795	0.008156	0.006804	0.006655	1.001	0.8160
B1C	0.006537	0.005301	0.008479	0.008762	1.297	1.653
B3C	0.02106	0.02228	0.003734	0.003597	0.1773	0.1614
B4C	0.02473	0.02486	0.003063	0.003381	0.1239	0.1360
B6C	0.001486	0.001319	0.007713	0.008112	5.190	6.150
B7C	0.001858	0.001606	0.007488	0.007173	4.030	4.466
B9C	0.0002531	0.0002646	0.008353	0.008503	33.00	32.14
B15C	0.01475	0.01548	0.004309	0.004349	0.2921	0.2809
B16C	0.01243	0.01257	0.006633	0.006476	0.5336	0.5152

Key: G=green band, NBE=near band edge emission, 50 indicates 50 hours of light exposure

Appendix 21: RGB Values and G/B Ratios

Table A21.1 Average UV fluorescent digital photograph RGB values and G/B ratios

	R	R50	G	G50	B	B50	G/B	G50/B50
W1C	100	95	199	183	106	90	1.877	2.033
W3C	72	64	158	139	116	89	1.362	1.562
W4C	70	71	158	137	133	99	1.188	1.384
W6C	101	95	194	185	99	92	1.960	2.011
W7C	78	76	148	145	66	58	2.242	2.500
W9C	115	108	251	242	159	152	1.579	1.592
W15C	75	72	171	160	128	115	1.336	1.391
W16C	85	85	193	183	122	108	1.582	1.694
WGumC	15	5	88	30	105	48	0.8381	0.6250
F1C	85	85	164	164	91	80	1.802	2.050
F3C	74	66	136	133	89	86	1.528	1.547
F4C	73	60	122	117	85	85	1.435	1.376
F6C	82	76	168	159	102	83	1.647	1.916
F7C	62	58	135	126	82	56	1.646	2.250
F9C	101	98	221	222	146	143	1.514	1.552
F15C	81	72	150	146	104	102	1.442	1.431
F16C	86	82	166	163	98	91	1.694	1.791
FGumC	29	7	183	120	209	153	0.8756	0.7843
B1C	130	122	215	212	115	112	1.870	1.893
B3C	100	86	159	153	99	114	1.606	1.342
B4C	101	109	153	166	110	126	1.391	1.317
B6C	128	97	215	182	121	108	1.777	1.685
B7C	102	73	168	140	88	86	1.909	1.628
B9C	137	124	254	254	164	168	1.549	1.512
B15C	122	114	197	195	133	138	1.481	1.413
B16C	127	119	213	212	122	123	1.746	1.724
BGumC	110	39	202	163	191	175	1.058	0.9314

Key: R=red channel, G=green channel, B=blue channel, 50 indicates 50 hours of light exposure

Table A21.2 Average UV fluorescent micrograph RGB values and G/B ratios

	R	R50	G	G50	B	B50	G/B	G50/B50
W1C	52	68	146	166	106	113	1.377	1.469
W3C	40	39	95	102	109	81	0.8716	1.259
W4C	43	43	93	104	114	94	0.8158	1.106
W6C	53	66	148	166	100	110	1.480	1.509
W7C	36	40	107	110	71	61	1.507	1.803
W9C	49	50	159	163	121	123	1.314	1.325
W15C	45	40	100	103	131	109	0.7634	0.9450
W16C	41	42	120	124	102	96	1.176	1.292
WGumC	16	7	37	16	71	31	0.5211	0.5161
F1C	70	65	166	169	119	134	1.395	1.261
F3C	49	49	115	108	119	134	0.9664	0.8060
F4C	59	62	112	111	141	162	0.7943	0.6852
F6C	73	65	172	164	117	108	1.470	1.519
F7C	46	40	124	117	84	80	1.476	1.463
F9C	76	66	196	187	161	147	1.217	1.272
F15C	54	61	117	132	143	159	0.8181	0.8302
F16C	56	56	144	150	113	126	1.274	1.190
FGumC	73	31	154	79	200	146	0.7700	0.5411
B1C	52	54	141	144	105	105	1.343	1.371
B3C	36	41	80	95	103	112	0.7767	0.8482
B4C	45	43	91	95	111	110	0.8198	0.8636
B6C	58	57	150	151	101	102	1.485	1.480
B7C	36	35	99	107	59	87	1.678	1.230
B9C	53	48	157	157	114	121	1.377	1.298
B15C	45	46	96	102	128	134	0.7500	0.7612
B16C	36	41	103	111	91	112	1.132	0.9911
BGumC	39	32	99	84	122	112	0.8115	0.7500

Key: R=red channel, G=green channel, B=blue channel, 50 indicates 50 hours of light exposure

Glossary of Terms

Absorption edge: the portion of a semiconductor's absorption or reflectance spectrum where a strong reflectance shifts to a weak one, or vice versa. It occurs near the UV region in zinc oxide where strong reflectance in the visible shifts to strong absorption in the UV. The absorption edge when the absorption coefficient is plotted over wavelength converted to eV can indicate the width of the band gap.

Acicular: needle-like particles, typical of zinc oxide produced by the *direct* method of production

Adsorption: the adhesion of atoms or molecules to a surface, either by hydrogen bonding, van der Walle forces, covalent bonding or electrostatic attraction. Water is frequently adsorbed onto zinc oxide surfaces.

Annealing: to heat a material, usually a metal, to high temperature to modify the crystal structure. In the case of zinc oxide, annealing reduces bulk defects but increases surface defects.

Band gap: the energy gap between the valence band and the conductance band. In conducting materials, these bands overlap, while in insulators they are very far apart, disallowing the transfer of electrons to the conductance band. Semiconductors have band gaps which are wide enough to maintain most electrons in the valence band in a resting state but which allows them to cross the band gap to the conductance band when energy is introduced which is as high or higher than the energy of the band gap.

Bleaching: a chemical process which involves breaking up of conjugated double bonds, or structures with alternating double and single bonds, usually by breaking

double bonds and replacing them with single bonds. Visible light tends to bleach organic dyes and paper while ultraviolet light causes discolouration by re-introducing the conjugated double bond structure.

Body-colour: The term 'body-colour' is now typically interchangeable with the term gouache, though body-colour once referred specifically to opaque pigments used in watercolour. Additionally, while gouache was made popular in the nineteenth century, body-colour has been a term used since the fifteenth century.

Cell parameters: the 'x,y,z' axes of crystal lattices. Crystals are arranged in a space delineated by the cell parameters *a, b,* and *c*, corresponding roughly to the x, y and z axes of the Cartesian coordinate system. Unlike the latter system, the angles between the cell parameters are often not 90° and are described by the crystal family to which they belong. Zinc oxide has a wurzite crystal structure in the hexagonal crystal family, meaning that both *a* and *b* are equal and delineated by the *a* parameter and the angle between the two *a* parameters is 120°. The angle between *a* and *c* is 90°.

Chemisorb: when a molecule is chemically bound to the surface of an adsorbing material.

Chinese white: a white zinc oxide watercolour paint marketed by Winsor and Newton in 1834. The first zinc oxide watercolour pigment to be commercially sold, it revolutionised watercolour painting by facilitating opaque watercolour painting and providing a safe, relatively stable alternative to lead-based white pigments. Zinc oxide watercolour paints are still marketed today as Chinese white.

CIELAB (CIE 1976 L*a*b*): a colour space invented to standardise the incremental changes perceived by human vision on a scale from -100 – 100 using three variables: L^* for lightness, a^* corresponding to a colour gradient of green to

red and *b** corresponding to a colour gradient from blue to yellow. The colour space is used for standardisation of colour measurements as well as colour representation in computer screens via RGB spaces and in device colour conversions as in the case of printers.

Conductance band: the energy level at which electrons in a material are free flowing and unbound to individual atoms. In conducting materials, this is the energy level when a material is not excited by added energy while in semiconductors, electrons jump to this level typically with the introduction of light or heat.

Conductivity: the ease at which electrons move over or through a material. A conductive material is one which allows the free movement of electrons.

Conjugated double bonds: a bond structure within a molecule consisting of alternating single and double bonds. The effect of conjugated double bond structures is the increased absorption of certain wavelengths of light, leading to visible darkening of the material.

Crystallite: a single crystal of a material, usually microscopic, which forms upon cooling of a material. Zinc oxide pigments contain many crystallites often fused together into agglomerate particles which themselves may clump together to form larger particles.

Deep acceptor: an acceptor is a positively-charged defect or impurity in a semiconductor which attracts electrons. A deep acceptor is one which is energetically far from the bottom of the conductance band, closer to the middle of the gap between the valence and conductance bands.

Deep donor: a donor is a negatively-charged defect or impurity which donates electrons to a material. A deep donor is one which is located far from the conductance band near the middle of the band gap.

Density Functional Theory: a method in solid-state physics of calculating the density of electrons in a material. The assumptions used to model electrons in this theory have improved but are still inadequate for accurately determining certain qualities such as band gaps and van der Waals forces.

***Direct* method of ZnO production (American method):** a method for producing zinc oxide which involves burning coal and zinc containing materials together in a furnace, producing zinc vapour and carbon monoxide. An ignition chamber converts these to zinc oxide and carbon dioxide. There are more elemental impurities and crystal defects in zinc oxides produced by this method when compared with those produced by the *indirect* or French method of production.

Doping: in semiconductor design, doping a material involves adding defects or impurities which introduce more holes or electrons or which add energy levels for electrons and holes to reside in.

Efflorescence: from the French meaning 'to flower out,' efflorescence from zinc oxide is the result of the pigment's conversion to zinc sulphate salts which have larger particle sizes and form long, needle-like particles. These sit on the surface or break up paint layers, causing the material to look chalky or milky. Sometimes 'flowers' of crystals are visible as the salts align in small rosettes. These sulphate salts are water soluble and typically removed with moisture.

Electron volt (eV): the kinetic energy of one electron accelerating from rest to one volt. The unit is the electron's charge multiplied by a volt with unit Joules/charge,

resulting in a unit of Joules. The energy required for a band gap jump is delineated in electron volts and can be derived from a proton's wavelength.

Fluorescence: an electron falling from an excited to a resting state emits a photon of light with wavelength proportional to the energy lost in the fall, resulting in the phenomenon of fluorescence.

Glazing: a painting method involving the application of thin, transparent layers of paint over an underpainting to slowly build colour. The result is often a more luminous colour with a less diffuse surface quality.

Gouache: a term arising from a paint developed in the eighteenth century marketed for opaque painting on paper. It contained more binding medium than watercolours and had a white pigment added for increased opacity.

Hemicellulose: a polymer constituent of paper consisting of several different sugar monomers which takes on an amorphous form and is easily hydrolysed. While cellulose polymers contain only glucose, hemicellulose can contain galactose, arabinose, xylose, etc. and does not form crystalline regions.

Hole: an energetically positive state left by an electron when it is excited or removed from its resting state. The hole is energetically unstable and attracts electrons in order to re-establish an electronically stable state.

***Indirect* method of ZnO production (French method):** a method of producing zinc oxide in which zinc metal is boiled, then the vapours burnt in an oxygen-rich atmosphere. The resulting zinc oxide powder is gathered into hoppers which separate them by purity. The resultant pigment consists of round, nodular crystallites maintained at an optimum size of 0.2-0.25 μm for best hiding power. This method creates the purest zinc oxide with the least crystal defects.

Insulator: a material in which electrons remain in the valence band and are not free-flowing. These materials have a band gap which is too wide for electrons to pass from the valence band to the conductance band by typical excitation methods that occur at room temperature.

Interstitial: a position within a crystal lattice which is not normally occupied by an atom is an interstitial position.

Irradiance: irradiance is a measurement of the radiant energy imparted to a material over a specific surface area. Irradiance is measured in watts per metre squared, while a watt is measured in Joules per second. Therefore, by multiplying the irradiance value of a light source by the time of exposure and area exposed, an energy value in Joules is obtained.

Lithographic film: a photographic film used to create high-contrast negatives. Lithographic film is well-suited to Russell-grams which require exposed areas to image darkly so that they can be easily detected.

Miller-Bravais index: a notational method for delineating the orientation of planes passing through crystal structures. Four terms delineate the reciprocal of the position of the plane against four axes: the first term references to the position along the first cell parameter *a*, the second delineates the position along the second *a* parameter, the third is the negative sum of the first two terms and the fourth refers to the position along the *c* parameter. The Miller-Bravais system is particularly good for hexagonal crystal structures as certain symmetries are more easily studied with a fourth term.

Miller index: a notational method for orienting planes within a crystal lattice. Similar to the Miller-Bravais index but without the third term. Miller indices are more widely applicable and are used for all crystal families.

Native-point defect: a crystal defect caused by a missing or displaced native ion rather than an impurity. For example, native point defects in zinc oxide all pertain to the locations or stoichiometry of zinc and oxygen ions within the crystal lattice.

Near-band-edge (NBE) emission: the near-band-edge emission in zinc oxide is the fluorescence associated with electrons falling from the conductance band back into holes in the valence band. This produces fluorescence in the near-UV. Additional wavelengths of fluorescence are associated with defects and impurities which create trap-states or deep acceptors which electrons can fall into. When this happens, a broad green fluorescent band is emitted. These wavelengths are associated with the shorter distance travelled by electrons falling into inter-band defects rather than back down into the valence band.

Nodular: crystallites produced by the *indirect* method of zinc oxide production are described as nodular in structure. This describes crystallites which are round in shape and may be somewhat cylindrical but are much shorter than the acicular crystallites associated with the *direct* method of production.

n-type semiconductor: an n-type semiconductor is one which maintains an excess of donor defects, negatively shifting the overall charge. The n in n-type stands for negative.

Photocatalysis: photocatalysis is a process by which photolytic reactions are accelerated by a catalyst. Typically, a catalyst creates electron-hole pairs which produce radicals which then take part in further reactions with other materials. Zinc

oxide can be an efficient photocatalyst in the presence of moisture and carbon-containing molecules.

p-type semiconductor: a p-type semiconductor is one in which an excess of holes are maintained, positively shifting the overall charge of the material. The p in p-type stands for positive.

Quenching: surrounding materials can quench fluorescence by absorbing fluoresced wavelengths of light, sometimes re-emitting at longer wavelengths. Some quenching is almost always observed in mixed materials and can even occur in pure materials when fluoresced wavelengths are within the absorbing regions of the material's reflectance spectrum.

Recombination: recombination refers to the return of an excited electron to a hole, cancelling the charges of both and returning the system to a neutral, relaxed state.

Russell-gram: an imaging method developed by W.J. Russell in the late nineteenth century for detecting degradation products using sensitised photographic films. Areas of peroxide and radical formation will 'image' on the film, creating a picture of deterioration for study. The technique has also been used for imaging watermarks.

Semiconductor: a material which possesses an energetic gap between valence and conductance bands but in which the band gap is narrow enough to allow for the excitation of electrons across the band gap.

Shallow acceptor: a defect or impurity which contributes holes to the band gap very close to the valence band maximum.

Shallow donor: a defect or impurity which contributes electrons to the conductance band very close to the conductance band minimum.

Spectral power distribution (SPD): indicates wavelength-dependent spectral irradiance for a light source. The irradiance in watts per metre squared is plotted against wavelength. SPDs are valuable for conservators as they indicate the energy emitted by light in the UV and IR ranges as well as the visible range.

Stoke's shift: the difference between the absorbed and emitted wavelengths of light is referred to as the Stoke's shift. This difference is unique to a material.

Trap state: a defect or impurity which 'traps' electrons which were previously free-flowing in the conductance band. They can then become excited again from the trap state but are not mobile while trapped. These trap states are also deep acceptors and can sometimes produce fluorescence.

Unit cell: the simplest representation of a crystal structure. A unit cell is the smallest repeatable unit comprised of the atoms in a crystal. This unit cell is tessellated to create a crystal.

Valence band: the energetic band in a crystal comprised of all valence electrons. Electrons in this band are typically bound to their atoms and are not free-flowing.

Wurzite crystal structure: a crystal habit within the hexagonal crystal family which is composed of atoms arranged in pyramids within a hexagonal unit cell. Zinc oxide along with a number of other semiconductors arrange themselves in the wurzite crystal habit.

List of References

Ackermann, R. (1801) *A treatise on Ackermann's superfine water colours: with directions how to prepare and use them: including succinct hints on drawing and painting.* London: R. Ackermann.

Advice sheet: caring for paper collections in museums (2009). Edinburgh.

Afsharpour, M. and Imani, S. (2017) 'Preventive protection of paper works by using nanocomposite coating of zinc oxide', *Journal of Cultural Heritage.* Elsevier Masson SAS, 25(October), pp. 142–148. doi: 10.1016/j.culher.2016.12.007.

Alivov, Y. I., Chukichev, M. V. and Nikitenko, V. A. (2004) 'Green luminescence band of zinc oxide films copper-doped by thermal diffusion', *Semiconductors,* 38(1), pp. 31–35. doi: 10.1134/1.1641129.

Anderson, D. M. W., Howlett, J. F. and McNab, C. G. A. (1985) 'The amino acid composition of the proteinaceous component of gum arabic (Acacia Senegal (L.) Willd.)', *Food Additives and Contaminants*, 2(3), pp. 159–164.

De Angelis, F. and Armelao, L. (2011) 'Optical properties of ZnO nanostructures: A hybrid DFT/TDDFT investigation', *Physical Chemistry Chemical Physics*, 13(2), pp. 467–475. doi: 10.1039/c0cp01234c.

Artesani, A., Bellei, S., Capogrosso, V., Cesaratto, A., Mosca, S., Nevin, A., Valentini, G. and Comelli, D. (2016) 'Photoluminescence properties of zinc white: an insight into its emission mechanisms through the study of historical artist

materials', *Applied Physics A: Materials Science and Processing.* Springer Berlin Heidelberg, 122(12), pp. 1–11. doi: 10.1007/s00339-016-0578-6.

Artesani, A., Gherardi, F., Nevin, A., Valentini, G. and Comelli, D. (2017) 'A photoluminescence study of the changes induced in the zinc white pigment by formation of zinc complexes', *Materials,* 10(340), pp. 1–12. doi: 10.3390/ma10040340.

Artesani, A., Gherardi, F., Mosca, S., Alberti, R., Nevin, A., Toniolo, L., Valentini, G. and Comelli, D. (2018) 'On the photoluminescence changes induced by ageing processes on zinc white paints', *Microchemical Journal.* Elsevier B.V., 139, pp. 467–474. doi: 10.1016/j.microc.2018.03.032.

Auer, G., Griebler, W.-D. and Jahn, B. (2005) 'White pigments', in Buxbaum, G. and Pfaff, G. (eds) *Industrial Inorganic Pigments.* 3rd edn. Weinheim, pp. 51–97.

Avery, K. J. (2002) *American Drawings and Watercolours in the Metropolitan Museum of Art Volume 1: A Catalogue of Works by Artists Born before 1835.* New York: The Metropolitan Museum of Art.

Bacci, M., Picollo, M., Trumpy, G., Tsukada, M. and Kunzelman, D. (2007) 'Non-Invasive identification of white pigments on 20th-century oil paintings by using fiber optic reflectance spectroscopy', *Journal of the American Institute for Conservation,* 46(1), pp. 27–37.

Bachhoffner, G. H. (1837) *Chemistry as applied to the fine arts.* London: J. Carpenter and Co.

Baldia, C. M. and Jakes, K. A. (2007) 'Photographic methods to detect colourants in archaeological textiles', *Journal of Archeological Science*, 34, pp. 519–525. doi: 10.1016/j.jas.2006.06.010.

Bandopadhyay, K. and Mitra, J. (2015) 'Zn interstitials and O vacancies responsible for n-type ZnO: what do the emission spectra reveal?', *RSC Advances. Royal Society of Chemistry,* 5(30), pp. 23540–23547. doi: 10.1039/C5RA00355E.

Bankhead, P. (2014) 'Analyzing fluorescence microscopy images with ImageJ', *ImageJ,* (1), pp. 1–195.

Bao, J., Shalish, I., Su, Z., Gurwitz, R., Capasso, F., Wang, X. and Ren, Zhifeng (2011) 'Photoinduced oxygen release and persistent photoconductivity in ZnO nanowires', *Nanoscale Research Letters*, 6, pp. 1–7. doi: 10.1186/1556-276X-6-404.

Barbur, J. L., Rodriguez-Carmona, M., Harlow, J. A., Mancuso, K., Neitz, J. and Neitz, M. (2008) 'A study of unusual Rayleigh matches in deutan deficiency', *Visual Neuroscience,* 25(3), pp. 507–516.

Barnard, G. (1871) *The theory and practice of landscape painting in water-colours.* 1st edn. London: Routledge, Warne & Routledge.

Barnes, P., Jaques, S. and Vickers, M. (2006) *Determination of size and strain, Birkbeck College, University of London.* Available at: http://pd.chem.ucl.ac.uk/pdnn/peaks/sizedet.htm (Accessed: 30 August 2018).

Baruah, S., Jaisai, M., Imani, R. and Nazhad, M. M. (2010) 'Photocatalytic paper using zinc oxide nanorods', *Science and Technology of Advanced Materials,* 11(055002), pp. 1–7. doi: 10.1088/1468-6996/11/5/055002.

Bellows, A. F., Hart, W. M., Cranch, C. P., Falconer, J. M. and Burling, G. (eds) (1868) *Water-Color Painting: Some Facts and Authorities in Relation to its Durability*. New York: American Society of Painters in Water-Colors.

Bertrand, L., Refregiers, M., Berrie, B., Echard, J.-P. and Thoury, M. (2013) 'A multiscalar photoluminescence approach to discriminate among semiconducting historical zinc white pigments', *Analyst,* 138(16), pp. 4463–4469.

Bindu, P. and Thomas, S. (2014) 'Estimation of lattice strain in ZnO nanoparticles: X-ray peak profile analysis', *Journal of Theoretical and Applied Physics*, 8(4), pp. 123–134. doi: 10.1007/s40094-014-0141-9.

Blashkov, I. V., Basov, L. L. and Lisachenko, A. A. (2017) 'Photocatalytic Reaction $NO + CO + h\nu \rightarrow CO_2 + 1/2N_2$ Activated on ZnO_{1-x} in the UV–Vis Region', *The Journal of Physical Chemistry C,* 121(51), pp. 28364–28372. doi: 10.1021/acs.jpcc.7b10143.

Bonaduce, I., Brecoulaki, H., Colombini, M. P., Lluveras, A., Restivo, V. and Ribechini, E. (2007) 'Gas chromatographic-mass spectrometric characterisation of plant gums in samples from painted works of art', *Journal of Chromatography A*, 1175(2), pp. 275–282. doi: 10.1016/j.chroma.2007.10.056.

Boni, M. (2011) 'Discovery and mining history of the "calamine "in SW Sardinia (Italy)', *History of Research in Mineral Resources*, pp. 25–32.

Bonosewicz, P., Hirschwald, W. and Neumann, G. (1986) 'Influence of surface processes on electrical, photochemical and thermodynamical properties of zinc oxide films', *Journal of the Electrochemical Society,* 133(11), pp. 2270–2278.

Brown, H. E. (1957) *Zinc oxide rediscovered.* New York: New Jersey Zinc Company.

Buxbaum, G. and Pfaff, G. (2005) *Industrial Inorganic Pigments*. 3rd Revise. Edited by G. Buxbaum and G. Pfaff. Weinheim: Wiley-VCH.

Capogrosso, V., Gabrieli, F., Bellei, S., Cartechini, L., Cesaratto, A., Trcera, N., Rosi, F., Valentini, G., Comelli, D. and Nevin, A. (2015) 'An integrated approach based on micro-mapping analytical techniques for the detection of impurities in historical Zn-based white pigments', *Journal of Analytical Atomic Spectrometry*. Royal Society of Chemistry, 30(3), pp. 828–838. doi: 10.1039/c4ja00385c.

Carden, M. L. (1991) 'Use of ultraviolet light as an aid to pigment identification', *ATP Bulletin*, 23(3), pp. 26–37.

Carmichael, J. W. (1859) *The art of marine painting in water-colours.* London: Winsor and Newton.

Carpenter, C. H. (1952) *382 photomicrographs of 91 papermaking fibers*. Revised ed. Syracuse, NY: State University of New York, College of Forestry.

Carter, H. A. (1996) 'The Chemistry of Paper Preservation: Part 2. The Yellowing of Paper and Conservation Bleaching', *Journal of Chemical Education*, 73(11), pp. 1068–1073. doi: 10.1021/ed073p1068.

Casadio, F. and Rose, V. (2013) 'High-resolution fluorescence mapping of impurities in historical zinc oxide pigments: hard X-ray nanoprobe applications to the paints of Pablo Picasso', *Applied Physics A: Materials Science and Processing*, 111(1), pp. 1–8. doi: 10.1007/s00339-012-7534-x.

Castle, M. and Keller, J. (2007) *Rolling Ball Background Subtraction (ImageJ)*. Available at: https://imagej.net/Rolling_Ball_Background_Subtraction (Accessed: 12 June 2018).

Chapman, J. G. (1858) *The American Drawing-Book: A Manual for the Amateur, and Basis of Study for the Professional Artist.* New York: J.S. Redfield.

Chen, H., Gu, S., Tang, K., Zhu, S., Zhu, Z., Ye, J., Zhang, R. and Zheng, Y. (2011) 'Origins of green band emission in high-temperature annealed N-doped ZnO', *Journal of Luminescence*. Elsevier, 131(6), pp. 1189–1192. doi: 10.1016/j.jlumin.2011.02.025.

Chiantore, O., Riedo, C. and Scalarone, D. (2009) 'Gas chromatography-mass spectrometric analysis of products from on-line pyrolysis/silylation of plant gums used as binding media', *International Journal of Mass Spectrometry*, 284(1), pp. 35–41. doi: 10.1016/j.ijms.2008.07.031.

Church, A. H. (1890) *The chemistry of paints and paintings*. 1st edn. London: Seeley, Service and Co. Limited. Available at: http://babel.hathitrust.org/cgi/pt?id=wu.89046887063;view=1up;seq=9.

Clark, J. H. (1807) *A practical essay on the art of colouring and painting landscapes in water colours: accompanied with ten engravings.* London: Edward Orme.

Clementi, C., Miliani, C., Verri, G., Sotiropoulou, S., Romani, A., Brunetti, B. G. and Sgamellotti, A. (2009) 'Application of the Kubelka-Munk correction for self-absorption of fluorescence emission in carmine lake paint layers', *Applied Spectroscopy,* 63(12), pp. 1323–1330. doi: 10.1366/000370209790109058.

Clementi, C., Rosi, F., Romani, A., Vivani, R., Brunetti, B. G. and Miliani, C. (2012) 'Photoluminescence properties of zinc oxide in paints: a study of the effect of self-absorption and passivation', *Applied Spectroscopy,* 66(10), pp. 1233–1241. doi: 10.1366/12-06643.

Cohn, M. B. and Rosenfield, R. (1977) *Wash and gouache: a study of the development of the materials of watercolor.* Cambridge: Center for Conservation and Technical Studies, Fogg Art Museum and the Foundation of the American Institute of Conservation.

Colbourne, J. (2006) 'Pigment, extender, or adulterant: a discussion on artists' white pigments in aqueous medium in the early twentieth century', in *ICON Edinburgh 2006.* Edinburgh: ICON, pp. 123–130.

Conte, A. M., Pulci, O., Del Sole, R., Knapik, A., Bagniuk, J., Lojewska, J., Teodonio, L. and Missori, M. (2012) 'Experimental and theoretical study of the yellowing of ancient paper', *e-Journal of Surface Science and Nanotechnology*, 10, pp. 569–574. doi: 10.1380/ejssnt.2012.569.

Cosentino, A. (2014) 'Identification of pigments by multispectral imaging; a flowchart method', *Heritage Science*, 2(8), pp. 1–12. doi: 10.1186/2050-7445-2-8.

Cox, S. F. J., Davis, E. A., Cottrell, S. P., King, P. J., Lord, J. S., Gil, J. M., Alberto, H. V., Vilão, R. C., Piroto Duarte, J., Ayres de Campos, N., Weidinger, A., Lichti, R. L. and Irvine, S. J.. (2001) 'Experimental confirmation of the predicted shallow donor hydrogen state in zinc oxide', *Physical Review Letters*, 86(12), pp. 2601–2604. doi: 10.1103/PhysRevLett.86.2601.

Cuttle, C. (2000) 'A proposal to reduce the exposure to light of museum objects without reducing illuminance or the level of visual satisfaction of museum visitors', *Journal of the American Institute for Conservation*, 39(2), pp. 229–244. doi: 10.2307/3180093.

Daniels, V. (1986) 'The Russell Effect and its use in non-destructive testing', *Philosophical Transactions of the Royal Society of London A: Mathematical Physical and Engineering Sciences*, 320(1554), pp. 285–293. doi: 10.1098/rsta.1986.0117.

Daniels, V. (1990) 'Discolouration of paper induced by pigments containing zinc', *Restaurator,* 11(1), pp. 236–243.

Daniels, V. (2001) 'The changing face of paper conservation science', *The Paper Conservator,* 25(1), pp. 65–70. doi: 10.1080/03094227.2001.9638682.

Daniels, V. (2007) 'Paper', in May, E. and Jones, M. (eds) *Conservation Science: Heritage Materials.* Cambridge: Royal Society of Chemistry, pp. 32–55. doi: 10.1039/9781847557629-00032.

Daruwalla, E. H. and Narsian, M. G. (1966) 'Detection and identification of acid-sensitive linkages in cellulose fiber substances', *Tappi,* 49(3), pp. 106–111.

Depew, H. A. (1941) 'Zinc oxide - a product of complex physical and chemical properties', *Rubber Chemistry and Technology*, 14(1), pp. 259–272.

Dhenadhayalan, N., Mythily, R. and Kumaran, R. (2014) 'Fluorescence spectral studies of Gum Arabic: Multi-emission of Gum Arabic in aqueous solution', *Journal of Luminescence*. Elsevier, 155, pp. 322–329. doi: 10.1016/j.jlumin.2014.06.022.

van Dijken, A., Meulenkamp, E. A., Vanmaekelbergh, D. and Meijerink, A. (2000) 'The Kinetics of the Radiative and Nonradiative Processes in Nanocrystalline ZnO Particles upon Photoexcitation', *The Journal of Physical Chemistry B*, 104(8), pp. 1715–1723. doi: 10.1021/jp993327z.

Dingle, R. (1969) 'Luminescent transitions associated with divalent copper impurities and the green emission from semiconducting zinc oxide', *Physical Review Letters*, 23(11), pp. 579–581.

Djurišić, A. B. and Leung, Y. H. (2006) 'Optical properties of ZnO nanostructures', *Small*, 2(8–9), pp. 944–961. doi: 10.1002/smll.200600134.

Dodd, A. C., McKinley, A. J., Saunders, M. and Tsuzuki, T. (2006) 'Effect of particle size on the photocatalytic activity of nanoparticulate zinc oxide', *Journal of Nanoparticle Research*, 8(1), pp. 43–51. doi: 10.1007/s11051-005-5131-z.

Doherty, B., Daveri, A., Clementi, C., Romani, A., Bioletti, S., Brunetti, B., Sgamellotti, A. and Miliani, C. (2013) 'The Book of Kells: A non-invasive MOLAB investigation by complementary spectroscopic techniques', *Spectrochimica Acta - Part A: Molecular and Biomolecular Spectroscopy*. doi: 10.1016/j.saa.2013.06.020.

Downs Jr, A. C. (1976) 'Zinc for paint and architectural use in the 19th century', *Bulletin of the Association for Preservation Technology*, 8(4), pp. 80–99.

Dror, Y., Cohen, Y. and Yerushalmi-Rozen, R. (2006) 'Structure of gum arabic in aqueous solution', *Journal of Polymer Science: Part B: Polymer Physics*, 44(22), pp. 3265–3271. doi: 10.1002/polb.20970.

Druzik, J. R. and Michalski, S. W. (2012) *Guidelines for Selecting Solid-State Lighting for Museums.* Los Angeles. doi: 10.13140/RG.2.1.3347.2080.

Dyer, J., Verri, G. and Cupitt, J. (2013) 'Multispectral imaging in reflectance and photo-induced luminescence modes: a user manual', *The British Museum, 7th framework program of Charisma Project.*

Ebert, B., Singer, B. and Grimaldi, N. (2012) 'Aquazol as a consolidant for matte paint on Vietnamese paintings', *Journal of the Institute of Conservation*, 35(1), pp. 62–76. doi: 10.1080/19455224.2012.672813.

Eibner, A. (1933) 'Les rayons ultraviolets appliquée a l'examen des couleurs et des agglutinants', *Mouseion*, 21–22, pp. 32–68.

El-Feky, O. M., Hassan, E. A., Fadel, S. M. and Hassan, Mohammad L. (2014) 'Use of ZnO nanoparticles for protecting oil paintings on paper support against dirt, fungal attack, and UV aging', *Journal of Cultural Heritage.* Elsevier Masson SAS, 15(2), pp. 165–172. doi: 10.1016/j.culher.2013.01.012.

Ellis, T. J. (1883) *Sketching from nature: a handbook for students and amateurs*. London: Macmillan and Co.

Ellmer, K. and Bikowski, A. (2016) 'Intrinsic and extrinsic doping of ZnO and ZnO alloys', *Journal of Physics D: Applied Physics.* IOP Publishing, 49(41), pp. 1–33. doi: 10.1088/0022-3727/49/41/413002.

Erhart, P. and Albe, K. (2006) 'Diffusion of zinc vacancies and interstitials in zinc oxide', *Applied Physics Letters,* 88(20), pp. 10–13. doi: 10.1063/1.2206559.

Fabbri, F., Villani, M., Catellani, A., Calzolari, A., Cicero, G., Calestani, D., Calestani, G., Zappettini, A., Dierre, B., Sekiguchi, T. and Salviati, G (2014) 'Zn vacancy induced green luminescence on non-polar surfaces in ZnO nanostructures', *Scientific reports*, 4(5158), pp. 1–5. doi: 10.1038/srep05158.

Feller, R. L. (1964) 'Control of deteriorating effects of light upon museum objects', *Museum International*, 17(2), pp. 57–98. doi: 10.1111/j.1468-0033.1964.tb01570.x.

Feller, R. L. (1966) 'Problems in retouching: chalking of intermediate layers', Bull. *American Group - IIC*, 7(1), pp. 32–34.

Feller, R. L. (1986) 'Barium sulfate - natural and synthetic', in Feller, R. L. (ed.) *Artists' pigments: a handbook of their history and characteristics Vol. 1.* London: Archetype Publications, pp. 47–64.

Feller, R. L. (1992) *Accelerated aging*, Cellulose. Available at: http://hdl.handle.net/1811/4918.

Feller, R. L., Lee, S. B. and Curran, M. (1985) 'Three fundamental aspects of cellulose deterioration', *Art and Archaeology Technical Abstracts*, 22(1), pp. 277–358.

Field, G. (1885) *Field's chromatography: a treatise on colours and pigments for the use of artists.* Edited by J. S. Taylor. Winsor and Newton.

Fielding, T. H. (1830) *An index of colours and mixed tints for the use of beginners in landscape and figure painting*. London.

Fielding, T. H. (1844) *Ackermann's manual of colours used in the different branches of water-colour painting.* London: Ackermann & Co.

Fleury, P. (1912) *The preparation and uses of white zinc paints*. 1st edn. Edited by D. Grant. London: Scott, Greenwood & Son.

Ford, B. (2014) 'The accelerated light fading of iron gall inks in air, hypoxia and near-anoxia', *ICOM-CC 17th Triennial Conference Preprints*, (Iii), p. art. 0604.

Foster, V. (1884) *Vere Foster's simple lessons in water-color, flowers: eight facsimiles of original water-color drawings and numerous outline drawings of flowers, after various artists, with full instructions for drawing and painting*. London: Blackie & Son.

Francia, L. (1813) *Progressive lessons tending to elucidate the character of trees, with the process of sketching, and painting them in water colours*. London: T. Clay.

Garside, D., Curran, K., Korenberg, C., MacDonald, L., Teunissen, K. and Robson, S. (2017) 'How is museum lighting selected? An insight into current practice in UK museums', *Journal of the Institute of Conservation*. Taylor & Francis, 40(1), pp. 3–14. doi: 10.1080/19455224.2016.1267025.

Gettens, R. J. and Stout, G. L. (1966) *Painting materials: a short encyclopedia*. New York: Dover Publications.

González, G. B. (2012) 'Investigating the defect structures in transparent conducting oxides using x-ray and neutron scattering techniques', *Materials,* 5(12), pp. 818–850. doi: 10.3390/ma5050818.

Gullick, T. J. and Timbs, J. (1859) *Painting properly explained...: with historical sketches of the progress of the art*. London: Kent and Co.

Gurwitz, R., Cohen, R. and Shalish, I. (2014) 'Interaction of light with the ZnO surface: Photon induced oxygen "breathing," oxygen vacancies, persistent photoconductivity, and persistent photovoltage', *Journal of Applied Physics*, 115(3). doi: 10.1063/1.4861413.

Harley, R. D. (2001) *Artists' pigments c. 1600-1835: a study in English documentary sources.* London: Archetype Publications.

Hassell, J. (1823) *The camera; or art of drawing in water colours: with instructions for sketching from nature.* 1st edn. London: W. Simpkin and R. Marshall.

Hermans, J., Keune, K., van Loon, A. and Iedema, P. (2016) 'The crystallization of metal soaps and fatty acids in oil paint model systems', *Physical Chemistry Chemical Physics.* Royal Society of Chemistry, 18(16), pp. 10896–10905. doi: 10.1039/C6CP00487C.

Hey, M. (1987) 'Chinese white - a potential source of trouble on paper?', in Vendl, A. et al. (eds) *Wiener Berichte uber Naturwissenschaft in der Kunst.* Vienna: ORAC, pp. 362–369.

Hill, L. J. K. and Bouwmeester, W. (2005) *Factsheet: conservation and lighting*. Edinburgh.

Holley, C. D. (1909) *The lead and zinc pigments.* 1st edn. New York: John Wiley & Sons.

Holmes, C. J. (1920) *Notes on the science of picture-making*. London: Chatto & Windus.

Horiba (2014) *A guidebook to particle size analysis*. Irvine: Horiba Instruments, Inc.

Isacco, E. and Darrah, J. (1993) 'The ultraviolet-infrared method of analysis, a scientific approach to the study of Indian miniatures', *Artibus Asiae*, pp. 470–491.

Jacobs, C. B., Maksov, A. B., Muckley, E. S., Collins, L., Mahjouri-Samani, M., Ievlev, A., Rouleau, C. M., Moon, J. W., Graham, D. E., Sumpter, B. G. and Ivanov, I. N. (2017) 'UV-activated ZnO films on a flexible substrate for room temperature O2 and H2O sensing', *Scientific Reports*, 7(1), pp. 1–10. doi: 10.1038/s41598-017-05265-5.

Jacobsen, A. E. and Gardner, W. H. (1941) 'Zinc soaps in paints: zinc oleates', *Industrial and Engineering Chemistry*, 33(10), pp. 1254–1256.

Janotti, A. and Van de Walle, C. G. (2009) 'Fundamentals of zinc oxide as a semiconductor', *Reports on Progress in Physics*, 72(12), p. 126501. doi: 10.1088/0034-4885/72/12/126501.

Janotti, A. and Van De Walle, C. G. (2007) 'Native point defects in ZnO', *Physical Review B - Condensed Matter and Materials Physics,* 76(16), pp. 1–22. doi: 10.1103/PhysRevB.76.165202.

Johns, C. (2002) *William Henry Hunt: Primroses and Bird's Nest, Tate.* Available at: http://www.tate.org.uk/art/artworks/hunt-primroses-and-birds-nest-n03564 (Accessed: 1 November 2018).

Jordan, G. and Mollon, J. D. (1993) 'The Nagel anomaloscope and seasonal variation of colour vision.', *Nature,* 363(June), pp. 546–549. doi: 10.1038/363546a0.

Jordan, G. and Mollon, J. D. (1995) 'Rayleigh matches and unique green', *Vision Research,* 35(5), pp. 613–620. doi: 10.1016/0042-6989(94)00153-D.

Kemp, F., Wise, A. and Hamilton, B. (2004) 'Re-inventing Diddy: the examination and treatment of a pastel drawing on paper by Grace Cossington Smith', *Collaboration and Connections Sydney Symposium*, pp. 115–124.

Khorsand Zak, A., Ebrahimizadeh Abrishami, M., Abd Majid, W. H., Yousefi, R. and Hosseini, S. M. (2011) 'Effects of annealing temperature on some structural and optical properties of ZnO nanoparticles prepared by a modified sol-gel combustion method', *Ceramics International*. Elsevier Ltd and Techna Group S.r.l., 37(1), pp. 393–398. doi: 10.1016/j.ceramint.2010.08.017.

Khorsand Zak, A., Razali, R., Abd Majid, W. H. and Darroudi, Majid (2011) 'Synthesis and characterization of a narrow size distribution of zinc oxide nanoparticles', *International Journal of Nanomedicine,* 6(1), pp. 1399–1403. doi: 10.2147/IJN.S19693.

Khorsand Zak, A., Abd. Majid, W. H., Abrishami, M. E. and Yousefi, R. (2011) 'X-ray analysis of ZnO nanoparticles by Williamson-Hall and size-strain plot methods', *Solid State Sciences,* 13(1), pp. 251–256. doi: 10.1016/j.solidstatesciences.2010.11.024.

Kirby, J. and Saunders, D. (2004) 'Fading and colour change of Prussian blue: Methods of manufacture and the influence of extenders', *National Gallery technical bulletin*, 25, pp. 73–99.

Klingshirn, C. (2007) 'ZnO: material, physics and applications', *ChemPhysChem,* 8(6), pp. 782–803. doi: 10.1002/cphc.200700002.

Krithiga, R., Sankar, S. and Subhashree, G. (2014) 'Augmentation of band gap and photoemission in ZnO by Li doping', *Journal of Materials Science: Materials in Electronics*, 25(12), pp. 5201–5207. doi: 10.1007/s10854-014-2289-0.

Kröger, F. A. and Vink, H. J. (1954) 'The origin of the fluorescence in self-activated ZnS, CdS, and ZnO', *The Journal of Chemical Physics*, 22(2), pp. 250–252. doi: 10.1063/1.1740044.

Kühn, H. (1986) 'Zinc white', in Feller, R. L. (ed.) *Artists Pigments: A Handbook of their History and Characteristics.* Cambridge: Cambridge University Press, pp. 169–186.

Kumar, S. G. and Rao, K. S. R. K. (2015) 'Zinc oxide based photocatalysis: Tailoring surface-bulk structure and related interfacial charge carrier dynamics for better environmental applications', *RSC Advances*. Royal Society of Chemistry, 5(5), pp. 3306–3351. doi: 10.1039/c4ra13299h.

Kwan, A. K. H., Mora, C. F. and Chan, H. C. (1999) 'Particle shape analysis of coarse aggregate using digital image processing', *Cement and Concrete Research,* 29(9), pp. 1403–1410. doi: 10.1016/S0008-8846(99)00105-2.

Landolt, H. and Börnstein, R. (1999) 'Zinc oxide (ZnO) crystal stucture, lattice parameters', in Madelung, O., Rössler, U., and Schulz, M. (eds) *Landolt-Börnstein - Group III Condensed Matter*. Berlin: Springer, pp. 1–5.

Leake, S. J. (2010) *Coherent X-ray Diffraction Imaging of Zinc Oxide Crystals.* University College London.

Lee, S. B., Bogaard, J. and Feller, R. L. (1989) 'Damaging Effects of Visible and near Ultraviolet-Radiation on Paper', *Acs Symposium Series*, 410(1), pp. 54–62.

Lee, S. B. and Feller, R. L. (1986) 'Influence of the hemicellulose fraction on thermal and photochemical discoloration of paper', in Needles, H. L. and Haig Zeronian, S. (eds) *Historic Textile and Paper Materials: Conservation and Characterization.* University of California, Davis, pp. 377–386.

Leitch, R. P. (1873) *A course of water-colour painting*. 1st edn. London, Paris and New York: Cassell, Petter and Galpin.

Lerwill, A. et al. (2015) 'Photochemical colour change for traditional watercolour pigments in low oxygen levels', *Studies in Conservation*, 60(1), pp. 15–32. doi: 10.1179/2047058413Y.0000000108.

Leverenz, H. and Seitz, F. (1939) 'Luminescent materials', *Journal of Applied Physics*, 10(1), pp. 479–493.

Li, D. and Haneda, H. (2003) 'Morphologies of zinc oxide particles and their effects on photocatalysis', *Chemosphere*, 51(2), pp. 129–137.

Li, M., Wilkinson, D. and Patchigolla, K. (2005) 'Comparison of particle size distributions measured using different techniques', *Particulate Science and Technology*, 23(3), pp. 265–284. doi: 10.1080/02726350590955912.

Liddie, C. A. (1998) '*S.S. BUDA' by G. Thomson: the conservation treatment and art historical study of a nineteenth century gouache seascape, with scientific investigation into the effects of zinc oxide pigment on cellulose*. Northumbria University.

Loe, D. L., Rowlands, E. and Watson, N. F. (1982) 'Preferred lighting conditions for the display of oil and watercolour paintings', *Lighting Research & Technology*, 14(4), pp. 173–192. doi: 10.1177/096032718201400401.

Łojewska, J., Miśkowiec, P., Łojewski, T. and Proniewicz, L. M. (2005) 'Kinetic approach to degradation of paper. In situ FTIR transmission studies on hydrolysis and oxidation', *e-PS*, 2(January 2005), pp. 1–12. Available at: www.e-PRESERVATIONScience.org%0A1.

Luo, Z., Dong, K., Guo, M., Lian, Z., Zhang, B., Wei, W. (2018) 'Preparation of Zinc Oxide Nanoparticles-Based Starch Paste and its Antifungal Performance as a Paper Adhesive', *Starch/Staerke*, 70(7–8), pp. 1–9. doi: 10.1002/star.201700211.

Lyon, R. A. (1934) 'Ultraviolet rays as aids to restorers', *Technical Studies in the Field of the Fine Arts*, 2, pp. 152–157.

Lyons, J. L., Varley, J. B., Steiauf, D., Janotti, A. and Van De Walle, C. G. (2017) 'First-principles characterization of native-defect-related optical transitions in ZnO', *Journal of Applied Physics*, 122(3). doi: 10.1063/1.4992128.

Manente, S., Micheluz, A., Ganzerla, R., Ravagnan, G. and Gambaro, A. (2012) 'Chemical and biological characterization of paper: A case study using a proposed methodological approach', *International Biodeterioration and Biodegradation*. Elsevier Ltd, 74, pp. 99–108. doi: 10.1016/j.ibiod.2012.03.008.

Markham, M. C. and Laidler, K. J. (1953) 'Kinetic study of photo-oxidations on the surface of zinc oxide in aqueous suspensions', *Journal of Physical Chemistry*, 57(3), pp. 363–389.

McVicker, J. E., Rapp, R. A. and Hirth, J. P. (1975) 'The sublimation of basal surfaces of zinc oxide', *The Journal of Chemical Physics*, 63(6), pp. 2646–2658. doi: 10.1063/1.431658.

Merrifield, M. P. (1851) *Practical directions for portrait painting in water-colours.* Second. London: Winsor and Newton.

Meyer, B. K., Sann, J., Hofmann, D. M., Neumann, C. and Zeuner, A. (2005) 'Shallow donors and acceptors in ZnO', *Semiconductor Science and Technology*, 20(4). doi: 10.1088/0268-1242/20/4/008.

Meyer, B., Rabaa, H. and Marx, D. (2006) 'Water adsorption on ZnO(10$\bar{1}$0): From single molecules to partially dissociated monolayers', *Physical Chemistry Chemical Physics,* 8(13), pp. 1513–1520. doi: 10.1039/b515604a.

Michalski, S. (2017) *Agent of deterioration: light, ultraviolet and infrared.* Available at: https://www.canada.ca/en/conservation-institute/services/agents-deterioration/light.html (Accessed: 14 October 2017).

Mikhailov, M. M., Neshchimenko, V. V. and Li, C. (2011) 'Comparative analysis of emission and absorption spectra of zinc oxide powders', *Journal of Surface Investigation. X-ray, Synchrotron and Neutron Techniques*, 5(4), pp. 775–779. doi: 10.1134/S1027451011070160.

Mishra, K. C., Schmidt, P. C., Johnson, K. H., DeBoer, B. G., Berkowitz, J. K. and Dale, E. A. (1990) 'Bands versus bonds in electronic-structure theory of metal oxides: Application to luminescence of copper in zinc oxides', *Physical Review B*, 42(2), pp. 1423–1430.

Moezzi, A., McDonagh, A. M. and Cortie, M. B. (2012) 'Zinc oxide particles: synthesis, properties and applications', *Chemical Engineering Journal.* Elsevier B.V., 185, pp. 1–22. doi: 10.1016/j.cej.2012.01.076.

Mollow, E. (1956) *Proceedings of the Conference on photoconductivity*, Kew Bulletin. New York: Wiley and Sons, Inc. doi: 10.2307/4108143.

Mora, C. F., Kwan, a. K. H. and Chan, H. C. (1998) 'Particle size distribution analysis of coarse aggregate using digital image processing', *Cement and Concrete Research*, 28(6), pp. 921–932. doi: 10.1016/S0008-8846(98)00043-X.

Morgan, S. W. K. (1985) *Zinc and its alloys and compounds*. Chichester: Ellis Horwood.

Morley-Smith, C. T. (1950) 'The development of anti-chalking french process zinc oxides', *Journal of Oil and Colour Chemists Association*, 33, pp. 484–501.

Morley-Smith, C. T. (1958) 'Zinc oxide - a reactive pigment', *Journal of Oil and Colour Chemists Association,* 74(2), pp. 85–97.

Muckley, W. J. (1882) *A handbook for painters and art students: on the character, nature, and use of colours...also short remarks on the practice of painting in oil and water colours.* Second. London: Bailliere, Tindall, and Cox.

Muckley, W. J. (1888) *A manual on flower painting in oil colours from nature: with instructions for preliminary practice; also a section on flower painting in water colours, etc.* Fifth. London: Winsor and Newton.

Nagle, P. G. (1928) 'The mercury vapour arc lamp: its uses in a rubber factory', *Rubber Chemistry and Technology,* 1(2), pp. 304–311.

Nevin, A., Cesaratto, A., Bellei, S., D'Andrea, C., Toniolo, L., Valentini, G. and Comelli, D. (2014) 'Time-Resolved Photoluminescence Spectroscopy and Imaging: New Approaches to the Analysis of Cultural Heritage and Its Degradation', *Sensors*, 14(4), pp. 6338–6355. doi: 10.3390/s140406338.

Newberg, J. T., Goodwin, C., Arble, C., Khalifa, Y., Boscoboinik, J. A. and Rani, S. (2018) 'ZnO(10$\bar{1}$0) surface hydroxylation under ambient water vapor', *Journal of Physical Chemistry B*, 122(2), pp. 472–478. doi: 10.1021/acs.jpcb.7b03335.

Niskanen, M., Kuisma, M., Cramariuc, O., Golovanov, V., Hukka, T. I., Tkachenko, N. and Rantala, T. T. (2013) 'Porphyrin adsorbed on the (10$\bar{1}$0) surface of the wurtzite structure of ZnO-conformation induced effects on the electron transfer characteristics', *Physical Chemistry Chemical Physics,* 15(40), pp. 17408–17418. doi: 10.1039/c3cp51685g.

Noble, P., van Loon, A. and Boon, J. J. (2005) 'Chemical changes in old master paintings II : darkening due to increased transparency as a result of metal soap formation', in *Proceedings of 14th Triennial ICOM-CC Meeting in The Hague*. I. Verger. London: James & James, pp. 496–503.

Oba, F., Togo, A., Tanaka, I., Paier, J. and Kresse, G. (2008) 'Defect energetics in ZnO: A hybrid Hartree-Fock density functional study', *Physical Review B - Condensed Matter and Materials Physics,* 77(24), pp. 3–8. doi: 10.1103/PhysRevB.77.245202.

Ormsby, B. A., Townsend, J. H., Singer, B. W. and Dean, J. R. (2005) 'British watercolour cakes from the eighteenth to the early twentieth century', *Studies in Conservation*, 50(1), pp. 45–66. doi: 10.2307/25487717.

Osmond, G. (2019) 'Zinc soaps: an overview of zinc oxide reactivity and consequences of soap formation in oil-based paintings', in Casadio, F. et al. (eds) *Metal Soaps in Art: Conservation and Research.* Cham, Switzerland: Springer, pp. 25–46.

Osmond, G., Ebert, B. and Drennan, J. (2014) 'Zinc oxide-centred deterioration in 20th century Vietnamese paintings by Nguyên Trong Kiêm (1933-1991)', *AICCM bulletin*, 34(1), pp. 4–14.

Osmond, G., Keune, K. and Boon, J. J. (2005) 'A study of zinc soap aggregates in a late 19th century painting by R.G. Rivers at the Queensland Art Gallery', *AICCM Bulletin,* 29(1), pp. 37–46. doi: 10.1179/bac.2005.29.1.004.

Pardeshi, S. K. and Patil, A. B. (2008) 'A simple route for photocatalytic degradation of phenol in aqueous zinc oxide suspension using solar energy', *Solar Energy*, 82(8), pp. 700–705. doi: 10.1016/j.solener.2008.02.007.

Park, C. H., Zhang, S. B. and Wei, S. H. (2002) 'Origin of p-type doping difficulty in ZnO: The impurity perspective', *Physical Review B - Condensed Matter and Materials Physics,* 66(7), pp. 732021–732023. doi: 10.1103/PhysRevB.66.073202.

Penfold, T. J., Szlachetko, J., Santomauro, F. G., Britz, A., Gawelda, W., Doumy, G., March, A. M., Southworth, S. H., Rittmann, J., Abela, R., Chergui, M. and Milne, C. J. (2018) 'Revealing hole trapping in zinc oxide nanoparticles by time-resolved X-ray spectroscopy', *Nature Communications*. Springer US, 9(1), pp. 1–9. doi: 10.1038/s41467-018-02870-4.

Perrin, T. E., Druzik, J. R. and Miller, N. J. (2014) *SSL adoption by museums: survey results, analysis, and recommendations*. Richland. Available at: http://energy.gov/sites/prod/files/2015/02/f19/gateway_museums-report_0.pdf.

Picollo, M., Bacci, M., Magrini, D., Radicati, B., Trumpy, G., Tsukada, M. and Kunzelman, D. (2007) 'Modern white pigments: their identification by means of noninvasive ultraviolet, visible, and infrared fiber optic reflectance spectroscopy', in *Modern Paints Uncovered: Proceedings from the Modern Paints Uncovered Symposium,* (May 16-19, 2006, Tate Modern, London). Getty Cons. London: Getty Conservation Institute, pp. 129–139.

Porck, H. J. (2000) *Rate of paper degradation: the predictive value of artificial aging tests*. Amsterdam: European commission on preservation and access. Available at: http://www.knaw.nl/ecpa/publ/porck2.pdf.

Potthast, A., Rosenau, T. and Kosma, P. (2006) 'Analysis of oxidized functionalities in cellulose', in *Advances in Polymer Science*, pp. 3–48. doi: 10.1007/12.

Remington, J. S. and Francis, W. (1954) *Pigments: their manufacture, properties, and use.* 3rd edn. London: Leonard Hill Ltd.

Rene de la Rie, E. (1982) 'Fluorescence of paint and varnish layers (part 1)', *Studies in Conservation*, 27(1), pp. 1–7.

Riedo, C., Scalarone, D. and Chiantore, O. (2013) 'Multivariate analysis of pyrolysis-GC/MS data for identification of polysaccharide binding media', *Analytical Methods*, 5(16), p. 4060. doi: 10.1039/c3ay40474a.

Rischbieth, J. R. (1950) 'Weathering tests on zinc oxide paints', *Journal of the Oil & Colour Chemists' Association*, 33(365), pp. 471–476.

Rodnyi, P. and Khodyuk, I. (2011) 'Optical and luminescence properties of zinc oxide (Review)', *Optics and Spectroscopy*, 111(5), pp. 776–785. doi: 10.1134/S0030400X11120216.

Romani, A., Clementi, C., Miliani, C. and Favaro, G. (2010) 'Fluorescence spectroscopy : A powerful technique for the noninvasive characterization of artwork', *Accounts of Chemical Research*, 43(6), pp. 837–846.

Rowbotham, T. and Rowbotham, T. L. (1850) *The art of landscape painting in water colours.* London: Winsor and Newton.

Rubin, T. R., Calvert, J. G., Rankin, G. T. and MacNevin, W. (1953) 'Photochemical synthesis of hydrogen peroxide at zinc oxide surfaces', *Journal of the American Chemical Society*, 75(12), pp. 2850–2853. doi: 10.1021/ja01108a017.

Ruskin, J. (1858) *The Elements of Drawing*. New York: Wiley & Halsted.

Ruskin, J. (1878) *Notes by John Ruskin on his drawings by J.M.W. Turner, R.A., exhibited at the Fine Art Society's galleries*. London: The Fine Art Society.

Russell, W. J. (1908) 'The action of resin and allied bodies on a photographic plate in the dark', *Proceedings of the Royal Society of London. Series B, Containing Papers of a Biological Character*, 80(541), pp. 376–387.

Russell, W. J. and Abney, W. D. W. (1888) *Report to the Science and Art Department of the Committee of Council on Education on the Action of Light on Water Colours.* London: Eyre and Spottiswoode.

Sáez-Pérez, M. P., Rodríguez-Gordillo, J. and Durán-Suárez, J. A. (2016) 'Synthetic white pigments (white titanium and white zinc) in different binding media. Influence of environmental agents', *Construction and Building Materials*, 114, pp. 151–161. doi: 10.1016/j.conbuildmat.2016.03.140.

Sasges, M., Robinson, J. and Daynouri, F. (2012) 'Ultraviolet lamp output measurement: a concise derivation of the Keitz equation', *Ozone: Science & Engineering,* 34(4), pp. 306–309. doi: 10.1080/01919512.2012.694322.

Sawicka, A., Burnstock, A., Izzo, F. C., Keune, K., Boon, J. J., Kirsch, K. and van den Berg, K. J. (2014) 'An investigation into the viability of removal of lead soap efflorescence from contemporary oil paintings', in *Issues in Contemporary Oil Painting*, pp. 311–332. doi: 10.1007/978-3-319-10100-2.

Scardi, P., Leoni, M. and Delhez, R. (2004) 'Line broadening analysis using integral breadth methods: a critical review', *Journal of Applied Crystallography,* 37(3), pp. 381–390. doi: 10.1107/S0021889804004583.

Schanda, J., Csuti, P. and Szabó, F. (2015) 'Colour fidelity for picture gallery illumination, Part 1: Determining the optimum light-emitting diode spectrum', *Lighting Research and Technology*, 47(5), pp. 513–521. doi: 10.1177/1477153514538643.

Sengupta, G., Mandal, N., Kundu, M., Sanyal, R. and Dutta, S. (1987) 'Morphology and surface defects of zinc oxide', *Journal of Colloid and Interface Science,* 117(2), pp. 301–309. doi: 10.1016/0021-9797(87)90388-2.

Seymour, P. (2007) *The artist's handbook: a complete professional guide to materials and techniques.* Second. London: Lee Press.

Shalish, I., Temkin, H. and Narayanamurti, V. (2004) 'Size-dependent surface luminescence in ZnO nanowires', *Physical Review B - Condensed Matter and Materials Physics*, 69(24), pp. 1–4. doi: 10.1103/PhysRevB.69.245401.

Shan, F. K., Liu, G. X., Lee, W. J., Lee, G. H., Kim, I. S. and Shin, B. C. (2005) 'Aging effect and origin of deep-level emission in ZnO thin film deposited by pulsed laser deposition', *Applied Physics Letters*, 86(221910), pp. 1–3.

Shi, G. A., Saboktakin, M., Stavola, M. and Pearton, S. J. (2004) '"Hidden hydrogen" in as-grown ZnO', *Applied Physics Letters,* 85(23), pp. 5601–5603. doi: 10.1063/1.1832736.

Silvester, G., Burnstock, A., Megens, L., Learner, T., Chiari, G. and van den Berg, K. J. (2014) 'A cause of water-sensitivity in modern oil paint films: the formation of magnesium sulphate', *Studies in Conservation*, 59(1), pp. 38–51. doi: 10.1179/2047058413Y.0000000085.

Simon, J. (2018) *British artists' suppliers, 1650-1950 – A*, *National Portrait Gallery*. Available at: https://www.npg.org.uk/research/programmes/directory-of-suppliers/a (Accessed: 20 May 2018).

Singer, B. W. and Liddie, C. A. (2005) 'A study of unusual degradation on a seascape painting associated with the use of zinc white pigment', *The Paper Conservator*, 29(1), pp. 5–14. doi: 10.1080/03094227.2005.9638483.

Singh, N. K., Saha, S. and Pal, A. (2015) 'Methyl red degradation under UV illumination and catalytic action of commercial ZnO: a parametric study', *Desalination and Water Treatment*, 56(4), pp. 1066–1076. doi: 10.1080/19443994.2014.942380.

Sloan, K. (2003) *Cozens family*, Oxford Art Online. Available at:

http://www.oxfordartonline.com/groveart/view/10.1093/gao/9781884446054.001.00

01/oao-9781884446054-e-7000020053 (Accessed: 20 May 2018).

Smith, S. (2010) *Guidelines for the environmental control for objects on display in FuturePlan*.

Sons, J. C. P. (1901) 'Catalogue of paints, oils, varnishes, brushes, artists' materials,

plate and window glass, mirrors and beveled plates, painters' and paper hangers'

supplies'. Available at:

https://archive.org/stream/catalogueofpaint00john#page/24/mode/2up.

Spotlight on Chinese white (2011) Winsor & Newton. Available at:

http://www.winsornewton.com/na/discover/articles-and-inspiration/spotlight-on-

chinese-white.

Srinivasan, G., Gopalakrishnan, N., Yu, Y. S., Kesavamoorthy, R. and Kumar, J.

(2008) 'Influence of post-deposition annealing on the structural and optical

properties of ZnO thin films prepared by sol-gel and spin-coating method',

Superlattices and Microstructures, 43(2), pp. 112–119. doi:

10.1016/j.spmi.2007.07.032.

Standage, H. C. (1887) *The artists' manual of pigments*. London: Crosby Lockwood

& Co.

Stavroudis, C., Doherty, T. and Wolbers, R. (2005) 'A new approach to cleaning I:

Using mixtures of concentrated stock solutions and a database to arrive at an optimal

aqueous cleaning system', *Newsletter (Western Association for Art Conservation)*,

27(2), pp. 17–28.

Steiauf, D., Lyons, J. L., Janotti, A. and Van De Walle, C. G. (2014) 'First-principles study of vacancy-assisted impurity diffusion in ZnO', *APL Materials*, 2(9). doi: 10.1063/1.4894195.

Stephenson, H. B. (1973) 'Zinc Oxide and Leaded Zinc Oxide', in Patton, T. C. (ed.) *Pigment Handbook*. New York, pp. 37–51.

Stutz, G. F. A. (1925) 'Observations of spectro-photometric measurements of paint vehicles and pigments in the ultra-violet', *Journal of the Franklin Institute*, 200(1), pp. 87–102.

Tauc, J. (1968) 'Optical properties and electronic structure of amorphous Ge and Si', *Materials Research Bulletin*, 3(1), pp. 37–46. doi: 10.1016/0025-5408(68)90023-8.

Taylor, J. S. (1887) *A Descriptive Handbook of Modern Water Colours: Illustrated with Actual Washes of the Pigments on Whatman's Drawing Paper. With an Introductory Essay on the Recent Water-colour Controversy*. London: Winsor and Newton.

Thomas, J. L. (2012) *Evaluation of reduced oxygen display and storage of watercolours, Doctoral thesis, UCL (University College London)*. University College London. Available at: http://discovery.ucl.ac.uk/1352730/.

Thomson, G. (1986) *The Museum Environment*. 2nd edn. Oxford: Butterworth Heinemann/Elsevier.

Townsend, J. H. (1993) 'The Materials of J . M . W . Turner : Pigments', *Studies in Conservation*, 38(4), pp. 231–254.

Townsend, J. H., Carlyle, L., Khandekar, N. and Woodcock, S. (1995) 'Later nineteenth-century pigments: evidence for additions and substitutions', *The Conservator*, 19(1), pp. 65–78.

Townsend, J. H., Ridge, J. and Hackney, S. (2004) Pre-Raphaelite Painting Techniques. Tate Publishing.

Townsend, J. H., Thomas, J., Hackney, S. and Lerwill, A. (2008) 'The benefits and risks of anoxic display for colorants', *Studies in Conservation*, 53(sup1), pp. 76–81. Available at: http://www.ingentaconnect.com/content/maney/sic/2008/00000053/A00102s1/art00015.

Vanheusden, K., Seager, C. H., Warren, W. L., Tallant, D. R. and Voigt, J. A. (1996) 'Correlation between photoluminescence and oxygen vacancies in ZnO phosphors', *Applied Physics Letters*, 68(3), pp. 403–405. doi: 10.1063/1.116699.

Verri, G., Clementi, C., Comelli, D., Cather, S. and Pique, F. (2008) 'Correction of ultraviolet-induced fluorescence spectra for the examination of polychromy', *Applied Spectroscopy*, 62(12), pp. 1295–1302.

Viezbicke, B. D., Patel, S., Davis, B. E. and Birnie, D. P. (2015) 'Evaluation of the Tauc method for optical absorption edge determination: ZnO thin films as a model system', *Physica Status Solidi* (B), 252(8), pp. 1700–1710. doi: 10.1002/pssb.201552007.

Viswanatha, R., Chakraborty, S., Basu, S. and Sarma, D. D. (2006) 'Blue-emitting copper-doped zinc oxide nanocrystals', *Journal of Physical Chemistry B*, 110(45), pp. 22310–22312. doi: 10.1021/jp065384f.

Wahl, R., Lauritsen, J. V., Besenbacher, F. and Kresse, Georg (2013) 'Stabilization mechanism for the polar ZnO(000$\bar{1}$)-O surface', *Physical Review B - Condensed Matter and Materials Physics*, 87(8), pp. 1–12. doi: 10.1103/PhysRevB.87.085313.

Van De Walle, C. G. (2000) 'Hydrogen as a cause of doping in zinc oxide', *Physical Review Letters,* 85(5), pp. 1012–1015. doi: 10.1103/PhysRevLett.85.1012.

Wang, L., Pu, Y., Fang, W., Dai, J., Zheng, C., Mo, C., Xiong, C. and Jiang, F. (2005) 'Effect of high-temperature annealing on the structural and optical properties of ZnO films', *Thin Solid Films*, 491(1–2), pp. 323–327. doi: 10.1016/j.tsf.2005.05.048.

van der Weerd, J., Geldof, M., van der Loeff, L. S., Heeren, R. M.A. and Boon, J. J. (2003) 'Zinc soap aggregate formation in "Falling Leaves (Les Alyscamps)" by Vincent van Gogh', *Zeitschrift für Kunsttechnologie und Konservierung,* 17(2), pp. 407–416.

Weidenkaff, A., Steinfeld, A., Wokaun, A., Auer, P. O., Eichler, B. and Reller, A. (1999) 'Direct solar thermal dissociation of zinc oxide: condensation and crystallisation of zinc in the presence of oxygen', *Solar Energy,* 65(1), pp. 59–69. doi: 10.1016/S0038-092X(98)00088-7.

Weintraub, S. (2010) 'Using risk assessment tools to evaluate the use of LEDs for the illumination of light-sensitive collections', *American Institute of Conservation News,* (September), pp. 14–17. Available at: http://www.apsnyc.com/LED for Art Applications_Steven Weintraub.pdf.

Wells, B. (2015) *Bandgap measurements of nonspecular materials using a bifurcated fiber optic method of diffuse reflectance*. Oregon State University.

Williams, P. A. and Phillips, G. O. (2009) 'Gum arabic', in Phillips, G. O. and Williams, P. A. (eds) *Handbook of Hydrocolloids*. Second. Elsevier, pp. 252–273.

Wilton, A. and Lyles, A. (1993) *The Great Age of British Watercolours: 1750-1880.* Munich: Prestel-Verlag.

Winter, G. and Whittem, R. N. (1950) 'Fluorescence and photo-chemical activity of zinc oxides', *Journal of the Oil and Colour Chemists' Association,* 33, pp. 477–483.

Yun, S. and Lim, S. (2011) 'Effect of Al-doping on the structure and optical properties of electrospun zinc oxide nanofiber films', *Journal of Colloid and Interface Science*. Elsevier Inc., 360(2), pp. 430–439. doi: 10.1016/j.jcis.2011.05.022.

Zerr, G. and Rübencamp, R. (1908) *A treatise on colour manufacture: a guide to the preparation, examination, and application of all the pigment colours in practical use.* 1st edn. London: C. Griffin and Company.

Zhang, S. B., Wei, S. H. and Zunger, A. (2001) 'Intrinsic n-type versus p-type doping asymmetry and the defect physics of ZnO', *Physical Review B - Condensed Matter and Materials Physics,* 63(7), pp. 1–7. doi: 10.1103/PhysRevB.63.075205.

Zhu, Y., Zhang, X., Li, R. and Li, Q. (2014) 'Planar-defect-rich zinc oxide nanoparticles assembled on carbon nanotube films as ultraviolet emitters and photocatalysts', *Scientific Reports*, 4(4728), pp. 1–7. doi: 10.1038/srep04728.